Analysis of the molecular mechanisms underlying the role of SREBP1 in Glioblastoma tumour development and progression

Analyse der molekularen Mechanismen, die der Rolle von SREBP1 bei der Entwicklung und Progression von Glioblastom-Tumoren zugrunde liegen

Doctoral thesis

for a doctoral degree

at the Graduate School of Life Sciences,

Julius-Maximilians-Universität Würzburg,

Section Biomedicine

submitted by

Sudha Rani Janaki Raman

From Bangalore

Würzburg 2021

Members of the Thesis committee:

Chairperson:

Primary Supervisor: Prof. Almut Schulze

Supervisor (Second): Prof. Svenja Meierjohann

Supervisor (Third): PD Dr. med. Dr. rer. nat. Matthias Kroiss

Submitted on:

Office stamp

Date of Public Defence:

Date of Receipt of Certificates:

Table of Contents

Summary

Glioblastoma (GB) is the most aggressive malignant adult brain tumour with a median survival rate of only 15 months. GB tumours are characterized by necrotic and hypoxic core, which leads to nutrient deficient areas contributing to invasive, diffuse-infiltrative and angiogenic nature of these tumours. Cells exposed to nutrient deficient conditions and are known to reprogram their metabolism to produce or procure macro molecules from their environment. This makes cancer cells uniquely dependent on transcriptional regulators and a window of opportunity to target them. Sterol regulatory element binding protein 1 (SREBP1) is a transcriptional regulator of *de-novo* fatty acid synthesis in cells. The aim of this thesis was to investigate if SREBP1 was involved in restructuring the transcriptional regulation of genes involved in fatty acid biosynthesis upon low serum condition, in mediating interaction with other cell types in the tumour bulk such as endothelial cells, in regulating cancer stem like cells and finally to study its upstream regulation in GB. Global transcriptional analysis on GB cells exposed to low serum conditions revealed that SREBP1 regulated several fatty acid biosynthesis and phospholipid metabolic processes. PLA2G3 was identified as a novel target of SREBP1 in GB that was uniquely regulated in low serum condition. Analysis of total fatty acid and lipid species revealed that loss of SREBP1 in low serum condition changes the proportion of saturated, MUFAs and PUFAs. These changes were not specific to loss of PLA2G3 but as a result of downregulation of many genes regulated by SREBP1 in the fatty acid biosynthetic pathway. Next, treatment of HUVEC's (endothelial cells) with condition medium from SREBP1-silenced U87 cells inhibited sprouting and tube formation capacity compared to the control condition, emphasizing the role of SREBP1 in angiogenesis and release of signalling mediators. Further, SREBP1 was shown to be important for proliferation of patient derived stem like cells and becomes indispensable for forming neurospheres in long term cultures, indicating its role in maintaining stemness. Also, inhibition of SREBP function by blocking the esterification of cholesterol using inhibitors targeting SOAT1 showed impairment in the viability of GB cells exposed to serum-depleted condition. Overall, SREBP1 plays an important role in maintaining tumour growth in nutrient deficient conditions and help in interaction with tumour microenvironment contributing to the aggressiveness of this tumour and poses itself as an attractive and unique target for GB treatment

Zusammenfassung

Das Glioblastoma (GB) ist der aggressivste bösartige Gehirntumor bei Erwachsenen mit einer medianen Überlebensrate von nur 15 Monaten. GB-Tumore zeichnen sich durch einen nekrotischen und hypoxischen Kern aus, der zu nährstoffarmen Bereichen führt, die zu invasiven, diffus-infiltrierenden und angiogenen Natur dieser Tumore beitragen. Zellen, die einem Nährstoffmangel ausgesetzt sind, sind dafür bekannt, ihren Stoffwechsel umzuprogrammieren, um Makromoleküle zu produzieren oder diese aus ihrer Umgebung zu beziehen. Dies macht Krebszellen in einzigartiger Weise abhängig von Transkriptionsregulatoren und eröffnet die Möglichkeit diese gezielt anzugreifen. Das sterol regulatory element binding protein 1 (SREBP1) ist ein Transkriptionsregulator der de-novo Fettsäuresynthese in Zellen.

Das Ziel dieser Arbeit war es zu erforschen, ob SREBP1 an der Umstrukturierung der Transkriptionsregulation der Gene involviert ist, die unter niedrigen Serumbedingungen an der Fettsäurebiosynthese beteiligt sind. Des Weiteren richtete sich die Arbeit darauf, ob SREBP1 die Interaktion mit anderen Zelltypen im Tumor wie den Endothelzellen vermittelt, ob es die stammzellähnlichen Krebszellen reguliert und letztlich, dessen Stromaufwärts-Regulierung in GB zu untersuchen.

Eine globale Transkriptionsanalyse von GB-Zellen, die niedrigen Serumbedingungen ausgesetzt waren, ergab, dass SREBP1 mehrere Fettsäurebiosynthese- und Phospholipid-Stoffwechselprozesse reguliert. Dabei wurde PLA2G3 als ein neuartiges Ziel von SREBP1 in GB identifiziert, welches unter geringen Serumbedingungen auf einzigartige Weise reguliert wurde. Die Analyse der gesamten Fettsäure- und Lipidspezies ergab, dass der Verlust von SREBP1 unter niedrigen Serumbedingungen das Verhältnis zwischen gesättigten, MUFAs und PUFAs verändert. Diese Veränderungen waren nicht spezifisch auf den Verlust von PLA2G3 zurückzuführen, sondern eine Folge der Herunterregulierung vieler Gene, die im Fettsäurebiosyntheseweg durch SREBP1 reguliert werden.

Als Nächstes zeigte die Behandlung von HUVECs (Endothelzellen) mit dem konditionierten Medium von SREBP1-stillgelegten U87 Zellen, dass die Sprieß- und Röhrenbildungsfähigkeit im Vergleich zur Kontrollbedingung gehemmt war. Dies unterstreicht die Rolle von SREBP1 bei der Angiogenese und der Freisetzung von

Signalmediatoren. Außerdem wurde nachgewiesen, dass SREBP1 wichtig für die Proliferation von aus Patienten stammenden stammzellähnlichen Zellen und für die Bildung von Neurosphären in Langzeitkulturen unverzichtbar ist, was auf die Rolle von SREBP1 bei der Aufrechterhaltung der Stammzellfähigkeit hindeutet. Auch die Hemmung der SREBP Funktion durch die Blockierung der Veresterung von Cholesterin mittels SOAT1-Inhibitoren wies eine Beeinträchtigung der Lebensfähigkeit von GB-Zellen auf, die einer serumarmen Bedingung ausgesetzt waren.

Zusammenfassend zeigt diese Arbeit, dass SREBP1 eine wichtige Rolle in der Aufrechterhaltung des Tumorwachstums unter nährstoffarmen Bedingungen und bei der Interaktion mit der Tumormikroumgebung spielt, die zur Aggressivität des Tumors beiträgt und sich somit als ein attraktives und einzigartiges Ziel für die Behandlung von GB darstellt.

Chapter 1: Introduction

1.1 Glioblastoma

Cells are the basic structural and functional building blocks of all organisms. Cell division and proliferation is an important part of our existence and survival. Generally, cells require growth signals to change from quiescent to proliferative phase. Our cells tightly regulate and control the production and release of these growth stimulating signals and hence maintain homeostasis of cell division and normal tissue architecture. Cancer cells re-program their cellular signalling to evade normal growth cycle and transform themselves into a chronic proliferative state. It is known that cancer cells accumulate different genetic mutations to attain this uncontrollable proliferative state. Mutations are one of the most important factors that governs the state of transformation of cells from normal to cancerous state (Hanahan and Weinberg, 2000). Depending on the type, location and the environment of the tumour bearing organ, they can acquire mutations that are in their favour to help them rewire their metabolism to support proliferation. Some tumours, such as glioblastoma (GB), are also known to have acquired several mutations that leads to heterogenous tumour bulk and makes cancer treatment more challenging and decreases overall survival rate in patients. GB is one of the most aggressive malignant brain tumours and is classified as grade IV tumours by the world health organization (WHO) and account for two thirds of all adult brain tumours (Ostrom et al., 2019; Perry and Wesseling, 2016). GB tumours can originate as primary or secondary tumours. Secondary tumours are formed through pre-existing lower grade gliomas and has better prognosis and treatment outcome and account only for about 10% of all GB cases (Lai et al., 2011). While primary GB account for almost 90% of the cases and have poor prognosis and poor survival rate. GB tumours also have high recurrence rate, high mortality with median survival rate of only 15 months (Stupp et al., 2005).

1.1.1 Classification of Glioblastoma

It dates back to mid 90’s when several researchers including remarkable work of Hans-Joachim Scherer a young German neuropathologist, started to distinguish

between primary and secondary GB (Peiffer and Kleihues, 1999). Only after establishing immunohistochemistry staining and analysis of GB tumours it was universally accepted to distinguish them into primary and secondary lesions (Ohgaki and Kleihues, 2013; Scheithauer, 2009). Further developments in the later years lead to establishment of distinguishable genetic traits between these two classes including identification of mutations in p53 and EGFR signalling (Collins, 1993; Watanabe et al., 1996). There were other significant contributions made to differentiate between primary and secondary GB, but not until it was identified that IDH mutations in GB patients showed better prognosis and overall survival (Parsons et al., 2008). This discovery led to bench marking of IDH1/2 mutations as the marker for astrocytoma grade II and anaplastic astrocytoma grade III, which are the precursors for secondary GB (Fig 1.1) (Nobusawa et al., 2009; Yan et al., 2009). IDH1/2 mutations occur early and are present in precursor cells which progress to form diffuse astrocytomas or oligodendrogliomas. Oligodendrogliomas likely show frequent mutations in 1p/19q loss whereas about 60-65% of the astrocytomas also incur TP53 mutations which progresses to grade IV secondary GB (Louis, 2006; Ohgaki and Kleihues, 2013). Overall, patients diagnosed with secondary GB have better prognosis and have a median survival rate of 2-5 years (Park et al., 2010).

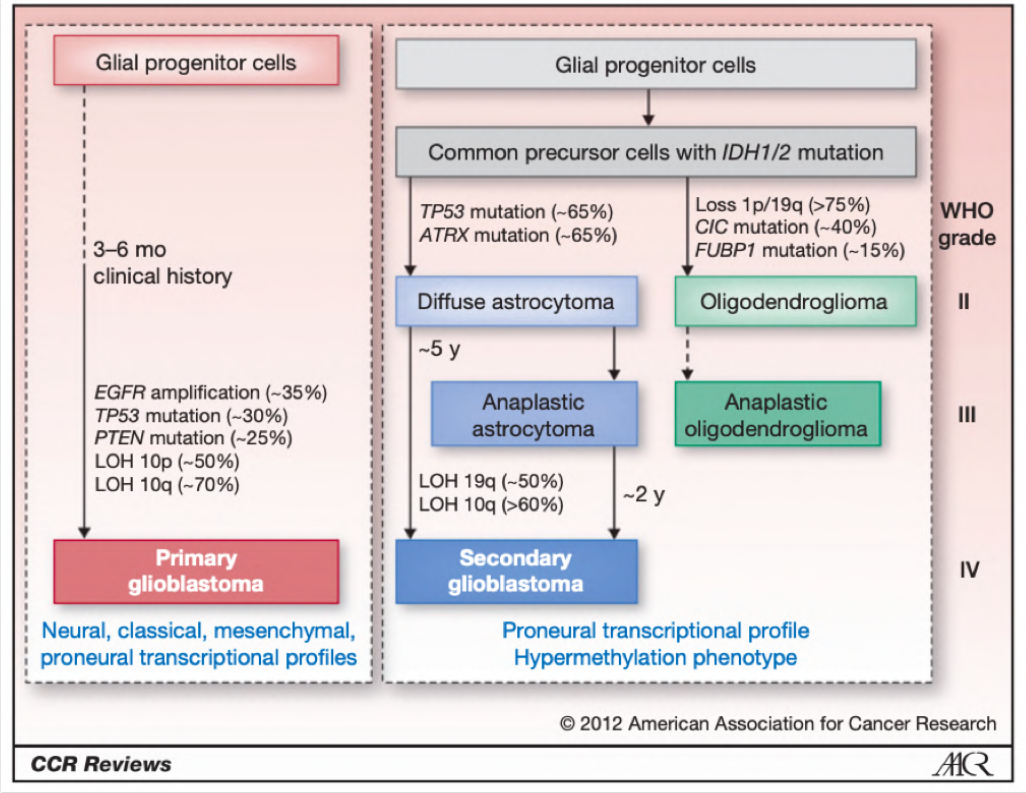

Figure 1.1: Genetic distinctions of primary and secondary GB

Glial cells are the source of origin for both primary and secondary gliomas. The primary GB are derived from glial cells that undergo mutations in either *EGFR, TP53, PTEN, LOH 10p or LOH 10q* and leads to tumour formation. The percentages mentioned are the rates of mutations seen in those genes in primary glioblastomas. While secondary GB are derived from lower grades tumours such as diffuse astrocytoma and anaplastic astrocytoma, which primarily are formed from *IDH1/IDH2* mutations in glial cells. Also, the secondary gliomas share their lineage with oligodendrogliomas. This image was obtained from (Ohgaki and Kleihues, 2013).

1.1.2 Primary Glioblastoma

Tumours that are classified as IDH1/2 WT account for about 90% of the GB cases. These tumours are called as primary GB as they do not arise from a lower grade tumour, most of them have acquired several mutations in EGFR, TP53, PTEN, LOH 10p or LOH 10q and are classified as WHO grade IV tumours (Figure 1.1). These tumours are incurable and have poor diagnosis, prognosis and disappointing outcomes. Patients with primary GB have only about 12-15 months of median survival rate (Ostrom *et al.*, 2019; Perry and Wesseling, 2016). Standard care of treatment for these tumours are surgical resection, followed by fractionated radiotherapy along with chemotherapy with an alkylating chemotherapeutic agent temozolomide. Surgical resection of brain tumours is challenging depending on the position of the tumours and the outcome varies from case-to-case basis. Even when the tumours are in a region reasonably accessible for resection it requires specialized and skilled neurosurgeons to remove the tumour bulk as much as possible without carving into the surrounding normal brain. This leads to some remaining tumour cells after resection that are incompletely treated by radio and chemotherapy. One other critical factor that makes it hard to treat these tumours with chemotherapy is the blood brain barrier (BBB). BBB is a specialized junction made of brain microvascular endothelial cells that controls the exchange of substances between brain and the rest of the body, protecting the brain neural cells from possible exposure to toxins and harmful compounds. Furthermore, microenvironment of the brain, their developmental complexity, epigenetic and genetic make-up is very different from the other organs. Hence, drugs that are used in the treatment of other type of tumours might not be suitable for brain tumour patients, thus making these tumours unique and hard to treat (Aldape et al., 2019). These tumours are also known to be resistant to available treatments and leads to relapse in almost all cases. They are known to grow fast and tend to be large tumours with hypoxic and

necrotic areas, contributing to the highly diffusive infiltrative, angiogenic nature of these tumours and making them the most aggressive malignant brain tumour. Also, they are highly heterogenic in nature, making the tumour bulk additionally complex and difficult to treat with a single agent. It is known that these tumours have cancer stem like cells that are resistant to chemo and radio therapy and are mostly responsible for relapse in patients with more aggressive tumours that are unresponsive to most available treatments (Golebiewska et al., 2013; Prasad et al., 2015).

Hence, there is a significant need to understand these tumours better and develop targeted therapies and combinatorial approach to aim at several aspects of GB rather than a single point care. Also, identifying factors that regulate processes specific to cancer cells and finding the window of opportunity to target the Achilles of cancer holds a priority in novel therapeutic strategies to reduce toxicity with the drugs and to increase the efficiency of the targeted approach. Overall, the path to improve GB patient treatment is to identify the mutational status of the patients, understand the pathways over expressed in them and develop treatments targeted towards the signalling regulators curbing the root of cancer growth. Also, it is important to understand, identify and target the signalling network that is essential for communication with different cell types (e.g., endothelial cells, macrophages, immune cells) present in the microenvironment to efficiently limit the growth of cancer cells and relapse.

1.2 Tumour angiogenesis

Angiogenesis is process of developing new blood vessels by endothelial cells in the existing vascular network. This process involves proliferation and migration of endothelial cells to required region for formation of new blood vessels. This process is tightly regulated by signalling network of pro- and anti-angiogenic molecules and is essential for wound healing and formation of new vasculature. Blood vessels are important to any mammalian cell as they obtain oxygen and nutrients for their survival from them. Every cell needs to be located as close as 100 to 200 µm to a blood vessel for proper diffusion of oxygen (Carmeliet and Jain, 2000; Hanahan and Weinberg, 2000). In cancer cells due to their high proliferation there is huge need for new blood vessels and without which tumours cannot grow beyond a critical size which is

dependent on the proximity to an existing blood vessel. Tumour angiogenesis was discovered nearly a 100 years ago and is recognized as one of the hallmarks of cancer (Hanahan and Weinberg, 2000). Studies in mice have shown that tumour angiogenesis is acquired by tumours through their mid-phase growth before they become full blown tumours, there is an angiogenic switch that transforms quiescent endothelial cells to proliferate to form new blood vessels (Hanahan and Folkman, 1996). Hence it is an important phenomenon for fast growing tumours and is point of intervention to target cancer with therapies.

GB tumours are characterized by vascular proliferation and is known to occur in 2 pathologically distinguished forms. First, an increased diffusion of densely populated array of small blood vessels, which are not obvious in H & E staining but detected using endothelial cells markers such as CD31. Second, microvascular proliferation of blood vessels also called as glomeruloid vessels, and they are unique to high grade GB and is used to grade tumours. These vessels are generally made up of proliferating endothelial cells and smooth muscle cells, and they are distributed haphazardly and irregularly over the necrotic regions of the tumour (Louis, 2006). The tumour blood vessels are structurally different from normal healthy blood vessels as they are permeable, have heterogenous morphological structures, lack pericytes making them thin and weak, have large pores and are leaky (Jain et al., 2007; Lupo et al., 2016). These structural abnormalities are also known to cause hypoxic region even with neoangiogenesis in tumour and are also responsible for improper delivery of chemotherapeutic drugs and lead to treatment failure.

1.2.1 Regulators of angiogenesis

The regulation of angiogenesis in malignant tumours is a complex process and is known to involve several signalling networks and cross talk between cancer cells and the endothelial cells. There are several factors that are responsible for inducing angiogenesis in tumours, and a well-known molecule synthesized by the cancer cells is the vascular endothelial growth factor (VEGF), which acts through the receptors present on the endothelial cells vascular endothelial growth factor receptor 1 (VEGFR1) and 2 to induce angiogenesis. VEGF is a homodimeric glycoprotein and is known to be involved in embryonic development and in wound healing processes in

adults (Carmeliet, 2005). VEGF is one of the growth factor produced by the tumour cells which is known to be involved in the angiogenic switch observed in endothelial cells involved in tumour angiogenesis (Carmeliet, 2005). VEGF signalling is upregulated in cancer and hypoxia is known to transcriptionally regulate VEGF in the tumour microenvironment (Carmeliet, 2005; Jain *et al.*, 2007). Current anti-angiogenic treatments are targeted at VEGF signalling, they focus on inhibiting the proliferation of endothelial cells, thereby stopping the nutrient and oxygen source from the tumour cells and stopping their proliferation.

There are several other signalling molecules known to be involved in angiogenesis, such as angiogenin, interleukin-8, prostaglandin E2 (PGE2), lysophosphatidic acid C18:1 (LPA C18:1) and others. These molecules are shown to either act on endothelial cells directly or activate other pathways to induce angiogenesis indirectly. Angiogenin is a polypeptide member of the RNAse A superfamily and is known to be important in cancer cell proliferation, survival and inducing angiogenesis. Angiogenin is released by the cancer cells into the tumour microenvironment and can enter other cells and can regulate important cellular signalling. Angiogenin is involved in rRNA transcription and ribosomal biogenesis in endothelial cells, hence can be important for endothelial cell proliferation (Kishimoto et al., 2005). Interleukin 8 (IL8) is a proinflammatory chemokine and is known to be released by tumour cells and is involved in paracrine signalling mediating metastasis, tumour angiogenesis and also in chemoresistance. IL8 is also linked to histological grading of brain tumours such as GBs, as these tumours secrete high levels of IL8 (David et al., 2016; Li et al., 2003; Ning et al., 2011; Shi and Wei, 2016). IL8 is shown to be directly involved in angiogenesis by maintaining endothelial cell proliferation and survival and regulating the expression of matrix metalloproteinase 2 (MMP-2) that is necessary for degradation of extracellular matrix to facilitate migration and sprouting (Li *et al.*, 2003).

Lipid mediators such as PGE2 and LPA C18:1 which are known to be involved in cell signalling regulation and cross talk between cells and the microenvironment have also been shown to be involved in regulating angiogenesis. PGE2 has been shown to regulate angiogenesis in tumour cells by increasing the secretion of VEGF in endothelial cells and that PGE2 is regulated downstream of PI3/AKT (Tamura et al.,

2006). LPA C18:1 is a known lipid mediator involved in regulation of various cellular functions and aids in cell growth, proliferation through G-coupled receptors LPARs. Their involvement in angiogenesis is studied in context of vascular development in healthy tissues and their role in pathological diseases. It has been shown that LPA C18:1 is involved in endothelial cell proliferation and migration, which is essential for neo-angiogenesis and is rendered important in wound healing processes. LPA C18:1 is also known to induce VEGFA expression in cancer endothelial cells via HIF-1α and contribute to aggressiveness of human cancers (Teo et al., 2009).

1.2.2 Challenges with anti-angiogenic therapies

Even though many targets that regulate angiogenesis in tumours are being extensively studied the available antiangiogenic therapies are mainly based on targeting VEGF signalling. Bevacizumab is one of the standard lines of treatment for antiangiogenic treatment for GB patients (Kim et al., 2018; Li et al., 2017b). Even though anti-angiogenic therapies show efficacy in earlier treatment period, it fails to be effective in long term as patients develop resistance to the treatments (Li *et al.*, 2017b). Though there are several possible explanations for treatment failure, the adaptation of tumour endothelial cells to the tumour micro environment and loss of chemotherapeutic drugs reaching the tumours due to loss of blood vessels, gives rise to heterogenous population of endothelial cells that show resistance to the treatment and contribute to tumour growth (Montemagno and Pages, 2020). The other important factor that leads to treatment failure with anti-VEGF treatment is that tumour angiogenesis is regulated by many other signalling molecules synthesized by cancer cells and only targeting VEGF is insufficient to completely block neo-vascularization in tumours. Hence, treatment with anti-angiogenic drugs should employ combinatorial approach with in-depth analysis of the tumour microenvironment to successfully design treatment strategies that would show efficacy in patients.

1.3 Tumour heterogeneity in primary GB

Heterogeneity is generally defined in clinical terms as state of being diverse, in tumours it is referred to both inter-tumour and intra-tumour heterogeneity. Inter-tumour

heterogeneity refers to a difference seen in different patients or population level variability. Intra-tumour heterogeneity refers to variability within individual tumours. The heterogeneity can be studied using samples collected from single time point for investigating spatial heterogeneity or collected from different time points to study clonal evolution, also called as longitudinal heterogeneity. Both spatial and longitudinal heterogeneity permits to understand histopathological changes, progression of the tumours and development of resistance. GB tumours are known for both inter and intra-tumour heterogeneity (Becker et al., 2021). GBs are known to be composed of diverse clonal and sub-clonal cell populations; cancer stem like cells and differentiated cells, non-tumour cells such as endothelial cells, inflammatory cells and also microglial cells, making their tumour microenvironment complex and hard to treat with single point care (Becker *et al.*, 2021; Hambardzumyan et al., 2016).

Availability of complete human genome sequence and swift improvements in high throughput omics technology has led to more comprehensive genomic analysis on human cancers. The cancer genome atlas (TCGA) performs genomic analysis on human cancer genomes and catalogues the main aberrations found in cancers using large cohorts of patient materials. GB was the first cancer to be evaluated by TCGA to perform multidimensional analysis to characterize its genome and transcriptome. The analysis was performed by using DNA copy number, gene expression and DNA methylation irregularities in 206 GB patients and major pathways that are deregulated in these tumours were identified. Receptor tyrosine kinase/ rat sarcoma virus protein/ phosphatidylinositol 3-kinases (RTK/RAS/PI3K), p53 signalling and retinoblastoma protein (RB) signalling were identified as 3 major signalling pathways frequently mutated in GB genome (Fig. 1.2) (Cancer Genome Atlas Research, 2008). Copy number analysis of 206 GB tumours and analysing the somatic aberrations in 91 GB patients with sequencing data showed at least one genetic alteration in the constituents of RB, p53 or RTK pathways. This study led to understanding of the genetic alterations found in different GB patients and the importance of genomic analysis of individual patients to design treatment strategies based on the aberration for a successful outcome.

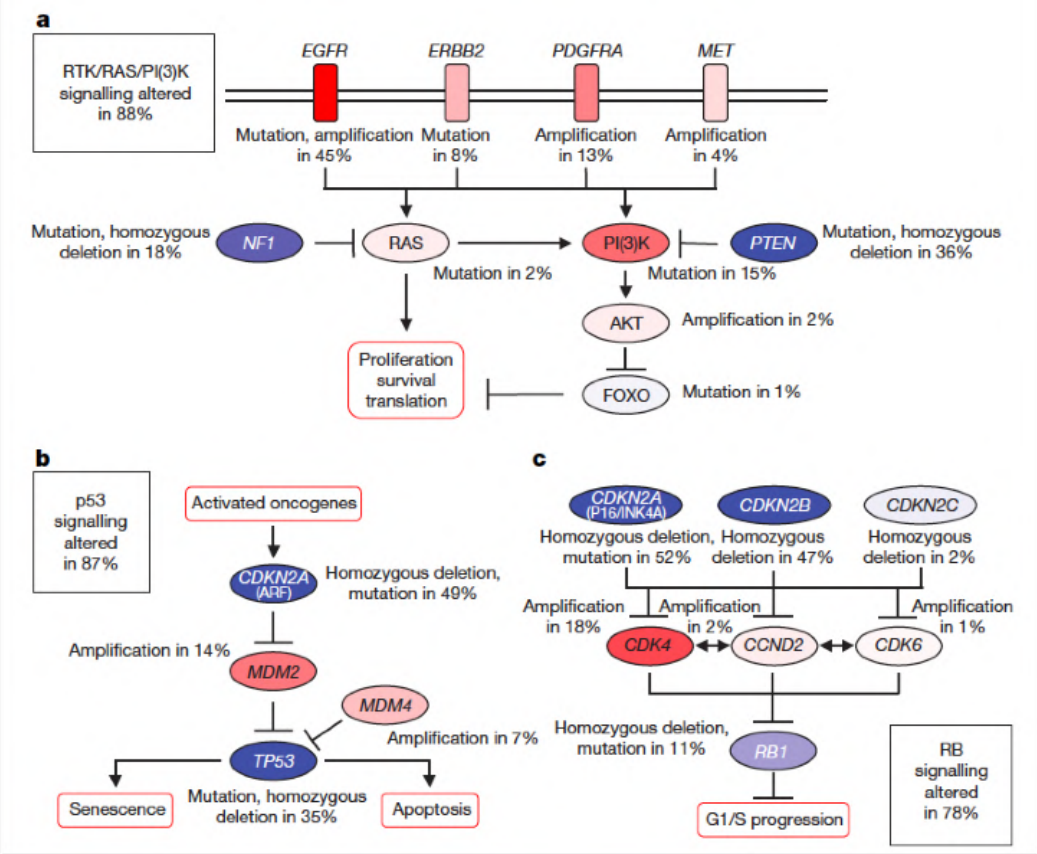

Figure 1.2: Identification of altered signalling pathways in GB by TCGA

This figure shows the mutations/amplifications found in 3 critical signalling pathways in GB patients. a. shows the signalling alteration in RTK/RAS/PI3K pathway which is altered in 88% of the cases. b. 87% of GB tumours showed mutations or amplifications accumulated in the p53 signalling cascade. c. 78% of amplification, mutation or gene deletion was seen in RB signalling. Genes that are indicated in red shows activating and blue shows inactivating aberrations. Darker shades represent higher frequently of alterations. This figure was taken from (Cancer Genome Atlas Research, 2008).

RTK/RAS/PI3K pathway was one of the most altered signalling cascades in GB in the TCGA analysis (Cancer Genome Atlas Research, 2008). This axis is particularly prominent in highly proliferative cells as it mediates growth factor signalling and uptake of nutrients and involves in regulation of biosynthesis of both proteins and lipids in cells. PI3Ks were first discovered as kinases phosphorylating the hydroxyl group of inositol lipids to increase the turnover of phosphatidylinositol in cells upon growth factor stimulation (Cantley et al., 1986; Whitman et al., 1985). RTKs are a family of cell surface receptors and respond to growth factors, hormones and signalling molecules (Regad, 2015). Autophosphorylation of RTKs upon external cues can promote to

recruitment of PI3Ks in cells. One of the main important downstream regulators of RTK/PI3K axis is AKT.

The serine/threonine kinase AKT, also known as protein kinase B (PKB) is known to have 3 isoforms: AKT1, AKT2 and AKT3 (Bellacosa et al., 2005). All 3 isoforms have been known to be involved in several important functional regulation in cells, AKT 1 is involved in embryonic growth, AKT3 in brain development, AKT1 and 3 are regulators of glucose homeostasis in cells (Lu et al., 2012; Vivanco and Sawyers, 2002). AKT is known to be involved in regulation of cell proliferation, nutrient sensing and uptake upon growth factor addition, angiogenesis regulation and diffuse invasiveness of tumour cells (Bellacosa *et al.*, 2005). AKT needs to be phosphorylated at 2 specific sites to be completely activated. PH-domain containing protein kinase 1 (PDK1) located close to the membrane localized AKT, phosphorylates AKT at T308 (Scheid et al., 2005). Rictor- mammalian target of rapamycin (mTOR) is known to be the kinase responsible for the second phosphorylation of AKT at S473 present in the carboxyl-terminal hydrophobic motif (Sarbassov et al., 2005). S473 phosphorylation of AKT is necessary for the translocation of AKT from plasma membrane to the nucleus. Nuclear localized AKT activates several downstream signalling pathways involved in both protein and lipid biosynthesis.

Mammalian target of rapamycin (mTORC) is a serine/threonine kinase which belongs to the PI3K related kinase family which forms the catalytic subunit of 2 distinct protein complexes, mTORC1 and mTORC2. mTORC1 has three components: mTOR, regulatory protein associated with mTOR (Raptor) and mammalian lethal with Sec13 protein 8 (mLST8, also known as GβL). Raptor is involved in substrate recruitment to the TOR signalling motif and helps in subcellular localization of mTORC1 (Kim et al., 2002). mLST8 is linked to the catalytic domain of the mTORC1 which is required for stabilization of kinase activation loop. It is shown that mLST8 is important for functioning of mTORC1 kinase activity in the cells (Yang et al., 2013). mTORC1 is regulated downstream of PI3K-AKT axis and responds to growth factors and nutrient depletion and is mainly involved in regulation of protein biosynthesis in cells. The tumour suppressor proteins TSC1 and TSC2 are negative regulators of mTORC1. They act on GTP-ase activating proteins such as Ras homolog enriched protein in brain (Rheb), which plays important role in mediating growth factor signalling and

nutrient sensing of mTORC1. AKT phosphorylates the TSC2, and this phosphorylation stops it from disassociating from the lysosomal membrane and inhibiting Rheb. Another mechanism of activation of mTORC1 in cells is dependent on MAP kinase ERK signalling, whose effector p90 RSK phosphorylates and inactivates TSC2 (Saxton and Sabatini, 2017).

mTORC1 promotes protein signalling in cells through 2 core effectors phosphorylation, p70S6 kinase 1 (S6K1) and eIF4E binding protein (4EBP1). mTORC1 is involved in direct phosphorylation of S6K1 at its hydrophobic motif site Threonine 389 and this phosphorylated form is further phosphorylated by PDK1 for its complete activation (Saxton and Sabatini, 2017). S6K1 phosphorylates many downstream targets and one important including eIF4B that regulates the formation of eIF4F complex (Holz et al., 2005). 4EBP1 independent of S6K1 inhibits eIF4E by binding and inhibits the formation of eIF4F complex and mTORC1 prevents 4EBP1 binding by phosphorylation at several sites (Raught and Gingras, 1999). These phosphorylation by mTORC1 and its downstream target S6K1 regulates mRNA transcription and translation, especially the mRNAs consisting of pyrimidine rich 50 TOP or “TOP-like” motifs which are involved in protein biosynthesis (Hsieh et al., 2012; Saxton and Sabatini, 2017; Thoreen et al., 2012). mTORC1 is also a key regulator of lipid biosynthesis in cells by regulating activity and stability of the transcription factor SREBP1 (Porstmann et al., 2008), which makes P13K-AKT-mTORC1-SREBP1 axis prominent in proliferating cells.

1.4 Fatty acids and lipid biosynthesis

Metabolic alteration is one of the hallmarks of cancer. Nutrient uptake and macromolecular biosynthesis are characteristics of proliferating cancer cells. Fatty acid and lipid biosynthesis is an essential process in synthesizing cellular membranes in newly formed cells and plays an important role in cancer growth and progression. Fatty acids, sphingolipids and cholesterol are the building blocks of more complex lipid structures that form cell membranes. Fatty acids consist of a polar head group and aliphatic hydrocarbons chains with variable number of carbon atoms and double bonds which gives rise to thousands of unique lipid species that provides cell membranes its structure, fluidity and dynamics. The fatty acids are classified based on the number of

double bonds, saturated fatty acids (without double bonds), mono-unsaturated fatty acids (MUFAs, one double bond) and polyunsaturated fatty acids (PUFAs, with two or more double bonds). Fatty acids are stored as triacylglycerols in lipid droplets when esterified with glycerol-3-phosphate and act as huge energy reserve in cells. Triacylglycerols can be used to be obtain ATP by combining three important metabolic pathways in cells, beta-oxidation, Krebs cycle and the oxidative phosphorylation (also known as the respiratory chain). When triacylglycerols are completely metabolized by all three pathways provide a great amount of ATP to the cells, for e.g., complete oxidation of one molecule of palmitate can yield up to 104 molecules of ATP (assuming non-integer phosphate/oxygen ratio) (Salway, 2017).

Lipids are the hydrophobic biomolecules that include phospholipids, sterols, glycolipids and mono-, di-, and tri-acyl glycerides. The main structural lipid in the cellular membrane is phospholipids. Phospholipids contains a polar headgroup with a phosphate group, hydrophobic region derived from diacylglycerol containing two fatty acyl chains, which are connected by glycerol moiety. Phospholipids are classified into 5 major groups: phosphatidylcholines (PC), phosphatidylethanolamine (PE), phosphatidylinositol (PI), phosphatidylserine (PS) and phosphatidic acid (PA). Among these lipids about more than 50% of cellular membrane lipids are made up of phosphatidylcholine (van Meer et al., 2008). This is because the PC molecules arrange themselves into a planar bilayer with hydrophobic tails facing each other and head groups on the outside which gives almost a cylindrical geometry to the membranes. Also, the diverse fatty acyl chains with varying lengths and double bonds give the asymmetrical nature to membrane and controls the fluidity and accommodates proteins and aid in cell signalling. Further the PC and other phospholipids present on membranes aid in compartmentalization of organelles for specific function in the cells. Especially, PE and cardiolipins present on mitochondrial membranes help in fission and fusion reactions (van Meer et al., 2008).

Even though lipids are continuously converted into each other and move from different membranes and cellular compartments, phospholipids are still synthesised in cells, and it mainly occurs in the ER. There are three ways of synthesizing phospholipids in cells: Kennedy pathway, Land’s cycle and phosphatidylethanolamine methyl transferase (PEMT) (Moessinger et al., 2014). Cells synthesize PC and PE via

Kennedy pathway via two main branches, choline and ethanolamine arms respectively. Phospholipid synthesis is activated by availability of CTP, which is further transferred to DAGs which are converted to PC and PE, and these reactions are catalysed by CTP phosphocholine cytidylyltransferase and membrane embedded choline phosphotransferase or choline/ethanolamine phosphotransferase (CEPT1/CPT1). In Land's cycle cells use phospholipases to cleave off one of the acyl chains, preferably on the sn-2 positions from the phospholipids and gives rise to lysophospholipids. Further, re-acylation of other acyl chains to those positions by lysophosphatidylcholine acyltransferases (LPCATs) which are recruited to the ER membrane creates new phospholipids (Moessinger *et al.*, 2014). These constant modifications of the acyl chains give additional fluidity to the cell membranes and in synthesizing essential lipid mediators or precursors necessary for producing signalling molecules downstream, that are involved in myriad of cellular functions.

1.4.1 Sterol regulatory element binding proteins (SREBPs)

SREBPs were discovered by Goldstein and Brown as proteins that bind to sterol regulatory elements (SRE), activating and mediating the final steps of low-density lipoproteins (Hua et al., 1993; Yokoyama et al., 1993). These proteins consist of n-terminal transcription activation domain, a middle hydrophobic region containing two hydrophobic transmembrane segments and a c-terminal regulatory domain. Enzymes involved in fatty acid biosynthesis are regulated by SREBPs, these proteins are from the family of basic-helix-loop-helix-leucine zipper transcription factors. There are three isoforms of SREBPs: SREBP1a and SREBP1c, splice variants of the *SREBF1* gene, and SREBP2 expressed by *SREBF2* (Horton, 2002). The difference between SREBP1a and SREBP1c is caused by the alternative splicing of the first exons that results in a difference of 113 amino acid stretch (Yokoyama *et al.*, 1993). The 3 isoforms of SREBP transcriptionally regulate genes involved in biosynthesis of fatty acids, cholesterol, triacylglycerols and phospholipids (Horton, 2002).

1.4.2 Upstream regulators of SREBPs activation

SREBPs are produced as inactive precursors that are located on the endoplasmic reticulum membranes (ER). These inactive precursors are bound to

protein called SREBP cleavage activating protein (SCAP). SREBP-SCAP complex needs to be translocated to Golgi bodies via coat protein complex II (COP-II) mediated transport for its activation as these proteins require proteolytic cleavage by proteases membrane-bound transcription factor site 1 protease and 2 (MBTPS1 and MBTPS2) located on the Golgi bodies. These proteolytic cleavage releases the n-terminal transactivation domain of SREBP which further travel to the nucleus and binds as homodimers to the SRE elements and transcriptionally regulates the genes involved in fatty acid biosynthesis (Fig 1.3a). Activation of SREBPs is controlled by the intracellular levels of sterols. When the sterol levels are high, there is conformational changes in SCAP which binds to insulin-induced genes (INSIGs) that retains the SREBP-SCAP complex in the ER membrane (Nohturfft and Zhang, 2009). SREBP1 processing can also be mediated by the levels of phosphatidyl choline (PC) content in the Golgi membranes. Low levels of PC in the Golgi membranes can mediate the translocation of the proteases MBTPS1 and MBTPS2 via COP I mediated vesicles from the Golgi to ER membrane to release the n-terminus of SREBP1 (Fig. 1.3b) (Walker et al., 2011).

There are several other mechanisms regulating the processing and stability of SREBPs. Activation of AKT induces accumulation of mature SREBP in the nucleus and is known to be a regulator of its activation and function via mTORC1 (Fleischmann and Iynedjian, 2000; Porstmann *et al.*, 2008). Phosphatidate phosphatase lipin 1 (LPIN1), an enzyme which converts phosphatidic acid to diacylglycerols (DAGs) is also known to be involved in activation of peroxisome proliferator-activated receptor-γ co-activator 1 α (PPARα) (Finck et al., 2006). LPIN1 binds the mature SREBPs in the nucleus to the nuclear lamina and thus prevents SREBPs binding to the SRE elements, which is necessary for its transcriptional activity. mTORC1 phosphorylates LPIN1 and retains it in the cytosol and prevents its binding to mature SREBPs in the nucleus and restores the transcriptional regulation of lipid biosynthesis in cells (Fig 1.3c) (Peterson et al., 2011). mTORC1 also regulates translocation of SREBP1 from ER to Golgi in hepatocytes by phosphorylating CREB regulated transcription co-activator 2 (CRTC2). SEC31A, a protein present in the COPII vesicles and is inhibited by CRTC2, phosphorylation of CRTC2 by mTORC1 restores the function of COPII mediated vesicles in the ER-Golgi translocation of SCAP-SREBP complex (Fig 1.3d) (Han et al., 2015). Another important regulator of SREBP activity is F-box and WD repeat domain

protein 7 (FBXW7). FBXW7 is a subunit of the E3-ubiquitin ligase complex and is involved in the degradation of proteins via ubiquitination. FBXW7 is phosphorylated by glycogen synthase 3 β (GSK3β) and only phosphorylated form of FBXW7 can bind to mature SREBPs and leads to its degradation (Bengoechea-Alonso and Ericsson, 2009; Sundqvist et al., 2005). GSK3β is negatively regulated by AKT and thus prevents the regulation of SREBPs by FBXW7 and maintains SREBP function (Fig 1.3c).

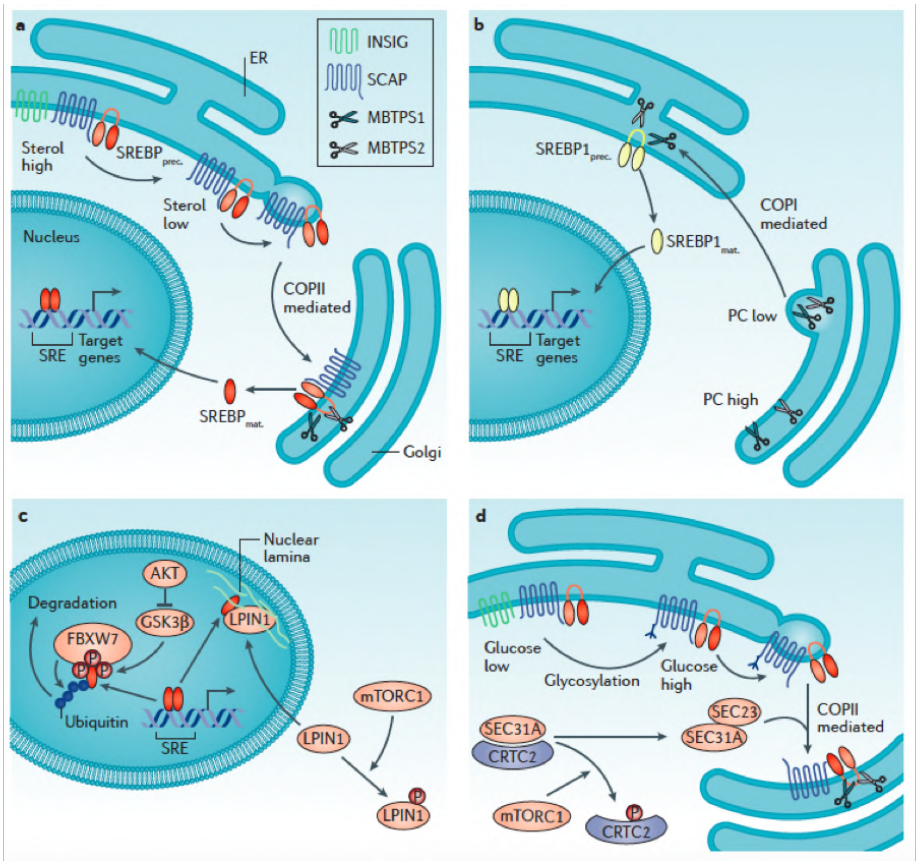

Figure 1.3: Upstream regulators of SREBPs

Shows multiple levels of regulation of SREBP activation.
a. shows the processing of full length SREBP by transmembrane processing when sterol levels are low by translocation of SREBP-SCAP complex from ER to Golgi complex via COP-II mediated vesicle transport and release of n-SREBP by the action of proteases MBTPS1 and MBTPS2 present on Golgi bodies.
b. shows the translocation of MBTPS1 and MBTPS2 via COP I mediated vesicles from Golgi bodies to ER membrane to cleave n-terminus of SREBP1 when the levels of phosphatidylcholine are low.
c. Regulation of stability of n-terminus of SREBP in the nucleus. LPIN1 binds to n-SREBP in the nucleus and retains it in the nuclear lamina and prevents its binding to the SRE elements, LPIN1 is phosphorylated by mTORC1 and contained in the cytoplasm and prevents its binding to SREBPs and hence regulates its activity in the nucleus. SREBPs stability in the nucleus is also controlled by F-box and WC repeat domain protein 7 (FBXW7), which upon phosphorylation by glycogen synthase kinase 3β (GSK3β) (negatively regulated by AKT) binds to the CDC4 phosphodegron motif on n-SREBPs and leads to its degradation.
d. mTORC1 regulates SREBPs ER-Golgi translocation through the phosphorylation of CREB-regulated transcription co-activator 2 (CRTC2), which negatively regulates the COP II-dependent

vesicle transport. Transmembrane processing of n-SREBPs occurs in high glucose condition by glycosylation of SCAP and releasing them from INSIGs.
This image is obtained from (Rohrig and Schulze, 2016).

SREBP processing is strictly controlled by the sterol levels in the cells and changes in the amount of sterol alters its processing and activation. There are several modes of regulation of sterol levels in the cells. Stimulation of ATP-binding cassette transporter (ABCA1) by p53 has been shown to increase the transport of cholesterol from the cell membrane to the ER, thus preventing the processing of SREBPs (Moon et al., 2019). Another important upstream regulator of SREBPs is sterol O-acyltransferase 1 (SOAT1, also known as ACAT1), an enzyme that regulates the conversion of cholesterol-to-cholesterol esters and their storage in lipid droplets. Cholesterol esterification reduces the free cholesterol pool and activates the processing of SREBPs, and thus maintains active fatty acid and cholesterol biosynthesis in proliferating cells (Yue et al., 2014). It has been shown that cholesterol esterification into lipid droplets is an important phenomenon for GB tumours and abrogating this process by inhibition of SOAT1 has direct implication on cancer cell proliferation and tumour growth *in vivo*. There are several drugs such as mitotane, avasimibe etc., that are being studied to target SOAT1 in different tumour types and, these drugs have shown effective inhibition in *in vivo* studies and in patients (Geng et al., 2016; Kroiss and Fassnacht, 2016; Sbiera et al., 2015). Inhibition of SOAT1 increases the free cholesterol levels in the cells and inactivates processing of SREBPs and shuts down the transcriptional regulation of genes involved in fatty acid and cholesterol biosynthesis (Geng *et al.*, 2016). Hence, SOAT1-SREBP axis is important for GB tumours and studies shedding light on the upstream signalling of SOAT1 holds utmost importance in improving GB treatment.

1.4.3 Fatty acid biosynthesis pathway

SREBPs transcriptionally regulates the genes involved in fatty acid and cholesterol biosynthesis in cells downstream of the PI3K-AKT-mTORC1 signalling. Aberrant activation of SREBPs and their target genes are seen in many types of cancer as proliferating cells have a huge demand for fatty acids and lipids for their newly synthesized membranes, they are also a great source for ATP synthesis and are crucial for synthesising signalling molecules essential for inter and intracellular

signalling. Upregulation of PI3/AKT axis regulates both protein biosynthesis and lipid biosynthesis in cells via mTORC1 and SREBPs and regulates uptake of macro molecules necessary to fuel these processes.

Glucose, glutamine and acetate are the three major sources of acetyl-CoA which is the main substrate for fatty acid biosynthesis in cells (Fig 1.4). Acetyl-CoA is converted to malonyl-CoA by the first enzyme in the fatty acid biosynthesis, acetyl-CoA carboxylase (Fig 1.4). ACC expression and its enzymatic activity is tightly controlled by upstream signalling regulators as this step is the crucial step in activating fatty acid biosynthesis in cells. High levels of Malonyl-CoA levels allosterically inhibit the rate limiting enzyme of β-oxidation, carnitine palmitoyltransferase-1 to promote fatty acid biosynthesis. ACC1 and 2 expression is transcriptionally regulated by SREBP1, and its inhibition is controlled by AMPK by phosphorylation at serine 80 and 221 (serine 79 and serine 212 in mice), respectively (Lally et al., 2019). Once malonyl-CoA is synthesized in the cells, it takes 6 subsequent condensation steps to synthesize 16 carbon chain saturated straight chain fatty acid, palmitic acid (C16:0). This reaction is catalysed by the multi-enzyme complex, fatty acid synthase (FASN), it contains an unique carboxyl terminal thioesterase domain that hydrolyses the fatty acid chain and is crucial for maintaining the carbon chain length (Fig 1.4) (Chakravarty et al., 2004). FASN is a direct target of SREBP1 and is strongly regulated when the cells are in nutrient and oxygen limiting condition and a target of MYC-SREBP1 regulation of fatty acid biosynthesis in cancer (Gouw et al., 2019). One molecule of palmitic acid requires 7 molecules of cofactor NADPH, hence a reaction that is energy rich and needs the cells to commit to fatty acid biosynthesis. It has been shown that FASN is upregulated in many types of cancer and known to be involved in metastasis formation after anti-angiogenic therapy (Chakravarty *et al.*, 2004; Sounni et al., 2014). FASN has been a therapeutical target in many drug and clinical trials due its unique and druggable thioesterase domain and its selective elevated expression in cancer cells (Chakravarty *et al.*, 2004).

1.4.4 Fatty acid modifying enzymes

Once palmitic acid is synthesized by cells, the fate of this fatty acid depends on desaturases and elongases to form one or more double bonds and increase in number

of carbon atoms, respectively. The essential fatty acids alpha-linolenic acid (omega-3 fatty acid) and linoleic acid (omega-6 fatty acid) and, palmitic acid synthesized by cells are all elongated by elongation of very long chain fatty acids (ELOVL) enzymes, also known as elongases (Fig 1.4). ELOVLs performs the regulatory step of condensation in elongation of fatty acids by using 2 carbons from malonyl-CoA and cofactor NADPH. ELOVLs are classified into 7 groups (ELOVL1-7), based on their substrate-specific elongation function (Jakobsson et al., 2006; Jump, 2009). ELOVL1, 3 and 6 are known to be involved in elongation of saturated and mono-unsaturated fatty acids. ELOVL-6 preferentially elongates palmitic acid (C16:0) and palmitoleic acid (C16:1). ELOVL-2, 4 and 5 preferentially elongate polyunsaturated fatty acids. ELOVL-5 specifically is involved in elongation of γ-linolenoyl-CoA (C18:3, n-6 CoA) and may elongate palmitoleic acid (C16:1). ELOVLs are involved with fatty acid desaturases (FADs) to produce fatty acids with different length and number of double bonds. ELOVL-2 and 5 function together with Δ5 and Δ6 desaturases to generate the end products of the alpha-linolenic acid (omega-3 fatty acid) and linoleic acid (omega-6 fatty acid), arachidonic acid (C20:4) and docosahexaenoic acid (C20:5) (Jump, 2009; Snaebjornsson et al., 2020).

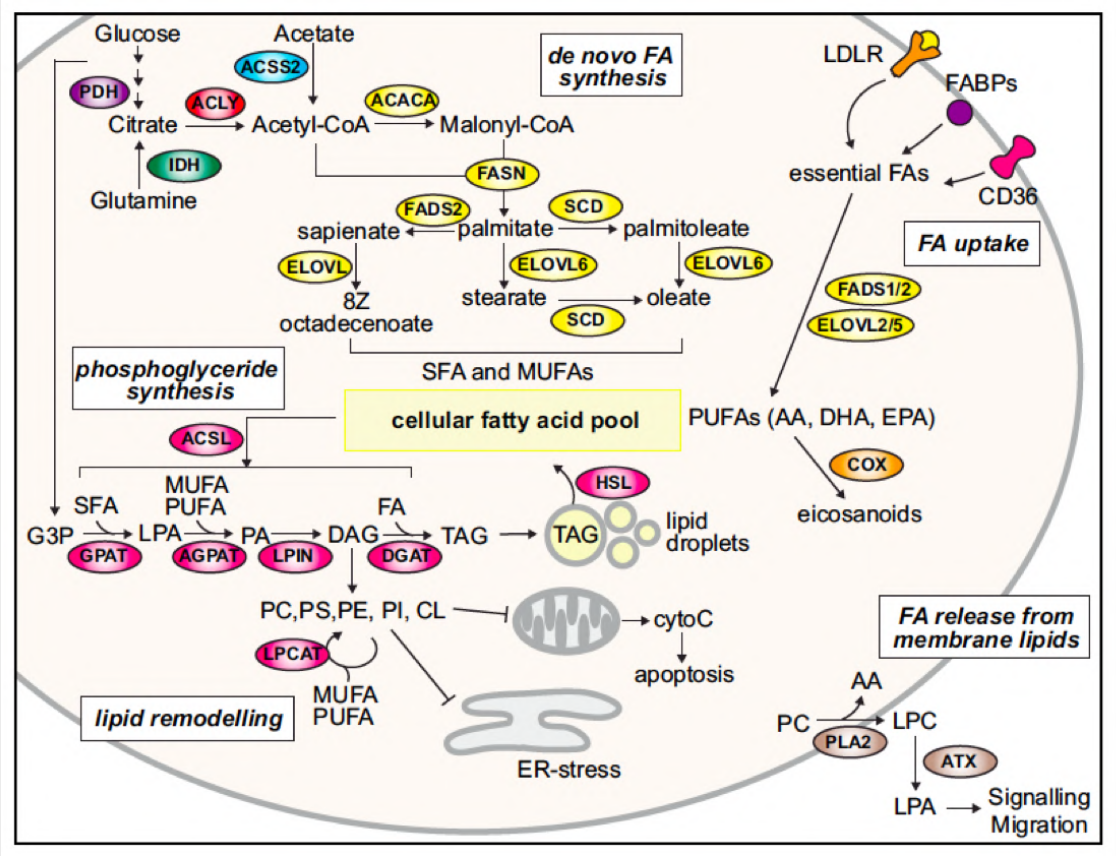

Figure 1.4: Schematic representation of procurement and synthesis of fatty acids and lipids in cancer cells

Main substrates used in biosynthesis of fatty acids are glucose, glutamine and/or acetate. Palmitate is the product of *de novo* fatty acid biosynthesis from these substrates, which is further elongated by elongases or desaturated by desaturases. Fatty acids are utilized as substrates to synthesize phosphoglycerides in the Land's cycle. Essential fatty acids are taken up by cells by different receptors/transporters into the cells and are modified with elongases and desaturases before incorporating into membrane lipids. Lipases are used to cleave of fatty acids from membrane lipids which are used as precursors for synthezing lipid mediators/signalling molecules. The amount of mono-unsaturated fatty acids present in the membranes is important for maintaining organelle structure and function. This image is obtained from (Snaebjornsson *et al.*, 2020).

Stearoyl-CoA desaturase is a ∆9-desaturase that catalyses the formation of double bond in palmitoyl-CoA and stearoyl-CoA to produce palmitoleoyl-CoA and Oleoyl-CoA respectively (Fig 1.4). Many studies have shown that inhibition of SCD in serum limited conditions in cancer cells leads to accumulation of saturated fatty acids and decreased levels of monounsaturated fatty acids and results in ER stress and apoptosis (Ariyama et al., 2010; Griffiths et al., 2013; Williams et al., 2013). Additionally, apoptosis induced due to SCD inhibition was rescued by addition of oleic acid (C18:1) or poly unsaturated fatty acids like linolenic acid (C18:2) or arachidonic acid (C20:4) (Ariyama *et al.*, 2010; Griffiths *et al.*, 2013; Williams *et al.*, 2013). Also, SCD inhibition in xenografts models of gastric and colon cancer lead to reduction in tumour formation and SCD knockdown in human prostate cancer cells reduced their ability to form orthotopic tumours (Mason et al., 2012; Peck et al., 2016; Roongta et al., 2011). These studies show the importance of SCD in tumour cells and the dependence of cancer cells on monounsaturated and polyunsaturated fatty acids. Especially, when cells are under nutrient deprivation, essential fatty acids are very limited, and this creates a unique dependence on *de novo* synthesized monounsaturated fatty acids to maintain fluidity in the membranes and avoid lipotoxicity and rigidity due to high levels of saturated fatty acids. SCD is expressed at high levels only in tumour cells compared to healthy cells, which gives an unique opportunity to target them with minimum side effects and efficiently eliminate cancer cells.

1.4.5 Phospholipases

Phospholipases are involved in mediating inter and intracellular signalling events. The phospholipases functions as phospholipid hydrolysing enzymes and act

on membrane lipids to produce free fatty acids and are involved in producing signalling lipid mediators. Phospholipases can be mainly categorized into 3 groups: phospholipases class A, C and D (PLA, PLC and PLD). They are grouped based on the enzymatic reaction they catalyse and their targets. PLA consists of PLA1 and PLA2, they act on glycerol groups of phospholipids at position sn-1 and sn-2 to generate one free fatty acid and n-acyl lysophospholipid. PLC acts on hydrolysing phosphatidylinositol and cleaves the bond between the glycerol and phosphate groups and generates phosphorylated base and DAGs. PLD acts on hydrolysing phosphatidylcholine and severs the phosphodiester bond and generates a free base (choline) and phosphatidic acid (PA) (Park et al., 2012).

The phospholipases are further divided into subgroups and isotopes based on the function, domains and regulatory mechanisms. The 3 major subtypes of PLA2 groups consists of secretary PLA2 (sPLA2), cytosolic PLA2 (cPLA2) and calcium independent PLA2 (iPLA2). These groups of PLA2s are categorized into eleven sPLA2s, six cPLA2s and nine iPLA2s. All sPLA2 consists of a signal sequence, calcium binding loop and a catalytic site (Park *et al.*, 2012). The 11 sPLA2s – IB, IIA, IIC, IID, IIE, IIF, III, V, X, XIIA and XIIB are further subdivided on structural basis into three branches: groups I/II/V/X, group III, and group XII (Murakami et al., 2005). The sPLA2s show unique tissue and cellular localization, tissue specific activities emphasising their roles in pathological events in the cells and are also linked to cancer. The human sPLA2 group III (sPLA2G3) is structurally unique compared to the other groups, the full length 55 kDa protein consists of a central sPLA2 domain (S), n-terminal domain (N) and a c-terminal domain (C). The human sPLA2 is most similar to the bee venom group III sPLA2 compared to the other groups, but bee venom sPLA2G3 does not contain N and C domains. Further investigation on the human sPLA2G3 showed that after cellular processing of the full-length protein, the S domain is the active domain that is mostly expressed in cells (Murakami *et al.*, 2005). sPLA2G3 mostly acts on fatty acyl chains on the sn-2 position and is known to release arachidonic acid from the membrane lipids in overexpressed cells and release prostaglandin E2 (PGE2) (Fig 1.4) (Murakami et al., 1999; Murakami et al., 2003). It is shown that PLA2G3 is a direct target of SREBP1 and is shown to be regulated transcriptionally by ChIP sequencing data and this regulation is conserved in humans, mouse, pigs and dogs (Gijs et al., 2015). PLA2G3 is shown to be overexpressed in several different types of cancer,

specifically in colorectal cancer overexpression of PLA2G3 is associated with cancer cell proliferation, aggressive metastasis and tumour angiogenesis (Murase et al., 2017). Since, PLA2G3 is a secreted phospholipase its inter- and intra-cellular functions are significant in pathological illness and cancer, as it contributes to cell communication in the tumour microenvironment and releasing of signalling molecules. Hence, PLA2G3 has become an important target of study in developing novel therapeutic strategies and understanding its role in several diseases.

Overall, fatty acid and lipid metabolism in addition to providing materials for synthesizing cell membranes are also involved in regulation of myriad of cellular functions and aid in energy metabolism, release of signalling molecules and facilitate inter- and intra-cellular communication. Hence, understanding the underlying mechanisms of fatty acid and lipid metabolism in GB could pave way for identifying the important nodes of regulation of tumour development, progression and reoccurrence. These in-depth understanding could be attributed in designing successful combinatorial approaches to improve better treatment outcomes for this dreadful disease.

1.5 Aims of the thesis

Fatty acids are essential biomolecules involved in membrane biogenesis, cellular bioenergetics and synthesis of signalling mediators. *De novo* fatty acid biosynthesis is one of the important axes in governing cancer cell proliferation under nutrient limiting conditions. Hence, this thesis mainly aims at investigating and understanding the role of the transcriptional factor SREBP1 in different aspects of GB. Specific aims of thesis are:

1. To profile transcriptional network of SREBP1 by RNA sequencing and to identify genes that are specifically regulated under low serum condition in GB. Further, evaluate the changes in fatty acid and lipid components controlled by SREBP1 by metabolomics approach.

2. To understand if SREBP1 played a role in crosstalk with endothelial cells and was involved in inducing angiogenesis in GB.

3. To explore if SREBP1 plays a role in growth and maintenance of cancer stem like cells, contributing to the tumour heterogeneity in GB.

4. To identify and unravel therapeutically targetable upstream regulator of SREBP1 in GB.

Chapter 2: Materials

2.1 Cell lines and bacteria strains

2.1.1 Human cell lines

Cell lines were routinely tested for mycoplasma contamination

Table-2.1.1: Cell lines

Name	Cell type	Origin
U87	human glioblastoma cell line, EGFR WT	CRUK-LRI Cell services
U251	human glioblastoma cell line, wildtype (p53+/+)	ATCC
HEK293T	Human embryonic kidney cell line	Prof. Eilers
NCH644	Human patient derived glioblastoma stem-like cells	Prof. Christel Herold-Mende, Heidelberg
HUVECs	Human umbilical vein endothelial cells	Promocell- C-12205

2.1.2 Bacteria strains

Escherichia coli DH5α and XL1 blue were used for plasmid amplification

2.2 Culture media and supplements

2.2.1 Eukaryotic cell culture media

All media and solutions were stored at 4°C and stocks at -20°C .

Table-2.2.1: Cell culture medium components

Name	Company	Catalog number	Use
DMEM	Sigma	D6429	Media for adherent cell cultivation
FBS	Sigma	F7524-500ML	Media supplements
Glutamine	Sigma	59202C	

Penicillin/Streptomycin	Sigma	4333	
DMEM/F-12	Life technologies	21331046	NCH644 cell cultivation
bFGF	Biomol	50361.50	
EGF	Invitrogen	PHG0311	
BIT Admixture	Pelo Biotech	PB-SH-033-0000	
Accutase	Sigma	A6964-100ML	
poly-HEMA	Sigma	P3932-10G	
Oleic Acid-Albumin from bovine serum	Sigma	O3008-5ML	Rescue experiments
Bovine serum albumin solution in 10% DPBS (fatty acid free)	Sigma	A1595-50ML	
M200	Thermo Fisher Scientific	M200500	Endothelial cell cultivation and angiogenesis assays
Methyl cellulose	Sigma	M0512-100G	
Growth Factor Reduced Matrigel	BD Biosciences / Labor Schubert & Weiss	356231	
Low Serum Growth Supplement (LSGS)	Life Technologies GmbH	S00310	
recombinant human VEGF	Life Technologies GmbH	PHC9394	Controls for sprouting assay
Prostaglandin E2	Bertin Pharma	14010	
Oleoyl-L-α-lysophosphatidic acid sodium salt	Sigma	L7260-1MG	
Arachidonic acid	Sigma	23401-50MG	PGE2 Rescue

2.2.2 Bacterial culture media

Table-2.2.2: Bacterial culture medium components

Name	Components and preparation
LB medium	10% (w/v) Bacto tryptone (Roth)
	0.5% (w/v) yeast extract (Roth)
	0.5% (w/v) yeast extract (Roth)
	1% (w/v) NaCl (Roth)
	autoclaved immediately after preparation
LB agar	LB-medium with 1.2% (w/v) agar-agar (Roth)
	autoclaved, heated in a microwave oven, cooled down to 50°C;
	antibiotics were added the medium poured into 10 cm dishes

All powder formulations were obtained from Roth. Stock solutions were prepared in ddH2O and sterile filtered before use.

Table-2.2.3: Antibiotics used for bacterial culture

Name	Final concentration
Ampicillin	100 µg/mL
Kanamycin	30 µg/mL
Chloramphenicol	25 µg/mL

2.3 Chemical & Reagents

All inhibitors were dissolved in manufacturer recommended solvent and stored at appropriate temperature recommended for the compounds.

Table-2.3.1: Chemical & Reagents

Name	Source	Catalog number	Use
NVPBKM120	Bertin Pharma	11587	PI3K inhibition (both alpha and beta)
MK2206	Bertin Pharma	11593	Akt inhibition (both 1 & 2)

Rapamycin	Bertin Pharma	13346	mTORC1 inhibition
SCD inhibitor II	Cayman Chemical / Biomol	CAY10566	SCD inhibition
Thioether amide-PC	Cayman Chemical / Biomol	62750-1	Secreted PLA2 inhibition
HA-130	Cayman Chemical / Biomol	Cay10498-5	Autotaxin inhibition
KI 16425	SML0971-5MG	Ki 16425- LPAR inhibitor	LPA receptor inhibition
Mitotane	Kindly provided by Dr. Matthias Kroiss		SOAT1 inhibition
ATR101			
Avasimibe	Sigma	PZ0190-5MG	
Doxycycline hydrochloride	Sigma	D9891-1G	Induction of shRNA sequences
Puromycin	InvivoGen / Cayla	ant-pr5	Selection marker
Hoechst	Sigma	B2261-25MG	Nuclear stain

2.4 Solutions, buffers and solvents

All solutions and buffers were prepared using ddH2O, unless otherwise indicated. All solutions were stored at RT, unless otherwise specified. All chemicals were purchased from Sigma and Roth.

Table-2.4.1: Stock solutions and buffers

Ampicillin stock solution	10 g ampicillin solubilized in 100 ml ddH2O and sterile filtered; aliquots stored at -20°C
Blocking solution for PVDF membrane	5% (w/v) BSA in TBS-T
Crystal violet solution	0.1% (w/v) crystal violet 20% (v/v) ethanol
Deoxynucleotide triphosphate (dNTP) (10 mM)	50 µl each dNTP (100 mM) mixed with 300 µL ddH2O to 500 µL final volume

DNA loading buffer (6x)	10 mM EDTA, pH 8.0; 0.2% (w/v) Orange G; 40% (w/v) sucrose; stored at -20°C
Miniprep lysis buffer	0.2 M NaOH; 0.2 M NaOH
Miniprep neutralization buffer	3 M NaOAc pH 4.8
Miniprep resuspension buffer	1:1000 RNAse in TE buffer; stored at 4°C
PBS 1x	137 mM NaCl; 2.7 mM KCl; 10.1 mM Na2HPO4; 1.76 mM KH2PO4; autoclaved
Phenol-chloroform	25 ml phenol; 24 ml chloroform; 1 ml isoamyl alcohol; prepare at least one day before using
Polybrene stock solution (4mg/ml)	200 mg dissolved in 50 ml H2O sterile filtered with 0.2 µM syringe filter
Polyethylenimin (PEI)	450 µl PEI (10%, MW 25,000 g/mol, Sigma), 150 µl HCl (2 N), 49.5 ml ddH2O
RIPA lysis buffer	50 mM HEPES, pH 7.9; 140 mM NaCl; 1 mM EDTA; 1% Triton X-100; 0.1% Na-deoxycholate; 0.1% SDS; stored at 4°C
SDS running buffer (1X)	25 mM Tris base, 250 mM glycine, 0.1% (v/v) SDS
SDS separating gel	7.5 - 12.5% (v/v) acrylamide/bisacrylamide, 375 mM Tris HCl pH 8.8, 0.1% (w/v) SDS, 0.1% (w/v) APS, 0.1% (v/v) TEMED
SDS stacking gel 4% (v/v) acrylamide/bisacrylamide	125 mM Tris HCl pH 6.8, 0.1% (w/v) SDS, 0.1% (w/v) APS, 0.1% (v/v) TEMED
Transfer buffer 10x	250 mM Tris base, 1.5 M glycine
Transfer buffer 1x	prepared by diluting Transfer buffer 10x with 15% (v/v) methanol
TBS (20 x)	500 mM Tris base, 2.8 M NaCl; adjusted to pH 7.4 with concentrated HCl
TBS-T	1 x TBS, 0.2% Tween-20
TE	10 mM Tris, pH 7.4; 1 mM EDTA, pH 8.0

Table-2.4.2: Solutions and buffers used in ChIP

Blocking solution for ChIP	5 mg/ml BSA in PBS; ; Stock solution at 5g/mL stored at -20
Lysis Buffer 1	5mM PIPES pH 8, 85 mM KCl, 0,5% NP40, 10 mM Glycine+ 1:1000 protease and phosphatase Inhibitors
Lysis Buffer 2	RIPA Buffer: 10 mM Tris/HCl pH 7.5, 150mM NaCl, 1mM EDTA, 1% NP-40, 1% Deoxycholic acid sodium salt, 0,1% SDS + 1:1000 protease and phosphatase Inhibitors
Wash Buffer I	20 mM Tris HCl pH 8.1; 150 mM NaCl; 2mM EDTA; 0.1% SDS; 1%Triton-X-100
Wash Buffer II	20 mM Tris HCl pH 8.1; 500 mM NaCl; 2mM EDTA; 0.1% SDS; 1%Triton-X-100
Wash Buffer III	10 mM Tris HCl pH 8.1; 250 mM LiCl; 1 mM EDTA; 1% NP-40; 1% Deoxycholic acid sodium salt
Proteinase K	10 mg/ml in ddH2O; stored at -20 °C

Table-2.4.3: Solvents used for Mass spectrometry samples preparation

Name	**Company**	**Catalog number**
Methanol LC-MS Opti Grade	Wicom	WIC 60301
Formic acid (for LC-MS)	Sigma	5330020050
Acetonitrile Hyper Grade for LC-MS	Analytics Shop	MC1000292500
n-Heptane	Millipore	1036541000
1-Butanol	Millipore	1019881000
Ethanol	Sigma	32205-2.5L-D
Dimethyl sulfoxide (DMSO for cell culture)	Sigma	41640-100ML
n-Hexane	Sigma	104367

2.5 Markers, enzymes and kits

Table-2.5.1: Markers

Name	Company
DNA marker Gene Ruler 1 kb Plus DNA ladder	Thermo Scientific
Protein marker Page Ruler Pre-Stained Protein Ladder	Thermo Scientific
Protein marker HiMark Pre-stained High molecular weight standard	Life Technologies

Table-2.5.2: Enzymes

Name	Company	Catalog number
M-MLV Reverse Transcriptase	Promega	M1705
Q5® High-Fidelity DNA Polymerase	NEB Freezer	M0491 L
RQ1 RNase-Free DNase	Promega Kabinett	M6101
Absolute QPCR SYBR Green Mix	Thermo Fisher Scientific	AB-1158/B
T4 DNA Ligase	NEB Freezer	M0202 S

Table-2.5.3: Kits

Name	Company	Catalog number
PGE2 CLIA kit- 96 wells	Enzo	ADI-910-001
Lysophosphatidic Acid (LPA) ELISA Kit	Antibodies-online	ABIN2039318
Proteome Profiler Human Angiogenesis Array Kit	R&D Systems	ARY007
Qiaquick Gel Extraction Kit (250)	Qiagen Kabinett	28706
QIAprep Spin Miniprep Kit (50)	Qiagen Kabinett	27104
Purelink Plasmid Maxi 25 Kit	Life Technologies GmbH	K210007

2.6 Nucleic acids

2.6.1 RT-qPCR Primers

Most of the oligos were synthetized by and obtained from Sigma. All oligos were synthetized at 0.025 µmole scale and purified by desalting (DST) unless otherwise indicated. Each primer was resuspended in Ampuwa H2O to 100 µM and used at 10

µM final concentration, unless otherwise specified. Stock and diluted primers were stored at -20°C.

Table-2.6.1: RT-qPCR primers

Name	Forward Sequences	Reverse Sequences
B2M	GTGCTCGCGCTACTCTCTC	GTCAACTTCAATGTCGGAT
ß-Actin	GCCTCGCCTTTGCCGAT	CGCGGCGATATCATCATCC
SREBP1	CGCTCCTCCATCAATGACA	TGCGCAAGACAGCAGATTTA
SCD	CCTAGAAGCTGAGAAACTGGTGA	ACATCATCAGCAAGCCAGGT
FASN	CAGGCACACACGATGGAC	CGGAGTGAATCTGGGTTGAT
PLA2G3	ACAGGGTGGCCTAAAACCTC	CAATCTGGTGCTCACACTGG
DDIT3	GGTATGAGGACCTGCAAGAGGT	CTTGTGACCTCTGCTGGTTCTG
FASN	CAGGCACACACGATGGAC	CGGAGTGAATCTGGGTTGAT
FABP7	CTGTTGTTAGCCTGGATGGAGAC	CTCATAGTGGCGAACAGCAACC
SREBP2	GAAAGGCGGACAACCCATAAT	AGAACGCCAGACTTGTGCATC
HMGCR	GTTCGGTGGCCTCTAGTGAG	GCATTCGAAAAAGTCTTGACAAC
HMGCS	AAGTCACACAAGATGCTACACCG	TCAGCGAAGACATCTGGTGCCA

2.6.2 ChIP Primers

Table-2.6.2: ChIP primers

Name	Forward Sequences	Reverse Sequences	Source
ACLY	CCTCTCTCCTCCCTGGACTC	CACACTGGGAAGTATGCTCTG	Gouw et al Myc ChIP Seq
ACACA	CCTTCTCCCGGTAACTGATTC	CCACATTCTGACACCAACTTC	

FASN (distal)	GAGGCTGCGAGTTTTCCAG	CCACGATTCGAGGAATCACT	
SCD	AGTTGGCCTGACCCTGAGAC	AGACAAGCACCTGGGATTTC	
RAB5B	CCGCCTCCATCACTCACCTG	GTCACCAACAAGTACGAGCAAGG	Reed et al SREBP1 ChIP Seq
FASN (proximal)	GCGCAGCCCCGACGCTCATT	CGGCGTATTTAAACCGCGG	

2.6.3 Cloning Primers

Table-2.6.3: Cloning primers

Name	**Forward Sequences**	**Reverse Sequences**
mirE-XhoI	TACAATACTCGAGAAGGTAT	ATTGCTGTTGACAGTGAGCG
mirE-EcoRI	TTAGATGAATTCTAGCCCCTT	GAAGTCCGAGGCAGTAGGCA
Sequencing primer	TGTTTGAATGAGGCTTCAGTAC	

2.6.4 shRNA sequences

Table-2.6.4: shRNA sequences

Target	**Name**	**Sequences**
SREBF1	LT3-BP1_01	TGCTGTTGACAGTGAGCGCTGCGGAGAAGCTGCCTATCAATAGTGAAGCCACAGATGTATTGATAGGCAGCTTCTCCGCATTGCCTACTGCCTCGGA
	LT3-BP1_03	TGCTGTTGACAGTGAGCGACCCAGTCTTTGAGGACAGCAATAGTGAAGCCACAGATGTATTGCTGTCCTCAAAGACTGGGCTGCCTACTGCCTCGGA
	LT3-BP1_04	TGCTGTTGACAGTGAGCGACACAAGGTACACAACTTTTAATAGTGAAGCCACAGATGTATTAAAAGTTGTGTACCTTGTGGTGCCTACTGCCTCGGA

	LT3-BP1_05	TGCTGTTGACAGTGAGCGCAAGGAAAATAAACA TCTTTTATAGTGAAGCCACAGATGTATAAAAGAT GTTTATTTTCCTTATGCCTACTGCCTCGGA
	LT3-BP1_06	TGCTGTTGACAGTGAGCGACAGCAGCTACTGAC AGTCACATAGTGAAGCCACAGATGTATGTGACT GTCAGTAGCTGCTGGTGCCTACTGCCTCGGA
	LKO-BP1_07 forward	CCGGCCAGAAACTCAAGCAGGAGAACTCGAGTT CTCCTGCTTGAGTTTCTGGTTTTT
	LKO-BP1_07 reverse	AATTAAAAACCAGAAACTCAAGCAGGAGAACTC GAGTTCTCCTGCTTGAGTTTCTGG
Scramble	LKO-Scr forward	CCGGCCTAAGGTTAAGTCGCCCTCGCTCGAGCG AGGGCGACTTAACCTTAGG
	LKO-Scr reverse	AATTCCTAAGGTTAAGTCGCCCTCGCTCGAGCG AGGGCGACTTAACCTTAGG
PLA2G3	LT3-PLA2G3_01	TGCTGTTGACAGTGAGCGCCAGGGTTGTGATGC AGATTAATAGTGAAGCCACAGATGTATTAATCTG CATCACAACCCTGTTGCCTACTGCCTCGGA
	LT3-PLA2G3_05	TGCTGTTGACAGTGAGCGAAGAGGTTGATGTAA CCTTTTATAGTGAAGCCACAGATGTATAAAAGGT TACATCAACCTCTCTGCCTACTGCCTCGGA
SOAT1	LT3-SOAT1_02	TGCTGTTGACAGTGAGCGACCGCAGTAATGTTC TGCACAATAGTGAAGCCACAGATGTATTGTGCA GAACATTACTGCGGG TGCCTACTGCCTCGGA
	LT3-SOAT1_03	TGCTGTTGACAGTGAGCGACCGGTTCA TCATTATATTCGATAGTGAAGCCACAG ATGTATCGAATATAATGATGAACCGGG TGCCTACTGCCTCGGA

2.6.5 Plasmids

All sequences cloned into the vectors refer to human sequences. All constructs were verified by Sanger sequencing, which was carried out by LCG Genomics.

Table-2.6.5: shRNA sequences

Name	Company	Catalog number	Provided by
psPAX.2	Addgene	12260	D. Trono
pMD2.G	Addgene	12259	D. Trono
Tet-pLKO-puro	Addgene	21915	D.Wiederschain
pLT3GEPIR			Prof. Zender

2.7 Antibodies

Table-2.7.1: primary antibodies

Name	Company	Catalog number	Size	Dilution
Rabbit anti-AKT	Cell Signaling	9272	60kDa	WB (1:1000)
Rabbit anti-Phospho-Akt (Ser473)	Cell Signaling	9271	60kDa	WB (1:1000)
Rabbit anti-p44/42 MAP Kinase (ERK)	Cell Signaling	9102	42-44kDa	WB (1:1000)
Mouse anti-Phospho-p44/42 MAP Kinase (Thr202/Tyr204) (E10) (pERK)	Cell Signaling	9106	42-44kDa	WB (1:1000)
Rabbit anti-S6 Ribosomal protein (5G10)	Cell Signaling	2217	32kDa	WB (1:1000)
Rabbit anti-phospho-S6 Ribosomal protein (Ser240/244) (pS6)	Cell Signaling	2215	32kDa	WB (1:1000)
SCD-1 (prestige antibody)	Sigma	HPA012107	32kDa	WB (1:1000)
Mouse anti-SREBP-1 (2A4)	BD PharMingen	557036	120, 70kDa	WB (1:500)

Mouse anti-SREBP-1 (2A4)	Home made		120, 70kDa	ChIP (1:30)
Rabbit anti-PLA2G3	Cell Signaling	3198	57kDa	WB (1:1000)
Mouse anti-SOAT-1	Abcam	ab39327	50-55kDa	WB (1:1000)
Mouse anti-beta-Actin (AC-15)	Sigma	A5441	42kDa	WB (1:10000)
Mouse anti-Vinculin (hVIN-1)	Santa Cruz	sc-25336	120kDa	WB (1:10000)
c-Myc (y-69)	abcam	ab32072	55kDa	ChIP and WB (1:1000)

Table-2.7.2: secondary antibodies

Name	**Company**	**Catalog number**	**Dilution**
IRDye® 800CW Donkey anti-Rabbit IgG (H + L)	LI-COR Biosciences GmbH	926-32213	WB (1:5000)
IRDye® 800CW Donkey anti-Mouse IgG (H + L)	LI-COR Biosciences GmbH	926-32212	WB (1:5000)

2.8 Consumables

Consumables such as cell culture dishes, reaction tubes, cryotubes, syringes, cuvettes and pipettes were purchased from the companies Eppendorf, Greiner, Nunc, Sarstedt and VWR.

Table-2.8.1: Equipment and membranes

Equipment	**Company**

Automated Electrophoresis	Experion Automated Electrophoresis System (Bio-Rad)
Chemiluminescence imaging	LAS-4000 mini (Fujifim)
Centrifuges	Avanti J-26 XP (Backman Coulter)
	Eppendorf 5417 R (Eppendorf)
	Eppendorf 5425 (Eppendorf)
	Eppendorf 5430 (Eppendorf)
	Galaxy MiniStar (VWR)
	Multifuge 1S-R (Heraeus)
Heating block	Dry Bath System (Starlab)
	Thermomixer® comfort (Eppendorf)
Immunoblot transfer chamber	PerfectBlue Tank Electro Blotter Web S (Peqlab)
Microscopes	Axiovert 40CFL (Zeiss)
	TCS SP5 (Leica)
PCR thermal cycler	C1000 Thermal cycler (Bio-Rad)
Photometer	Multiscan Ascent (Thermo Labsystems)
	UltrospecTM 3100 pro UV/Visible (Amersham Biosciences)
	Spectrofluorometer NanoDrop 1000 (Thermo Scientific)
Power supply Power	Pac (Bio-Rad)
	Consort EV231/EV243 (Roth)
Protein Sample Loading Buffer and PVDF Membrane	Li-COR Biosciences GmbH - 926-31097
Quantitative RT-PCR machine	StepOne plus (Applied Biosystem)
SDS-PAGE system	Minigel (Bio-Rad)

	Mini-PROTEAN Tetra Cell (Bio-Rad)
Sterile bench	HeraSafe (Heraeus)
Ultrasonifier	Digital Sonifier W-250 D (Branson)
Vortex mixer	Vortex-Genie 2 (Scientific Industries)
Water bath	Julabo ED-5M water bath (Julabo)
	Memmert waterbath (Memmert)
Whatman filter paper	Gel Blotting Paper (Schleicher and Schuell)
Ultrapure water, Millipore water purification system	Milli-Q Merck Millipore, Darmstadt, Germany
Dionex Ultimate 3000 UHPLC system hyphenated with a Q Exactive mass spectrometer (QE-MS) equipped with a HESI probe	Thermo Scientific, Bremen, Germany
UPLC-precolumn, Acclaim 120 C8 (5 µm particles, 10 × 2 mm)	Thermo Scientific, Bremen, Germany)
UPLC-column, Acclaim RSLC 120 C8 (2.2 µm particles, 50 × 2.1 mm)	Thermo Scientific, Bremen, Germany)

2.9 Software and online programs

Table-2.9.1: Software and online programs

Software	**Source**
ApE plasmid	editor by M. Wayne Davis
BD FACSDiva v6.1.2	BD Biosciences
EndNote 20.1	Clarivate Analytics
Illustrator, Photoshop	Acrobat Adobe Inc.
Image J	by Wayne Rasband

Mac OS X	Apple Inc.
Image Studio lite	Licor inc.
Stepone software v2.3	Applied Biosystem
Trace Finder	Thermo Scientific
Microsoft office package	Microsoft inc.
Prism4	GraphPad Software Inc.
HarmonyR High Content Imaging and Analysis Software	PerkinElmer
UCSC Genome Bioinformatics	http://genome.ucsc.edu

Chapter 3: Methods

3.1 Cell biology methods

3.1.1 Thawing of eukaryotic cell lines

Cells frozen in cryotubes were placed in a water bath at 37°C for few minutes and immediately transferred to 10mL appropriate medium used for culturing the cells. The cell suspension was centrifuged at 1200 rpm for 5 minutes. After centrifugation the supernatant was removed, and the cell pellet was re-suspended in 1 mL fresh culture medium and plated on appropriate cell culture dish with fresh medium.

3.1.2 Cultivation of eukaryotic cell lines

Monolayer cell cultivation:

U87 (CRUK-LRI), U251 (ATCC), NCH644 (C. Herold-Mende, Heidelberg) and HEK293-T (obtained from Prof. M. Eilers) cells were cultured as adherent cells in DMEM (D6546, Sigma) media supplemented with 10% foetal bovine serum, 2mM L-glutamine (Sigma) and 100units/ml penicillin/100µg/ml streptomycin (Sigma). Cells were cultivated in a cell incubator at 37°C, 5% CO2 and a relative humidity of 95%.

Human umbilical vein endothelial cells (HUVECs) (Promocell) were cultured in M200 (Thermo Fisher Scientific) media supplemented with 1% low serum growth supplement (LSGS) (Thermo Fisher Scientific) and 100units/ml penicillin/100µg/ml streptomycin (Sigma). Cells were cultivated in a cell incubator at 37°C, 5% CO2 and a relative humidity of 95%. The day after thawing, fresh medium was added to these cells for promoting cell growth *in vitro*.

Neurosphere cell cultivation:

NCH644 (C. Herold-Mende) were cultured as neurospheres in GSC media 1: DMEM F12 (Life technologies) media supplemented with 2mM L-glutamine (Sigma),

100units/ ml penicillin/100 µg/ml streptomycin (Sigma), 20ng/mL bFGF (Biomol), 20 ng/mL EGF (Invitrogen) and 2% BIT Admixture (Pelo-Biotech). Cells were cultivated in low attachment surface flasks (Sarstedt) and incubated at 37°C, 5% CO2 and a relative humidity of 95%.

U87 cells were grown in low adhesion 6-well plates coated with poly-HEMA (Poly 2-hydroxyethyl methacrylate; Sigma). 20,000 to 50,000 cells were plated per well with 2mL GSC media 2: DMEM F12 (Life technologies) supplemented with 2mM glutamine (Sigma), 100units/ml penicillin/100µg/ml streptomycin (Sigma), 20ng/mL bFGF (Peprotech 100-18B), 20ng/mL EGF (Peprotech AF-100-15), 10ng/mL LIF (Peprotech 0300-05) and 2% B27 (Thermo Fisher Scientific 12587010). Cells were cultivated in a cell incubator at 37°C, 5% CO2 and a relative humidity of 95%.

3.1.3 Cell passaging

Cells grown in monolayer were passaged every 3-5days approximately at 80-90% confluency. The medium was aspirated, and the cells were washed with PBS before addition of appropriate volume of trypsin to the cells based on the size of the dish and placed at 37°C, 5% CO2 and a relative humidity of 95% for cell detachment process. After detachment, the cells were collected in medium containing serum at 4:1 ratio to the volume of trypsin for its inactivation and centrifuged at 1200 rpm for 5 minutes. Supernatant was aspirated and the cell pellet was dissolved in cell culture medium and depending on the requirement, only fraction of the cells was cultivated on a dish with fresh medium. Some cells like HUVECs were split as low as 1:1 as they only grew *in vitro* with more than 50% confluency.

Cells grown as neurospheres were passaged every 5days approximately when they reached size of 500nm. The cells were collected in a 15 mL falcon tube and the neurospheres were allowed to settle down for 5 minutes at the bottom of the tube. Medium was removed by gently pipetting it out, without disturbing the neurospheres. After that, 1 mL accutase (Sigma) was added to the neurospheres by slowly pipetting up and down and then transferred to an Eppendorf tube and put in a block heater at 37°C, 1000 rpm for 5 minutes for mechanical dissociation of the neurospheres. After dissociation, cells were centrifuged at 900rpm for 3 minutes and the accutase was

removed by pipetting. Cell pellet was dissolved in 1 mL medium, and a fraction was plated on the same flask (flasks were re-used up to 2 times) or new flask.

3.1.4 Cell freezing

For monolayer culture the cells were harvested by trypsinization, as described above. After centrifugation, cell pellet from an 80% confluent 10 cm dish was resuspended in 2 mL freezing medium (8% DMSO + 20% FBS + 72% culture medium). One mL of cell suspension was transferred to cryotubes and immediately transferred into a freezing container filled with isopropanol and placed overnight at -80°C. Then the cryotubes were stored in liquid nitrogen tanks for long term storage.

For neurosphere culture the cells were collected in a 15 mL falcon tube and the neurospheres were allowed to settle down for 5 minutes at the bottom of the tube. Medium was removed by gently pipetting it out, without disturbing the neurospheres. The cells were resuspended in 2 mL freezing medium (8% DMSO + 92% culture medium). One mL of cell suspension was transferred to cryotubes and immediately transferred into a freezing container filled with isopropanol and placed overnight at -80°C. Then the cryotubes were stored in liquid nitrogen tanks for long term storage.

3.1.5 Sprouting assay

HUVECs after trypsinization and counting were resuspended in M200 medium with 1% LSGS supplement and 0.25% methylcellulose (Sigma). The resuspension was made such that 25 µL consisted of 1000 cells and would be one hanging drop. The hanging drops were made by pipetting the solution on to a non-adherent 10 cm petri dish. The plates were flipped carefully and incubated for 24 hours at 37 °C 5% CO2 and a relative humidity of 95%. To prevent the hanging drops to dry out, 10 mL PBS were added to the bottom of the dish. The spheroids were collected from the hanging drops with PBS containing 10% FCS into a 50 mL falcon tube by using 5mL/plate. The collected spheroids were centrifuged at 300g for 5 minutes. The supernatant was aspirated carefully without disrupting the pellet. The spheroids were resuspended in a solution containing 43% collagen (3.5mg/mL stock Corning / OMNILAB GmbH & Co. KG), 16.5% FCS (Sigma), 10.3% of 1% methyl cellulose solution, 14.3% of M200

medium, 15% NaHCO3 (15.6 mg/mL) and 1% NaOH (1 M). The solution was mixed gently on ice to stop polymerization in the tube. 250uL of the solution per well was transferred to 48-well plate and let it polymerize at 37degree °C for 30 minutes. 250uL of the test medium was added on to the collagen gel and the plate was incubated at 37 °C, 5% CO2 and a relative humidity of 95% for a minimum of 16 hours. The medium was aspirated from the wells and the spheroids were fixed with 4% paraformaldehyde (PFA) in PBS for 20 minutes at RT and then washed twice with PBS and stored in PBS at 4°C. PFA procedure was performed in chemical hood. Spheroids were imaged on a bright field microscope and the sprout length was analyzed using ImageJ.

3.1.6 Tube formation assay

For tube formation assay the Matrigel was thawed overnight at 4°C and always used on ice. 150 µL of Matrigel (BD Biosciences / Labor Schubert & Weiss) was added to wells on a 24-well plate on ice and incubated at 37°C for 1hour. HUVECs (Promocell) were trypsinized and counted and 120K cells were resuspended in 500 µL appropriate test medium and added to solidified Matrigel. The plates were incubated at 37 °C, 5% CO2 and a relative humidity of 95% for a minimum of 16 hours. Pictures were taken on a brightfield microscope and analyzed using ImageJ for quantification of number of tubes, number of branching points and number of loops.

3.1.7 Neurosphere formation assay

Primary neurospheres were formed in 96-well plates coated with poly-HEMA, by plating 300 cells in 0.125 mL GSC1 media with 2.5 µM doxycycline (Sigma) or ethanol (Sigma) in the medium. The plates were incubated at 37 °C, 5% CO2 and a relative humidity of 95%. Doxycycline was added every 48 hours. 8 to 10 days after plating, neurospheres formed in a well were counted (at least 4 wells were counted) and the neurosphere size was quantified (at least 10 neurospheres) by Image J software.

3.1.8 Neurosphere formation assay with 0.5 % methyl cellulose

Primary neurospheres were formed in 24-well plates coated with poly-HEMA, by plating 5,000 cells in 0.5 mL with 0.5% methylcellulose GSC media 1. per well with

2.5 µM doxycycline or ethanol in the medium. The plates were incubated at 37 °C, 5% CO2 and a relative humidity of 95%. Doxycycline/ethanol was added every 48 hours. 8 to 10 days after plating, neurospheres formed in a well were counted (at least 4 wells were counted) and the neurosphere size was quantified (10 neurospheres) by Image J software. Neurospheres were then collected to a 15 mL falcon, centrifuged at 700 rpm for 3 minutes and re-suspended in accutase for mechanical dissociation of the neurospheres in a block heater at 37 °C, 1000rpm for 5 minutes. After dissociation, cells were centrifuged at 900rpm for 3 minutes and the accutase was removed. Cell pellet was dissolved in 0.5 to 1 mL medium and cells were counted for re-plating in the same conditions for the secondary and tertiary generations of neurospheres.

3.1.9 Cell transfection by Polyethyleneimine (PEI)

Cells were washed twice with PBS and medium was changed to transfection medium (DMEM with 2%FCS without antibiotics). In an Eppendorf tube 700 µl DMEM (Sigma) was mixed with 30 µL PEI solution (1µg/µL) and incubated for 5 minutes at RT; in a second Eppendorf tube 700 µL DMEM was mixed with the appropriate amount of plasmid DNA. The reactions were mixed and incubated 20 minutes at RT. The mix was added dropwise to the cells for both lentiviral and retroviral production.

3.1.10 Production of lentiviruses

Five million HEK293T cells were plated in 10 cm dishes. The day after, medium was changed to DMEM 2% FBS without antibiotics. The cells were transfected by PEI, using 12 µg lentiviral expression plasmid (LT3GEPIR), 9 µg packaging plasmid (psPAX2) and 3 µg envelop plasmid (pMD2.G). Cells were incubated in a biosafety level 2 (BSL-2) incubator and the following steps were performed in a BSL-2 environment. After 24 hours, transfection medium was replaced by DMEM 10% FBS with antibiotics (Pen/Strep). Viral supernatants were harvested 48 hours post-transfection, collected into a 15 mL falcon tube and filtered using a 0.45 µm syringe-filter, aliquoted in cryotubes and stored at -80°C.

3.1.11 Infection of adherent cells with lentiviruses

This lentiviral procedure was used for infecting U87 cells with shRNAs targeting *SREBF1*, *SOAT1* and *PLA2G3* used in the thesis. Five hundred thousand U87 cells were plated in a 10 cm dish the day before infection. The infections were performed in a BSL-2 environment. Viral supernatants (2 mL) were mixed with 8 ml fresh medium and polybrene was added to a final concentration of 5 µg/ml. After 48 hours post-infection, cells were selected with puromycin (1 µg/mL) with fresh medium. The puromycin concentration was selected by a kill curve experiment on healthy cells.

3.1.12 Infection of suspension cells with lentiviruses

This lentiviral procedure was used for infecting NCH644 cells with shRNAs targeting *SREBF1* and *SOAT1* used in the thesis. Cells were dissociated and 500,000 cells/plasmid were plated in a well of Poly-HEMA coated 6-well plate with 2 mL medium. 3 mL virus supernatants were thawed in a water bath at 37° and ultra-centrifuged for 90 minutes at 25.000 rpm, 4°C, to discard the FBS-containing medium and re-suspend in 1 mL stem cell medium. Polybrene was added to the viral supernatants to the final concentration of 5 µg/ml and added to the wells. After 72 hours post-infection, neurospheres were dissociated and selected with puromycin (1 µg/mL) with fresh medium.

3.1.13 Crystal violet staining

This procedure was followed for cells seeded in 6-well plates or 10 cm dishes. Cells were fixed for 20 minutes with 4% PFA in PBS at RT in a chemical hood. The cells were washed with PBS to remove residual PFA. Then the cells were incubated for 30 minutes with crystal violet solution. The crystal violet solution was removed, and the plates were washed with distilled water and air-dried overnight. The colour intensity was quantified by de-staining the cells with 10% w/v acetic acid solution. All samples were diluted 1:2 or 1:4 with water, depending on the colour saturation, and the absorbance was measured at 550 nm in a microplate reader.

3.1.14 Cell Number Assay using Operetta

For the determination of cell number, 15,000 U87 and U251 cells were cultured per well and treated with appropriate inhibitors in 96-well plates (Greiner) and fixed in 3.7% PFA in PBS for 10 minutes. After washing with PBS, cells were permeabilized with 0.2% Triton X-100/PBS with 2.5 µg/ml Hoechst (Stock 5 mg/mL, Sigma) for 5 minutes. Images were acquired using the Operetta™ High Content Screening System (PerkinElmer) with the following settings: objective: 20 x WD; optical mode: non-confocal; excitation: 50 %. Ten images per well were acquired and analysis was performed with the HarmonyR High Content Imaging and Analysis Software (Perkin Elmer) by Ursula Eilers and Christina Schülein-Völk.

3.2 Molecular biology methods

3.2.1 RNA isolation

Medium from monolayer cells was aspirated and cells were lysed directly on the plate with 1 mL peqGOLD TriFast (Peqlab); neurospheres were collected to a 15 mL falcon, centrifuged 700 rpm for 3 minutes, the medium was removed, and cells were lysed with 1 mL peqGOLD TriFast. Lysed cells were transferred to RNAse-free Eppendorf tubes and incubated at RT for 5 minutes and either RNA was extracted after that, or the tubes were stored at -80 °C. 200 µl chloroform per 1mL of TriFast was added and the suspension was mixed by turning the tube upside down 15 times and incubated at RT for 10 minutes. Samples were centrifuged for 15 minutes at 14,000 rpm, at 4°C. The upper aqueous phase containing the RNA was transferred into a new reaction tube. To precipitate the RNA, 500 µl isopropanol was added and the samples were incubated on ice for 15 minutes followed by centrifugation for 15 minutes at 14,000 rpm, at 4 °C. The supernatant was carefully discarded, and the RNA pellet was washed twice with 70% EtOH. The pellet was air-dried and solubilized in 50 µl RNAse free ddH2O. The RNA was stored at -80°C.

RNA used for RNA-sequencing was isolated with the RNeasy Mini Kit and additional DNase I digestion according to manufacturer's protocol.

3.2.2 DNA isolation with phenol-chloroform

DNA was used for chromatin immunoprecipitation (ChIP) analysis. One volume of phenol-chloroform-isoamyl alcohol solution was added to the de-crosslinked chromatin and the mix was vortexed for 30 seconds. Samples were centrifuged at 14,000 rpm for 10 minutes at RT and the upper phase containing the DNA was transferred to a new reaction tube. 900 µL 100% EtOH, 38 µL Na-acetate pH 5.2 and 3 µL Glyco blue were added to the mix. The samples were briefly vortexed and incubated at -80°C for 40 minutes. Afterwards, samples were centrifuged at 14,000 rpm for 30 minutes at 4°C. The DNA pellet was washed with 80% EtOH, air-dried and resuspended in TE buffer or ddH2O.

3.2.3 cDNA synthesis

In order to perform the quantitative reverse transcriptase PCR reaction, 2 µg of extracted RNA in a total volume of 8 µL was reverse transcribed into complementary DNA (cDNA). Reactions were set up as follows: 2 µg RNA in 7µL water, 2.25 µL of HexaN (stock 0.5 µg/ µL, Roche), 1 µL of dNTP (stock 10 mM, Invitrogen), 1 µL of DNAse I (Promega) and 1.25 µL of DNAse buffer (Promega). The mixture was incubated for 15 minutes at 37°C, 15 minutes at 70°C and at least 2 minutes at 4°C. After that, 4 µL of M-MLV RT buffer (5x stock, Invitrogen), 2.4 µL of ddH2O, 0.1 µL of RNAseOUT (Invitrogen) and 1 µL of M-MLV RT (Invitrogen) was added to each reaction and incubated for 10 minutes at 25°C, 50 minutes at 42°C and 15 minutes at 70°C (to inactivate M-MLV RT). The cDNA was stored at -20°C.

3.2.4 Polymerase chain reaction (PCR)

The reaction mixture contained 4 µL cDNA (1/10 diluted), 5 µl SYBRGreen Mix (Thermo Scientific) and 1 µL forward and reverse primers (2.5 µM). The reaction was performed in a quantitative RT-PCR machine as follows:

Step	*Cycles*	*Temperature*	*Time*
Initial denaturation	1	95 °C	10 min
Denaturation	45	95 °C	15 sec
Annealing and extension		60 °C	1 min
Melting curve	1	95 °C	15 sec
		60 °C	1 min

		95 °C	1 sec

Each sample was analysed in technical duplicate. Raw data were expressed as Ct (threshold cycle), i.e., the cycle in which the fluorescence is above the background. For qPCR experiments, *B2M* or *ß-Actin* was used as housekeeping gene for internal normalization. qPCR data were analysed according to the double Delta Ct method, i.e., the fold induction relative to a control was calculated. First, the average Ct value was calculated. The difference of Ct between average housekeeping gene and the target gene was calculated per each condition (ΔCt). The standard deviation of the ΔCt was calculated and the difference of ΔCt between the control (or monolayer) and the treated (or neurospheres) sample was then quantified (ΔΔCT). The relative expression per each condition was calculated (relative expression =2^- ΔΔCT).

ChIP data were analyzed according to the Percent input method, i.e., the enrichment of the immune-precipitated sample over the amount of chromatin. Typically, 1% chromatin was used as input sample. First, the average Ct value of the input sample was calculated. Using this value, the percentage input subtracted was calculated per each immune-precipitated sample (nonspecific adjustment): Ct_{ChIP} - Average Ct_{input}. The percentage of input was calculated per each immune-precipitated sample: 0.5^ percentage input subtracted.

3.2.5 Gel electrophoresis

Gels were prepared according to the expected size of the DNA fragments. The appropriate amount of agarose was boiled in TAE, briefly cooled down, supplemented with 0.4 µg/ml ethidium bromide and poured into a gel chamber with combs depending on the volume of the sample to be loaded. The samples were mixed with DNA loading buffer (1:5) and loaded into each well of the gel, as well as a DNA ladder. The separation was performed at 120 V for one hour and the DNA fragments were visualized on a UV trans-illuminator.

3.2.6 Extraction and purification of DNA fragments

DNA fragments of the required size were cut out of the agarose gel and extracted with the gel extraction kit according to the manufacturer's protocol (Monarch DNA Gel Extraction Kit, NEB or Qiaquick Gel Extraction Kit, Qiagen).

3.2.7 Nucleic acid quantification

DNA and RNA concentration were determined using the NanoDrop 1000. The absorbance was measured at 260 nm. To assess the purity of the nucleic acid solution, the ratio of absorbance at 260 and 280 nm was determined. A ratio of 1.8 for DNA and 2 for RNA indicate a pure preparation, i.e., without protein contaminants. RNA used for library preparation for RNA-Sequencing, was quantified with the Experion Automated Electrophoresis System from Bio-Rad, following the manufacturer's protocol.

3.2.8 Digestion of DNA fragments

Restriction enzymes from New England Biolabs were used following the manufacturer's protocol, namely the recommended restriction buffers and enzyme amounts. For cloning, EcoRI-HF and XhoI restriction enzymes were used. Cutsmart buffer (NEB) was used for digestion.

3.2.9 Ligation of DNA fragments

A control reaction without insert was included as negative control. Ligation was set up as follows: 2µL of 50ng/µL linearized vector, 1µL of 20ng/µL fragment, 1 µL T4 ligase, 2 µL 10x T4 ligase buffer, 9 µL ddH2O. The ligation reaction was performed by incubating the mixture overnight at 4°C.

3.2.10 Transformation of competent cells with plasmid DNA

Competent bacteria prepared in-house was thawed on ice and 100 µL were mixed with the plasmid DNA. The bacteria were incubated on ice for 30 minutes, followed by a heat shock for one minute at 42 °C. The reactions were shortly placed on ice for 2 minutes and the mix was plated on carbenicillin LB-agar plate. Bacteria

without plasmid DNA was used as negative control. LB agar plates were placed up-side-down and incubated at 37°C overnight.

3.2.11 Preparation of plasmid DNA from bacteria

3.2.11.1 MiniPrep

A minimum of 3 bacterial colonies were picked and grown overnight in 3 mL LB with ampicillin in 15 mL falcon tubes at 37°C with shaking. Bacteria culture was transferred to an Eppendorf tube and the rest was stored at 4°C. PureYeld Plasmid MiniPrep Kit (Promega) was used according to manufacturer's instructions. DNA was stored at -20°C.

3.2.11.2 MaxiPrep

Bacterial colonies that were sequenced and selected were grown in 200 mL LB medium with ampicillin (5 mL) and grown overnight at 37°C with shaking. Bacteria culture was processed according to the manufacturer's protocol (PureLink HiPure Plasmid Maxiprep Kit, Life Technologies). The purified plasmid DNA was solubilized in TE and adjusted to a concentration of 1 µg/µL.

3.3 Biochemical methods

3.3.1 Whole cell protein lysates

For monolayer cells, the medium was aspirated, and the cells were scraped in ice cold PBS and centrifuged to remove PBS. RIPA lysis buffer containing protease and phosphatase inhibitors was added to the pellet and incubated for 15 minutes on ice. Neurospheres were collected to a 15 mL falcon and centrifuged at 700 rpm for 3 minutes; the medium was removed, and cells were washed with PBS by centrifugation. Neurospheres were then incubated with the same lysis buffer for 15 minutes on ice.

After cell lysis, all samples were centrifuged at 14,000 rpm for 15 minutes, at 4°C and cleared lysates were transferred to new Eppendorf tubes. Lysates were stored at -20°C or, alternatively, samples were directly prepared for SDS-PAGE.

3.3.2 Protein quantification by BCA assay

To determine the protein concentration of protein lysates, the bicinchoninic acid (BCA) assay (Thermo Scientific) was applied. A BCA solution mix was prepared by mixing BCA buffer A and BCA buffer B in a 50:1 proportion. 4 µl of sample (diluted 1:10) or water (as a blank) were mixed with 200 µl of BCA solution mix, incubated for 30 minutes at 37 °C and absorbance was measured at 550 nm. Protein concentrations were determined using a BSA standard curve.

3.3.3 SDS-PAGE

The appropriate amount of 4x loading buffer was added to protein lysates (20 - 30µg) and samples were boiled at 95°C for 5 minutes. Protein samples and pre-stained protein ladder (Thermo Scientific) were loaded into the gel pockets. SDS polyacrylamide gels (7.5% - 12%) were used for separating the proteins according to their molecular weight. The electrophoresis was performed using SDS-PAGE chambers (Biorad) filled with 1x SDS running buffer at 80-120 V.

3.3.4 Immunoblot

After separating protein lysates by SDS-PAGE, proteins were transferred onto a PVDF membrane. The PVDF membrane was activated by incubation in methanol for 30 seconds, followed by 2 minutes in H2O. The membrane was equilibrated in the 1x transfer buffer before proceeding to the immunoblot assembly. The immunoblot sandwich was assembled in transfer buffer and the cassette was placed into the tank, which was filled with 1x transfer buffer. The transfer was carried out at 4°C, at 300 mA for 1 hour and 45 minutes. Afterwards, the membrane was stained with Ponceau to check for efficient transfer and washed with water. Membranes were incubated in blocking solution (LI-COR or 5% BSA in 1x TBS-T) for 1 hour at RT under constant shaking. After blocking, the membrane was incubated with the primary antibody at 4°C

overnight. On the next day, the membrane was washed 3 times for 10 minutes with 1x TBS-T and incubated for 1 hour with the secondary antibody (diluted in LI-COR or 5% milk in 1x TBS-T) followed by additional 3 washing steps of 5 minutes each with 1x TBS-T. Fluorescent signals were detected with a LI-COR Odyssey Infrared scanner.

3.3.5 Proteome profiler human angiogenesis array analysis

Media samples were collected from cells and centrifuged to remove cell debris and transferred to fresh tubes. The media samples were stored at -80°C until use and repeated freeze-thaw cycles were avoided. Proteome Profiler Human Angiogenesis Array Kit from R&D Systems (ARY007) was used according to manufacturer's instructions. The data was analysed and quantified using ImageJ software.

3.3.6 ELISA

Media samples without FCS were collected from cells and centrifuged to remove cell debris and transferred to fresh tubes. The media samples were stored at -80°C until use and repeated freeze-thaw cycles were avoided. The PGE2 CLIA kit from Enzo (ADI-910-001PGE2) is a competitive immunoassay used for the quantitative sensitive determination of Prostaglandin E2. Lysophosphatidic Acid (LPA) ELISA Kit from Antibodies-online (ABIN2039318) that employs competitive inhibition enzyme immunoassay technique was used for determination of LPA in the samples. The manufacturer's instructions were followed for effective measurement, analysis and interpretation of the data collected from ELISA assays.

3.4 RNA sequencing

RNA sequencing data used in the thesis for U87 cells with SREBP1 silencing was performed by Charlene Brault and analysed by Carsten Ade (AG Prof. Eilers) and Susanne Walz (Bioinformatics Core Unit of the Comprehensive Cancer Center Mainfranken). Compilation of 72 gene list and GO analysis utilizing gene expression data of cells over-expressing SREBP1 and knockdown of SREBP1 was performed by

Prof. Schulze. RNA-Seq data on monolayer and neurosphere comparison was performed by Joana Peixoto and analysed by Susanne Walz.

3.4.1 Library preparation

The experiment was performed in triplicate for each condition. RNA for RNAseq was extracted using the RNeasy Mini kit (Qiagen) and eluted in 40 µL RNAase free H2O. RNA samples were kept in ice and RNA concentration was measured using a standard sense chip for Bioanalyzer. One µg/µL RNA per each condition was used for library preparation. The library was prepared using the NEBNext Ultra RNA library prep kit for Illumina and the NEBNext Multiplex Oligos for Illumina (Dual Index Primers Set 1), according to the manufacturer's instructions. H2O was used as negative control to check the purity of the preparation. The amplification by PCR was performed for 12 cycles and the PCR products were purified using the Agencourt AMPure XP beads. The quality of the purified DNA was verified on the Bioanalyzer before performing the sequencing, using the Illumina GAIIx sequencer. All samples were mixed at equimolar concentration of 300nM.

3.4.2 Data analysis

Base calling was performed with Illumina's CASAVA software and overall sequencing quality was tested using the FastQC script. Reads were aligned to the human genome (hg19) with TopHat2 and Bowtie v0.12.8 using default parameters (Langmead 2010, Kim, Pertea et al. 2013). Mapped reads per gene (EnsEMBL GRCh37, release 74) were counted using the "summarizeOverlaps" function in the GenomicAlignments R package, non-expressed genes were removed (mean read count per gene over all samples >1) and TMM normalized with EdgeR. Gene set enrichment analysis was performed with the C2, C5 and Hallmark collection from the MSigDB v5.2 with default parameters and 1000 permutations (Subramanian, Tamayo et al. 2005, Liberzon, Subramanian et al. 2011). Principle component analysis (PCA) was performed with the prcomp function from R after centering sequencing depth-normalized expression values of all expressed genes (n=18,457).

3.5 Metabolic assays

3.5.1 Total fatty acid analysis

Media from cells were aspirated and the cells were washed and scraped in cold 154 mM ammonium acetate and centrifuged at 1500 rpm for 5 minutes. 190 µL cold MeOH and 47 µL cold H2O was added to the cell pellet. 20 µL Standard-Mix (containing 5 mM each of Lamivudine, tridecanoic acid, nonadecanoic acid and Ibuprofen in MeOH / CHCl3 (1/1; v/v)) was added, followed by addition of 30 µL 0.2 M HCl, 90 µL CHCl3, 100 µL CHCl3 and 100 µL H2O. After addition of each solvent, the samples were mixed vigorously. Finally, they were centrifuged at 14,000 rpm for 5 minutes and the lower phase was transferred to a new tube and evaporated at 45 °C under nitrogen gas flow. The samples were resuspended in 0.5 mL 0.3 M KOH in MeOH/H2O (9/1; v/v; freshly prepared) and heated at 80 °C for 1 hour. 50 µL formic acid was added to the lower phase and upper phase containing fatty acids was extracted twice with 0.5 mL hexane. The samples were evaporated at 45 °C under nitrogen gas flow and resuspended in 100 µl of isopropanol (iPrOH). The samples were manually injected by direct injection on to the mass spectrometer (MS). The scan rage was selected at 150-400, polarity to negative, acquisition time to 0.75 minutes.

3.5.2 Lipidomics

Media from cells were aspirated and the cells were washed and scraped in cold 154 mM ammonium acetate and centrifuged at 1500 rpm for 5 minutes. 280 µL of n-Butanol / Methanol (3/1, v/v) was added to the cell pellet, followed by addition of (Hexanoyl-sphingomyelin and 1,2-Dimyristinoyl-glycero-3-phosphocholine) in n-Butanol / Methanol (3/1 v/v) and 20 µL 1 mM standard (1,2-Dimyristinoyl-glycero-3-phospho-L-serine (DGPS) in PBS. 20 µl n-Butanol / Methanol (3/1, v/v) + 20 µl 1% Acetic Acid (in water) was added and mixed and samples were ultrasonicated. Then 300 µL heptane / ethyl acetate (3/1, v/v) and 280 µL 1% acetic acid (in water) was added and the samples were sonicated and mixed. Upper phase was transferred to new tubes. This procedure was repeated twice, and the upper phases were combined and evaporated at 35 °C under nitrogen gas flow. For 250 µL media samples the same

procedure was followed but 280 µL 1% Acetic acid was replaced by 28 µL of 10% Acetic acid.

For LC/MS analysis, samples were dissolved in 100 µl of iPrOH. Mobile phase A consisted of CH3CN/H2O/FA (10/89.9/0.1, v/v/v) and mobile phase B consisted of CH3CN/H2O/FA (90/9.9/0.1, v/v/v). With application of 3 µL sample to the C8 column (at 40 °C), the separation was performed with a gradient: 20% solvent B for 2 minutes, followed by a linear increase to 100% solvent B within 5 minutes, then maintaining 100% B for 27 minutes, then returning to 20% B in 1 minute and 5 minutes 20% solvent B for column equilibration before each injection. The flow rate was maintained at 350 µL/minute. The eluent was directed to the ESI source of the QE-MS from 2 minutes to 29 minutes after sample injection. MS scan parameters used were the following: full MS in positive/negative mode, runtime: 2 minutes - 29 minutes; resolution: 70,000, AGC-target: 3E6; maximum Injection Time: 200 ms and scan range: 200 - 1500 m/z. HESI source parameters were: sheath gas flow rate: 30; auxiliary gas flow rate: 10; sweep gas flow rate: 3; spray voltage: 2.5 kV in positive mode and 3.6 kV in negative mode; capillary temperature: 320 °C; S-lens RF level: 55.0 and aux gas heater temperature: 120 °C. Peaks corresponding to the calculated lipid masses (MIM +/- H+ ± 2 mMU) were integrated using TraceFinder software (Thermo Scientific, Bremen, Germany).

3.5.3 Thin layer chromatography (TLC)

Samples prepared for lipidomic analysis were used for thin layer chromatography. Samples were evaporated with speed vac and redissolved in 10 µl CHCl3/MeOH (1/1; v/v). 5 µl of the extract was applied to a TLC plate (20cm*20cm), at 1.5 cm from the bottom of the plate. First solvent line was drawn at 5 cm and the plate was immersed in “Polar Solvent”: CHCl3/MeOH/20%AcOH (65/25/5; v/v/v). The second solvent line was drawn at 12 cm and the plate immersed in “Medium polar Solvent”: Hexane/Acetic Acid Ethylester/AcOH (59/10/1; v/v/v); and the third solvent line was drawn at 15 cm and the plate immersed in “Unpolar Solvent”: Hexane/Acetic Acid Ethylester (9/1; v/v). The TLC plate was dried using a hair dryer and the plate was stained by dipping the plate into “SuperMix” (2.5% Molybdatophosphate, 1% Cer-IV-Sulfate, 6% H2SO4 in H2O) and heating at 200 °C until bands appear. Standards (in

MeOH/CHCl3; 1/1) used at 1 mg/ml each were the following: oleic acid, triolein, cholesterol, cholesterolpalmitate, phosphatidylcholines (from egg yolk) and Sphingomyelines (from egg yolk).

3.6 Statistical analysis

Quantitative data were displayed and analysed using GraphPad Prism 7.0. Data are presented as mean values with error bars representing standard deviation (SD) or standard error of mean (SEM), as described in figure legends. P-values were calculated by using two-tailed unpaired student t-test and considered to be statistically significant when smaller than 0.05.

Chapter 4: Results

4.1 SREBP1 regulation in Glioblastoma

Proliferating cells need to synthesize and obtain macromolecules that are the basic building blocks of the cell. Cancer cells are highly proliferative and are in great demand for procuring necessary macromolecules. When cancer cells are exposed to metabolic stress due to lack of access to necessary nutrients, they re-wire their metabolism to *de novo* synthesis to accommodate for the changes relative to the environment (DeBerardinis et al., 2008; Zhu and Thompson, 2019). This flexibility of cancer cells promotes their growth and progression in harsh microenvironments and also becomes a target for therapeutic intervention.

4.1.1 Low serum levels upregulate SREBP1 in Glioblastoma

When glioblastoma (GB) cells were cultured in low serum (1% FCS) condition, they significantly upregulated their *de novo* fatty acid synthesis. U87 and U251 grown in media containing 1% FCS had higher levels of mature SREBP1 protein, enhanced *SREBF1* mRNA levels and elevated expression of the target gene *SCD* compared to cells in 10% FCS condition (Fig 4.1A and B). This is consistent with an increase in the transcriptional output of the SREBP1 target gene network observed previously (Griffiths *et al.*, 2013; Lewis et al., 2015).

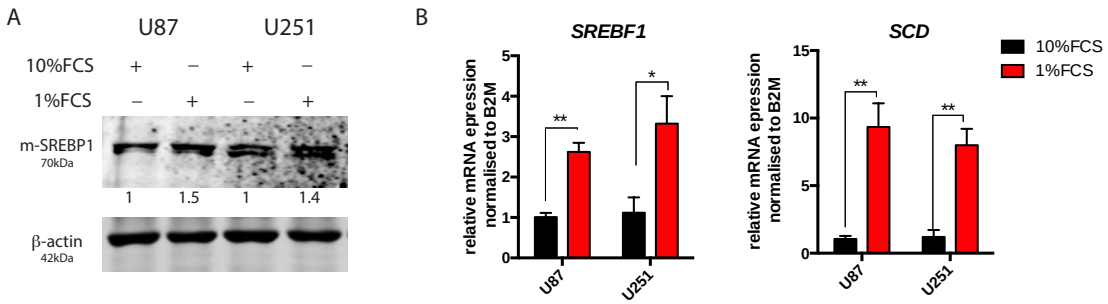

Figure 4. 1: Low serum in the media upregulates both SREBP1 protein and mRNA levels and induces expression of the target genes

A) Western Blot (WB) showing higher levels of mature SREBP1 (m-SREBP1) upon low serum (1% FCS) treatment compared to 10% FCS condition in two Glioblastoma cell lines (U87 and U251).

Cells were washed in PBS and grown in media containing 1% or 10% FCS for 24hours. Signal intensities were normalized to β-actin and are shown relative to 10% FCS controls.

B) qRT-PCR to quantify mRNA levels of *SREBF1* and *SCD* under the same conditions as in (A). mRNA levels are shown relative to 10% FCS condition. Bars represent mean ± SEM (n=3). p-values were calculated using a two tailed student's t-test (p-values are represented as * ≤ 0.05, ** ≤ 0.01).

The cells grown in low serum condition also have reduced growth factors available compared to full serum media. Growth factor signalling is important to direct cells to take up nutrients or switch to *de novo* synthesis (Palm and Thompson, 2017; Vander Heiden et al., 2001). To understand whether the upregulated fatty acid pathway seen in GB cells upon low serum treatment was a consequence of reduced growth factors, U87 cells were grown in 1% FCS, 10% FCS or in a serum substitute that does not contain lipids or cholesterol but is supplemented with growth factors (Panex basic) for 24hours. Cells grown in both 1% FCS and serum substitute without lipids/cholesterol but with growth factors were able to increase SREBP activity and upregulate enzymes involved in fatty acid and cholesterol biosynthesis compared to cells grown in 10% FCS media (Fig 4.2). Hence, low serum conditions can upregulate fatty acid metabolism in GB cells even in media containing reduced growth factors. But it also needs to be noted that cells grown in serum substitute with growth factors had further increase in mRNA levels of the genes involved in fatty acid and cholesterol biosynthesis compared to low serum condition without growth factors. Further investigation is required to understand the consequences of absence of growth factors which is not addressed in the current study.

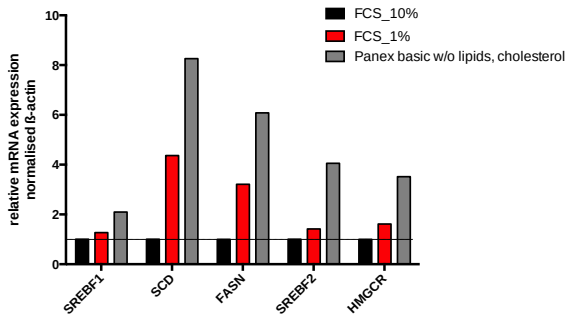

Figure 4. 2: Low amounts of lipids and cholesterol in the medium lead to the upregulation of SREBF1 and its target genes

qRT-PCR showing mRNA levels of *SREBF1*, *SREBF2* and their targets *SCD, FASN* and *HMGCR* in U87 cells in medium containing 10% and 1% FCS or serum substitute (Panex basic without lipids/cholesterol). mRNA levels are shown relative to 10% FCS. The cells were washed in PBS and treatment was performed for 24hours. Bars represent n=1.

4.1.2 shRNA mediated genetic ablation of SREBF1 with 2 different vector systems

To study the loss of SREBP1 in GB cells, different shRNA sequences targeting *SREBF1* were introduced into two different vector backbones to understand the effects of loss of SREBP1 and to avoid conclusions based on potential off-target effects.

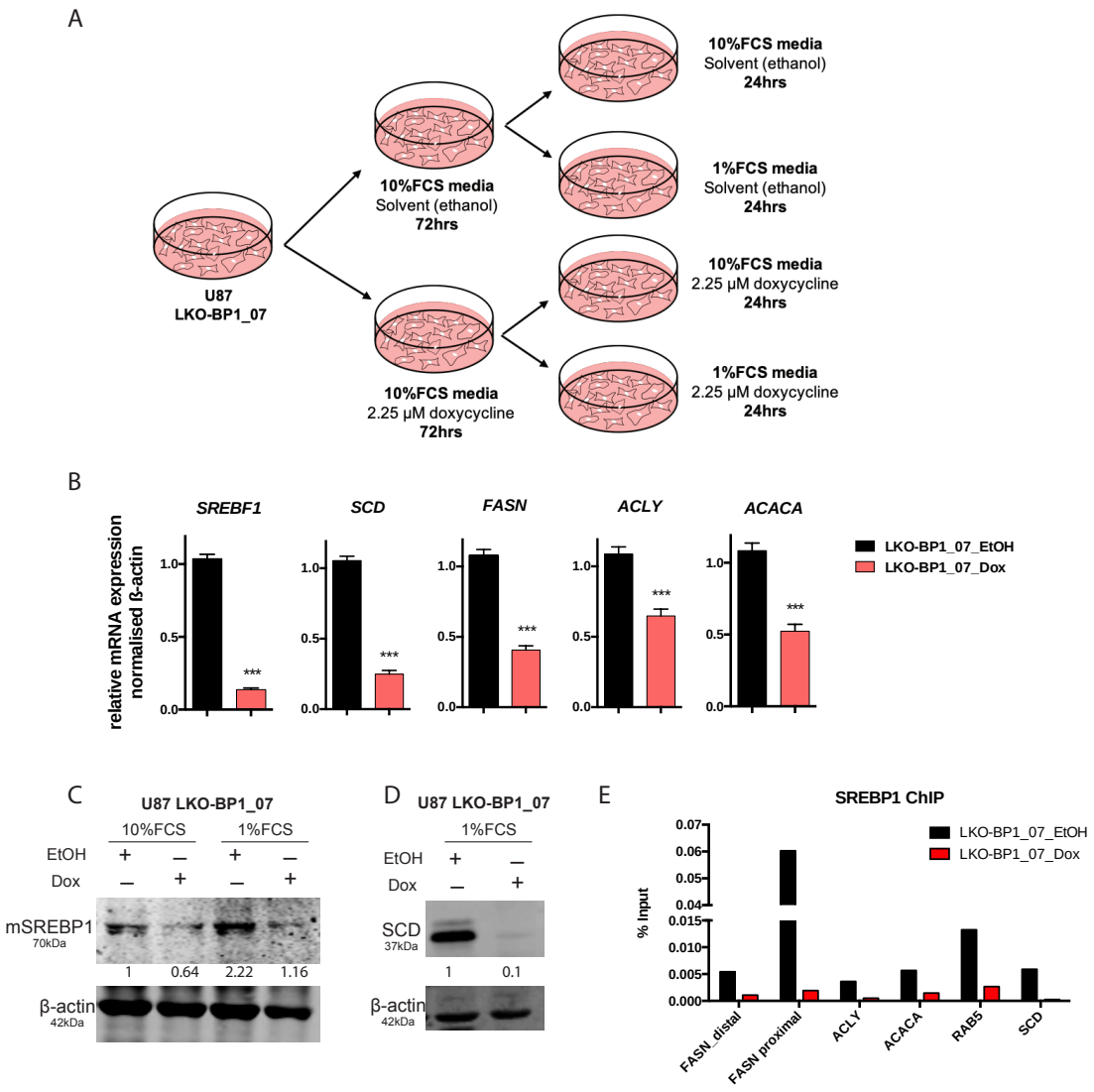

Figure 4.3: SREBP1 knockdown leads to the downregulation of genes involved in fatty acid biosynthesis and a decrease in its binding to the promoter regions of target genes

A) Schematic representation of time course of low serum treatment with shRNA mediated knockdown of SREBP1 with doxycycline. Cells were seeded in 10%FCS media and treated with ethanol (solvent control) or 2.25 µM doxycycline for 72 hours. The cells were washed with PBS and media was changed to 1% or 10% FCS with ethanol (solvent control) or 2.25 µM doxycycline for the last 24hours.

B) qRT-PCR showing mRNA levels of *SREBF1, SCD, FASN, ACLY* and *ACACA* in U87 cells. Cells expressing shSREBP1_07 were treated as shown in A, only 1% FCS treated samples were used for this analysis. Bars represent mean ± SEM (n=12). p-values were calculated using a two tailed student's t-test (p-values are represented as *** ≤ 0.001).
C) WB showing the mature form of SREBP1 upon SREBP1 knockdown in medium containing 10% or 1% FCS (as in A). Signal intensities were normalized to β-actin and are shown relative to the 10% FCS solvent control.
D) WB showing protein levels of SCD upon knockdown of SREBP1 in medium containing 1% FCS under the same conditions as in B. Signal intensities were normalized to β-actin and are shown relative to the solvent control.
E) ChIP qRT-PCR showing binding of SREBP1 to promoter regions of selected target genes in cells cultured under the same conditions as in B. Bars represent percent of input chromatin (n=1).

U87 cells transduced with a doxycycline (Dox) inducible pLKO-Tet-On vector with shRNA targeting *SREBF1* (LKO-BP1_07) were grown in 10% FCS with 2.25 µM Dox or solvent control (ethanol) for 72 hours. Cells were washed with PBS and the medium was changed to media containing 1% or 10% FCS with 2.25 µM Dox or ethanol control (as represented in Fig 4.3A). Dox induction of shRNA mediated knockdown of SREBP1 was confirmed by reduction of mRNA levels of *SREBF1* and its targets *SCD*, *FASN*, *ACLY* and *ACACA* (Fig 4.3B). The mature form of SREBP1 (Fig 4.3C) and protein levels of its target SCD (Fig 4.3D) were also strongly reduced upon Dox treatment. These results were also confirmed by a reduction of binding of SREBP1 to the promoter regions of several SREBP1 target genes by chromatin immuno precipitation (ChIP) (Fig 4.3E).

For the second vector system, five shRNA sequences targeting *SREBF1* were obtained from genome-wide sensor-based shRNA predictions (Fellmann et al., 2013) and were introduced into U87 cells via the pLT3-GEPIR Dox inducible vector system. To check the knock down of *SREBF1* with these shRNA sequences, cells were treated with 2.25 µM Dox or solvent (ethanol) for 72 hours in media with 10% FCS. Expression of all shRNA sequences resulted in a reduction of mRNA levels of the SREBP1 target gene *SCD* (Fig 4.4) but only shRNA sequences 01, 03 and 06 showed efficient reduction of mRNA levels of *SREBF1* (Fig 4.4).

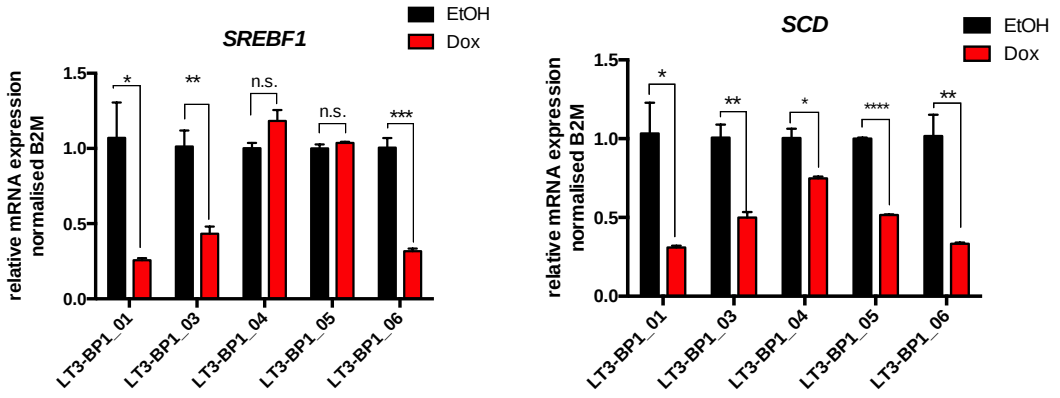

Figure 4.4: Selection of optimal shRNA sequences targeting SREBF1 using the pLT3-GEPIR Dox inducible system

qRT-PCR showing mRNA levels of *SREBF1* and *SCD*. Cells transduced with lentiviral vectors (pLT3-GEPIR) encoding different shRNA sequences targeting SREBP1 (shSREBP1_01, 03, 04, 05 and 06) were treated with 2.25 µM Dox or ethanol (solvent control) for 72 hours in 10% FCS medium. mRNA levels are shown relative to solvent control. Bars represent mean ± SEM (n=3). p-values were calculated using a two tailed student's t-test (p-values are represented as * ≤ 0.05, ** ≤ 0.01, *** ≤ 0.001 and **** ≤ 0.0001).

The shRNA sequences 01, 03 and 06 that showed efficient *SREBF1* silencing were further validated by treating cells in 10% FCS media containing 2.25 µM Dox or solvent (ethanol) for 72 hours and the media was changed to 1% or 10% FCS 2.25 µM Dox or solvent (ethanol) for an additional 24hours (as shown in Fig 4.3A). mRNA levels of *SREBF1* and its target *SCD* were reduced by all 3 shRNA sequences (Fig 4.5). shRNA sequences 01 and 06 both showed a more efficient reduction of *SREBF1* and *SCD* levels in both 10% and 1% serum conditions compared to sequence 03. As it had been shown previously that silencing of SREBP1 induces ER stress in cells depleted of exogenous lipids (Griffiths *et al.*, 2013), mRNA levels of the ER-stress gene *DDIT3* (CHOP) was used to check if the depletion of SREBP1 was sufficient to induce ER stress. Only induction of sequences 01 and 06 indeed triggered ER stress in 1% serum conditions (Fig 4.5), confirming previous results. Further, silencing efficiency and induction of ER-stress was also confirmed by including cells expressing a non-targeting control (shRenilla). The results obtained in this experiment showed that Dox treatment of shRenilla expressing cells does not alter the expression of *SREBF1* or *SCD* and does not induce ER-stress, as indicated by the lack of DDIT3 induction (Fig 4.6).

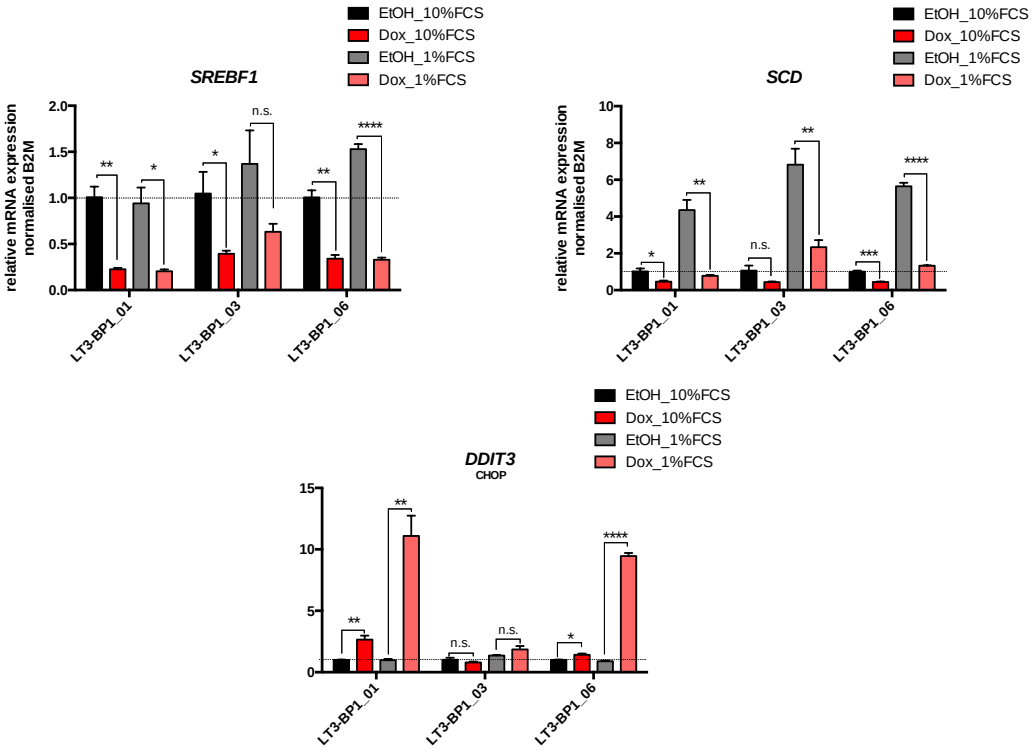

Figure 4.5: Validation of shRNAs targeting SREBF1 in PLT3-GEPIR Dox inducible system

qRT-PCR showing mRNA levels of *SREBF1*, *SCD* and *DDIT3*. Cells expressing shRNA sequences targeting SREBP1 (shSREBP1_01, 03 and 06) were grown in 10% FCS with 2.25 µM Dox or ethanol (solvent control) for 72 hours. Cells were washed with PBS and medium was changed to media containing 1% or 10% FCS with 2.25 µM Dox or ethanol (solvent control) (as represented in Fig 4.3A). mRNA levels are shown relative to the ethanol control of each cell line. Bars represent mean ± SEM (n=3). p-values were calculated using a two tailed student's t-test (p-values are represented as * ≤ 0.05, ** ≤ 0.01, *** ≤ 0.001 and **** ≤ 0.0001).

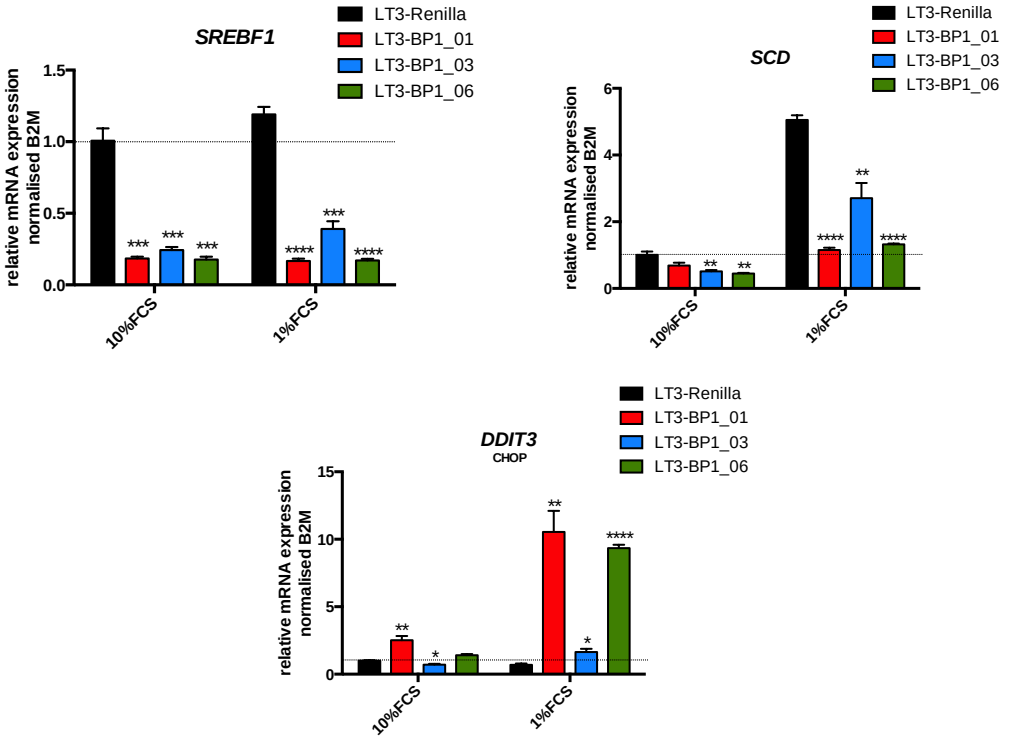

Figure 4.6: Validation of shRNAs targeting SREBF1 in the PLT3-GEPIR Dox inducible system with shRenilla control

qRT-PCR showing mRNA levels of *SREBF1*, *SCD* and *DDIT3*. mRNA levels are shown relative to shRenilla. Cells expressing either non-targeting controls (LT3-Renilla) or sequences targeting SREBP1 (LT3-BP1_01, LT3-BP1_02 or LT3-BP1_03) were treated with 2.25 μM Dox or solvent (ethanol) for 72 hours in medium containing 10% FCS. Cells were washed with PBS and medium was changed to media containing 1% or 10% FCS with 2.25 μM Dox or ethanol (solvent control) (as represented in Fig 4.3A). Bars represent mean ± SEM (n=3). p-values were calculated using a two tailed student's t-test (p-values are represented as * ≤ 0.05, ** ≤ 0.01, *** ≤ 0.001 and **** ≤ 0.0001).

The cells expressing shRNA sequences 01 and 06 were further investigated by cell viability assays. Cells were grown in 10% FCS media containing 2.25 μM Dox or solvent (ethanol) for 72 hours and the media was changed to 1% or 10% FCS with 2.25 μM Dox or solvent (ethanol) for an additional 24hours (as shown in Fig 4.3A). Cells grown in low serum conditions are under ER stress and showed significant reduction in cell viability upon SREBP1 knock down (Fig 4.7). Sequences 01 and 06 were therefore considered validated and used for further experiments.

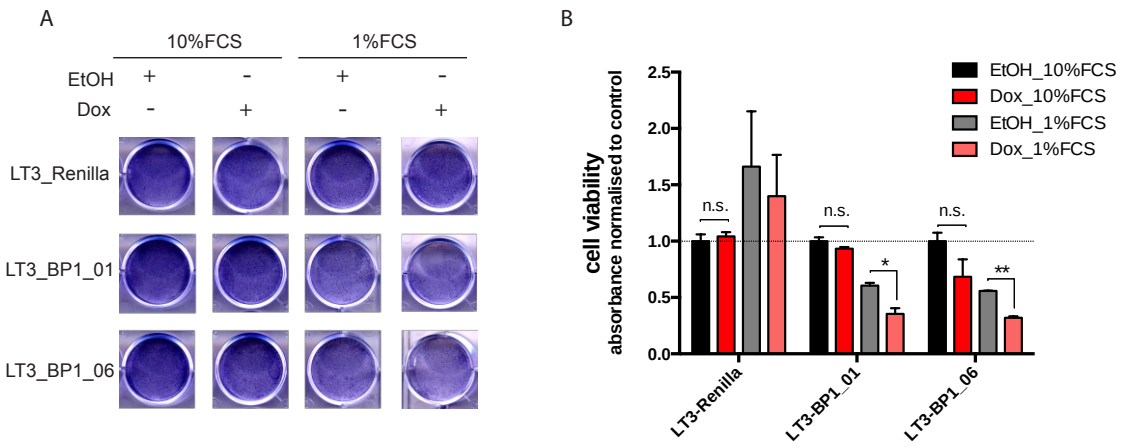

Figure 4.7: Decrease in cell viability upon SREBP1 knockdown and low serum treatment using the pLT3-GEPIR Dox inducible system

A) U87 cells expressing inducible shRNA sequences targeting SREBP1 were treated with 2.25 µM Dox or solvent (ethanol) in medium containing 10% FCS for 72 hours. Cells were washed with PBS and medium was changed to media containing 1% or 10% FCS with 2.25 µM Dox or ethanol (solvent control) (as represented in Fig 4.3A). Cell viability was determined by crystal violet staining.

B) Quantification of crystal violet staining in (A). Values were normalized to ethanol control in 10% FCS. Bars represent mean ± SEM (n=3). p-values were calculated using a two tailed student's t-test (p-values are represented as * ≤ 0.05 and ** ≤ 0.01).

4.1.3 Proliferation of U87 cells with SREBP1 knockdown

U87 cells with shRNA sequences targeting SREBP1 in two different vector systems, LKO-BP1_07 and LT3-BP1_06, and their respective controls, LKO-Scr and LT3-Renilla, were grown in medium containing 10%, 1% or 0% FCS to study cell proliferation in a time course experiment (Fig 4.8A).

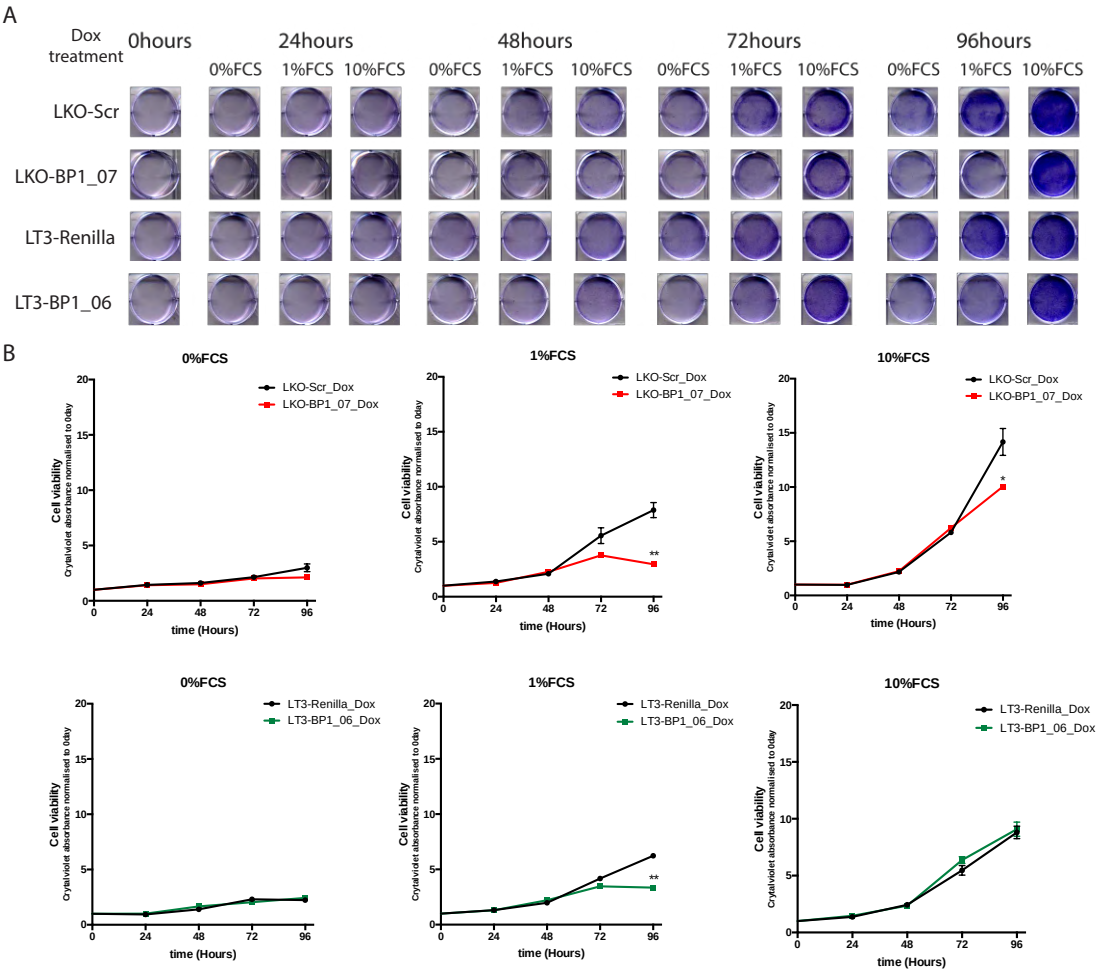

Figure 4.8: Cell proliferation upon SREBP1 knockdown in different FCS concentrations

A) Crystal violet staining of cells expressing shRNA sequences targeting SREBP1 (shSREBP1_07 and shSREBP1_06) or non-targeting controls (shScr and shRenilla) treated with 2.25 µM Dox in medium containing 0%, 1% or 10% FCS for 24, 48, 72 and 96 hours. The cells were washed with PBS after 24 hours of seeding in 10% FCS medium (referred to as 0 hours control) and media containing 10%, 1% or 0% FCS were added to cells and treated for 24, 48, 72 and 96hours with 2.25 µM Dox.

B) Quantification of crystal violet staining in (A) shown as growth curves. The values of quantification are normalized to the 0 hours control for each cell line. Each point on the curve represent the mean ± SEM (n=3). p-values were calculated using a two tailed student's t-test (p-values are represented as * ≤ 0.05, ** ≤ 0.01).

Induction of shRNA with Dox was started at 0 hours and cell growth was monitored over 96 hours. Cells expressing shBP1 in both vector systems showed similar growth rates in 10% FCS compared to the control cell lines at 24, 48 and 72 hours after Dox treatment, while LKO-BP1_07 cells showed a significant reduction in cell number at the 96-hour time point (Fig 4.8B, left graphs). In contrast, silencing of SREBP1 using both vector systems in medium containing 1% FCS resulted in a moderate reduction in growth after 72 hours and a significant reduction after 96 hour of Dox treatment compared to control cells (Fig 4.8B, middle graphs). This indicates that SREBP1 proficient cells have the ability to upregulate *de novo* fatty acid synthesis and sustain proliferation even with reduced availability of fatty acids from the medium. Nevertheless, their proliferation rate was reduced by about 50% compared to cells grown in 10% FCS condition. However, cells grown in 0% FCS showed an overall impaired proliferation, which was not further reduced by SREBP1 depletion (Fig 4.8B, right graphs).

4.2 The transcriptional signature controlled by SREBP1 in GB cells

To understand the global effect of SREBP1 knockdown in GB cells, a genome-wide RNA sequencing (RNAseq) analysis was performed in U87 cells expressing the pLKO-TetOn vector encoding either a non-targeting sequence (shScr) or a sequence targeting SREBP1 (shBP1_07). Cells were grown in 10% FCS with 2.25 µM Dox or solvent (ethanol) for 48 hours. After this time, cells were washed with PBS and the medium was changed to media containing 1% or 10% FCS with 2.25 µM Dox or ethanol and cells were incubated for a further 24 hours. This experiment was performed by C. Brault (Biochemistry and Molecular Biology, Biocenter Würzburg). RNAseq and data analysis was performed by C. Ade and S. Walz (Biochemistry and Molecular Biology, Biocenter, Würzburg and Comprehensive Cancer Center Mainfranken).

4.2.1 Analysis of the SREBP1 gene expression network

RNA seq data analysis revealed that knockdown of SREBP1 resulted in changes in regulation of number of genes in both 10% and 1% FCS treated cells (Fig 4.9A). Even though there were substantial number of genes that were regulated similarly in both conditions (number of genes overlapped in the Venn diagram in Fig. 4.9A), cells in 1% FCS condition showed evidently more regulation. Results from the RNAseq analysis were validated by performing RT-qPCR on the same RNA samples. mRNA levels of the previously identified SREBP1 target genes, *SCD, FASN, FADS1, FADS2* and *FABP3* were analysed. All genes showed upregulation in the 1% FCS conditions compared to 10% FCS, indicating induction of *de novo* fatty acid synthesis (Fig. 4.9B). Also, the strong downregulation of these genes upon SREBP1 knockdown confirmed the RNAseq data and placed these genes into the SREBP1 transcriptional network.

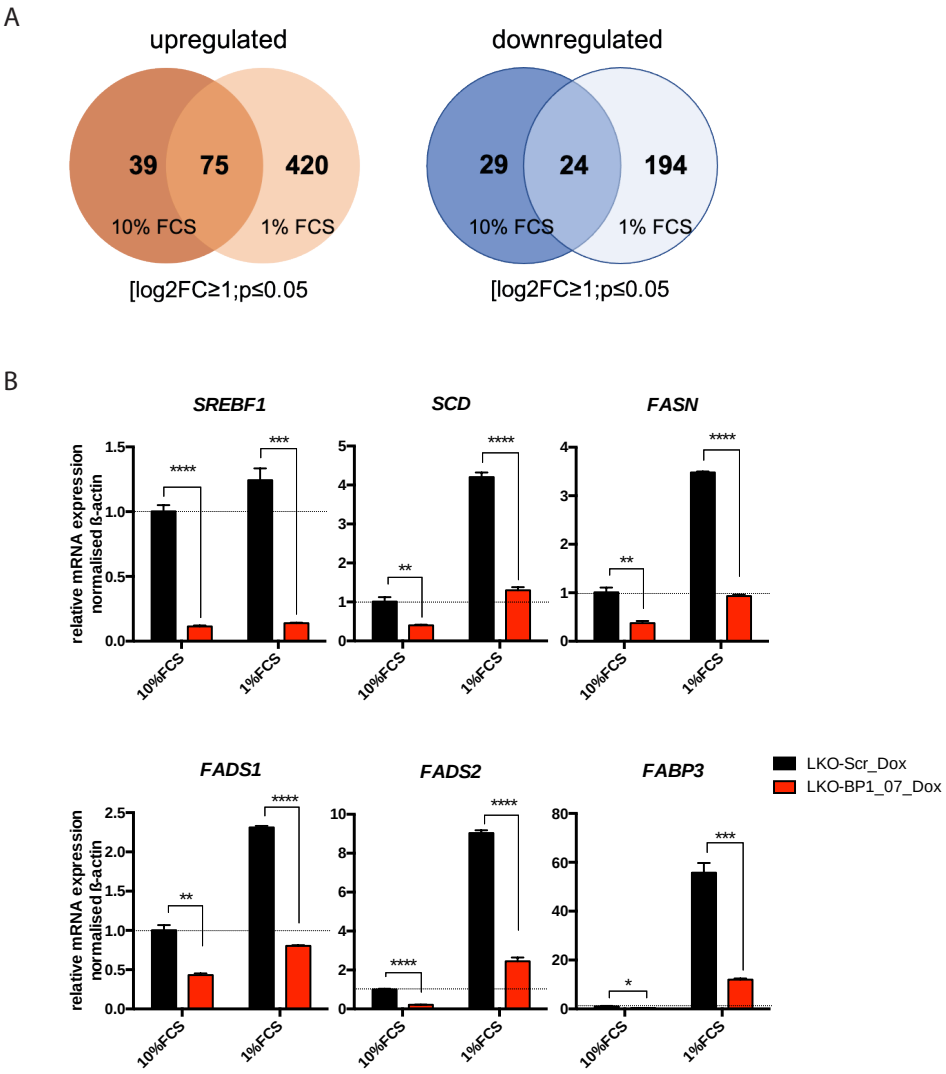

Figure 4.9: SREBF1 knockdown leads to downregulation of the transcriptional output of SREBP1

A) Venn diagrams showing summary of number of genes upregulated or downregulated upon SREP1 knockdown in both 10% and 1% FCS media, obtained from RNAseq data. Cells were seeded in 10%FCS media and treated with ethanol (solvent control) or 2.25 µM Dox for 72 hours. The cells were washed with PBS and media was changed to 1% or 10% FCS with ethanol (solvent control) or 2.25 µM Dox for the last 24hours.

B) qRT-PCR showing mRNA levels of *SREBF1*, *SCD, FASN, FADS1, FADS2* and *FABP3*. mRNA levels are shown relative to the 10% FCS condition of the control. Same samples were used in the RNA seq experiment. Bars represent mean ± SEM (n=3). p-values were calculated using a two tailed student's t-test (p-values are represented as * ≤ 0.05, ** ≤ 0.01, *** ≤ 0.001 and **** ≤ 0.0001).

Gene set enrichment analysis (GSEA) showed that genes associated with Horton SREBP1 targets gene set (Horton et al., 2003) were strongly reduced upon SREBP1 knock down in cells cultured in 1% FCS (Fig. 4.10). Furthermore, genes associated to

the Ishida E2F targets gene set involved in cell cycle control (Ishida et al., 2001) also showed reduced expression in SREBP1 knock down cells, indicating reduced proliferation (Fig 4.10). Additionally, genes associated with the response to Salirasib, an inhibitor of the farnesylation of Ras (Blum et al., 2007), and tumour necrosis factor (TNF) (Phong et al., 2010) were strongly induced upon SREBP1 knockdown, indicating a pro-inflammatory response compared to control cells (Fig 4.10).

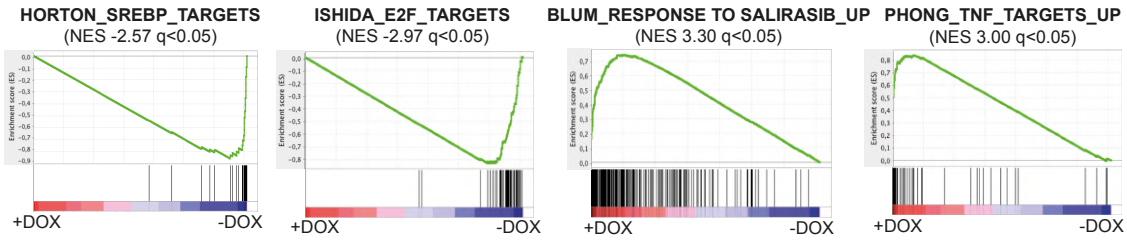

Figure 4.10: Gene Set Enrichment Analysis of transcriptional changes upon SREBP1 knockdown

Gene Set Enrichment Analysis (GSEA) of RNAseq data comparing control (-DOX) to SREBP1 knockdown (+DOX) in U87 cells cultured in 1% FCS. Enrichment plots of HORTON_SREBP_TARGETS (Horton *et al.*, 2003), ISHIDA_E2F_TARGETS (Ishida *et al.*, 2001), BLUM_RESPONSE_TO_SALIRASIB_UP (Blum *et al.*, 2007) and PHONG_TNF_TARGETS_UP (Phong *et al.*, 2010) are shown. Cells expressing shSREBP1_07 were seeded in 10% FCS media and treated with 2.25 µM Dox or solvent (ethanol) for 48 hours. The cells were then washed with PBS and media was changed to 1% FCS with 2.25 µM Dox or solvent for the last 24hours.

Gene expression data previously generated in U87 cells with tamoxifen (TX)-inducible activation of SREBP1 (Lewis *et al.*, 2015) were combined with the RNA-seq data generated with knockdown of SREBP1 to define a list of consensus genes regulated by SREBP1 in glioma cells. Despite the different platforms used in both experiments (Illumina bead array versus RNAseq), 72 genes showed overlapping but opposing regulation and are shown in a Venn diagram (Fig 4.11A). Performing gene ontology (GO) enrichment analysis using the DAVID pathway analysis tool (https://david.ncifcrf.gov/) with these 72 genes revealed a strong association with lipid/fatty acid synthesis and metabolism pathways (Fig 4.11B). Phospholipid metabolic process was one of the pathways that was identified in this analysis and the individual genes in this pathway were also significantly downregulated in the RNAseq analysis of U87 cells after SREBP1 knockdown (Fig 4.11C). Downregulation of the most regulated gene in the pathway, *PLA2G3*, was confirmed by RT-qPCR (Fig 4.11D).

Interestingly, this experiment showed that *PLA2G3* mRNA is strongly induced in cells exposed to low serum containing medium (Fig. 4.11D).

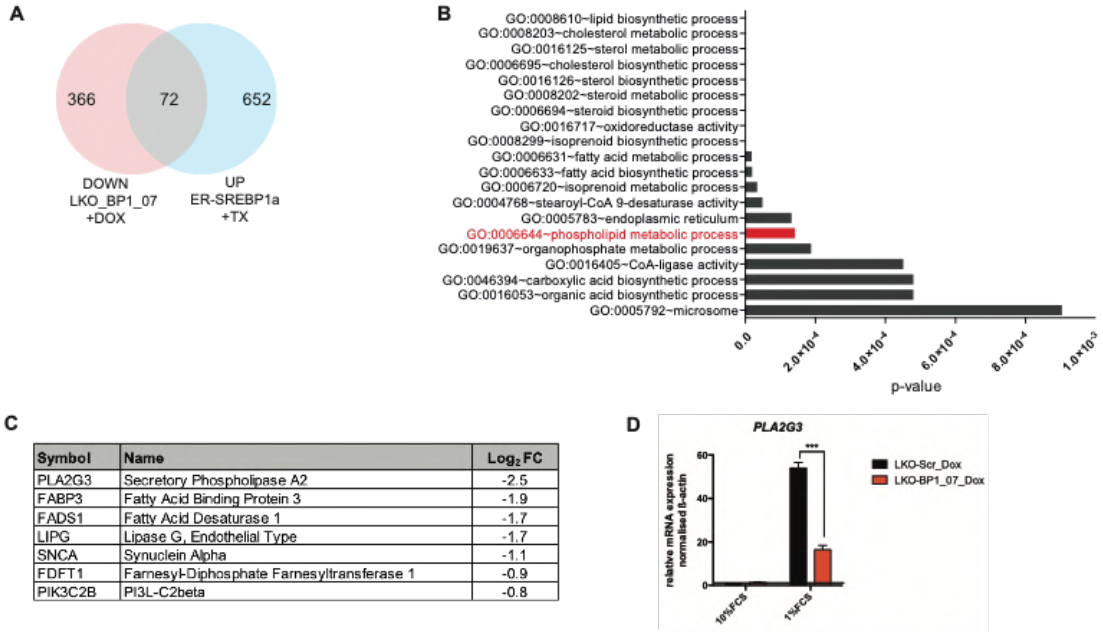

Symbol	Name	Log_2 FC
PLA2G3	Secretory Phospholipase A2	-2.5
FABP3	Fatty Acid Binding Protein 3	-1.9
FADS1	Fatty Acid Desaturase 1	-1.7
LIPG	Lipase G, Endothelial Type	-1.7
SNCA	Synuclein Alpha	-1.1
FDFT1	Farnesyl-Diphosphate Farnesyltransferase 1	-0.9
PIK3C2B	PI3L-C2beta	-0.8

Figure 4.11: SREBP1 regulates genes mapping to fatty acid and cholesterol biosynthesis and phospholipid metabolic processes

A) Venn diagram showing genes downregulated upon SREBP1 silencing (LKO_BP1_07 + DOX, RNAseq data) and upregulated upon SREBP1 activation (ER-SREBP1a + TX, Illumina bead array, data from Lewis et al.) in U87 cells. 72 genes were found to be regulated in both datasets.
B) Gene ontology (GO) pathway enrichment analysis of the 72 genes list.
C) Log_2-fold change (log_2 FC) of genes in the phospholipid metabolic process GO term upon SREBP1 knockdown.
D) qRT-PCR showing mRNA levels of *PLA2G3*. mRNA levels are shown relative to 10% FCS condition of the control. RNA samples from the experiments described in 4.10 were used to perform qPCR. Bars represent mean ± SEM (n=3). p-values were calculated using a two tailed student's t-test (p-values are represented as *** ≤ 0.001).

4.2.2 Validation of PLA2G3 as SREBP1 target gene

The reduction in mRNA levels of PLA2G3 observed upon knockdown of SREBP1 was confirmed using U87 cells expressing shRNA sequences shBP1_01 and 06 in the pLT3-GEPIR vector system. U87 cells with LT3-Renilla, LT3- BP1_01 and LT3-BP1_06 were treated with 2.25µM Dox or solvent (ethanol) in medium containing 10% FCS for 72 hours and incubated in medium containing 1% or 10% FCS with 2.25 µM Dox or solvent (ethanol) for further 24 hours (as shown in Fig 4.3A). WB analysis

showed that protein levels of PLA2G3 were reduced upon knockdown of SREBP1 in both 10% and 1% FCS samples (Fig 4.12A). PLA2G3 protein is detected as several bands representing different glycosylated forms, with a sharp band at 53 kDa (Murakami *et al.*, 2005). Interestingly, the experiment also showed that the strong induction of *PLA2G3* mRNA observed after exposure to medium containing 1% FCS (Fig. 4.11D) was not accompanied by a respective induction of PLA2G3 protein (Fig. 4.12A). However, mRNA levels of *PLA2G3* were reduced by all three shRNA sequences targeting SREBP1 in cells cultured in 1% FCS (Fig 4.12B).

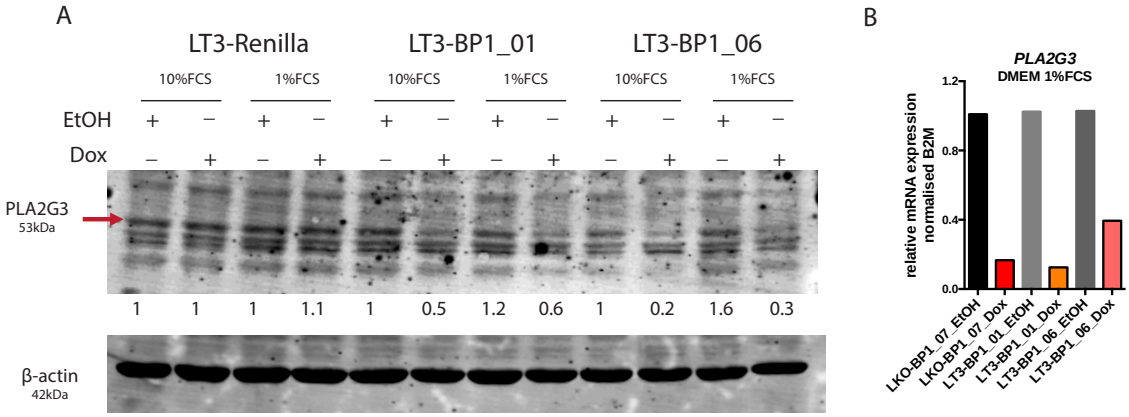

Figure 4.12: Decrease in PLA2G3 protein and mRNA levels upon SREBP1 knockdown

A) WB showing protein levels of PLA2G3 upon knockdown of SREBP1. Cells expressing shRNA sequences targeting SREBP1 (LT3-BP1_01 and LT3-BP1_06) or non-targeting controls (shRenilla) were seeded in 10% FCS media and treated with 2.25 µM Dox or ethanol (solvent control) for 72 hours. The cells were then washed with PBS and media was changed to 10% or 1% FCS with 2.25 µM Dox or ethanol (solvent control) for the last 24 hours. Signal intensities are normalized to β-actin and relative to the control sample. Red arrow shows the 53kDa band for PLA2G3 according to the predicted protein size and the specification sheet of the antibody.

B) qRT-PCR showing mRNA levels of *PLA2G3* upon SREBP1 knockdown in 1% FCS medium. Cells expressing shRNA sequences targeting SREBP1 (LKO-BP1_07, LT3-BP1_01 or LT3-BP1_06) were treated as described in A. Bars represent relative mRNA expression normalised to B2M (n=1).

The duration of Dox treatment needed to efficiently deplete *SREBF1* mRNA and cause an optimal reduction in target gene expression was also investigated. U87 LKO-Scr and LKO-BP1_07 cells were grown in medium containing 10% FCS and treated with 2.25 µM Dox for 0, 48 and 72 hours and then incubated with medium containing 0% FCS with 2.25 µM Dox for an additional 24 hours. It was observed that 96 hours of Dox treatment resulted in an 80% reduction of SREBF1 mRNA and a 60% reduction

in SCD expression (Fig 4.13A and B). Moreover, *PLA2G3* expression was reduced by about 50% after 96 hours of Dox treatment (Fig 4.13C).

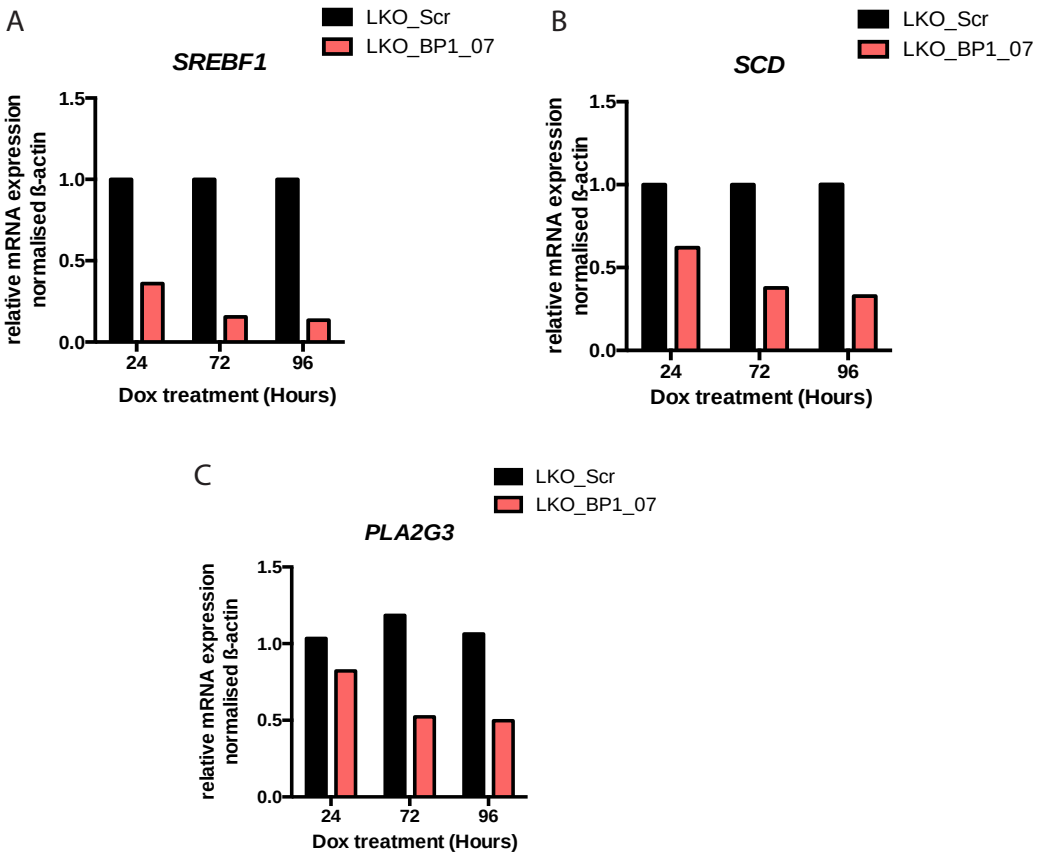

Figure 4.13: Time course of doxycycline treatment to induce knockdown of SREBF1 and downregulation of SCD and PLA2G3

A) qRT-PCR showing mRNA levels of *SREBF1* upon knockdown of SREBP1. Cells expressing LKO-Scr and LKO-BP1_07 were treated with Dox for the indicated time intervals. Cells were seeded in 10%FCS media and treated with 2.25 µM Dox for 0, 24, 48 and 72 hours. The cells were then washed with PBS and media was changed to media containing 0% FCS with 2.25 µM Dox for the last 24hours. Bars represent relative mRNA expression normalised to beta-actin (n=1).
B) qRT-PCR showing mRNA levels of *SCD* under the same conditions as in (A).
C) qRT-PCR showing mRNA levels of *PLA2G3* under the same conditions as in (A).

U87 cells with shRNAs targeting *PLA2G3* expressed from the pLT3-GEPIR vector were also generated, with the shRNA sequences obtained from Fellmann et al (Fellmann *et al.*, 2013). U87 shRen, shPLA2G3_01 and shPLA2G3_05 cells were

grown in 10% FCS with 2.25 µM Dox for 72 hours, cells were washed with PBS and the medium was changed to media containing 1% FCS with 2.25 µM Dox. A reduction in both PLA2G3 protein and mRNA levels was observed upon induction of shRNA expression (Fig 4.14A and B). Also, this analysis showed that the sharp band at 53 kDa was reduced upon PLA2G3 knockdown similar to what was observed after SREBP1 silencing (Fig 4.14A). However, PLA2G3 knockdown also reduced additional bands detected with the antibody, while SREBP1 knockdown mainly reduced the 53 kDa band (compare Fig 4.12A and 4.14A). It is possible that SREBP1 only controls the expression of specific products of the *PLA2G3* gene. Moreover, PLA2G3 is a secreted protein, and the different bands could represent differentially glycosylated forms (Murakami *et al.*, 2005). Further work is required to determine the mechanism by which SREBP1 selectively controls the expression of specific PLA2G3 forms.

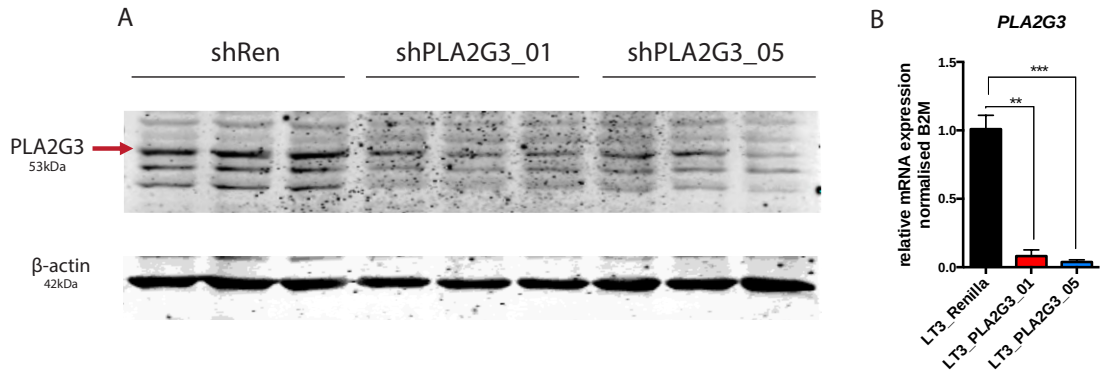

Figure 4.14: Decrease in PLA2G3 protein and mRNA levels upon PLA2G3 knockdown

A) WB shows protein levels of PLA2G3 upon knockdown in 1% FCS medium. Cells expressing shRenilla, shPLA2G3_01 and 05 were seeded in 10%FCS media and treated with 2.25 µM Dox for 72hours. The cells were washed with PBS and media was changed to media containing 1% FCS with 2.25 µM Dox for 24hours. Three different replicates for each cell lines are shown.

B) qRT-PCR showing mRNA levels of *PLA2G3* upon knockdown under the same conditions as in (A). Bars represent mean ± SEM (n=3). p-values were calculated using a two tailed student's t-test (p-values are represented as ** ≤ 0.01 and *** ≤ 0.001).

Time course of doxycycline treatment to efficiently reduce *PLA2G3* mRNA was tested by treating U87 shRen, shPLA2G3_01 and shPLA2G3_05 in medium containing 10%FCS and treated with 2.25 µM Dox for 0, 48 and 72 hours and then incubated with medium containing 0%FCS with 2.25 µM Dox for an additional 24 hours. It was evident that 96hours of Dox treatment was required to achieve about 80% reduction of *PLA2G3* expression with both shRNA sequences (Fig 4.15).

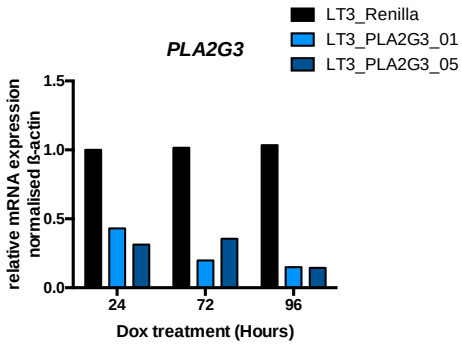

Figure 4.15: Time course of doxycycline treatment to induce knockdown of PLA2G3

qRT-PCR showing mRNA levels of *PLA2G3* upon knockdown. Cells were treated with 2.25 µM Dox for the indicated times. Cells were seeded in 10% FCS media and treated with 2.25 µM Dox for 0, 48 and 72 hours. The cells were then washed with PBS and media was changed to media containing 0% FCS with 2.25 µM Dox for an additional 24hours. Bars represent relative mRNA expression normalised to beta-actin (n=1).

The effect of PLAG3 silencing on cell viability was also determined. For this, cells expressing shRNA sequences targeting PLA2G3 (LT3-PLA2G3_01 and LT3-PLA2G3_05) or control LT3-Renilla were grown in medium containing 10% FCS with 2.25 µM Dox for 72 hours and cells were washed with PBS and the medium was changed to media containing 0% FCS with 2.25 µM Dox. Despite the strong induction of PLA2G3 expression under reduced serum conditions (see Fig. 4.11D), cell viability was not reduced upon PLA2G3 silencing (Fig 4.16A-B).

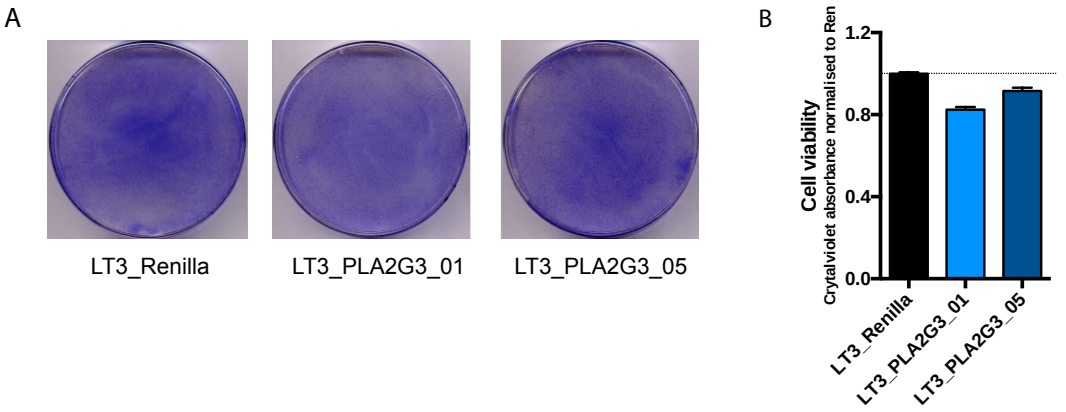

Figure 4.16: Cell viability of U87 cells upon PLA2G3 knockdown under serum starvation

A) Crystal violet staining of U87 cells expressing shRNAs targeting PLA2G3 (LT3-PLA3G3_01 and LT3-PLA2G3_05) or control (LT3-Renilla) were treated with 2.25 µM Dox for 72 hours in medium containing 10% FCS. Cells were washed with PBS and the medium was changed to media

containing 0% FCS with 2.25 µM Dox for an additional 24hours. Cells were then fixed and stained with crystal violet.

B) Quantification of crystal violet staining shown in (A). The O.D. values are normalized to the shRenilla control. Bars represent mean ± SEM (n=1, each in technical triplicate).

Together, the results presented in this chapter define the transcriptional network of SREBP1 in GB cells. They identify SCD and PLA2G3 as important target genes of SREBP1 in this cancer entity and demonstrate that SREBP1-dependent induction of SCD is essential for GB cells to prevent the induction of ER stress and support cell viability under conditions of reduced exogenous lipid availability. In contrast, the results indicate that PLA2G3 is not essential for GB cell viability *in vitro*, but that this enzyme may support a non-cell autonomous function that could only be relevant *in vivo*. Further experiments, for example exposing cells to different growth conditions, are required to reveal a potential role of PLA2G3 in GB cells viability *in vitro*.

4.3 Analysis of total fatty acids and lipid profile in U87 cells upon SREBP1 and PLA2G3 knockdown

SREBP1 transcriptionally controls genes involved in fatty acid biosynthesis and upon its knockdown a significant reduction of these genes was observed (see Fig 4.9 to 4.11). It has been previously shown that depletion of SREBP1 strongly impacts cellular fatty acid and lipid species in immortalised human retinal pigment epithelial cells (Griffiths *et al.*, 2013). Hence, analysing changes in fatty acids and lipids upon SREBP1 and PLA2G3 knockdown in U87 cells might help to better understand their potential roles in the regulation of GB growth.

4.3.1 Analysis of global changes in fatty acids and lipids

Thin layer chromatography (TLC) was performed on lipid extracts obtained from U87 cells expressing either LKO-Scr or LKO-BP1_07. Cells were treated with 2.25 µM Dox for 72 hours in medium containing 10% FCS, after which cells were washed with PBS and the medium was changed to media containing 1% FCS with 2.25 µM Dox. Lipids were extracted using Butanol and methanol (BuMe) extraction method. Levels of total phosphatidylcholines, sphingomyelins, cholesterol, free fatty acids, triglycerides and cholesterol esters were analysed, using respective standards. No significant changes in the total levels of these lipid/ fatty acid species were observed (Fig 4.17). Hence, it was concluded that a more detailed profiling of fatty acids and lipid classes should be performed.

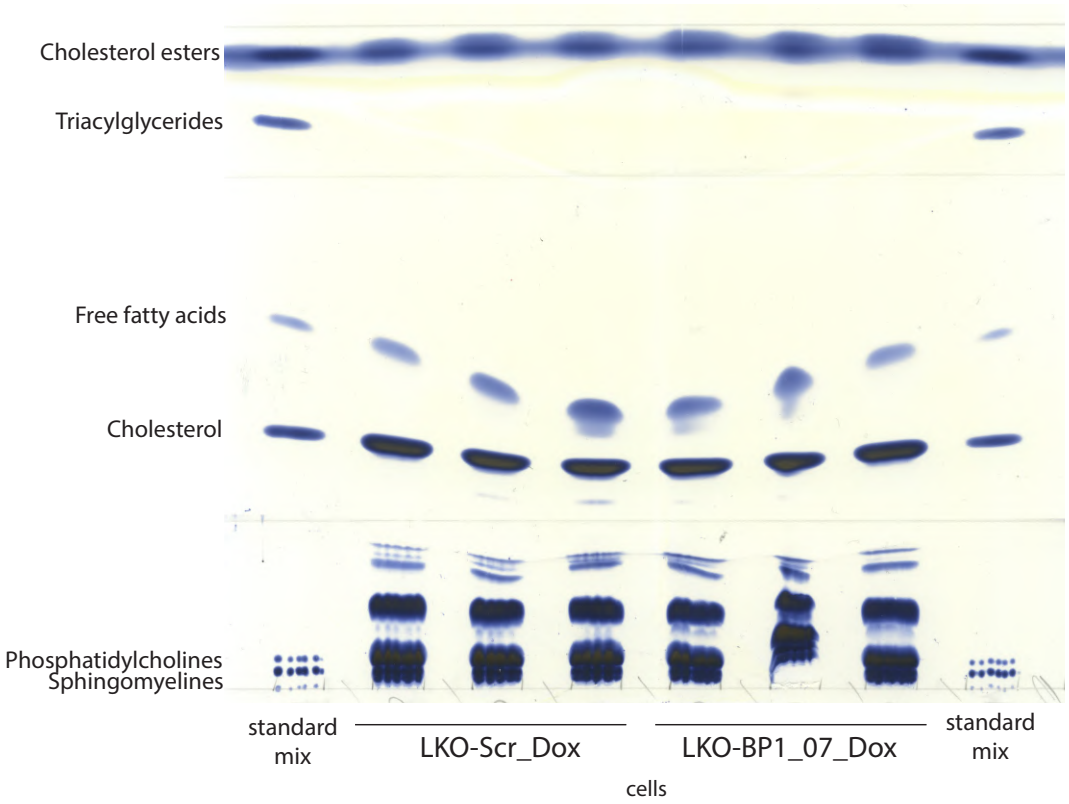

Figure 4.17: Lipid profiling by thin layer chromatography (TLC) in U87 cells upon SREBP1 knockdown

TLC showing different lipid species in control and SREBP1 knockdown cells. Cells expressing shScr (LKO-Scr) and shSREBP1_07 (LKO-BP1_07) were grown in 10%FCS with 2.25 µM Dox for 72 hours. Subsequently, cells were washed with PBS and the medium was changed to media containing 1% FCS with 2.25 µM Dox for a further 24 hours. Total lipids were extracted and resolved by TLC with cholesterol esters, triacylglycerides, free fatty acids, cholesterol, phosphatidylcholines and sphingomyelins as standard (n=3).

4.3.2 Analysis of changes in fatty acid profile upon SREBP1 knockdown

To analyse whether SREBP1 depletion causes alterations in the fatty acid composition in GB cells, total (hydrolysed) fatty acids were extracted from U87 cells expressing shBP1_07 (LKO-BP1_07). Cells were treated with 2.25 µM Dox or solvent (ethanol) for 72 hours in media containing 10% FCS and subsequently washed with PBS, after which the medium was changed to media containing 0% FCS with 2.25 µM Dox or solvent (ethanol) for an additional 24 hours. Fatty acids were extracted using Bligh and Dyer two phase extraction and analysed by MS following direct injection. Spectra were used to calculate relative contribution of each fatty acid species to the total fatty acid pool (Fig. 4.18A).

Upon SREBP1 knockdown, a significant downregulation of the mono-unsaturated fatty acids palmitoleic acid (C16:1) and oleic acid (C18:1) was observed, while the saturated fatty acid palmitic acid (C16:0) was upregulated (Fig 4.18A). This confirms earlier results in human retinal pigment epithelial cells (Griffiths *et al.*, 2013). A relative accumulation of essential fatty acids, including linoleic acid (C18:2), linolenic acid (C18:3), di-homo-linolenic acid (C20:3), arachidonic acid (C20:4), eicosapentaenoic acid (C20:5), docosapentaenoic acid (C22:5) and docosahexaenoic acid (C22:6) was also observed (Fig 4.18A). Furthermore, the ratios of monounsaturated to saturated fatty acids (C16:1/C16:0 and C18:1/C16:0) were also reduced upon SREBP1 silencing (Fig 4.18B), consistent with a reduction in the activity of the D9 fatty acid desaturase SCD and the fatty acid elongase ELOVL6. In addition, the observed decrease in the ratio of eicosadienoic acid and linoleic acid (C20:2/C18:2) (Fig. 4.18B) could be indicative of reduced ELOVL5 activity which is also a known target gene of SREBP1.

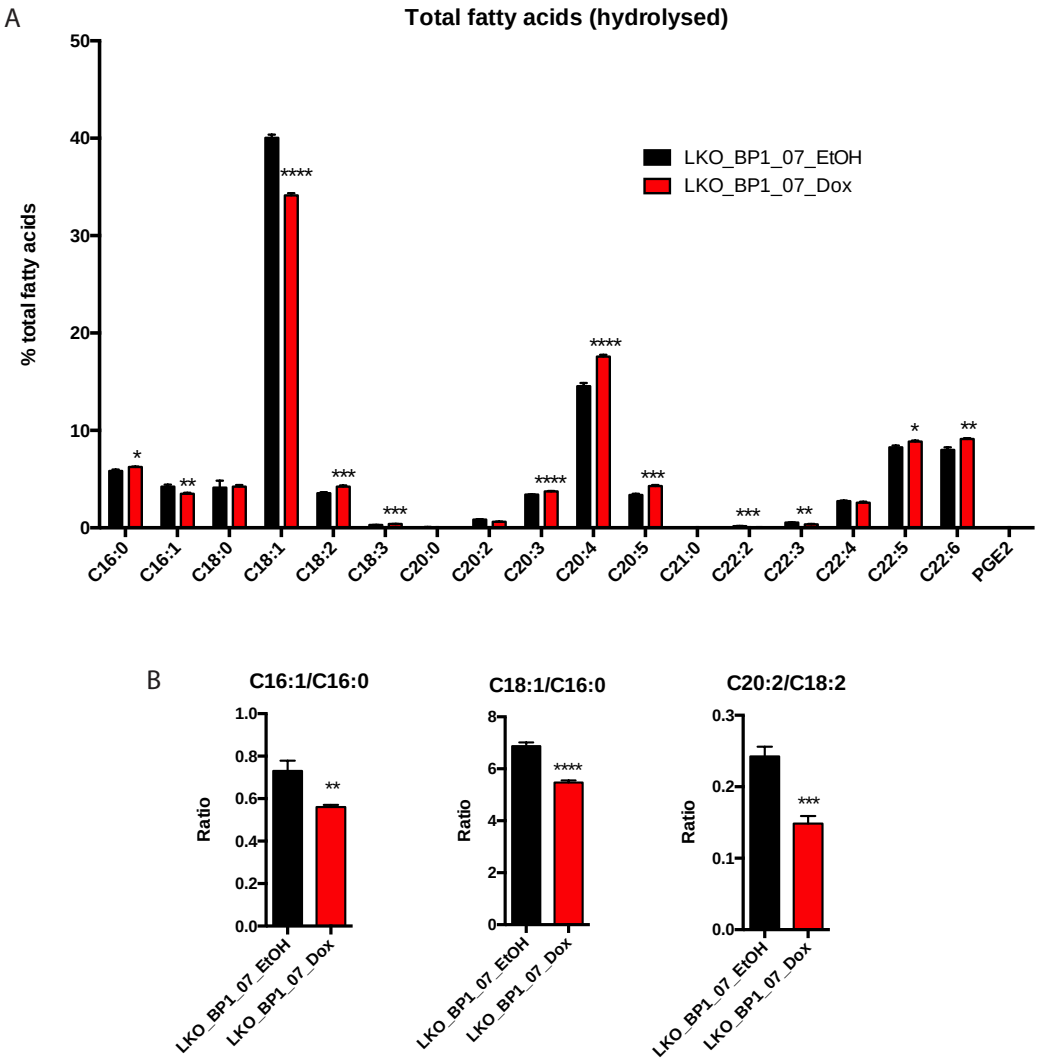

Figure 4.18: Changes in total fatty acid profile in U87 cells upon SREBP1 knockdown with the pLKO-Tet-On vector system

A) Overall changes in total fatty acid composition upon SREBP1 knockdown. Cells with shSREBP1_07 (LKO-BP1_07) were treated with 2.25 µM Dox or ethanol (solvent control) in medium containing 10%FCS for 72 hours. Cells were washed with PBS and the medium was changed to media containing 0% FCS with 2.25 µM Dox or ethanol (solvent control) for 24hours. Fatty acids were extracted and analysed by MS following direct injection. Bars represent mean ± SEM (n=3).

B) Changes in the ratios of palmitoleic acid over palmitic acid (C16:1/C16:0), oleic acid over palmitic acid (C18:1/C16:0) and eicosadienoic acid over linoleic acid (C20:2/C18:2) upon SREBP1 knockdown. Bars represent mean ± SEM (n=3).
p-values were calculated using a two tailed student's t-test (p-values are represented as ** ≤ 0.01, *** ≤ 0.001 and **** ≤ 0.0001).

To confirm these results, total (hydrolysed) fatty acids were extracted from U87 cells expressing shRenilla (LT3-Ren), shBP1_01 (LT3-BP1_01) and shBP1_06 (LT3-BP1_06). Cells were treated with 2.25 µM Dox for 72 hours in media containing 10%

FCS. Subsequently, cells were washed with PBS and the medium was changed to media containing 0% FCS with 2.25 μM Dox for 24 hours. Fatty acids were extracted and analysed by MS following direct injection. Spectra were used to calculate relative contribution of each fatty acid species to the total fatty acid pool (Fig. 4.19A). Upon SREBP1 knockdown, the same changes in oleic acid (C18:1), palmitic acid (C16:0), linoleic acid (C18:2), linolenic acid (C18:3), arachidonic acid (C20:4), eicosapentaenoic acid (C20:5), docosapentaenoic acid (C22:5) and docosahexaenoic acid (C22:6) previously observed with the LKO vector system were confirmed (Fig 4.19A). However, levels of eicosadienoic acid (C20:2), di-homo-linolenic acid (C20:3), docosadienoic acid (C22:2) and docosatrienoic acid (C22:3) were reduced following SREBP1 depletion using the LT3-GEPIR vector system (Fig 4.19A). Similar to the results observed with the LKO vector system, the ratios of C18:1/C16:0 and C20:2/C18:2 were also decreased, again consistent with a reduction in SCD and ELOVL6 activity following SREBP1 depletion (Fig 4.19B).

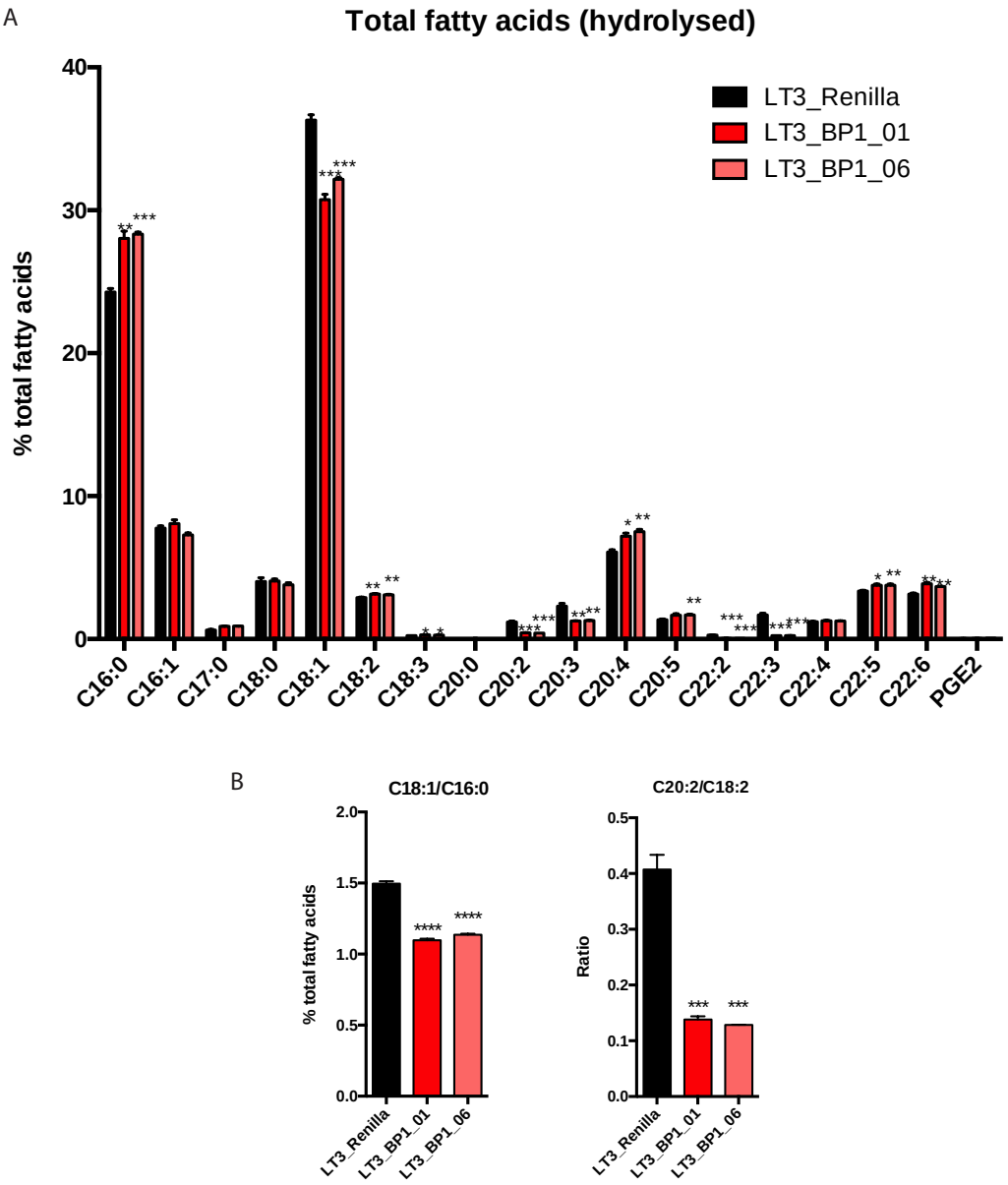

Figure 4.19: Changes in total fatty acid profile in U87 cells upon SREBP1 knockdown using the pLT3-GEPIR vector system

A) Overall changes in total fatty acid profile upon SREBP1 knockdown with two shRNAs sequences targeting *SREBF1* (LT3-BP1_01 and LT3-06) compared to a non-targeting control (LT3-Renilla). Cells were grown in medium containing 10% FCS with 2.25 µM Dox for 72 hours, washed with PBS and the medium was changed to media containing 0% FCS with 2.25 µM Dox for 24 hours. Fatty acids were extracted and analysed by MS following direct injection. Bars represent mean ± SEM (n=3).

B) Ratio of oleic acid over palmitic acid (C18:1/C16:0) and eicosadienoic acid over linoleic acid (C20:2/C18:2) upon SREBP1 knockdown. Bars represent mean ± SEM (n=3).
p-values were calculated using a two tailed student's t-test (p-values are represented as * ≤ 0.05, ** ≤ 0.01, *** ≤ 0.001 and **** ≤ 0.0001).

4.3.3 Analysis of changes in fatty acid profile upon PLA2G3 knockdown and comparison to SREBP1 knockdown

In addition, changes in total (hydrolysed) fatty acid levels were investigated upon PLA2G3 knockdown in U87 cells. For this, cells expressing either shRenilla (LT3-Renilla) or two independent sequences targeting PLA2G3 (LT3-PL2G3_01 or LT3-PLA2G3_05) were treated with 2.25 µM Dox for 72 hours in media containing 10% FCS. After this, cells were washed with PBS and the medium was changed to media containing 0% FCS with 2.25 µM Dox for 24 hours. Fatty acids were extracted and analysed by MS following direct injection. Spectra were used to calculate relative contribution of each fatty acid species to the total fatty acid pool (Fig. 4.20). This analysis showed that levels of the mono-unsaturated fatty acid oleic acid (C18:1) was moderately decreased upon PLA2G3 depletion (Fig 4.20). The essential fatty acids linoleic acid (C18:2), arachidonic acid (C20:4), eicosapentaenoic acid (C20:5), docosapentaenoic acid (C22:5) and docosahexaenoic acid (C22:6) were increased, while eicosadienoic acid (C20:2), di-homo-linolenic acid (C20:3) and docosatrienoic acid (C22:3) were reduced (Fig 4.20). However, the increase in C22:5 and C22:6 was only significant in one of the two sequences.

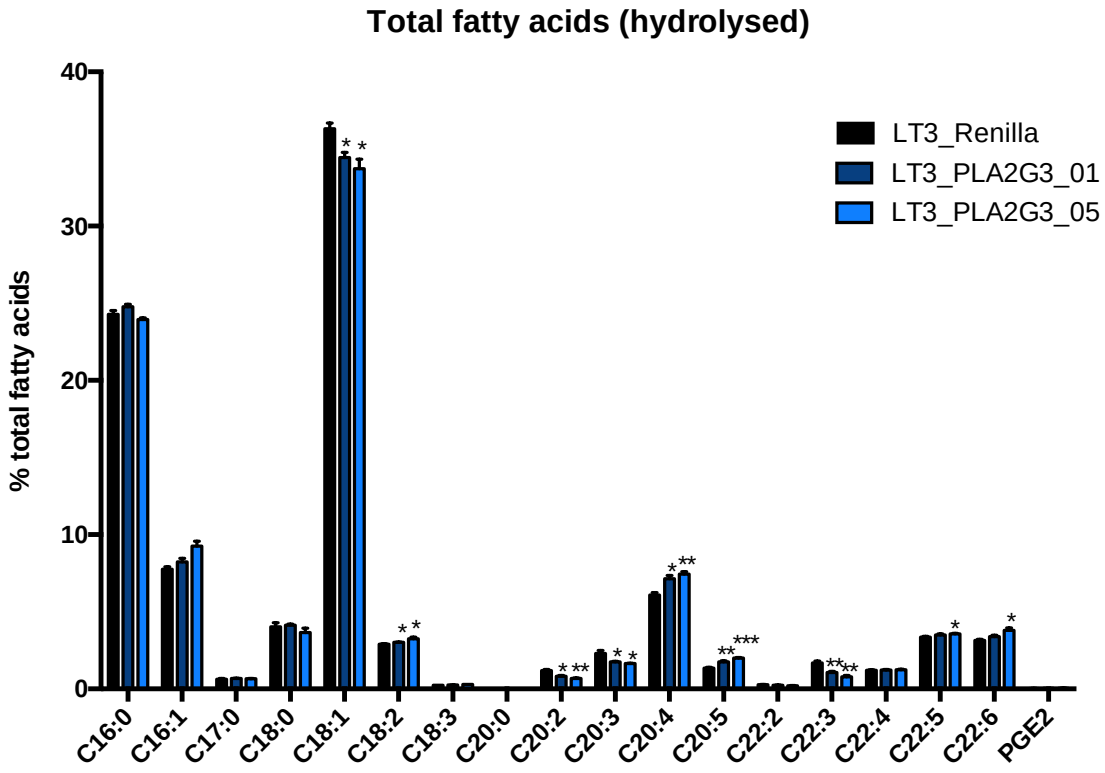

Figure 4.20: Changes in total fatty acid profile in U87 cells upon PLA2G3 knockdown with the pLT3-GEPIR vector system

Overall changes in total fatty acid profile upon PLA2G3 knockdown using two independent shRNA sequences (LT3-PLA2G3_01 and LT3-PLA2G3_05) compared to a non-targeting control (LT3-Renilla). Cells were grown in 10% FCS with 2.25 µM Dox for 72 hours, washed with PBS and the medium was changed to media containing 0% FCS with 2.25 µM dox for 24 hours. Fatty acids were extracted and analysed by MS following direct injection. Bars represent mean ± SEM (n=3). p-values were calculated using a two tailed student's t-test (p-values are represented as * ≤ 0.05, ** ≤ 0.01 and *** ≤ 0.001).

Direct comparison of the effect of PLA2G3 and SREBP1 silencing on cellular fatty acid profiles revealed that the decrease in oleic acid (C18:1) and the increase in linoleic acid (C18:2), arachidonic acid (C20:4) and eicosapentaenoic acid (C20:5) was similar after SREBP1 or PLA2G3 knockdown (Fig 4.21). However, the increase in C20:5 after induction of shBP1_01, while showing a similar trend as the other samples, failed to reach significance (Fig. 4.21, right graph).

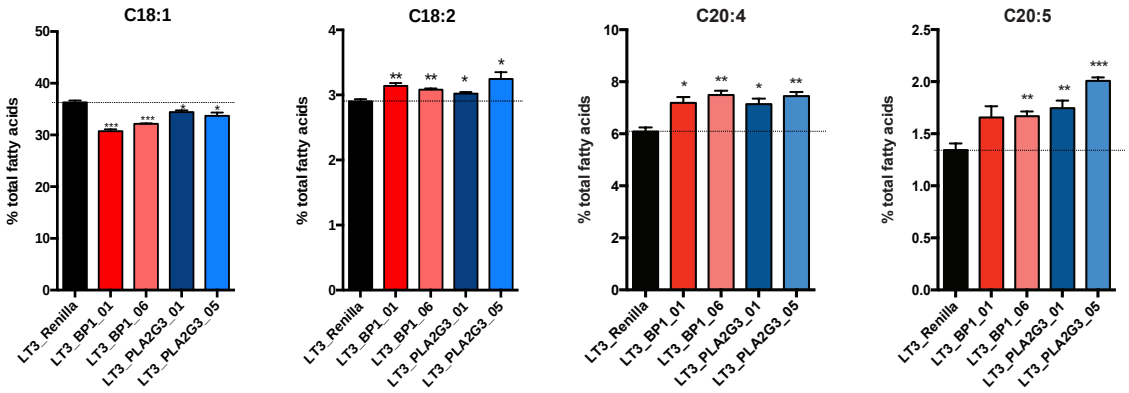

Figure 4.21: Comparison of changes in mono- and polyunsaturated fatty acids upon SREBP1 or PLA2G3 knockdown

Decrease in the mono-unsaturated fatty acid oleic acid (C18:1) and increase in the polyunsaturated fatty acids linoleic acid (C18:2), arachidonic acid (C20:4) and eicosapentaenoic acid (C20:5) upon SREBP1 or PLA2G3 knockdown in the experiments described in Figs. 4.19 and 4.20. Bars represent mean ± SEM (n=3).
p-values were calculated using a two tailed student's t-test (p-values are represented as * ≤ 0.05, ** ≤ 0.01 and *** ≤ 0.001).

4.3.4 Analysis of changes in cellular lipids upon SREBP1 knockdown

To understand the implications of SREBP1 knockdown on different cellular lipid species, lipidomic analysis was performed in U87 cells expressing shScr or shBP1_07 sequences in the LKO vector system. Cells were treated with 2.25 µM Dox for 72 hours in media containing 10% FCS. After this, cells were washed with PBS and the medium was changed to media containing 1% FCS with 2.25 µM Dox for 24 hours. Lipids were extracted using the butanol/methanol method and analysed by LC-MS. As no standards for every lipid class were used in this experiment, the data is presented as the fraction of each individual lipid species normalised to the total amount of lipids within each class. Only selected lipids that showed alterations after SREBP1 knockdown are shown. It should be noted that this was an exploratory experiment to optimise extraction and analysis procedures. For the phosphatidylcholine (PC) lipid class, a significant increase in the fraction of PC-(32:0), PC-(34:0), PC-(36:0) and PC-(38:0) was observed following SREBP1 knockdown, while the fraction of PC-(32:2) and PC-(36:2) were reduced (Fig 4.22A). In addition, among the phosphatidylethanolamine (PE) species, a decrease in PE-(32:2) and PE-(36:2) and a significant increase in PE-(38:4) was observed (Fig 4.22B).

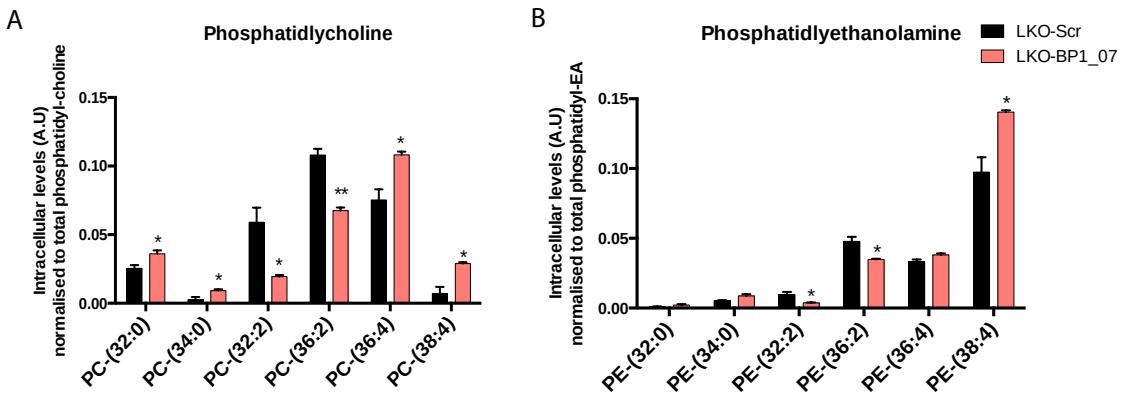

Figure 4.22: Changes in selected phosphatidylcholine and phosphatidylethanolamine species upon SREBP1 knockdown

A) Distribution of phosphatidylcholine (PC) species upon SREBP1 knockdown. Cells expressing shScr (LKO-Scr) and shSREBP1_07 (LKO-BP1_07) were grown in 10%FCS with 2.25 µM Dox for 72 hours. Cells were then washed with PBS and the medium was changed to media containing 1% FCS with 2.25 µM Dox for 24 hours. Total lipids were extracted using butanol/methanol and analysed by LC-MS. Bars represent mean ± SEM (n=3).
B) Distribution of phosphatidylethanolamine (PE) species upon SREBP1 knockdown. Cells were treated as described in (A).
p-values were calculated using a two tailed student's t-test (p-values are represented as * ≤ 0.05, ** ≤ 0.01, *** ≤ 0.001 and **** ≤ 0.0001).

In the lysophosphatidylcholine (LPC) lipid class, small but significant accumulation of LPC-(16:0), LPC-(18:0), LPC-(18:2), LPC-(18:3) and LPC-(20:3) was observed, while the mono-unsaturated species LPC-(16:1) and LPC-(18:1) were reduced (Fig 4.23A). In the lysophosphatidylethanolamine (LPE) class, there was a slight accumulation of LPE-(18:0), LPE-(18:2), LPE-(C18:3), LPE-(20:0), and a reduction in LPE-(22:5) and LPE-(22:6) (Fig 4.23B). Interestingly, LPE-(20:4), containing arachidonic acid as the acyl group, was increased upon SREBP1 depletion (Fig 4.23B).

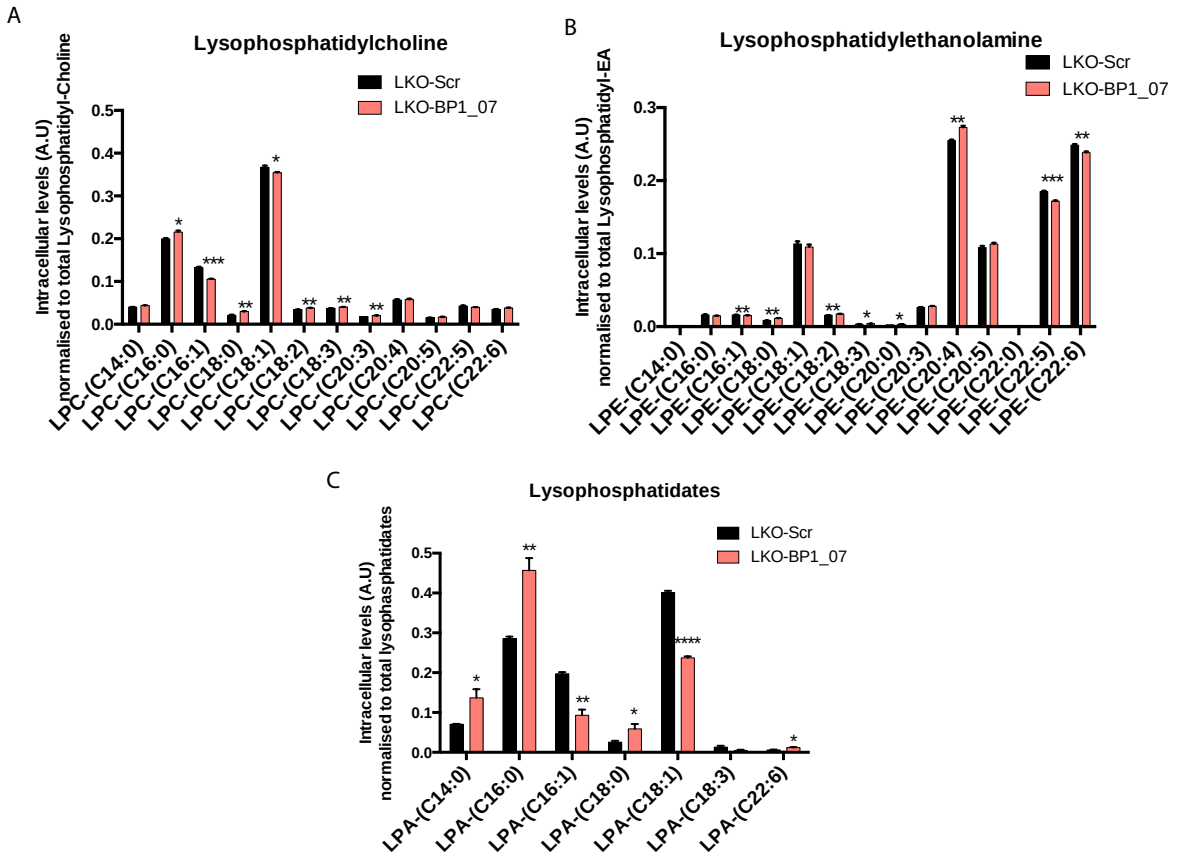

Figure 4.23: Changes in lysophospholipid species upon SREBP1 knockdown

A) Distribution of lysophosphatidylcholine (LPC) species containing fatty acids with different chain length and degree of saturation upon SREBP1 knockdown in the same samples described in Fig. 4.22.

B) Distribution of different lysophosphatidylethanolamine (LPE) species upon SREBP1 knockdown.

C) Distribution of different lysophosphatidate (LPA) species upon SREBP1 knockdown.

Bars represent mean ± SEM (n=3). p-values were calculated using a two tailed student's t-test (p-values are represented as * ≤ 0.05, ** ≤ 0.01, *** ≤ 0.001 and **** ≤ 0.0001).

In addition, the experiment showed a significant accumulation of lysophosphatidates (LPA) species containing saturated fatty acids, in particular LPA-(14:0), LPA-(16:0), LPA-(18:0), while LPA species containing mono-unsaturated fatty acids, i.e., LPA-(16:1) and LPA-(18:1), were strongly reduced (Fig 4.23C).

Due to the specific reduction in unsaturated fatty acid species within the total fatty acid pool observed upon SREBP1 knockdown (see Fig. 4.18), the ratio of unsaturated/saturated lipid molecules of the same carbon chain length was analysed to determine the implications of altered fatty acid desaturation on each lipid class. These ratios are shown as a heat map displaying the log2 fold change between

SREBP1 knockdown and control samples (Fig 4.24). This analysis revealed an overall reduction of unsaturated lipid species following SREBP1 depletion. Importantly, a major reduction in lipid desaturation was observed across all lipid classes, in particular LPA, PC and PE. In contrast, desaturation in LPC and LPE species was only moderately reduced.

As LPA is also an intermediate in the synthesis of PC and PE, this result suggests that SREBP1 is required for the generation of mono-unsaturated fatty acids to provide substrates for *de novo* synthesis of phosphoglycerides, including PC and PE. In contrast, LPC and LPE are produced by the removal of an acyl-group from PC and PE, respectively, by the action of different phospholipases, including PLA2G3, as part of the lipid remodelling process. Here, the changes in desaturation were much less pronounced.

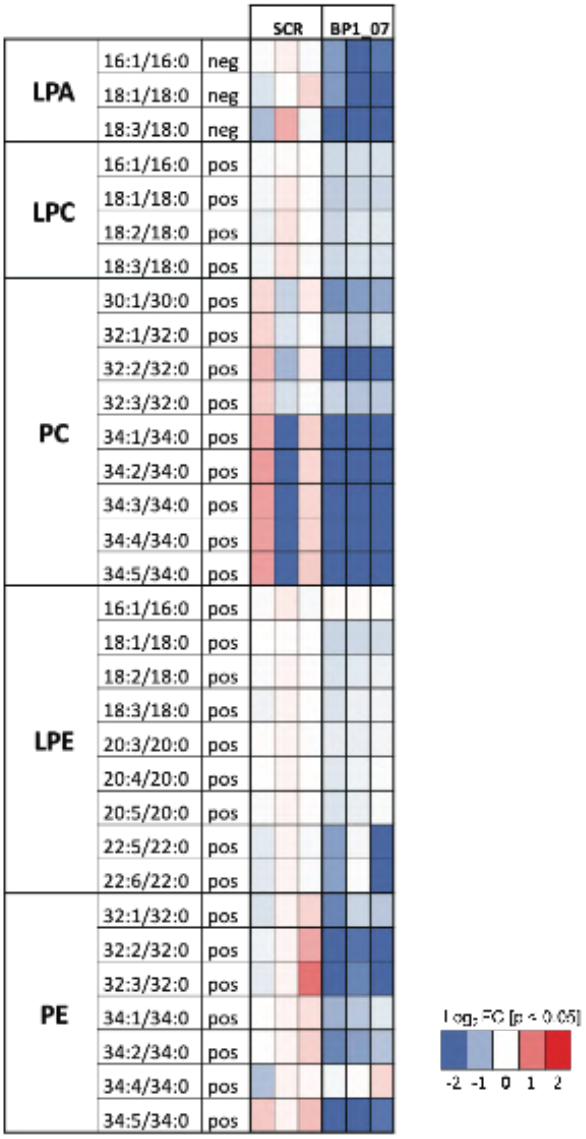

Figure 4.24: Decrease in the ratio of desaturated/saturated lipid species upon SREBP1 knockdown

Heat map showing the log2 fold change of the ratios of unsaturated over saturated lipid species in SREBP1 knockdown compared to control cells. Values were calculated from data shown in Fig 4.22 and 4.23.

4.3.5 Analysis of changes in different lipid species upon PLA2G3 knockdown and comparison to knockdown of SREBP1

In order to define similarities and differences in the effect of SREBP1 and PLA2G3 silencing on cellular lipid composition, changes in several lipid classes upon PLA2G3 knockdown were analysed. U87 cells expressing shRen (LT3-Renilla), shPLA2G3_01 (LT3-PLA2G3_01) and shPLA2G3_05 (LT3-PLA2G3_05) were treated with 2.25 µM Dox for 72 hours in media containing 10% FCS. Cells were then washed with PBS and the medium was changed to media containing 1% FCS with 2.25 µM Dox for 24 hours. Lipids were extracted using the butanol/methanol method and analysed by LC-MS. In contrast to the results observed with SREBP1, no consistently significant changes in PC, PE, LPC and LPA were found upon PLA2G3 knockdown (Fig 4.25A-E). The only significant changes were small reductions in LPE-(16:1), LPE-(18:2) and LPE-(20:3) (Fig 4.25D).

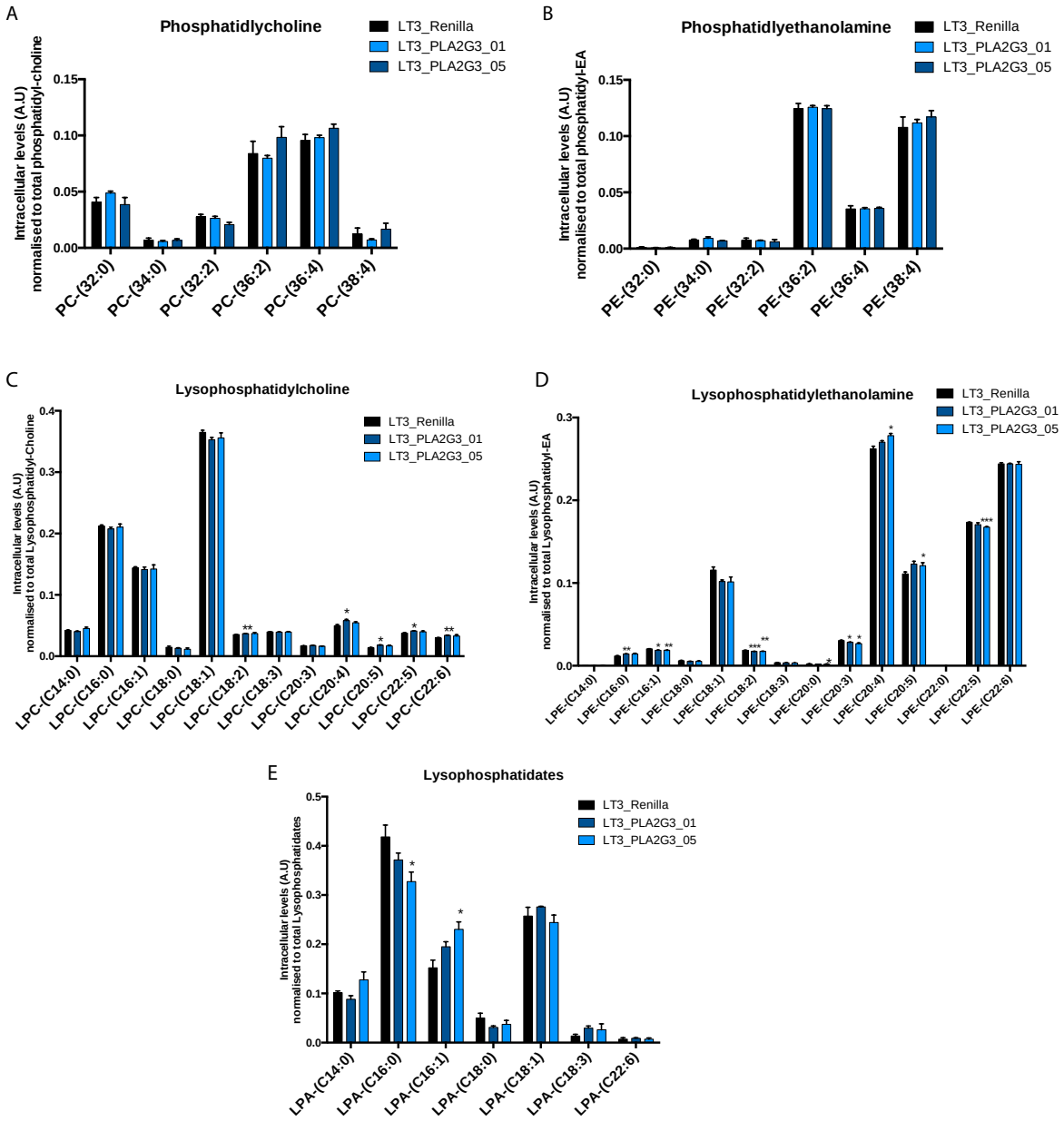

Figure 4.25: Changes in phosphatidylcholine, phosphatidylethanolamine and lysophospholipid species upon PLA2G3 knockdown

A) Distribution of phosphatidylcholines (PC) species upon PLA2G3 knockdown. Cells expressing shRenilla (LT3_Renilla), shPLA2G3_01 (LT3_PLA2G3_01) and shPLA2G3_05 (LT3-PLA2G3_05) were grown in 10% FCS with 2.25 µM Dox for 72 hours. Cells were then washed with PBS and the medium was changed to media containing 1% FCS with 2.25 µM Dox for 24 hours. Total lipids were extracted using butanol/methanol and analysed by LC-MS.
B) Distribution of phosphatidylethanolamine (PE) species upon PLA2G3 knockdown.
C) Distribution of lysophosphatidylcholines (LPC) species upon PLA2G3 knockdown.
D) Distribution of lysophosphatidylethanolamine (LPE) species upon SREBP1 knockdown.
E) Distribution of lysophosphatidates (LPA) species upon SREBP1 knockdown.
Bars represent mean ± SEM (n=3). p-values were calculated using a two tailed student's t-test (p-values are represented as * ≤ 0.05, ** ≤ 0.01, *** ≤ 0.001 and **** ≤ 0.0001).

The experiments described in this chapter demonstrate the substantial impact of SREBP1 depletion on the cellular lipid pool. Importantly, SREBP1 depletion reduces the fraction of mono-unsaturated fatty acids, which can be observed in the total fatty acid pool but also in different species of membrane phospholipids and lysophospholipids. Interestingly, some membrane lipids containing poly-unsaturated fatty acids were increased upon SREBP1 silencing, suggesting that SREBP1 reduces the abundance of poly-unsaturated lipid species, mainly derived from exogenous essential fatty acids, such as linoleic acid and alpha-linoleic acid. Importantly, changing the abundance of poly-unsaturated fatty acid containing lipids in the plasma membrane could have important consequences of GB cells viability and migration. Furthermore, the results also reveal that modulation of PLA2G3, a target gene of SREBP1, does not phenocopy the effect of SREBP1 depletion on the cellular lipid pool. It is more likely that concomitant regulation of several SREBP1 target genes, most importantly SCD, is required to shape the cellular lipid pool downstream of SREBP1.

4.4 SREBP1 regulates tumour angiogenesis

GB tumours show rapid growth and are known to have extensive regions of tumour hypoxia and areas with reduced access to nutrients from the blood supply. These conditions might force tumour cells to induce *de novo* synthesis of necessary metabolites and produce angiogenesis-stimulating signalling molecules to have access to new blood vessels, which is a feature of these tumours (Jain *et al.*, 2007).

4.4.1 HUVEC sprouting and tube formation assay

As SREBP1 transcriptionally regulates the secreted phospholipase PLA2G3, which is involved in the production of lipid mediators (see Fig. 4.10A), it was investigated whether this function of SREBP1 could be involved in the modulation of angiogenesis. To test this hypothesis, conditioned medium (CM) was collected from U87 cells expressing shScr (LKO-Scr) or shBP1_07 (LKO-BP1_07) which had been grown in the presence of 2.25 μM Dox for 72 hours in media containing 10% FCS, washed with PBS and switched to basic endothelial growth medium (M200) with 2.25 μM Dox for 24 hours. This medium was then tested for its ability to induce the sprouting of primary human umbilical cord endothelial cells (HUVECs) embedded as spheroids in a collagen matrix. As positive controls for endothelial cell sprouting, vascular endothelial growth factor (VEGF), which is known to induce angiogenesis (Leung et al., 1989) and growth factor supplement (LSGS), a mixture of several pro-angiogenic factors, were used. Blank endothelial growth medium (M200) was used as a negative control to assess the functionality of the assay. Indeed, both VEGF and LSGS were able to induce strong endothelial cell sprouting while minimal or no sprouting was observed in M200 blank media (Fig 4.26A). Interestingly, CM from U87 cells expressing the non-targeting RNAi sequence (shScr) induced endothelial cell sprouting to a similar extent as VEGF or LSGS, indicating that U87 cells secrete pro-angiogenic factors (Fig 4.26B). Moreover, silencing of SREBP1 significantly reduced the ability of U87 cells to produce CM that induces HUVEC sprouting (Fig 4.26B-C).

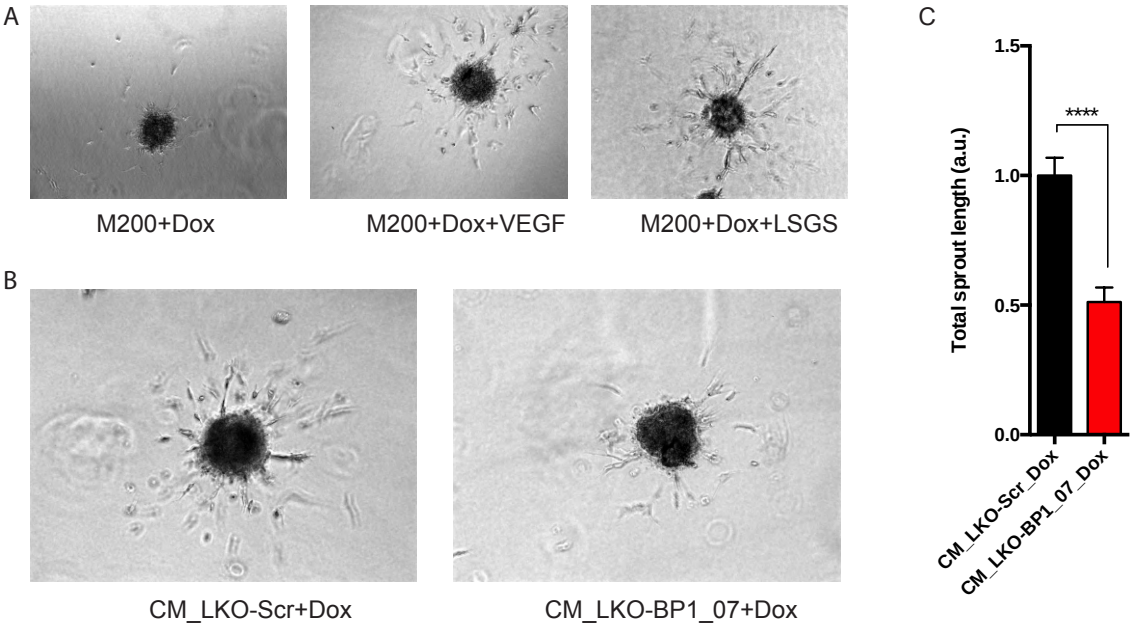

Figure 4.26: Silencing of SREBP1 reduces the ability of conditioned medium from U87 cells to induce the sprouting of primary human endothelial cells

A) Representative images of spheroids of HUVEC cells embedded in a collagen matrix and incubated with basic culture medium (M200) or medium supplemented with 50 ng/mL vascular endothelial growth factor (VEGF) or with full growth supplement 1% LSGS.

B) Representative images of spheroids of HUVEC cells embedded in a collagen matrix incubated with CM from U87 cells expressing shScr or shBP1_07. Cells were first grown in medium containing 10% FCS with 2.25 µM Dox for 72 hours, then washed with PBS and changed to M200 supplemented with 2.25 µM Dox for an additional 24 hours.

C) Quantification of spheroids treated as in B. 20 spheroids were used for the quantification in each condition. Total sprout length is shown as fold change normalized to CM from shScr control cells. p-values were calculated using a two tailed student's t-test (p-values are represented as **** ≤ 0.0001).

All spheroid images were taken at 10X magnification on a bright field microscope and quantified using Image J.

The results obtained by sprouting assays with SREBP1 knockdown using the shBP1_07 sequence in the LKO vector system were also re-confirmed by using all 3 shRNA sequences (shBP1_07, shBP1_01 and 06) in a tube formation assay. Again, U87 cells were grown with 2.25 µM Dox or solvent control (ethanol) for 72 hours in media containing 10% FCS. After this, cells were washed with PBS and the medium was changed to blank M200 media with 2.25 µM Dox or solvent control (ethanol) and CM was collected after 24 hours. HUVECs treated with CM obtained from all three SREBP1 knock down cell populations showed a significant reduction in the number of loops and number of tubes formed compared to HUVECs treated with CM from control

cells (Fig 4.27A, B and D). The number of branching points was significantly reduced in cells expression LT3-BP1_01 and LT3-BP1_6, while the results for LKO-BP1_07 failed to reach significance (Fig. 4.27C). Hence, it was concluded that SREBP1 plays an important role in the induction of angiogenesis in GB.

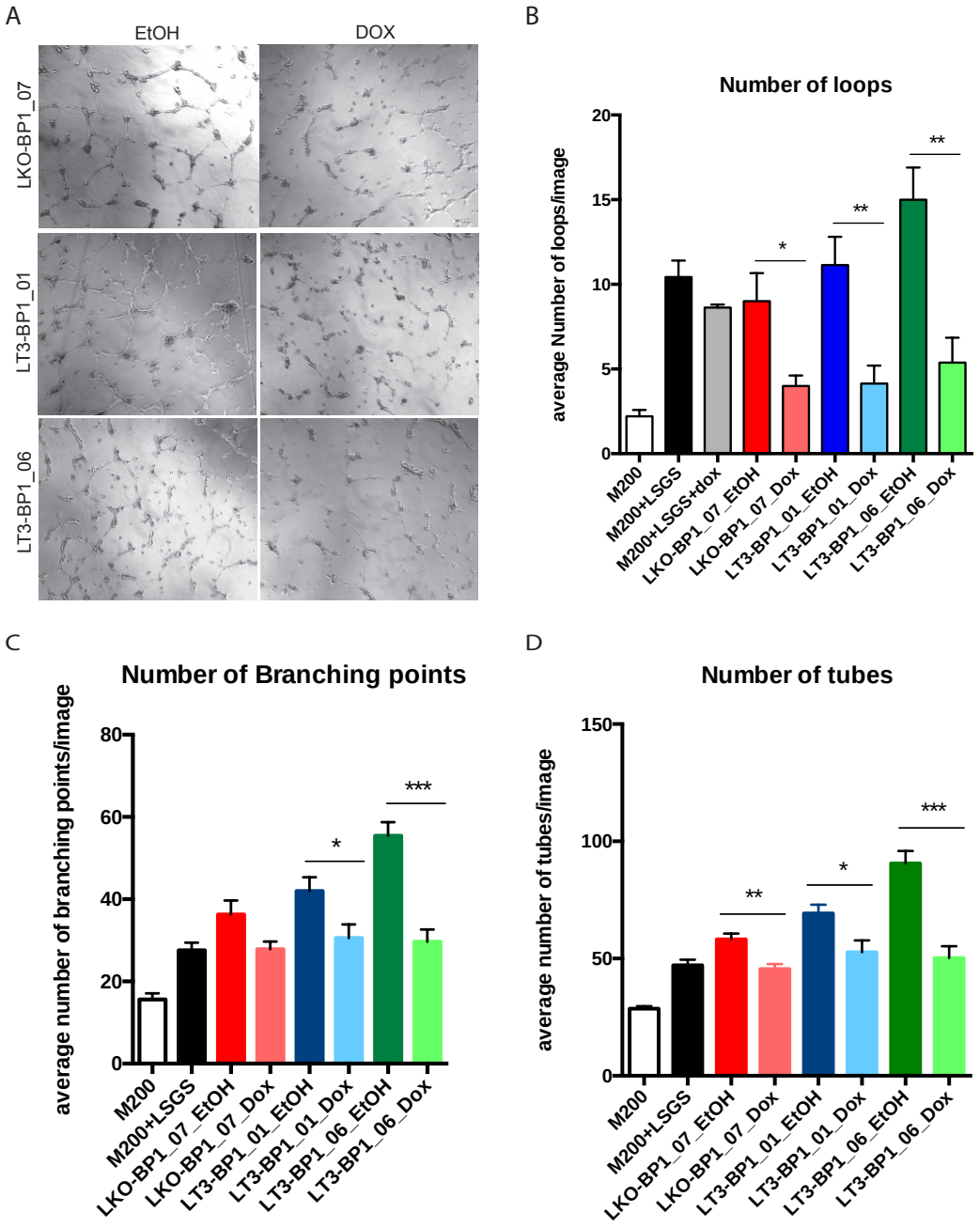

Figure 4.27: Conditioned medium from U87 cells with SREBP1 knockdown decreases tube formation in primary Endothelial cells

A) Representative images of human umbilical cord endothelial cells (HUVEC) in a tube formation assay seeded on a thin layer of matrigel in 24 well plates and incubated with CM from U87 cells expressing different shRNA sequences targeting SREBP1. U87 shBP1_07 (LKO-BP1_07), shBP1_01 (LT3-BP1_01) or shBP1_06 (LT3-BP1_06) were grown in 10%FCS with 2.25 µM Dox

or ethanol (EtOH, solvent control) for 72 hours, washed with PBS and changed to M200 medium with 2.25 µM Dox or ethanol (solvent control).

B) Quantification of number of loops formed by HUVECs grown as in A. 6 images were used for the quantification in each condition.

C) Quantification of number of branching points formed by HUVECs grown as in A.

D) Quantification of number of tubes formed by HUVECs grown as in A.

p-values were calculated using a two tailed student's t-test (p-values are represented as * ≤ 0.05, ** ≤ 0.01, *** ≤ 0.001 and **** ≤ 0.0001).

All images were taken at 10X magnification on a bright field microscope and quantified on Image J.

4.4.2 Conditioned medium analysis to identify the factors inducing angiogenesis in U87 cells

To further understand the role of SREBP1 in angiogenesis, CM was analysed to identify factors, like proteins and lipid mediators, that could be involved in inducing angiogenesis. Human angiogenesis array kit is a commercially available protein screening kit for a set of 55 known human angiogenesis related proteins. CM from SREBP1 proficient or deficient cells was incubated with the antibody-spotted membrane and signals were developed (Fig 4.28A). The cut-off was set to 0.05 for signal intensities to be considered as above background for the analysis performed on ImageJ (Fig 4.28C). The result of this analysis showed that several important proteins known to be involved in angiogenesis, including angiogenin, IGFBP1, IL-8 and VEGFA, were altered in CM obtained from SREBP1 knockdown cells compared to controls (Fig 4.28C). It should be noted, however, that this experiment was only exploratory and performed with a single biological replicate.

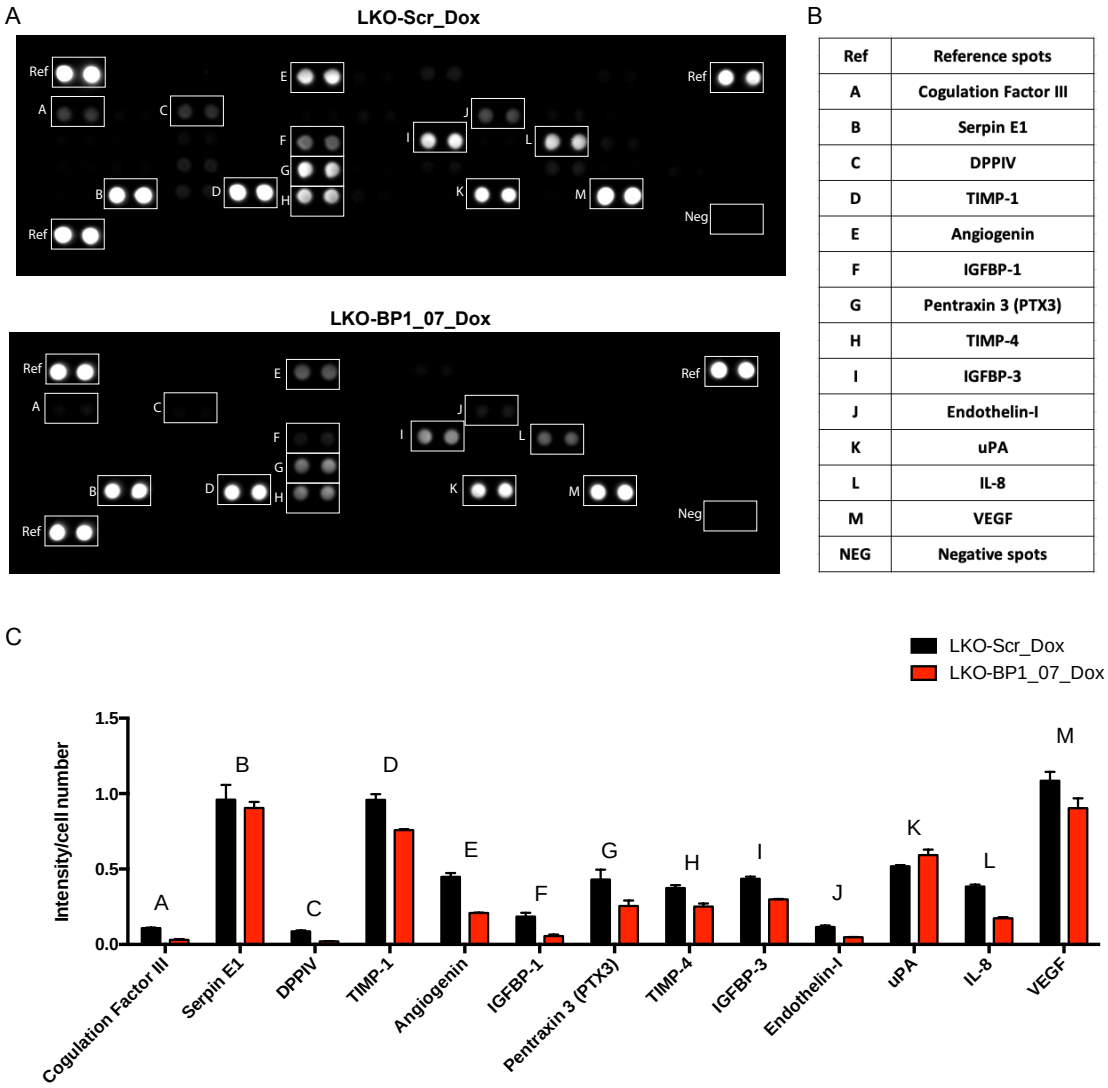

Ref	Reference spots
A	Cogulation Factor III
B	Serpin E1
C	DPPIV
D	TIMP-1
E	Angiogenin
F	IGFBP-1
G	Pentraxin 3 (PTX3)
H	TIMP-4
I	IGFBP-3
J	Endothelin-I
K	uPA
L	IL-8
M	VEGF
NEG	Negative spots

Figure 4.28: Quantification of angiogenesis-related proteins in conditioned medium of SREBP1 knockdown and control U87 cells

A) Detection of angiogenesis-related proteins using an antibody array spotted in duplicates. CM from U87 cells expressing shScr (LKO-Scr) or shBP1_07 (LKO-BP1_07) were grown in 10% FCS with 2.25 µM Dox for 72 hours. Cells were washed with PBS and the medium was changed to blank M200 supplemented with 2.25 µM Dox for 24 hours.
B) List of proteins represented on the antibody array.
C) Relative changes of secreted angiogenesis factors in CM from SREBP1 knockdown and control cells. Signal intensities shown in (C) were normalised to intensities in control cells. Bars represent mean ± SEM of the duplicate spots.

VEGF is one of the best-known stimulator of angiogenesis (Leung *et al.*, 1989). As the signal for VEGF showed a reduction in CM from SREBP1 knockdown cells in the angiogenesis antibody array, this protein was investigated in more detail. However,

immunoblot analysis of VEGF in total lysates of U87 cells showed no reduction in expression of the protein (Fig 4.30A).

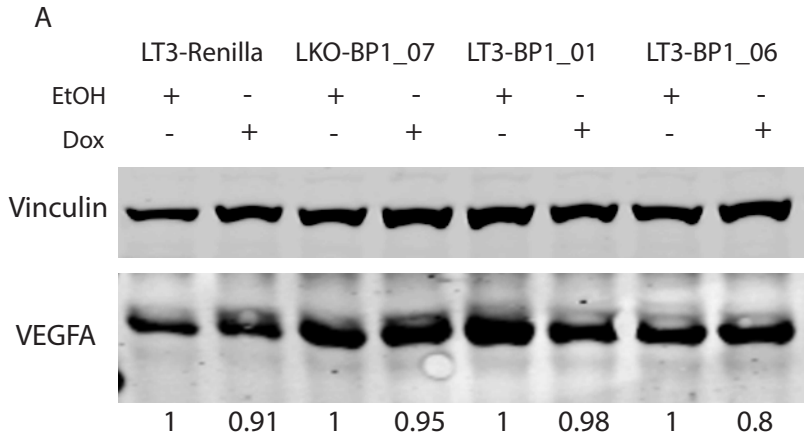

Figure 4.29: SREBP1 knockdown in U87 cells does not alter VEGF protein levels

A) WB shows VEGF protein levels in U87 cells with shRenilla, shBP1_07, shBP1_01 and shBP1_06. Cells were treated with 2.25 µM Dox or ethanol (solvent control) in 10%FCS for 72 hours and cells were washed with PBS and the medium was changed to media containing 0% with 2.25 µM Dox or ethanol (solvent control) for 24hours.

These results suggest that SREBP1 does not have a major effect on the production of VEGF in U87 cells. However, other known angiogenic stimulators involved in tumour angiogenesis, such as angiogenin (Sheng and Xu, 2016), endothelin-I and IL-8 (David *et al.*, 2016) showed substantial reduction upon SREBP1 silencing. Further investigation is necessary to understand the role of SREBP1 in the context of the changes in these proteins and their possible role in angiogenesis in GB.

4.4.3 Lipid mediators induce angiogenesis

In addition to secreted proteins, lipid mediators can also contribute to the induction of tumour angiogenesis. As the analysis of fatty acids and lipids in U87 cells with SREBP1 knockdown showed significant differences in fatty acid species that function as precursors of lipid mediators that might be involved in angiogenesis, the potential role of lipid mediators in the induction of angiogenesis downstream of SREBP1 was further investigated. To identify important nodes in the SREBP1 network involved in this process, the SREBP1 pathway was intercepted at different levels.

First, to understand whether these lipid mediators are present in the CM and were capable of inducing angiogenesis in a sprouting assay, CM derived from U87 was subjected to different treatments and extraction protocols and subsequently tested for its ability to induce HUVEC sprouting. CM was collected from U87 expressing shScr which were cultured in M200 media supplemented with 0.1% DMSO for 24 hours (N.B. DMSO was added as this also served as control for inhibitor treatments performed in the following experiments). The CM was then either boiled at 95° C for 10 minutes to denature and inactivate any protein-based angiogenic factors or subjected to a lipid extraction protocol (Folch extraction, with the resulting lipid-containing pellet being resuspended in M200 medium). Both treated media were then compared to untreated CM or CM derived from U87 cells after silencing of SREBP1 using the established protocol. Similar to the previous results (Fig 4.26), CM from U87 shScr cells was able to induce substantial sprouting of HUVEC cells, which was significantly reduced following SREBP1 silencing (Fig 4.30A-B). Interestingly, it was evident that the media that was boiled at 95 °C and the lipids extracted from CM were clearly able to induce HUVEC sprouting similar to the unmodified CM (Fig 4.30A-B).

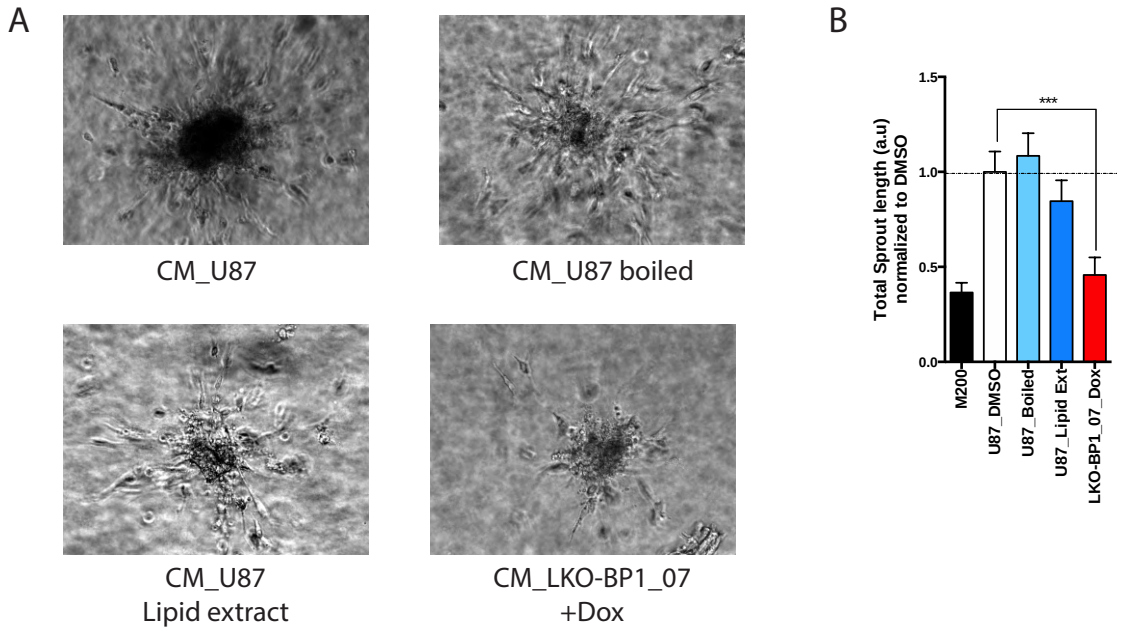

Figure 4.30: Lipids extracted from conditioned medium from U87 cells induce sprouting in primary endothelial cells

A) Representative images of spheroids of endothelial cells (HUVEC) embedded in a collagen matrix incubated with CM from U87 cells (CM_U87). The same medium was also boiled at 95 °C for 10 mins to denature all proteins (CM_U87_boiled) or used to extract lipids that were then

resuspended in M200 and used in the assay (CM_U87 Lipid extract). As a comparison, CM from U87 cells after SREBP1 silencing was also used (CM_LKO-BP1_07 +Dox).

B) Quantification of results shown in A. Total sprout length is shown as fold change normalised to U87_DMSO control. Blank M200 medium represents the negative control for the assay. (at least 12 spheroids were used for each quantification).
p-values were calculated using a two tailed student's t-test (p-values are represented as *** ≤ 0.001).
The spheroid images were taken at 20X magnification on a brightfield microscope and quantified using Image J.

As these results indicate that non-protein factors that can be extracted with the lipid fraction can mediate HUVEC sprouting, it was investigated whether individual lipid mediators could be candidates for this function. The first factor tested here was lysophosphatidic acid (C18:1), a lipid mediator involved in the induction of cell motility and angiogenesis. HUVECs spheroids were incubated with 10 μM lysophosphatidic acid (LPA-C18:1), or with lipid extracts from M200 media to which 10 μM LPA-C18:1 had been added prior to extraction. In addition, medium containing 10 μM LPAC18:1 was used in the presence of 10 μM of a small molecule inhibition of the LPA receptor (KI16425). As can be seen in Figure 4.31A-B, LPA-C18:1 both directly added to the medium or after lipid extraction was able to induce HUVEC sprouting. Moreover, treating HUVEC cells with the LPA receptor inhibitor prevented the induction of sprouting by LPA-C18:1 (Fig 4.31A-B). Thus, it can be concluded that LPA is a lipid mediator that is able to induce endothelial cell sprouting via activation of the LPA receptor. It is thus possible that modulation of the cellular lipid network by SREBP1 alters the production of LPA-C18:1 to affect angiogenesis in GB.

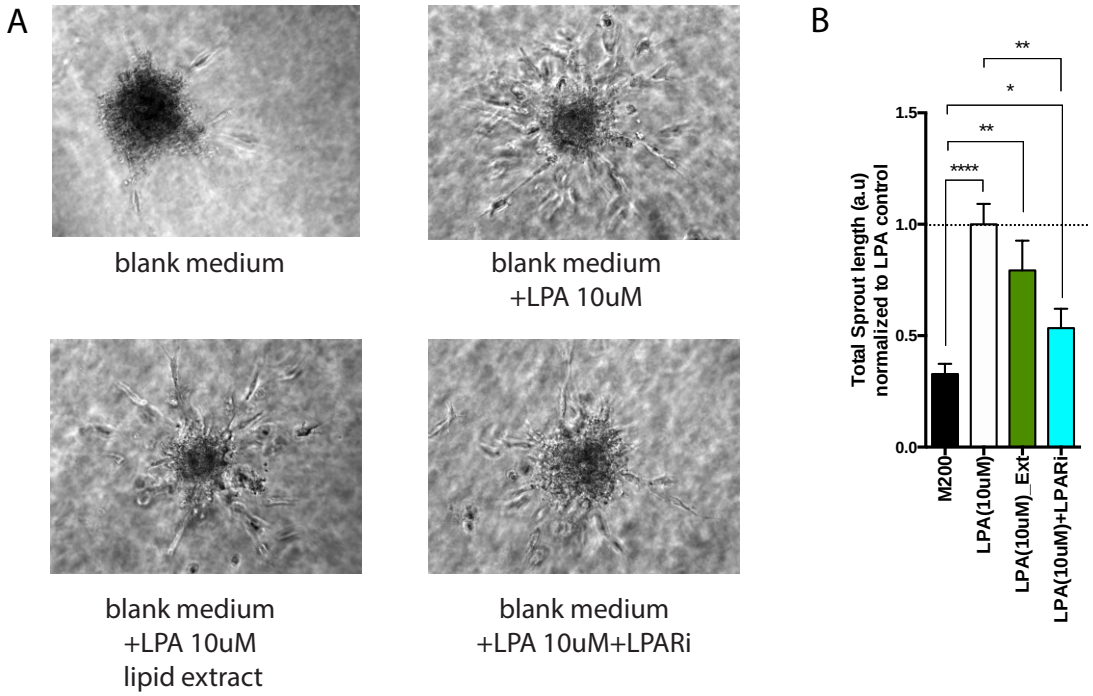

Figure 4.31: Lysophosphatidic acid (LPA-C18:1) induces sprouting in primary endothelial cells

A) Representative images of spheroids of endothelial cells (HUVEC) embedded in a collagen matrix incubated with either blank M200 medium, M200 medium with 10 μM LPA-C18:1 (blank medium _LPA 10μM), with lipids extracted from M200 medium to which 10 μM LPA-C18:1 had been added (blank medium +LAP10μM lipid extract) or 10 μM LPA-C18:1 plus 10 μM of the LPA receptor inhibitor KI16425 (blank medium+LPA 10μM+LPARi).

B) Quantification of spheroids shown in A. Total sprout length is shown as fold change normalised to U87 CM from a parallel experiment. M200 represents negative control for the assay. (at least 12 spheroids were used for quantification).
p-values were calculated using a two tailed student's t-test (p-values are represented as * ≤ 0.05, ** ≤ 0.01, *** ≤ 0.001 and **** ≤ 0.0001).
All spheroid images were taken at 20X magnification on a brightfield microscope and quantified using Image J.

Another lipid mediator that could be involved in the induction of angiogenesis is prostaglandin E2 (PGE2), a product arising from the metabolism of arachidonic acid (C20:4) that has previously been shown to induce angiogenesis (Form and Auerbach, 1983). To test the effect of PGE2 on angiogenesis, HUVEC spheroids were incubated with M200 media containing 2 μM or 10 μM of PGE2 and sprouting length was measured. The results clearly show that PGE2 was able to induce HUVEC sprouting in a concentration dependent manner (Fig 4.32A-B).

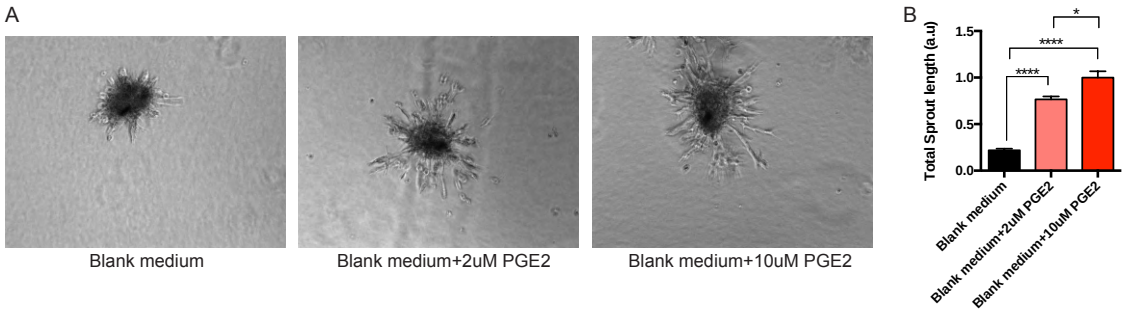

Figure 4.32: Prostaglandin E2 induces sprouting in primary endothelial cells

A) Representative images of spheroids of endothelial cells (HUVEC) embedded in a collagen matrix and incubated with blank M200 medium and M200 medium supplemented with either 2 µM or 10 µM of prostaglandin E2 (PGE2).

B) Quantification of spheroids shown in A. Total sprout length is shown as fold change normalised to U87 CM from a parallel experiment. Blank medium represents the negative control for the assay. (at least 12 spheroids were used for quantification).
p-values were calculated using a two tailed student's t-test (p-values are represented as * ≤ 0.05 and **** ≤ 0.0001).
All spheroid images were taken at 10X magnification on a bright field microscope and quantified using Image J.

4.4.4 Inhibition of enzymes in the SERBP1 network blocks endothelial cell sprouting

To further understand whether the SREBP1 pathway affects the synthesis of lipid mediators that are contributing to the induction of angiogenesis, the pathway was further dissected and interrogated using selective inhibitors for different points. In particular, the contribution of SCD, PLA2G3, autotaxin (ATX1) and the LPA receptor (LPAR) to the induction of HUVEC sprouting were investigated.

To be able to distinguish the effect of the inhibitors on the ability of U87 cells to produce pro-angiogenic factors from a direct effect of the inhibitors on sprouting in HUVEC cells, two types of inhibitor treatment were performed: pre-treatment (a) or post-treatment (b) as represented in Fig 4.33A. Pre-treatment: CM was collected from U87 cells which were treated with inhibitors in M200 media for 24 hours. Post-treatment: CM was collected from U87 cells incubated in M200 media for 24 hours and inhibitors were added to the CM before using it on HUVECs (4.33A). The controls for this assay were CM obtained from U87 cells incubated in M200 media treated with

solvent alone and CM from U87 cells after SREBP1 knockdown (already shown in Fig 4.30).

The CM obtained from pre-treatment with the SCD inhibitor CAY10566 (100 nM) showed significant reduction in endothelial cell sprouting while there was no change observed when the inhibitor (100 nM) was added to U87 CM (post-treatment) (Fig 4.33B-D). These results suggest that SCD activity is required for U87 cells to produce the pro-angiogenic factors secreted by the cells.

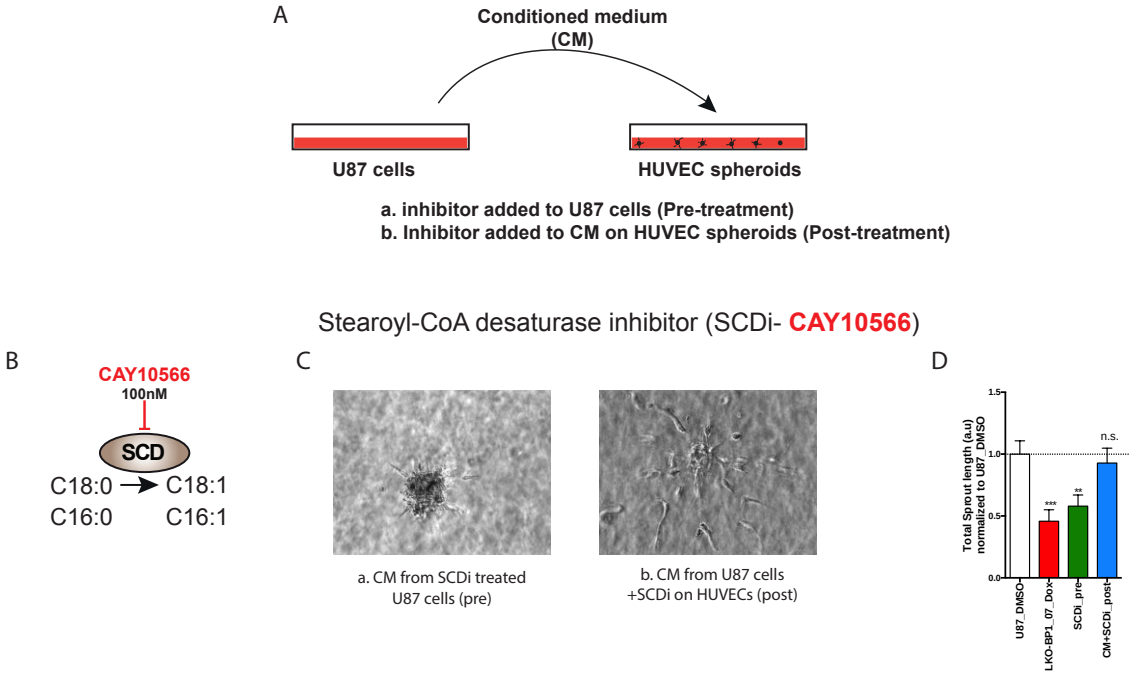

Figure 4.33: Inhibition of SCD blocks the ability of U87 cells to produce endothelial cell sprouting-inducing factors

A) Diagram of the experimental conditions for the inhibitor experiments. For experimental condition a, CM was obtained from U87 cells treated with the inhibitor for 24 hours (pre-treatment). For experimental condition b, the inhibitor was added after the CM had been removed prior to its addition to the endothelial cells (post-treatment).
B) Diagram showing the reactions affected by the SCD inhibitor used for the experiment.
C) Representative images of spheroids of endothelial cells (HUVEC) embedded in a collagen matrix and incubated with CM from U87 cells treated with M200 medium supplemented with 100nM CAY10566 (SCDi_pre). In comparison, HUVEC cells were incubated with conditioned medium to which 100nM CAY10566 had been added post incubation (CM+SCDi_post).
D) Quantification of spheroids shown in C. Total sprout length is shown as fold change normalized over U87 control. Data obtained with CM from U87 cells incubated in M200 media and treated with solvent alone (U87_DMSO) and CM from U87 cells after SREBP1 knockdown (LKO-BP1_Dox) already shown in Fig 4.30 are included as controls. (at least 12 spheroids were used for quantification).

p-values were calculated using a two tailed student's t-test (p-values are represented as ** ≤ 0.01).
The spheroid images were taken at 20X magnification on a bright field microscope and quantified using Image J.

In a similar experiment, CM obtained from U87 cells treated with 2 μM of an inhibitor targeting secreted phospholipases, thioetheramide-PC, showed a significant reduction in its ability to induce endothelial cell sprouting, while there was no change observed when the inhibitor (2 μM) was added to U87 CM using the post-treatment protocol (Fig 4.34 A-C).

As the used inhibitor could affect several secreted phospholipases, the involvement of PLA2G3 in the induction of endothelial cell sprouting was further investigated using a gene silencing strategy. U87 cells expressing shRNA targeting PLA2G3 (shPLA2G3_01 and 05) and control cells with shRenilla were treated with 2.25 μM Dox for 72 hours in media containing 10% FCS. After this, cells were washed with PBS and the medium was changed to M200 media with 2.25 μM Dox for 24 hours. CM from these cells was used in a HUVEC sprouting assay. Indeed, spheroids treated with CM obtained from PLA2G3 knockdown cells showed a significant reduction in sprouting compared to the control cells (Fig 4.34 D-E), confirming the importance of PLA2G3 in the induction of pro-angiogenic factors by U87 cells.

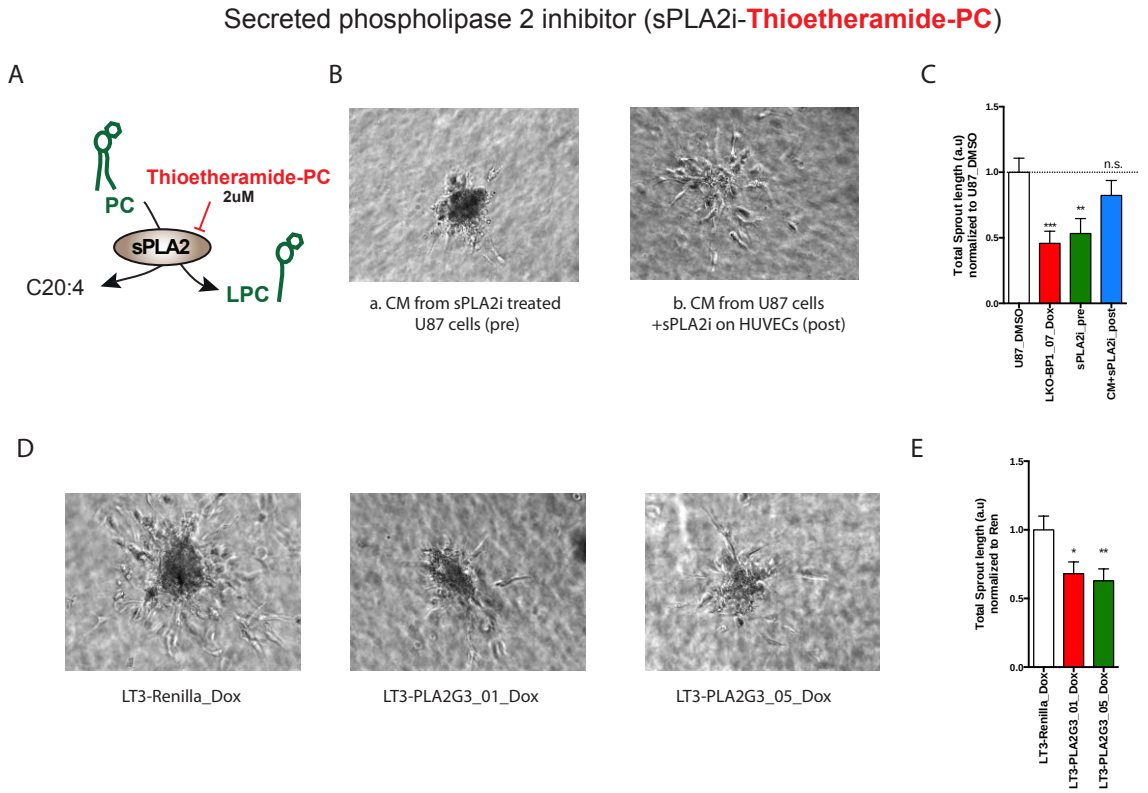

Figure 4.34: Inhibition or silencing of PLA2G3 reduces the ability of U87 cells to produce factors that induce sprouting in primary endothelial cells

A) Diagram of the function of the secreted sPLA2 inhibitor used for the experiment and the reaction affected by the inhibitor.

B) Representative images of spheroids of endothelial cells (HUVEC) embedded in a collagen matrix and incubated with CM from U87 cells treated with 2 µM sPLA2i thioetheramide-PC or with CM from U87 cells to which 2 µM sPLA2i had been added post-incubation.

C) Quantification of spheroids shown in B. Total sprout length is shown as fold change normalised to U87 controls. Data obtained with CM from U87 cells incubated in M200 media and treated with solvent alone (U87_DMSO) and CM from U87 cells after SREBP1 knockdown (LKO-BP1_Dox) already shown in Fig 4.30 are included as controls. (at least 12 spheroids were used for quantification).

D) Representative images of spheroids of endothelial cells (HUVEC) embedded in a collagen matrix and incubated with CM from U87 cells expressing shRenilla (LT3-Renilla_Dox), shPLA2G3_01 (LT3-PLA2G3_01_Dox) or shPLA2G3_05 (LT3-PLA2G3_05_Dox). Cells were first grown in medium containing 10% FCS with 2.25 µM Dox for 72 hours, then washed with PBS and changed to M200 supplemented with 2.25 µM Dox for an additional 24 hours before CM was collected.

E) Quantification of spheroids of shown in D. Total sprout length is shown as fold change normalized over shRenilla condition. (at least 12 spheroids were used for quantification).
p-values were calculated using a two tailed student's t-test (p-values are represented as * ≤ 0.05, ** ≤ 0.01 and *** ≤ 0.001).
The spheroid images were taken at 20X magnification on a brightfield microscope and quantified using Image J.

As a third potential factor involved in the production of lipid mediators by U87 cells, the lysophospholipid lipase autotaxin (ATX) was investigated. ATX catalyses the reaction of conversion of LPC to LPA (Fig. 4.35A). Furthermore, the effect of blocking the LPAR on HUVEC cell sprouting was also investigated (Fig. 4.35D). In contrast to the inhibition of SCD and PLA2G3, which only showed an effect on sprouting of endothelial cells in pre-treated CM, both inhibitors to autotaxin (HA-130 used at 10 µM) or LPAR (KI 16425 used at 10 µM) showed a significant reduction in endothelial cell sprouting with CM obtained from both pre- and post-treatment (Fig 4.35 B, C, E and F). This indicates that these two proteins exert their function on molecules already produced by U87 cells. For example, ATX, a secreted protein, could be used to convert secreted LPC into LPA that then induces sprouting in HUVEC cells. Similarly, the LPAR could be required to allow the induction of HUVEC sprouting by LPA present in the CM.

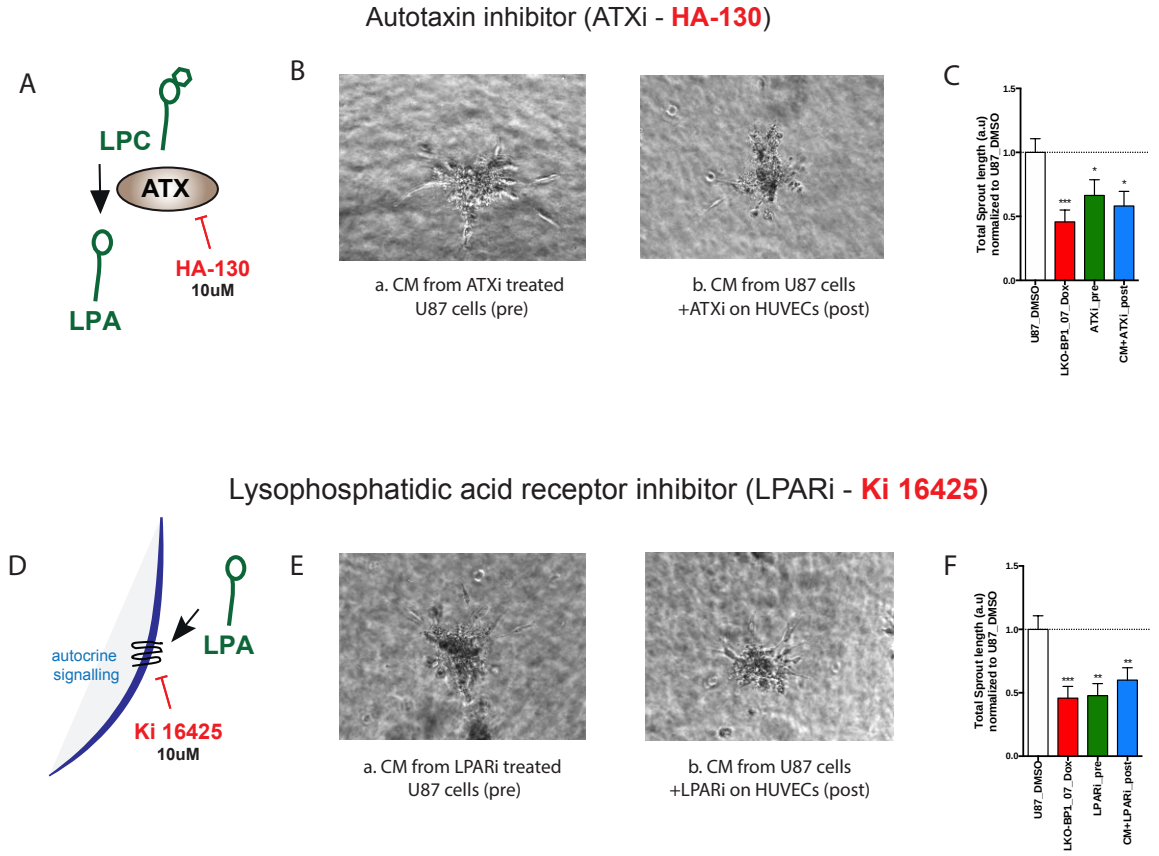

Figure 4.35: Inhibition of autotaxin or LPAR reduces the ability of U87 cells to produce and use factors that induce sprouting in primary endothelial cells

A) Diagram showing the function of the autotaxin inhibitor used for the experiment.
B) Representative images of spheroids of endothelial cells embedded in a collagen matrix and incubated with CM from U87 cells treated with 10 µM ATXi HA-130 or with CM from U87 cells to which 10 µM ATXi had been added using the post-treatment protocol.

C) Quantification of spheroids shown in B. Total sprout length is shown as fold change normalised to U87 controls. Data obtained with CM from U87 cells incubated in M200 media and treated with solvent alone (U87_DMSO) and CM from U87 cells after SREBP1 knockdown (LKO-BP1_Dox) already shown in Fig 4.30 are included as controls. (at least 12 spheroids were used for quantification).
D) Diagram showing the mode of action of the LPA receptor inhibitor used for the experiment.
E) Representative images of spheroids of endothelial cells embedded in a collagen matrix and incubated with CM from U87 cells treated with 10 μM LPARi KI 16425 or with CM from U87 cells to which 10 μM LPARi had been added using the post-treatment protocol.
F) Quantification of spheroids shown in E. Total sprout length is shown as fold change normalised to U87 controls. Data obtained with CM from U87 cells incubated in M200 media and treated with solvent alone (U87_DMSO) and CM from U87 cells after SREBP1 knockdown (LKO-BP1_Dox) already shown in Fig 4.30 are included as controls. (at least 12 spheroids were used for quantification).
p-values were calculated using a two tailed student's t-test (p-values are represented as * ≤ 0.05, ** ≤ 0.01 and *** ≤ 0.001).
The spheroid images were taken at 10X magnification on a brightfield microscope and quantified using Image J.

4.5.5 Analysis of fatty acids and lipids in conditioned medium from U87 cells

As the previous experiments suggested that lipid-based factors may play a major role in the induction of endothelial sprouting by U87 cells, CM were subjected to lipidome analysis. Lipid analysis of CM was performed similar to the lipid analysis performed in total cell extracts (as discussed in chapter 4.3) in a stepwise manner: global lipid analysis with TLC, fatty acid profiling and media lipidomics.

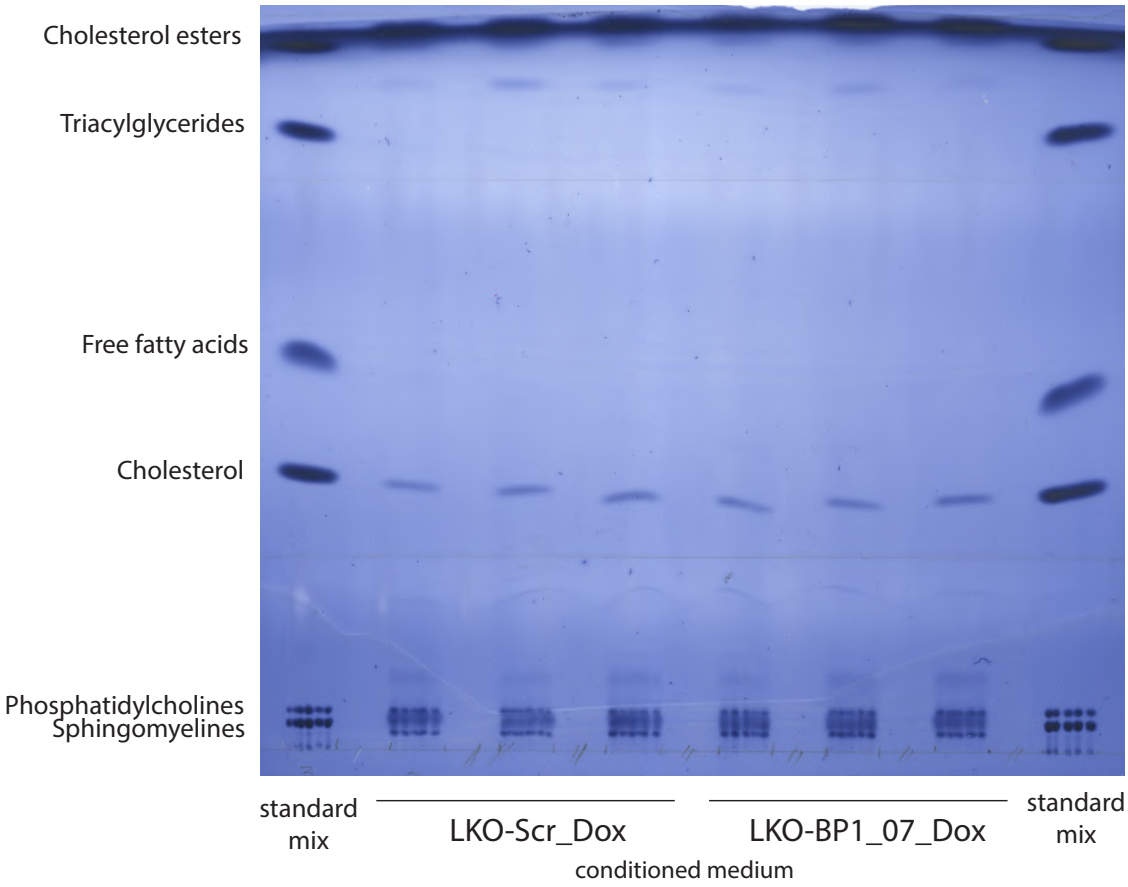

Figure 4.36: Lipid profiling by thin layer chromatography (TLC) in conditioned medium of U87 cells upon SREBP1 knockdown

TLC shows different lipid species in CM obtained by U87 cells expressing shScr or shBP1_07 in the LKO vector system. Cells were grown in 10% FCS with 2.25 µM Dox for 72 hours. After this, cells were washed with PBS and the medium was changed to media containing 1% FCS with 2.25 µM Dox for 24 hours. Total Lipids were extracted using a simple chloroform free BUME extraction and analysed by TLC (n=3).

Thin layer chromatography of lipid extracts from CM obtained from U87 cells expressing either shScr or shBP1_07 was performed. Cells were treated with 2.25 µM Dox for 72 hours in media containing 10% FCS. After this, cells were washed with PBS and the medium was changed to media containing 1% FCS with 2.25 µM Dox for 24 hours. Phosphatidylcholines, sphingomyelins, cholesterol, free fatty acids, triglycerides and cholesterol esters were analysed with respective standards. No significant differences in the overall levels of these lipids or fatty acid species was observed in SREBP1 depleted cells compared to the controls (data not shown?).

In a parallel experiment, total (hydrolysed) fatty acids and free (non-hydrolysed) fatty acids extracted from CM from SREBP1 silenced and control cells were analysed by MS following direct injection. The relative fraction of each fatty acid species within the total and free fatty acid pool was calculated and is displayed in Fig. 4.37. Upon SREBP1 knockdown, there were no significant changes in the mono-unsaturated total fatty acids, palmitoleic (C16:1) and oleic acid (C18:1) present in the total fatty acid pool (Fig. 4.37A). At the same time, accumulation of several poly-unsaturated fatty acids was observed in the total fatty acid pool, including linoleic acid (C18:2), di-homo-linolenic acid (C20:3), arachidonic acid (C20:4), eicosapentaenoic acid (C20:5), docosatetraenoic acid (C22:4), docosapentaenoic acid (C22:5) and docosahexaenoic acid (C22:6) (Fig 4.37A). In contrast, free fatty acids in the CM obtained from SREBP1 knockdown cells showed a significant reduction in mono-unsaturated fatty acids palmitoleic (C16:1) and oleic acid (C18:1), while no changes in essential fatty acids were observed (Fig 4.37B).

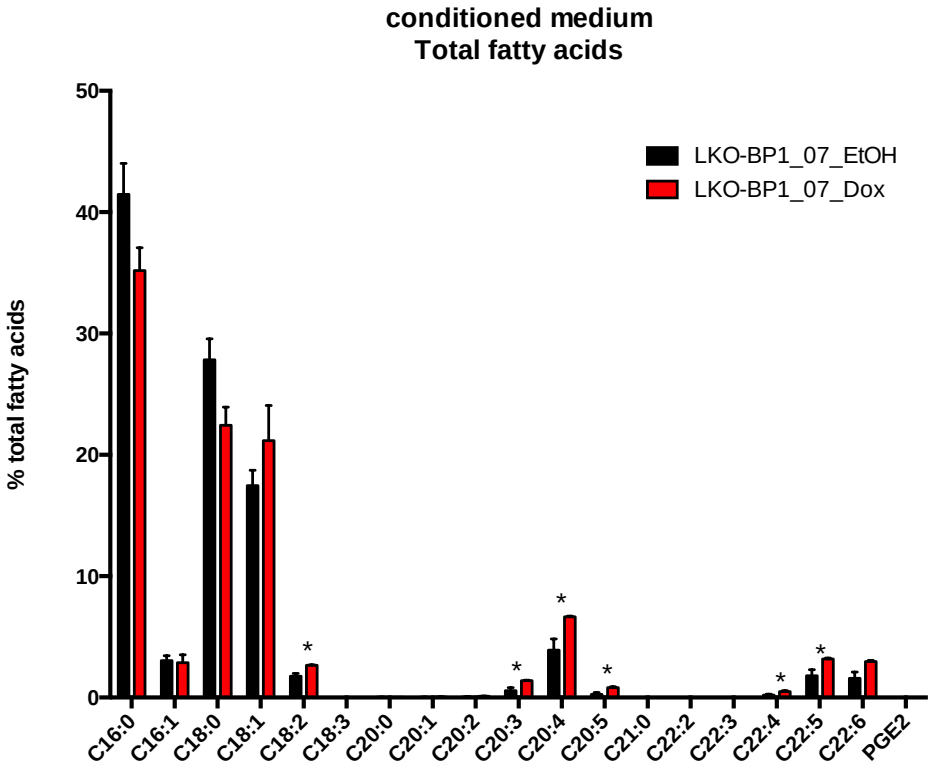
conditioned medium
Total fatty acids
% total fatty acids
LKO-BP1_07_EtOH
LKO-BP1_07_Dox
C16:0
C16:1
C18:0
C18:1
C18:2
C18:3
C20:0
C20:1
C20:2
C20:3
C20:4
C20:5
C21:0
C22:2
C22:3
C22:4
C22:5
C22:6
PGE2

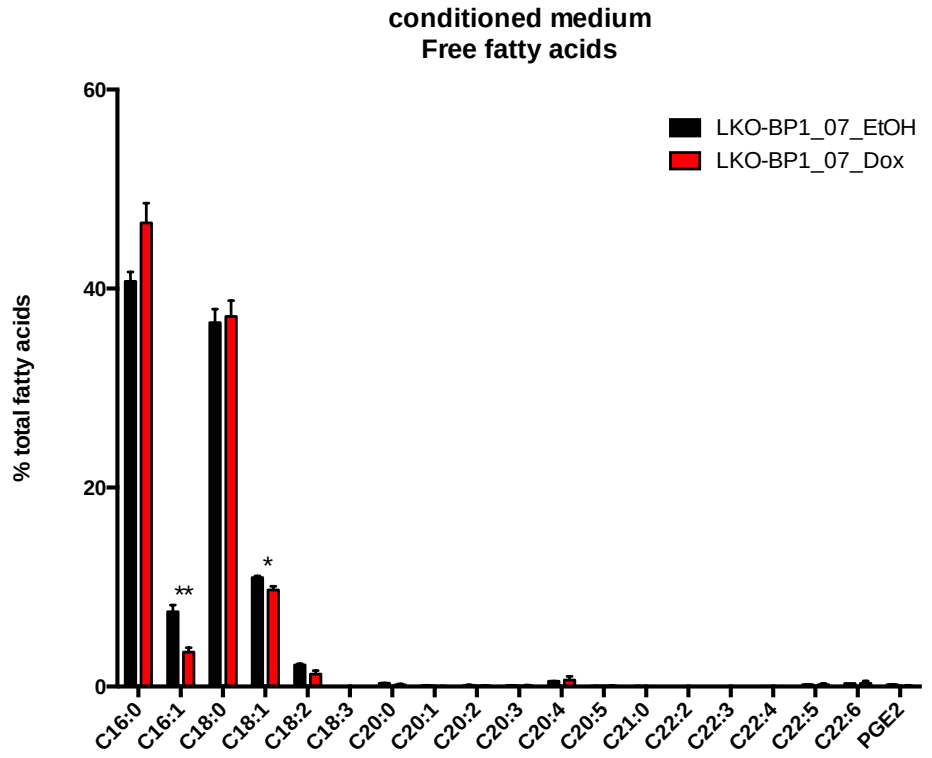
conditioned medium
Free fatty acids
% total fatty acids
LKO-BP1_07_EtOH
LKO-BP1_07_Dox
C16:0
C16:1
C18:0
C18:1
C18:2
C18:3
C20:0
C20:1
C20:2
C20:3
C20:4
C20:5
C21:0
C22:2
C22:3
C22:4
C22:5
C22:6
PGE2

Figure 4.37: Changes in total and free fatty acid profile in conditioned medium from U87 cells upon SREBP1 knockdown using the pLKO-Tet-On vector system

A) Overall changes in total fatty acids in CM obtained from U87 cells expressing shBP1_07 (LKO-BP1_07). Cells were grown in 10% FCS with 2.25 µM Dox or ethanol (solvent) for 72 hours. After this, cells were washed with PBS and the medium was changed to media containing 0% FCS with 2.25 µM Dox or solvent for 24 hours. Total fatty acids were extracted, hydrolysed and detected by MS following direct injection. Relative abundance of each fatty acid species is shown relative to the total fatty acid pool (n=3).

B) Overall changes in the free fatty acid profile of CM obtained from U87 cells expressing shBP1_07 (LKO-BP1_07). Cells were treated as described in A. Free fatty acids were extracted and detected by MS following direct injection. Relative abundance of each fatty acid species is shown relative to the total fatty acid pool (n=3).

p-values were calculated using a two tailed student's t-test (p-values are represented as * ≤ 0.05 and ** ≤ 0.01).

Although fatty acid profiling already revealed interesting differences in the relative abundance of several fatty acid species upon SREBP1 knockdown, the focus of this analysis was the identification of specific lipid mediators, such as PGE2 and LPA, that could be the downstream products of the SREBP1 network that are involved in angiogenesis, as suggested by results discussed above. Hence, measuring these specific mediators was crucial to determine whether their levels were modified by SREBP1 knockdown. The analysis of the CM (shown in Fig 4.37) suggested that the levels of PGE2 were too low for detection by MS without applying a further purification strategy. Nevertheless, we observed a trend towards reduced levels for PGE2 following SREBP1 silencing (Fig 4.38A), albeit with high variance of the data. Hence, a commercially available ELISA specifically designed for measuring PGE2 was used to analyse the CM obtained from SREBP1 silenced and control U87 cells. Indeed, CM from cells with SREBP1 knockdown showed a significant reduction in PGE2 levels compared to the control condition (Fig 4.38B). Moreover, CM was also obtained from U87 cells expressing shSREBP1_07 treated with 2.25 µM Dox for 72 hours in media containing 10% FCS. After this, cells were washed with PBS and the medium was changed to media containing 0% FCS with 2.25 µM Dox together with 100 µM oleic acid (C18:1) or 100 µM arachidonic acid (C20:4) during the last 24 hours. Oleic acid was added to rescue the loss of monounsaturated fatty acids, which were decreased upon SREBP1 knockdown, while arachidonic acid was added to provide a substrate for the synthesis of PGE2. The latter condition was chosen as it was hypothesised that SREBP1 silencing inhibits the release of arachidonic acid from membrane phospholipids by blocking the expression of PLA2G3 (discussed above). This is

supported by the accumulation of arachidonic acid in the total fatty acid pool observed in SREBP1 silenced cells (Fig. 4.18A and 4.19A). This experiment showed that addition of 100 µM oleic acid (C18:1) resulted only in a mild increase in PGE2 levels in CM from SREBP1 silenced U87 cells (Fig 4.38B). In contrast, addition of 100 µM arachidonic acid (C20:4) resulted in about 60 times higher levels of PGE2 compared to SREBP1 knockdown cells (Fig 4.38B). This result shows that U87 cells retain the ability to synthesize PGE2, even after SREBP1 silencing, but lack sufficient amounts of arachidonic acid as rate-limiting substrate for PGE2 synthesis.

Furthermore, PGE2 levels were also analysed in CM obtained from U87 cells expressing shPLA2G3 (shPLA2G3_01 and 05) or controls expressing shRenilla treated similarly as described above. While silencing of PLA2G3 using sequence 01 resulted in a significant decrease in PGE2 levels (Fig 4.38C), this was not recapitulated with the second sequence, despite both sequences resulting in a substantial depletion of PLA2G3 protein and mRNA (see Fig. 4.14A-B). Hence, reduction of PGE2 levels upon knock down of PLA2G3 remains inconclusive and needs further experiments to unravel a direct role of PLA2G3 in the regulation of PGE2 synthesis by SREBP1.

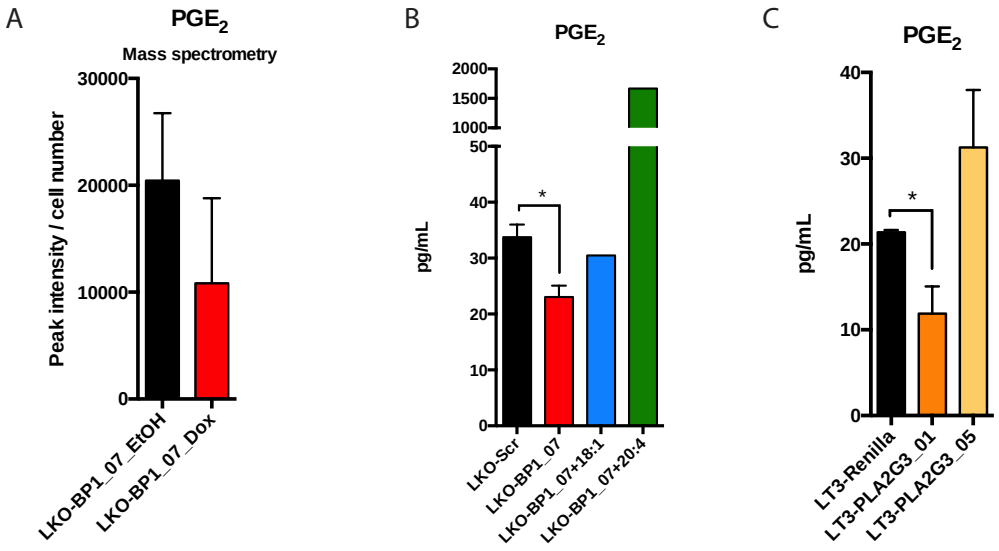

Figure 4.38: Prostaglandin E2 levels in conditioned medium from U87 cells with SREBP1 or PLA2G3 knockdown

A) PGE_2 levels measured by MS following direct injection in CM obtained from U87 cells expressing shBP1_07 (LKO-BP1_07). Cells were grown in 10% FCS with 2.25 µM Dox or ethanol (EtOH) for 72 hours. Afterwards, cells were washed with PBS and the medium was changed to media containing 0% FCS with 2.25 µM Dox or ethanol for 24 hours. Total fatty acids were extracted,

hydrolysed and detected by MS following direct injection. Peak intensity was normalised to cell number (n=3).

B) PGE_2 levels measured by ELISA in CM obtained from U87 cells expressing shScr or shBP1_07 were treated as in A. In addition, 100 µM oleic acid (C18:1) or 100 µM arachidonic acid (C20:4) were added during the last 24 hours.

C) PGE_2 levels measured by ELISA in CM obtained by U87 cells expressing shRenilla, shPLA2G3_01 and shPLA2G3_06 cells. Cells were treated as described in A.

Bars represent mean ± SEM (n=3). p-values were calculated using a two tailed student's t-test (p-values are represented as * ≤ 0.05, ** ≤ 0.01, *** ≤ 0.001 and **** ≤ 0.0001).

The second lipid mediator that could be implicated in the induction of angiogenesis downstream of SREBP1 is LPA. This lipid is produced by the reaction catalysed by the secreted lysophospholipid lipase autotaxin which removes the head groups from different lysophospholipids to release LPA. Importantly, the nature of the LPA species produced by this reaction is governed by the relative availability of lysophospholipids containing different acyl-chains, with LPA-18:1 being among the most important molecules for signalling events. Several factors, among them SREBP1 (as discussed in chapter 4.3), can therefore play a role in determining the output of the ATX reaction.

As PGE2 levels were affected by SREBP1 knockdown, synthesis of LPA, which is also branching from the same upstream reaction, could also be affected. LPA in the CM (described and used in Fig 4.36) was measured by LC-MS but, as the levels were very close to the detection limit, the results were inconclusive (Fig 4.39A). Also, measurement of LPA in CM obtained from cells with the 3 shRNA sequences targeting SREBP1 (shBP1_07, 01 and 06) compared to the control cells shScr and shRenilla did not lead to conclusive results (Fig 4.39B). One potential problem could be that the commercial kits detects total LPA levels and not specifically LPA C18:1. Also, total LPA measurement in CM obtained from PLA2G3 knockdown (shPLA2G3_01 and 05) cells showed no difference compared to the control cells (Fig 4.39B).

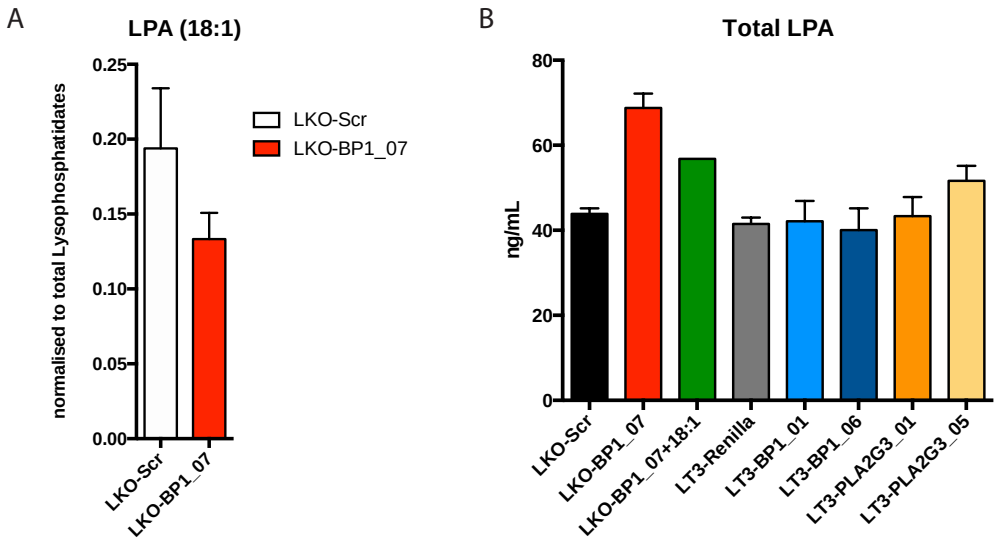

Figure 4.39: Lysophosphatidic acid C18:1 or total LPA in conditioned medium from U87 cells with SREBP1 or PLA2G3 knockdown

A) LPA C18:1 levels were measured by MS following direct injection in CM obtained from U87 cells expressing shScr (LKO-Scr) or shBP1_07 (LKO-BO1_07) (see Fig. 4.36) (n=3).

B) Total LPA levels measured by ELISA in CM obtained by U87 cells with shScr, shBP1_07, shBP1_07 cells treated with oleic acid (C18:1), shRenilla, shBP1_01, shBP1_06, shPLA2G3_01 and shPLA2G3_05. Cells were treated as described before (see Fig. 4.38) (n=3).

As efficient measurement of C18:1 LPA was technically challenging and required further optimization of the extraction and measurement on LC-MS, a rescue experiment was performed by adding increasing amounts of C18:1 LPA (1nM, 10nM, 100nM, 1µM and 10µM) into CM collected from U87 cells with SREBP1 knockdown. LPA addition at the 100nM concentration started to rescue endothelial cell sprouting and reached the same levels as sprouting induced by CM from control cells at the 1µM and 10µM concentration (Fig 4.40A-B).

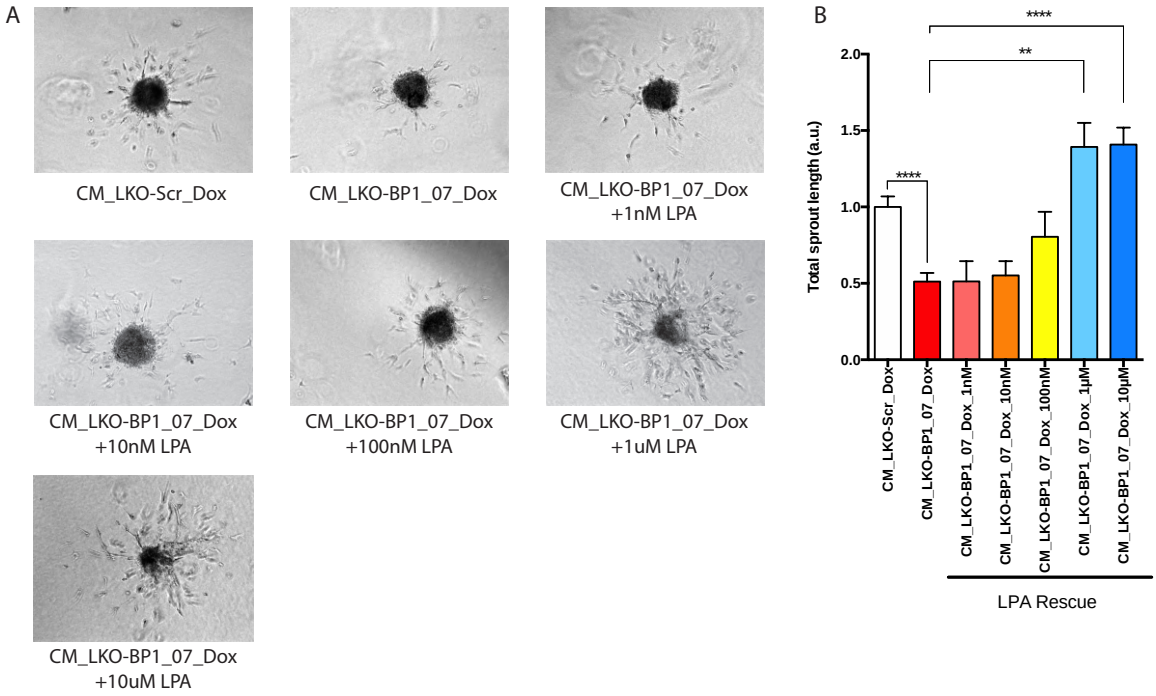

Figure 4.40: Lysophosphatidic acid C18:1 *rescue* decreased sprouting in primary endothelial cells with conditioned medium from U87 cells upon SREBP1 knockdown

A) Representative images of spheroids of endothelial cells (HUVEC) embedded in a collagen matrix and incubated with CM from U87 cells from shScr or shBP1_07 cells. In addition, different concentration of LPA C18:1 (1nM, 10nM, 100nM, 1 µM or 10 µM) were added to the CM from shBP1_07 cells. CM were obtained from cells grown in 10% FCS with 2.25 µM Dox for 72 hours after which cells were washed with PBS and the medium was changed to M200 media containing 0% FCS with 2.25 µM Dox for 24 hours.

B) Quantification of spheroids shown in A. Total sprout length is shown as fold change normalised to shScr control. (at least 5 spheroids were used for quantification for the rescue conditions).
p-values were calculated using a two tailed student's t-test (p-values are represented as ** ≤ 0.01 and **** ≤ 0.0001).
The spheroid images were taken at 10X magnification on a brightfield microscope and quantified using Image J.

4.4.6 SREBP1 ablation reduces blood vessel density in subcutaneous tumours

Even though measurement of lipid mediators that could be potentially involved in angiogenesis in GB needs more detailed experiments with improved technical strategies, analysing whether SREBP1 knockdown could also alter blood vessel formation *in vivo* was crucial. This analysis was performed on archival tissue material from subcutaneous tumours obtained by injecting U87 cells expressing shScr or

shBP1_07 into the dorsal flank of immunocompromised mice (ICRF nude strain) treated with or without Dox from an experiment performed by Caroline Lewis, Susana Ros and Bradley Spencer Dene. SREBP1 knockdown had been previously shown to significantly reduce both volume and weight of the tumours and established the importance of SREBP1 in tumour formation (Griffiths *et al.*, 2013). Upon further inspection of the tumours (images shown in Fig 4.41A), it was clear that SREBP1 silenced tumours were paler than the control tumours. Histological analysis by staining for murine endomucin (EMCM) protein (performed by Bradley Spencer Dene, CRUK London Research Institute) of those tumours revealed that blood vessel density was significantly reduced upon SREBP1 silencing (Fig 4.41B-D).

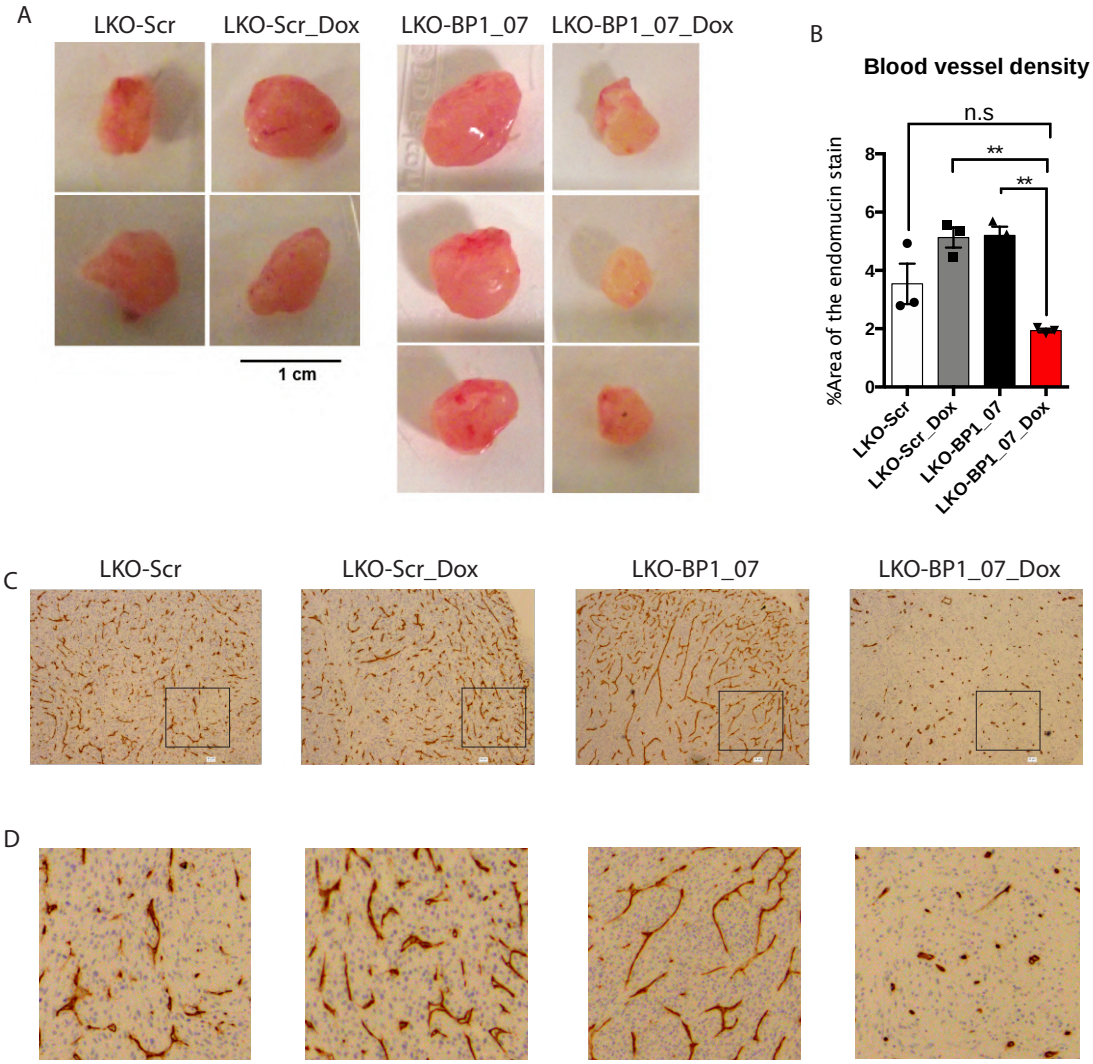

Figure 4.41: Subcutaneous xenograft tumours of U87 cells with SREBP1 knockdown show significant reduction of blood vessel density

A) Representative images of subcutaneous tumours of U87 cells expressing shScr (LKO-Scr) or shBP1_07 (LKO-shBP1_07) injected into immunocompromised mice treated with or without Dox starting at day 8 post-implantation. Tumours were extracted at day 30 post-implantation.
B) Quantification of blood vessel density of the tumours shown in A. Tissue sections were stained for murine endomucin and total signal areas were quantified from tumours of 3 individual mice for each condition.
C) Representative images of murine endomucin staining detecting blood vessels in the tumour sections.
D) Magnifications of images shown in C (square box in C indicates magnified region).
p-values were calculated using a two tailed student's t-test (p-values are represented as ** ≤ 0.01).

Collectively, the results discussed in this chapter indicate that altered lipid synthesis downstream of SREBP1 shapes the extracellular lipidome and potentially alters the availability of lipid mediators, including PGE2 and LPA, that contribute to the induction of endothelial sprouting and could thus promote tumour angiogenesis. This is summarised as a model for the regulation of angiogenesis by SREBP1 in GB (Fig 4.42). Further experiments are required to evaluate the specific nodes and the complex molecular regulation involved in angiogenesis.

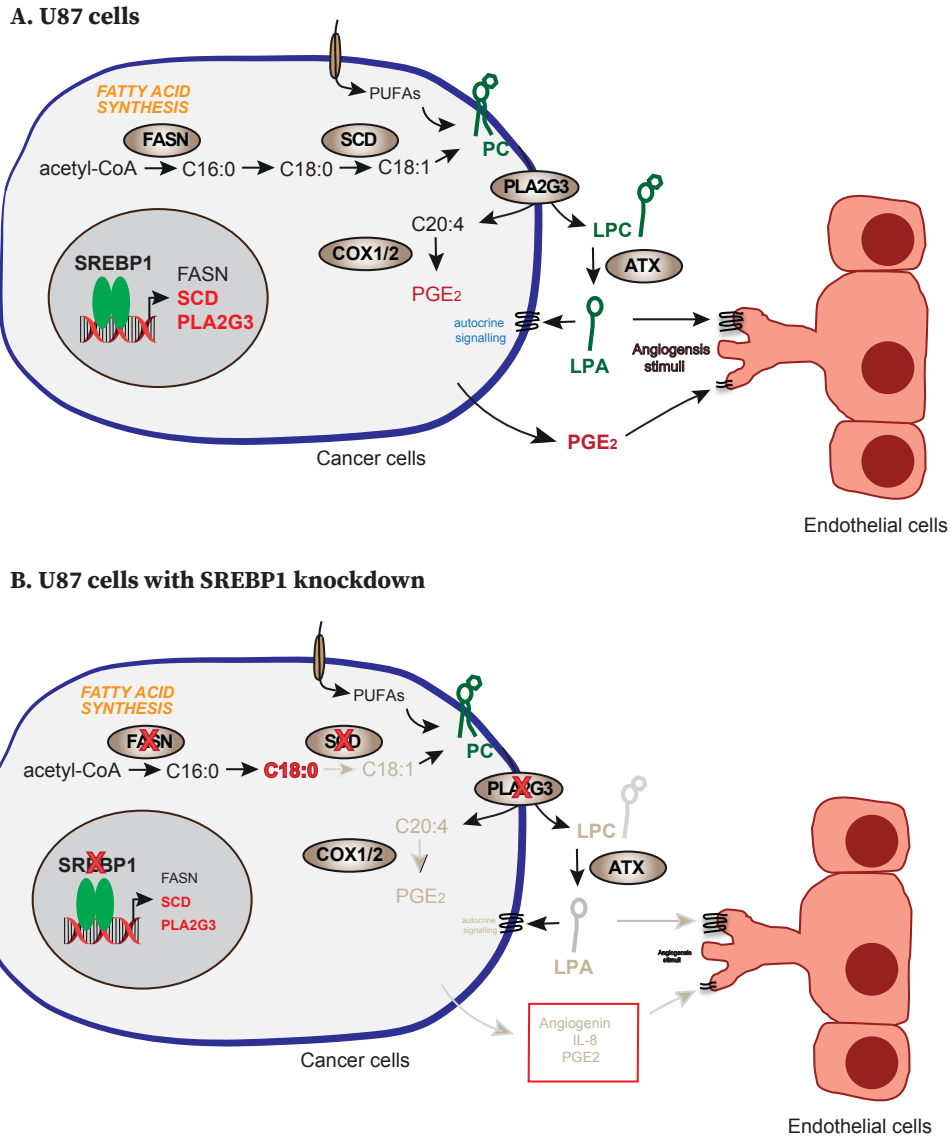

Figure 4.42: Model for angiogenesis regulation by SREBP1 network in GB

4.5 SREBP1 plays an important role in survival and proliferation of glioblastoma stem like cells

Glioblastoma tumours are the most aggressive type of brain tumour and known to recur in almost all patients despite surgery, radio- and chemotherapy (Osuka and Van Meir, 2017). There is a large body of literature studying the presence of stem like cells in GB, which are known to be resistant to the treatments and could be responsible for tumour recurrence. Hence, analysing the metabolic phenotype and adaptations in these types of cells could be crucial and utmost necessary to improve current therapeutic strategies and enhance the survival of GB patients.

Metabolic adaptations also occur in response to environmental cues determined by the nutrients available to the cells in the tumour bulk. As discussed in the earlier chapters, SREBP1 becomes important in cancer cells needing to survive in metabolically deprived conditions by supporting the switch to *de novo* fatty acid synthesis. Investigating and analysing the role of SREBP1 in GB stem like cells might reveal whether these cells have inherently rewired their SREBP1 network compared to differentiated cancer cells and determine whether SREBP1 is required to maintain the stem cell phenotype.

4.5.1 SREBP1 target genes are upregulated in glioblastoma stem-like cells

GB stem like cells (GSC) used in this study were from a patient derived GB NCH644 cell line which are usually cultured as neurospheres in suspension cultures using a defined medium. In order to study metabolic differences between GSCs and differentiated cells, two culture systems were used: cells grown in monolayer culture (differentiated) or cells grown as neurospheres (stem like enriched population) (Fig 4.43A). Monolayer cultures are grown in media containing serum (FCS), which gives rise to a mixed population that contains a majority of differentiated cells and only a small number of stem like cells. Neurosphere cultures are grown in serum free media supplemented with growth factors (including transferrin, insulin, basic EGF and basic FGF; either provided as part of a supplement mix or added individually) and selectively

enrich the stem-like cell population. U87 cells grown in similar conditions were also used as a comparison.

NCH644 and U87 cells were grown in monolayer and neurosphere cultures (Fig. 4.43A) and RNA prepared from the cells was analysed by RNA-seq by Joana Peixoto (Biochemistry and Molecular Biology, Biocenter Würzburg). Data analysis was performed by S. Walz (Comprehensive Cancer Center Mainfranken). In parallel, metabolites were extracted from the same cell populations and used for metabolomics by LC-MS. These data are described in (Peixoto et al., 2021). GSEA analysis of the U87 data showed that HORTON SREBP1 targets are upregulated in neurospheres compared to cells grown in monolayer (Fig 4.43B). Also, qPCR analysis of the same RNA samples showed that the SREBP1 targets *SCD, PLA2G3* and *FABP3* are upregulated in NCH644 neurospheres compared to monolayer cells, with *FABP3* only showing a trend towards upregulation (Fig 4.43C). Levels of *GFAP* mRNA (highly expressed by differentiated GB cells) were largely downregulated showing that neurosphere culture selects for stem-like cell population (Fig 4.43C). SCD protein levels were also upregulated in neurospheres compared to monolayer culture (Fig 4.43D). Overall, these results show that GSC upregulate the SREBP1 network.

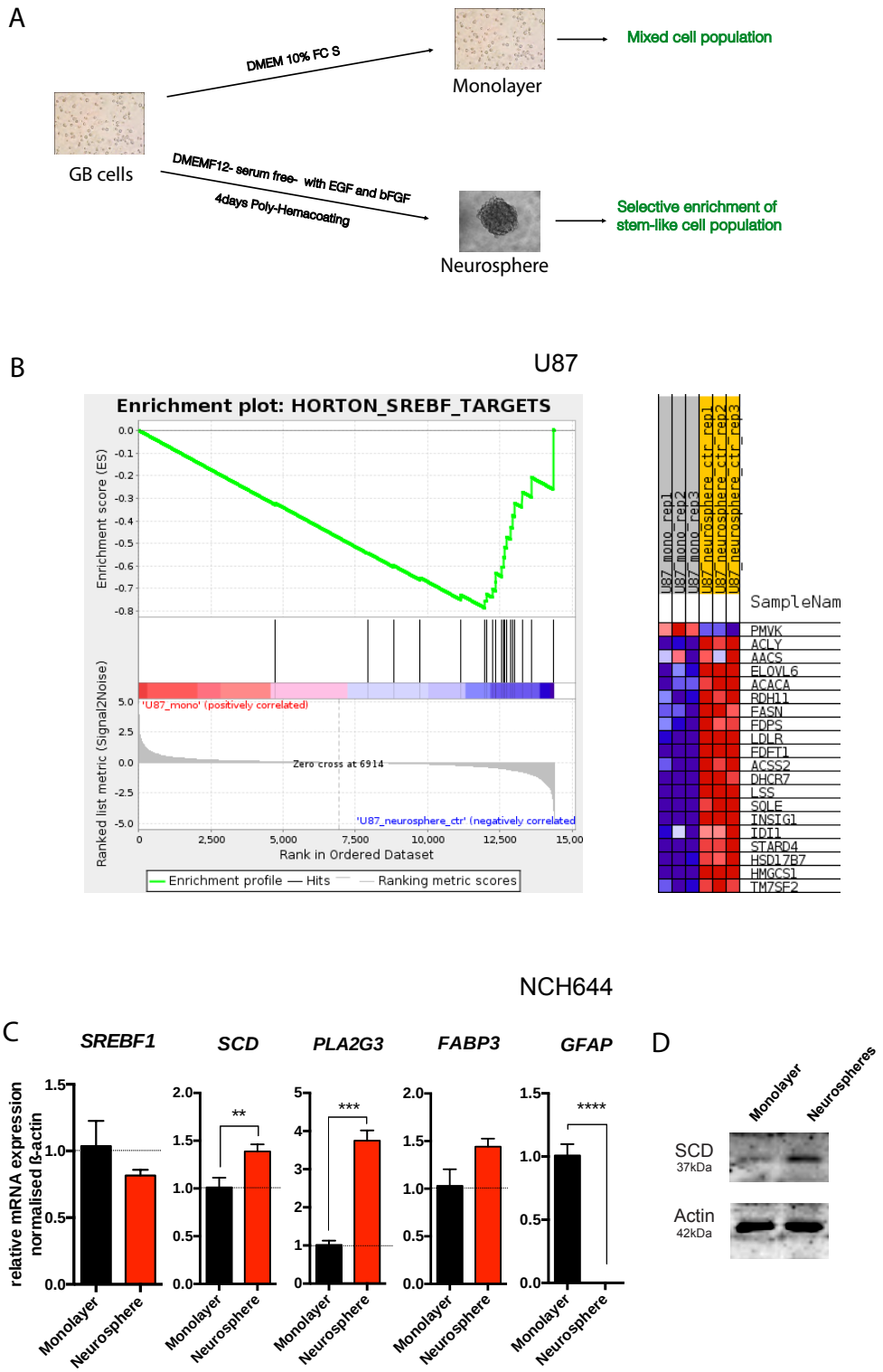

Figure 4.43: Glioblastoma stem like cells grown as neurospheres upregulate SREBP1 target genes

A) Diagram representing the experimental conditions used where NCH644 patient-derived GB stem cells or U87 cells were grown either as monolayer cultures in DMEM supplemented with 10% FCS or as neurospheres in suspension cultures in serum-free DMEM/F12 medium with B27 supplement, EGF and bFGF (both 20 ng/ml).

B) Enrichment plots of HORTON SREBP1 targets showing upregulation in U87 neurospheres compared to monolayer cultures. Neurospheres were generated by plating U87 in serum free media and culturing them for 4 days. Monolayer cells were grown adherent with media containing 10% FCS for 4 days.
C) qRT-PCR showing mRNA levels of *SREBF1*, *SCD, PLA2G3, FABP3 and GFAP* in NCH644 monolayer and neurosphere conditions. Neurospheres were generated by plating NCH644 in serum free media and culturing them for 4 days. Monolayer cells were grown adherent with media containing 10% FCS for 4 days. mRNA levels are shown relative to monolayer condition. Bars represent mean ± SEM (n=3). p-values were calculated using a two tailed student's t-test (p-values are represented as ** ≤ 0.01, *** ≤ 0.001 and **** ≤ 0.0001).
D) WB showing higher levels of SCD in NCH644 neurospheres compared to monolayer cultures.

4.5.2 Cell proliferation is reduced upon knockdown of SREBP1 in glioblastoma stem-like cells

To investigate the role of SREBP1 in GSC, shRNAs targeting SREBP1 (LT3-BP1_01 and 06) that were previously validated in U87 cells were introduced into NCH644 cells. NCH644 cells expressing shRen, shBP1_01 and shBP1_06 were cultured in GSCs media containing 2.25 µM Dox or ethanol (solvent control) to form neurospheres for 6 days (Fig 4.44A). mRNA levels of *SREBF1*, *SCD* and *PLA2G3* were reduced upon SREBP1 knockdown in NCH644 cells grown as neurospheres (Fig 4.44B). Also, cell numbers were significantly reduced upon loss of SREBP1 with both shRNA sequences compared to the shRenilla control cells (Fig 4.44C). Furthermore, analysis of fatty acids in NCH644 neurospheres upon SREBP1 knockdown showed a trend towards a reduction in the ratio of monounsaturated to saturated fatty acids and accumulation of arachidonic acid (C20:4) (Fig 4.44D), similar to the findings obtained in U87 cells described in chapter 4.3.

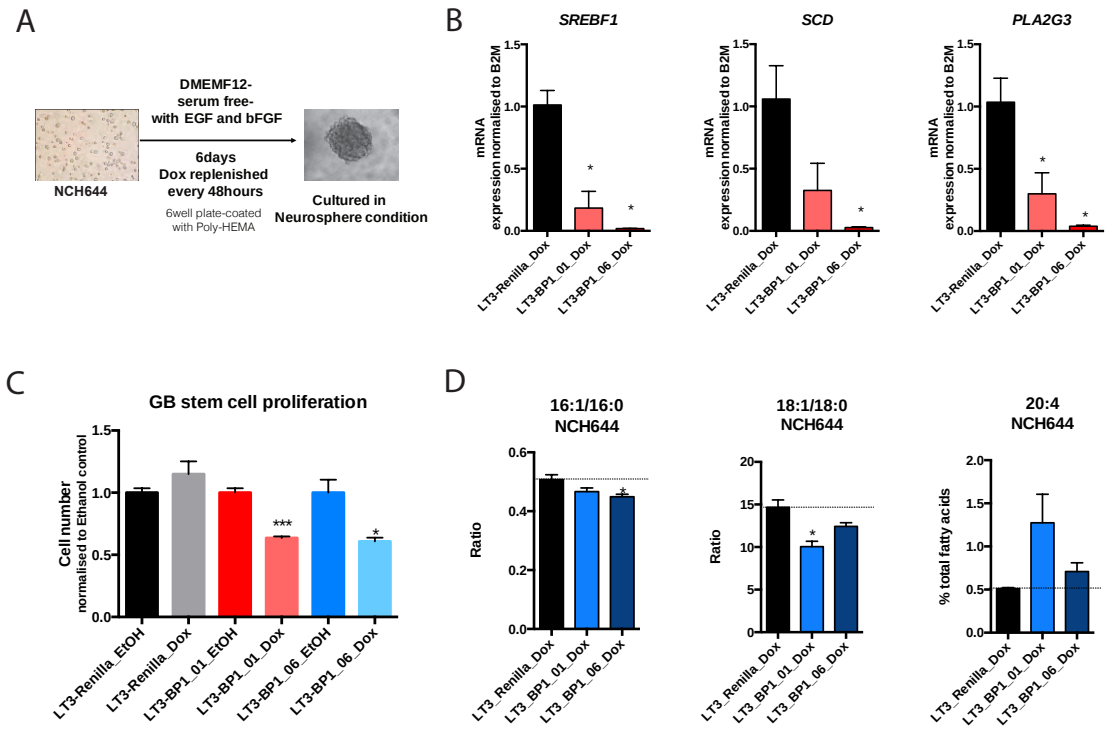

Figure 4.44: SREBP1 knockdown reduces proliferation of Glioblastoma stem like cells

A) Diagram representing the experimental conditions where NCH644 patient derived GSC were grown as neurospheres for 6 days in the presence of 2.25 µM Dox or ethanol (solvent).

B) qRT-PCR showing mRNA levels of *SREBF1*, *SCD and PLA2G3* in NCH644 cells expressing shRenilla (LT3-Renilla), shBP1_01 (LT3-BP1_01) and 06 (LT3-BP1_06) sequences. The cells were cultured in GSC media 1 containing 2.25 µM Dox to form neurospheres for 6 days. mRNA levels are shown relative to shRenilla condition.

C) Cell number of NCH644 cells expressing shRenilla, shBP1_01 and 06 sequences which were cultured as is (B). After 6 days, neurospheres were dissociated and cell numbers were determined by counting. Values are normalised to shRenilla treated with ethanol (n=3).

D) Parallel cultures were used for total fatty acid extraction and analysed by MS following direct injection. Ratio of palmitoleic acid over palmitic acid (C16:1/C16:0), oleic acid over stearic acid (C18:1/C18:0) and levels of arachidonic acid in SREBP1 silenced and control cells.

Bars represent mean ± SEM (n=3). p-values were calculated using a two tailed student's t-test (p-values are represented as * ≤ 0.05, *** ≤ 0.001).

4.5.3 Capacity to form neurospheres is reduced upon knockdown of SREBP1 in glioblastoma stem-like cells

SREBP1 knockdown was induced in a neurosphere formation assay by growing NCH644 cells expressing shRen, shBP1_01 and shBP1_06 in GSC media containing 2.25 µM Dox or ethanol (solvent) for 10 days while replenishing Dox/ethanol every 48 hours. After this time, multiple representative images of the cultures were taken and analysed for the number of neurospheres per area and neurosphere size (area of individual neurospheres) using imageJ analysis. Furthermore, all remaining

neurospheres were collected and segregated, and total cell number was determined by cell counting. As shown in Figure 4.45D, SREBP1 knockdown did not alter the size of the neurospheres formed. In contrast, neurospheres number and the cells number at the end of the 10-day assay was significantly reduced following SREBP1 silencing in NCH644 cells (Fig 4.45B-C). Also, it was confirmed that SREBP1 silencing was maintained for 10 days as a reduction of mRNA levels of *SREBF1* and *SCD* was observed (Fig 4.45E).

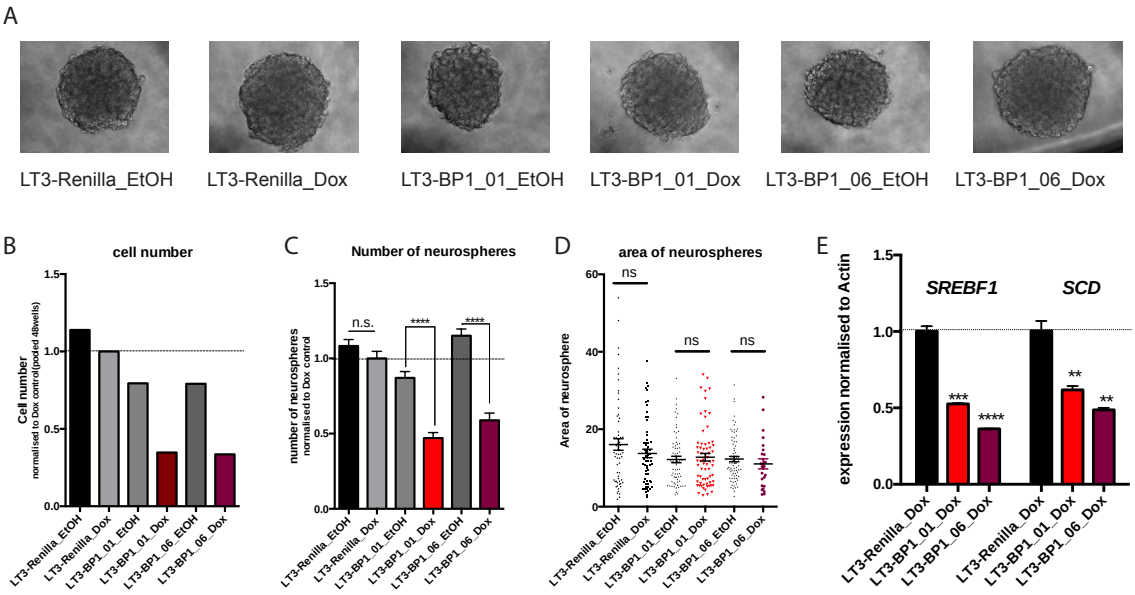

Figure 4.45: SREBP1 knockdown reduces number of neurospheres of glioblastoma stem like cells in a neurosphere formation assay

A) Representative images of neurospheres of NCH644 cells expressing shRenilla (LT3-Renilla), shBP1_01 (LT3-BP1_01) and 06 (LT3-BP1_06) sequences either treated with ethanol or Dox. Neurospheres were grown in GSC media 1 containing 2.25 µM Dox or ethanol (solvent) to form neurospheres for 10 days with Dox and ethanol being replaced every 48 hours in a 96 well plate. Each condition had 48 wells. Spheroid images were taken at 20X magnification on a bright field microscope.

B) Cell number of cells treated with the same conditions shown in A. All 48 wells were pooled for the cell count for each condition.

C) Number of neurospheres treated with the same conditions shown in A. 16 wells were counted for each condition.

C) Area of neurospheres treated with the same conditions shown in A. Image of all neurospheres in 3 wells were taken and area of each neurosphere was quantified on ImageJ.

D) qRT-PCR showing mRNA levels of *SREBF1* and *SCD* in neurospheres treated as in A (only Dox samples are shown here). mRNA levels are shown relative to shRenilla Dox.
Bars represent mean ± SEM (n=3). p-values were calculated using a two tailed student's t-test (p-values are represented as * ≤ 0.05, ** ≤ 0.01, *** ≤ 0.001 and **** ≤ 0.0001).

To understand if SREBP1 is involved in the maintenance of GB stemness and not just required for cell proliferation, the neurosphere formation assay was performed by adding 0.5% methyl cellulose to the culture medium, to increase viscosity, and by lowering the cell number seeded into wells do prevent cells from aggregating. Using this technique, the resulting neurospheres are expected to derive from individual cells. NCH644 cells expressing shRen, shBP1_01 and shBP1_06 were seeded in GSCs media containing 0.5% methyl cellulose and the same growth factors and supplements as used in the previous assays. To induce silencing, 2.25 μM Dox or ethanol (solvent control) was added and cells were incubated to form neurospheres for 10days, with Dox and ethanol being replenished every 48 hours. In addition, 100 μM oleic acid coupled to BSA or BSA alone was also added as control. This assay also involved the serial generation of neurospheres (Fig 4.46A) to test the effect on long-term maintenance of the stem cell population. For this, neurospheres formed after 10 days were dissociated and cells were seeded at equal cell number to initiate the formation of secondary neurospheres. This process was then repeated for the formation of tertiary neurospheres.

Interestingly, the number of neurospheres in the primary neurosphere generation was significantly reduced upon SREBP1 silencing and was restored by the addition of oleic acid. These results were consistent for both shRNA sequences targeting SREBP1, using shRenilla as control cells (Fig 4.46A). Cell counting at the end of 10 days after harvesting of primary neurospheres also revealed a reduction in cell number in SREBP1 knockdown cells, and addition of oleic acid was again able to rescue this decrease in cell number (Fig 4.46B). However, it was also observed that addition of oleic acid resulted in increased cell numbers in control cells, suggesting that oleic acid has a positive effect on GSC proliferation. Importantly, despite reduction in the number of neurospheres and the reduced cell number observed upon SREBP1 silencing, there was no reduction in the area of the individual neurospheres (Fig 4.46C).

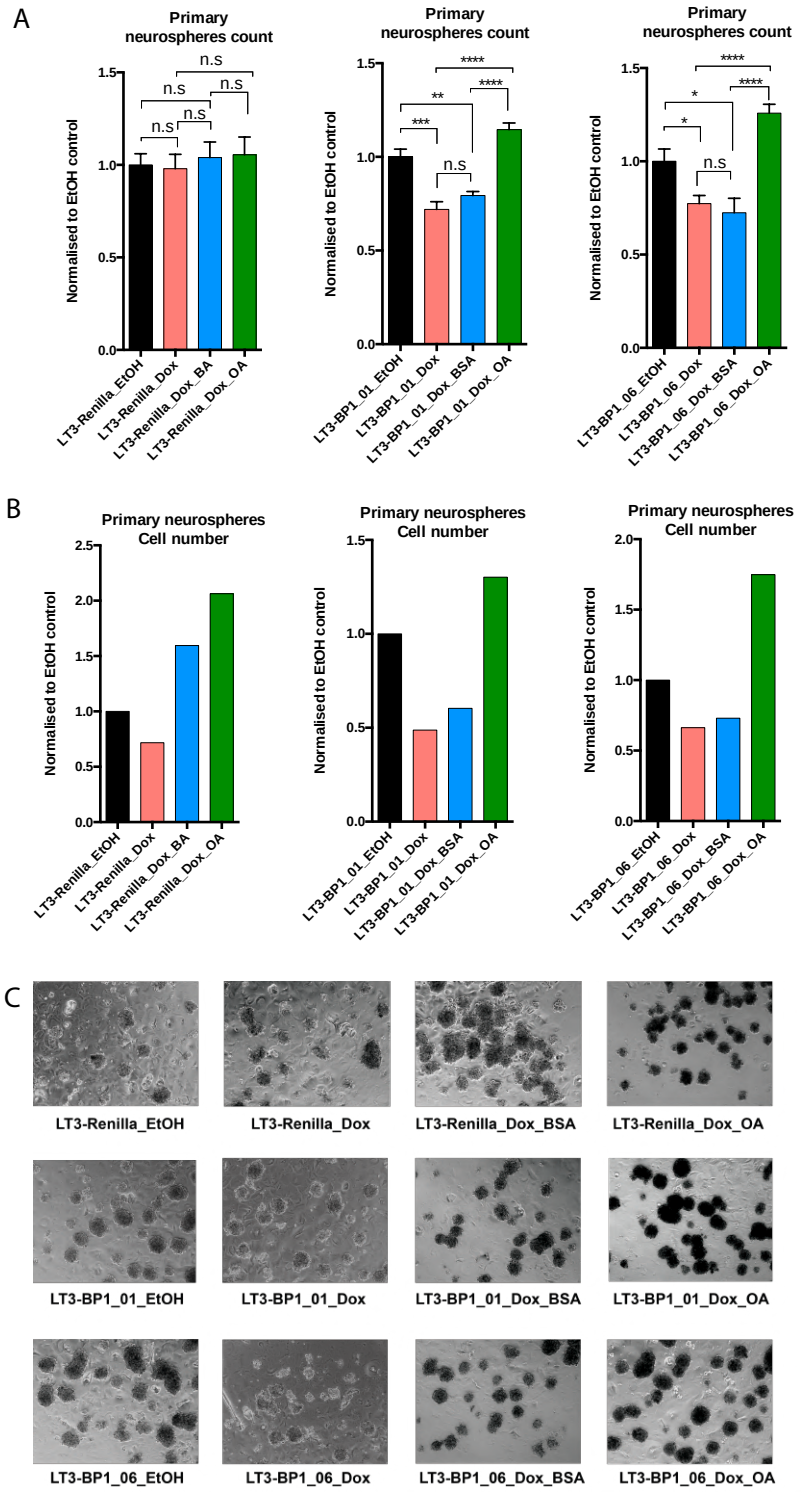

Figure 4.46: SREBP1 knockdown reduces number of primary neurospheres of GB stem like cells in a neurosphere formation assay and can be rescued by oleic acid

A) Number of neurospheres in a primary neurosphere assay in NCH644 cells expressing shRenilla (LT3-Renilla), shBP1_01 (LT3-BP1_01) or shBP1_06 (LT3-BP1_06). Cells were seeded in 48-well plates in GSC media 1 with 0.5% methyl cellulose supplemented with either 2.25 µM Dox, BSA, 100 µM BSA-coupled oleic acid or ethanol (solvent) and incubated to form neurospheres for 10 days. Dox and ethanol were replenished every 48 hours. Every condition has 12 wells. After 10 days, all neurospheres from 6 wells were counted per condition.

B) Total cell number of neurospheres collected from primary neurosphere cultures shown in C. 12 wells were combined for each data point.
C) Representative images of primary neurospheres of NCH644 cells grown in same conditions as in A. The spheroid images were taken at 5X magnification on a brightfield microscope.
p-values were calculated using a two tailed student's t-test (p-values are represented as * ≤ 0.05, ** ≤ 0.01, *** ≤ 0.001 and **** ≤ 0.0001).

Number of neurospheres in the secondary neurosphere generation was also significantly reduced upon SREBP1 silencing and rescued by the addition of oleic acid. These results were also consistent for both shRNA sequences targeting SREBP1 (shBP1_01 and 06) and using shRenilla as control (Fig 4.47A). Cell counting at secondary neurospheres after 10 days of culture also revealed a reduction in cell number following SREBP1 knockdown and the addition of oleic acid was able to restore this (4.47B). However, it has to be noted that there was a substantial effect of Dox on cell number also in the non-targeting control. However, as the BSA treated samples of control cells did not show this reduction in cell number, it is hard to conclude about a potential Dox effect (Fig 4.47B). Also, neurosphere size (area of each individual neurosphere) did not alter upon SREBP1 silencing in secondary neurosphere cultures (Fig 4.47C).

During the preparation of the tertiary neurospheres, it was noted that only a small number of cells remained in the SREBP1 silenced populations. Moreover, these cells had lost GFP-positivity, indicating that cells expressing the shRNA hairpin had been de-selected. Thus, conclusions from experiments with tertiary neurospheres were hard to interpret and hence not included here.

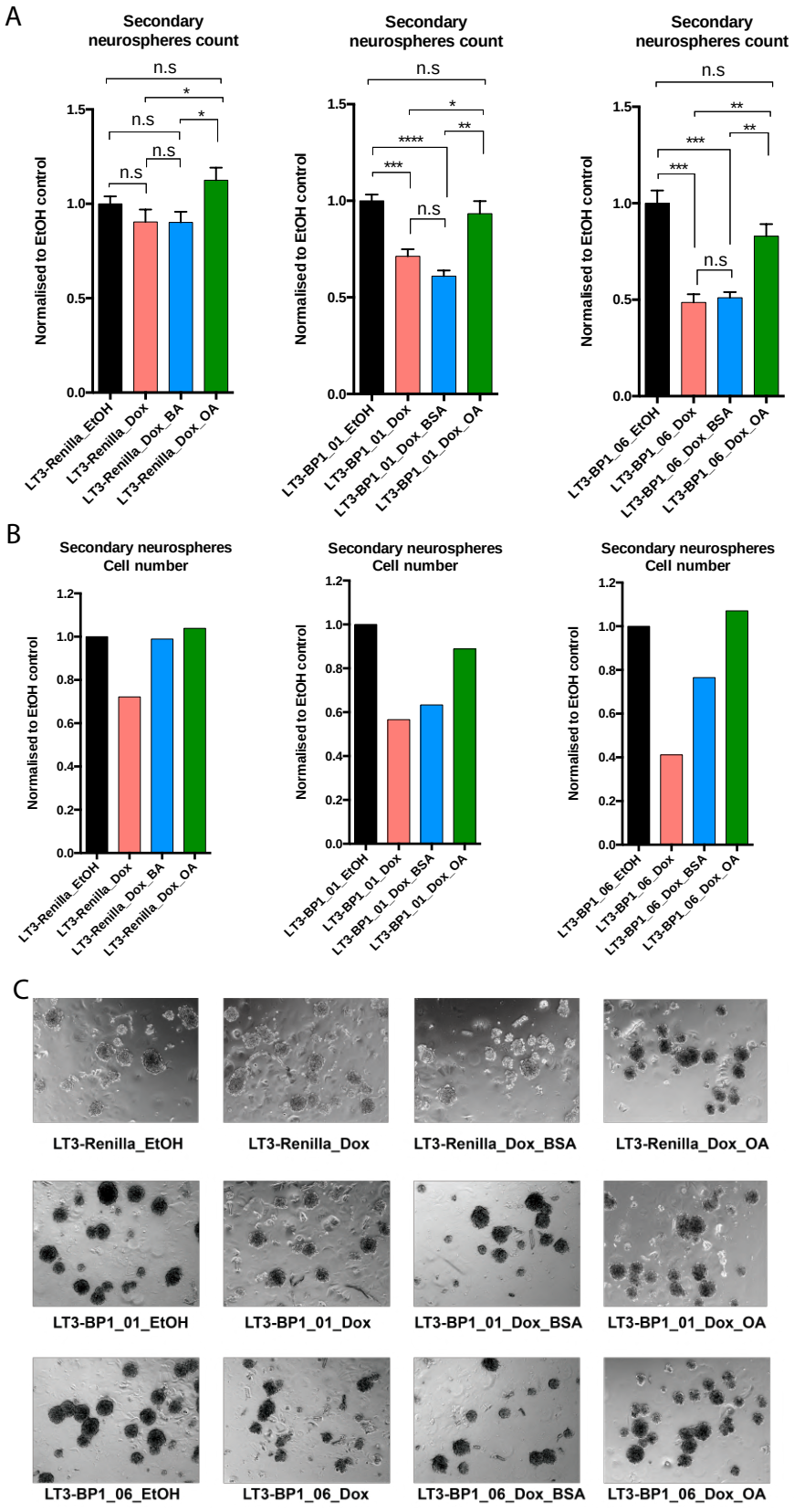
A
Secondary neurospheres count
Normalised to EtOH control
n.s
*
**
***
****
LT3-Renilla_EtOH
LT3-Renilla_Dox
LT3-Renilla_Dox_BA
LT3-Renilla_Dox_OA
LT3-BP1_01_EtOH
LT3-BP1_01_Dox
LT3-BP1_01_Dox_BSA
LT3-BP1_01_Dox_OA
LT3-BP1_06_EtOH
LT3-BP1_06_Dox
LT3-BP1_06_Dox_BSA
LT3-BP1_06_Dox_OA
B
Secondary neurospheres Cell number
C
LT3-Renilla_EtOH
LT3-Renilla_Dox
LT3-Renilla_Dox_BSA
LT3-Renilla_Dox_OA
LT3-BP1_01_EtOH
LT3-BP1_01_Dox
LT3-BP1_01_Dox_BSA
LT3-BP1_01_Dox_OA
LT3-BP1_06_EtOH
LT3-BP1_06_Dox
LT3-BP1_06_Dox_BSA
LT3-BP1_06_Dox_OA

Figure 4.47: SREBP1 knockdown reduces number of secondary neurospheres of GB stem like cells in a neurosphere formation assay and can be rescued by oleic acid

A) Number of neurospheres formed in secondary neurosphere cultures from NCH644 cells expressing shRenilla (LT3-Renilla), shBP1_01(LT3-BP1_01) or shBP1_06 (LT3-BP1_06) treated as described in Fig 4.46. Every condition has 12 wells. After 10 days, all neurospheres from 6 wells were counted per condition.
B) Total cell number of secondary neurosphere cultures grown in same conditions as A. 12 wells were combined for each data point.
C) Representative images of secondary neurospheres of NCH644 cells grown in same conditions as A. The spheroid images were taken at 5X magnification on a bright field microscope.
p-values were calculated using a two tailed student's t-test (p-values are represented as * ≤ 0.05, ** ≤ 0.01, *** ≤ 0.001 and **** ≤ 0.0001).

The results of the neurosphere assay performed in medium containing 0.5% methyl cellulose was further confirmed in U87 cells. For these cells expressing shScr and shBP1_07 were seeded in GSC media supplemented with 0.5% methyl cellulose, growth factors and supplements, treated with 2.25 µM Dox or ethanol (solvent control) and cultured for 10 days to form neurospheres. Dox and ethanol was replenished every 48 hours. It should be noted that U87 cells are not generally grown in neurosphere culture and were not adapted to the GSC medium before the assay. Nevertheless, it was observed that U87 cells readily form neurospheres under these conditions, indicating that normal cultures contain a substantial number of stem like cells.

A significant reduction in the number of neurospheres formed by U87 cells was observed upon SREBP1 knock down compared to solvent control (Fig 4.48A). However, it should be noted that shScr cells treated with Dox also displayed a significant reduction in the number of neurospheres. Nevertheless, SREBP1 silencing also resulted in a significant reduction of neurosphere number compared to shScr cells treated with Dox (Fig 4.48A) and further experimentation is required to resolve the effect of Dox on U87 neurosphere formation. In addition, total cell number was strongly reduced in neurosphere cultures after SREBP1 silencing compared to both solvent and Dox treated controls. Here, Dox did not induce an alteration in cell number (Fig 4.48B). In contrast to the results obtained with NCH644 cells, U87 cells upon SREBP1 knockdown also showed a significant reduction in neurosphere size, indicated by the area of individual neurospheres in the culture (Fig 4.48C-D).

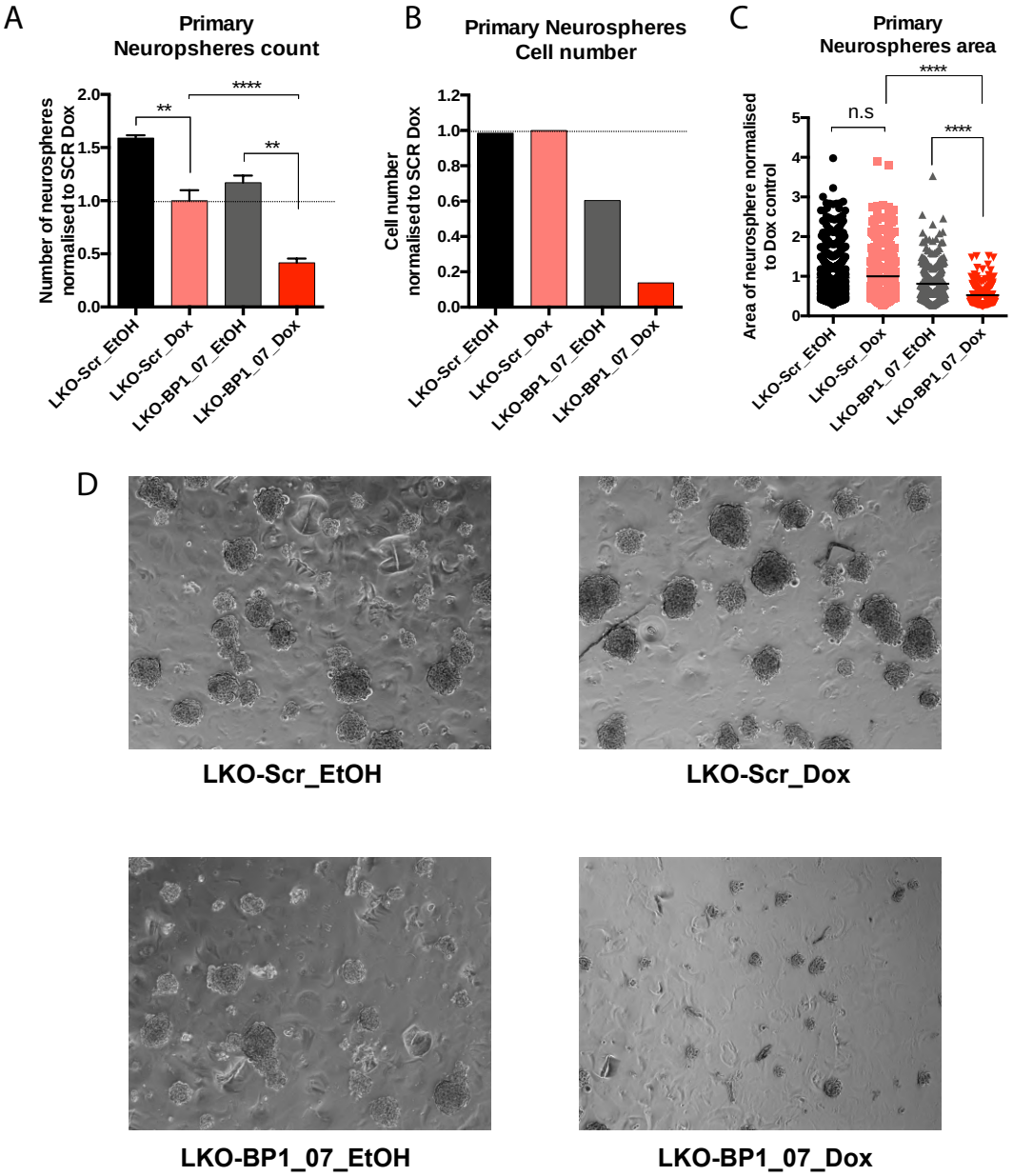

Figure 4.48: SREBP1 knockdown reduces number of primary neurospheres of U87 cells

A) Number of neurospheres collected from primary neurosphere cultures of U87 cells expressing shScr or shBP1_07. Cells were seeded in GSC media 2 containing 0.5% methyl cellulose supplemented with 2.25 µM Dox or ethanol (solvent) and incubated to form neurospheres for 10 days. Dox and ethanol was replenished every 48 hours. After 10 days, neurospheres from 6 wells were counted for each condition.

B) Total cell number of primary neurosphere cultures grown in same conditions as A. Neurospheres from 12 wells were combined for each data point.

C) Areas of individual neurospheres from primary neurosphere cultures shown in A. 6 parallel wells per condition were analysed.

D) Representative images of primary neurospheres of U87 cells shown in A. Images were taken at 5X magnification on a brightfield microscope.

p-values were calculated using a two tailed student's t-test (p-values are represented as * ≤ 0.05, ** ≤ 0.01, *** ≤ 0.001 and **** ≤ 0.0001).

Similar to the experiments conducted in NCH644 cells, cells from the primary neurosphere assays were also collected and seeded into secondary neurosphere cultures and treated in an equivalent manner. Neurosphere number was reduced upon SREBP1 silencing also in secondary neurospheres similar to primary neurospheres and also the Dox effect was still present in the control (Fig 4.49A). However, a strong reduction in total cell number in the secondary neurosphere cultures was only observed in the SREBP1 silencing condition, as seen in primary neurospheres (Fig 4.49B). Furthermore, SREBP1 knockdown significantly reduced neurosphere size compared to the Dox control (Fig 4.49C).

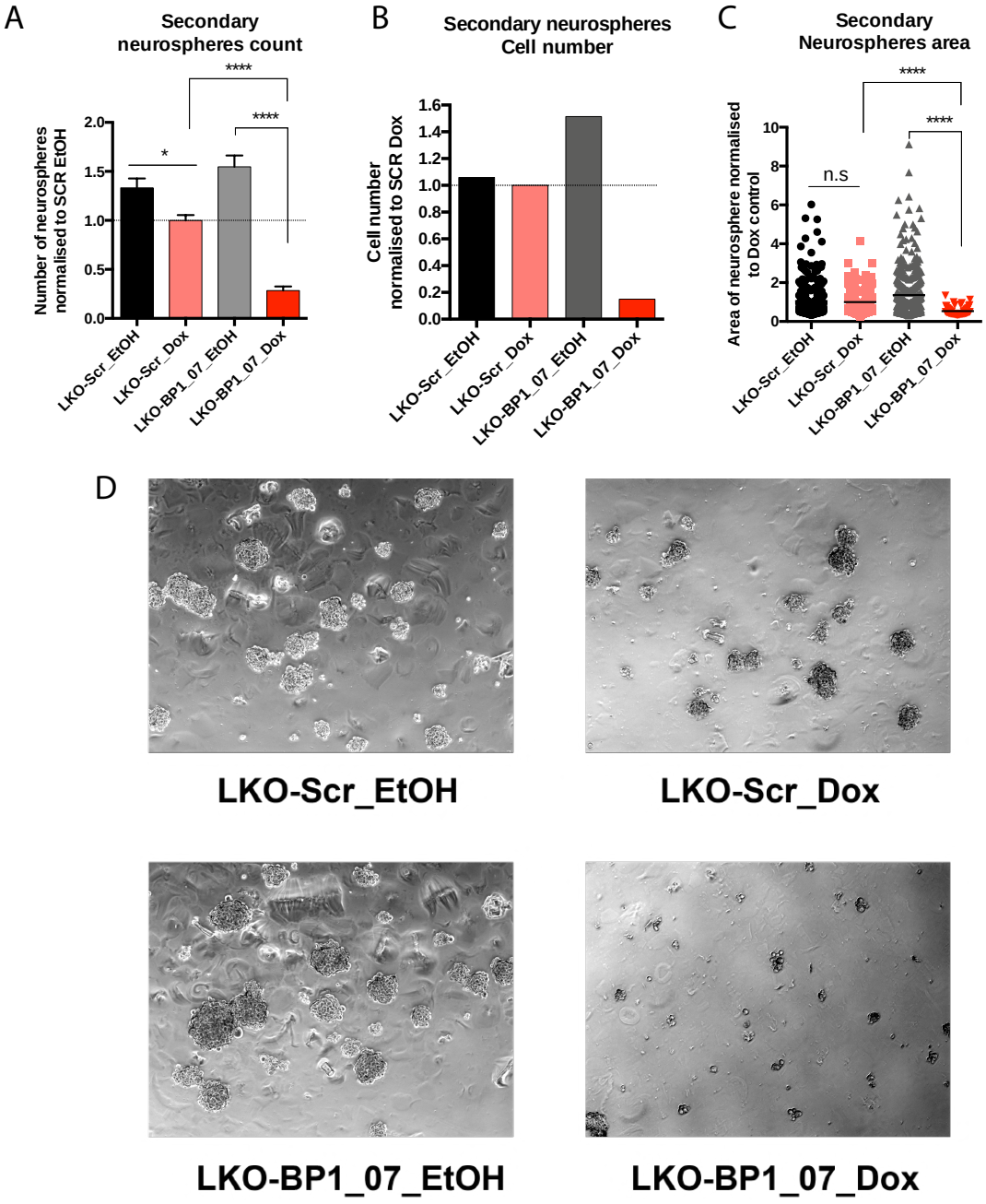

Figure 4.49: SREBP1 knockdown reduces number of secondary neurospheres of U87 cells

E) A) Number of neurospheres in secondary neurosphere cultures of U87 cells expressing shScr or shBP1_07 treated as described in Fig 4.48. After 10 days, neurospheres from 6 wells were counted for each condition.

A) B) Total cell number of neurospheres collected from secondary neurosphere cultures grown in same conditions as A. Neurospheres from 12 wells were combined for each data point.

B) C) Neurosphere size (area of individual neurospheres) collected from secondary neurosphere cultures grown in same conditions as A. All neurospheres in 6 wells were quantified for each condition on ImageJ.

C) D) Representative images of secondary neurospheres of U87 cells grown in same conditions as A. The spheroid images were taken at 5X magnification on a bright field microscope.

It was evident that there was a drastic reduction in the number and size of secondary neurospheres (Fig 4.49C-D) and there were far too few cells left to conduct experiments with tertiary neurosphere cultures. U87 cells, unlike NCH644 cells, did not exhibit loss of shRNA expression after long-term culture and still showed clear results upon SREBP1 silencing even after two neurosphere generations. However, there were not enough cells left to be seeded for tertiary neurosphere cultures. It could be interesting to repeat these experiments in U87 cells that have been adapted to neurosphere culture. Further experiments are also required to understand the differences seen in U87 and NCH644 cells.

4.6 Upstream regulation of SREBP1 by SOAT1

SOAT1 (also referred to as ACAT1) regulates the esterification of cholesterol-to-cholesterol esters and their compartmentalisation into lipid droplets (Geng *et al.*, 2016; Lee et al., 2018; Peck and Schulze, 2014; Yue *et al.*, 2014), thereby regulating the sterol levels that control the activity of the SREBP1 pathway. SOAT1 can strongly regulate SREBP1 and its target gene network in GB and could be a potential therapeutic target for the treatment of GB patients, as there are already bio-available drugs targeting SOAT1 used in different types of tumours (Cheng et al., 2018; Kroiss and Fassnacht, 2016; Lee et al., 2015).

To investigate the role of SOAT1 in GB, two shRNA sequences targeting SOAT1 were obtained from the Fellmann shRNA predictions (Fellmann *et al.*, 2013) and introduced into the pLT3-GEPIR doxycycline inducible system. Silencing efficiency in U87 cells expressing shSOAT1_02 and shSOAT1_03 sequences was validated using shRenilla cells as control. Cells were treated with 2.25 µM Dox or ethanol (solvent control) for 72 hours in medium containing 10%FCS. Afterwards, cells were washed with PBS and media was changed to 10% or 1% FCS containing media with 2.25 µM Dox or ethanol (solvent control) for 24 hours. *SOAT1* mRNA levels were significantly reduced upon SOAT1 knockdown in both 1% and 10% FCS compared to the solvent control (Fig 4.50A). Also, mRNA levels of *SOAT1* were analysed by comparing it to shRenilla cells treated with Dox, to avoid any fluctuations in the mRNA levels induced by Dox treatment, and it was clear that reduction in the SOAT1 mRNA was still strong and significant in this comparison (Fig 4.50B).

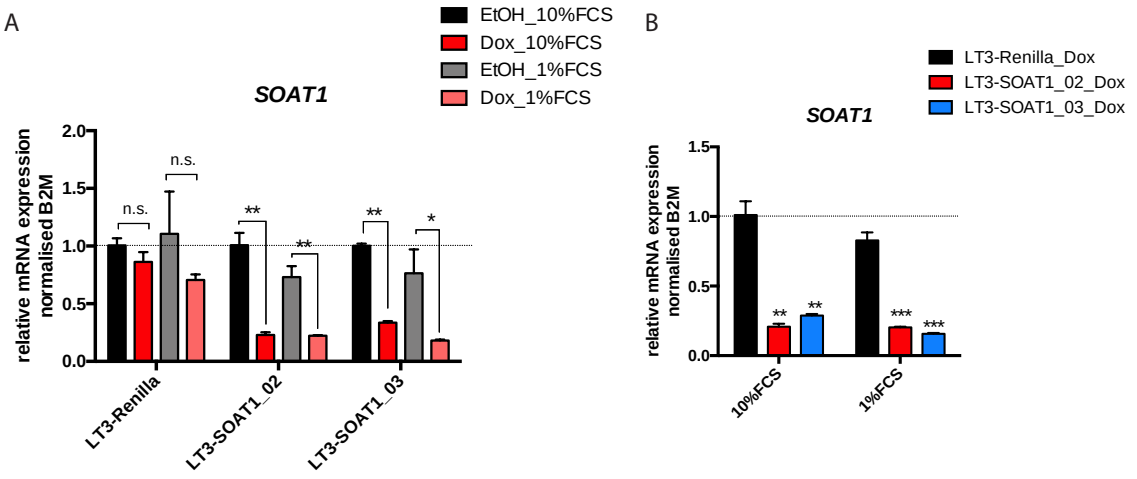

Figure 4.50: Validation of shRNAs targeting SOAT1 in PLT3-GEPIR dox inducible system

A) qRT-PCR showing mRNA levels of SOAT1. Cells expressing shRenilla (LT3-Renilla), shSOAT1_02 (LT3-SOAT1_02) and 03 (LT3-SOAT1_03) were treated with 2.25 μM Dox or ethanol (solvent control) in 10%FCS for 72 hours. Afterwards, cells were washed with PBS and the medium was changed to media containing 10% or 1% FCS with 2.25 μM Dox or ethanol (solvent control) for 24hours. mRNA levels are shown relative to shRenilla ethanol control.
B) Data for Dox treated samples presented as in A but normalised to shRenilla.
Bars represent mean ± SEM (n=3). p-values were calculated using a two tailed student's t-test (p-values are represented as * ≤ 0.05, ** ≤ 0.01 and *** ≤ 0.001).

4.6.1 SOAT1 knockdown or inhibition reduces expression of SREBP targets

Both shRNA sequences (shSOAT1_02 and 03) targeting SOAT1 were further analysed for efficient knockdown by checking SOAT1 protein levels. Cells were grown in the presence of 2.25 μM Dox or ethanol (solvent control) for 72 hours in medium containing 10% FCS. Afterwards, cells were washed with PBS and media was changed to 10% or 1%FCS containing media with 2.25 μM Dox or ethanol (solvent control) for 24 hours. The adrenal cortical carcinoma cell line NCI-H295 was used as a positive control, as these cells are known to display strong expression of SOAT1. NCI-H295 were grown in RPMI1640 medium supplemented with 10% FCS, 5.2 ng/mL sodium selenite, 100 μg/mL transferrin and 5 μg/mL insulin (Fig 4.51A). Induction of both shRNA sequences reduced SOAT1 protein levels in cells cultured in the 10% FCS condition (Fig 4.51A). Cells grown in the 1% FCS condition expressed lower levels of SOAT1 protein compared to the 10% FCS condition and it was difficult to conclude whether its levels were further reduced following knockdown (Fig. 4.51A).

Nevertheless, SOAT1 mRNA levels were substantially reduced by the induction of both shRNA hairpins following Dox treatment in either 10% or 1% FCS conditions (Fig. 4.51B-C, left graphs). It should be noted that the experiment shown in Fig. 4.51C was only performed in duplicate, preventing statistical assessment. Interestingly, mRNA levels of the SREBP targets *SCD* and *HMGCR* were significantly reduced upon SOAT1 knock down only in 10% FCS, with both sequences showing this effect (Fig 4.51B). But even though SOAT1 was efficiently silenced in cells cultured in 1% FCS, there was no detectable regulation of *SCD* and only a small reduction in *HMGCR* mRNA levels (Fig 4.51C). This indicates that regulation of cholesterol esterification by SOAT1 may have a stronger effect on SREBP2, which is the transcription factor primarily involved in the control of HMGCR expression.

Next, the effect of SOAT1 silencing on cell viability was determined. U87 cells expressing shRenilla, shSOAT1_02 or 03 were grown in media containing 10% or 1% FCS with 2.25 µM Dox or ethanol (solvent control) for 72 hours. Cells grown in low serum conditions showed reduced cell viability upon SOAT1 knock down (Fig 4.52A-B). Even though there was no change in *SCD* levels upon SOAT1 knockdown in cells cultured in 1% FCS, it was still important to investigate whether loss of viability was accompanied by the induction of ER stress, which can be induced by the inhibition of SREBP1 in lipid depleted conditions. However, *DDIT3* levels were reduced upon SOAT1 knockdown rather than upregulated and hence it was concluded that loss of SOAT1 did not reduce cell viability through the induction of ER stress (Fig 4.53). It should also be noted that the shRenilla cells showed a strong decrease in DDIT3 expression upon Dox treatment, even though this result was not significant. Nevertheless, the mechanism by which SOAT1 regulates cell viability in GB cells cultured in 1% FCS condition still needs to be determined.

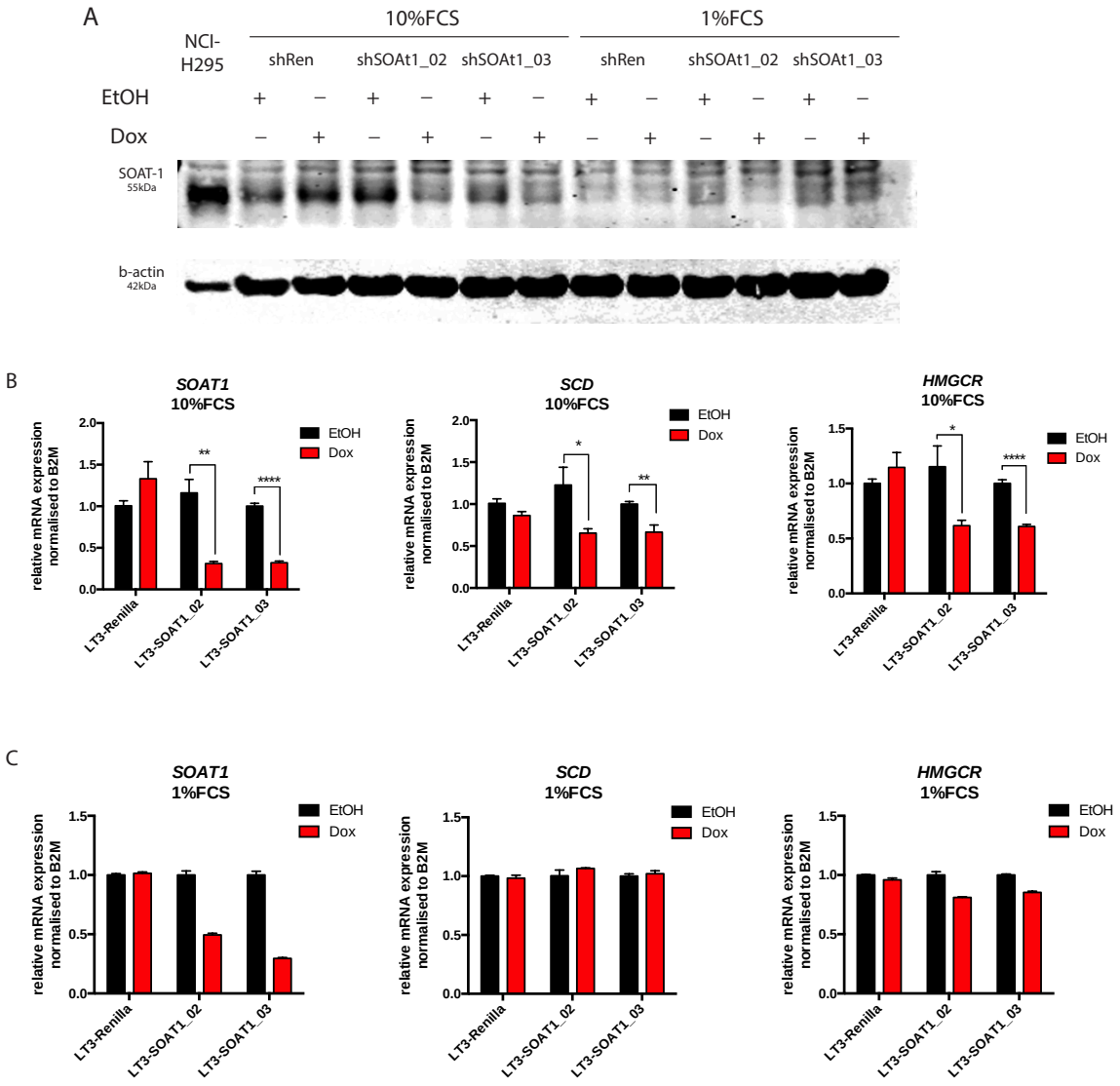

Figure 4.51: SOAT1 knockdown reduces mRNA levels of SREBP targets

A) WB shows SOAT1 protein levels in U87 cells expressing shRenilla (LT3-Renilla), shSOAT1_02 (LT3-SOAT1_02) or shSOAT1_03 (LT3-SOAT1_03). Cells were treated with 2.25 µM Dox or ethanol (solvent control) in medium containing 10% FCS for 72 hours. Afterwards, cells were washed with PBS and the medium was changed to media containing 10% or 1% FCS with 2.25 µM Dox or ethanol (solvent control) for 24 hours. β-actin serves as loading control. NCI-H295 cells serve as positive control for SOAT1 protein and were grown in RPMI1640 medium supplemented with 10% FCS, 5.2 ng/mL sodium selenite, 100 µg/mL transferrin and 5 µg/mL insulin.

B) qRT-PCR showing mRNA levels of *SOAT1*, *SCD* and *HMGCR* under the same conditions as in (A) but only the 10% FCS samples are shown. mRNA levels are shown relative to shRenilla ethanol condition. Bars represent mean ± SEM (n=4).
p-values were calculated using a two tailed student's t-test (p-values are represented as * ≤ 0.05, ** ≤ 0.01 and **** ≤ 0.0001).

C) qRT-PCR showing mRNA levels of *SOAT1*, *SCD* and *HMGCR* under the same conditions as in (A) but only 1% FCS samples are shown. mRNA levels are shown relative to shRenilla ethanol condition. Bars represent mean ± SEM (n=2).

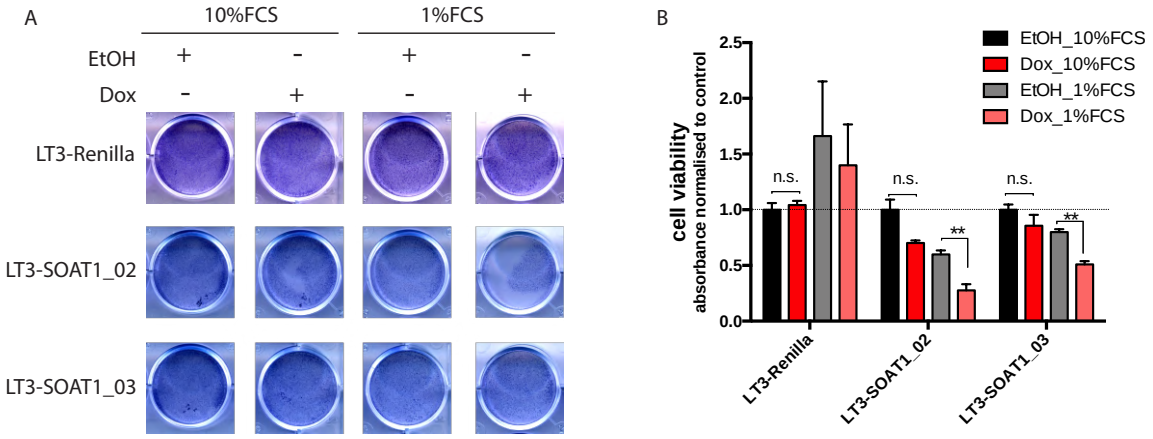

Figure 4.52: Decrease in cell viability upon SOAT1 knockdown in U87 cells upon low serum treatment

A) Crystal violet staining of U87 cells after SOAT1 silencing compared to control. U87 cells expressing shRenilla (LT3-Renilla), shSOAT1_02 (LT3-SOAT1_02) and shSOAT1_03 (LT3-SOAT1_03) were treated with 2.25 µM Dox or ethanol (solvent control) in medium containing 10% FCS for 72 hours. Afterwards, cells were washed with PBS and the medium was changed to media containing 10% or 1% FCS with 2.25 µM Dox or ethanol (solvent control) for 24hours. Cells were fixed and total protein was stained with crystal violet.

B) Quantification of crystal violet staining in (A). The values of quantification are normalised to ethanol treated cells in 10% FCS condition. Bars represent mean ± SEM (n=3). p-values were calculated using a two tailed student's t-test (p-values are represented as ** ≤ 0.01, n.s.= not significant).

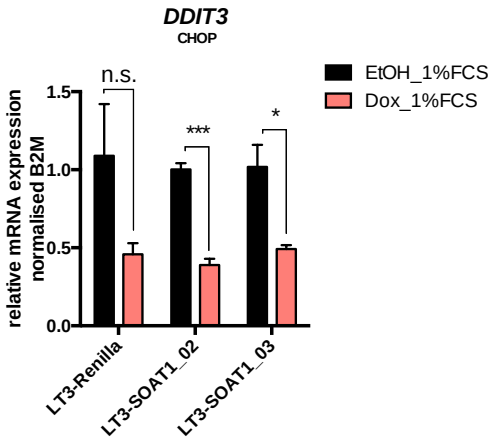

Figure 4.53: SOAT1 knockdown in U87 cells cultured in 1% FCS does not induce DDIT3 expression

qRT-PCR showing mRNA levels of the ER-stress gene *DDIT3*. mRNA levels are shown relative to ethanol control. Cells were treated as described in 4.52. Bars represent mean ± SEM (n=3). p-values were calculated using a two tailed student's t-test (p-values are represented as, ** ≤ 0.01 and *** ≤ 0.001).

To investigate the effect of SOAT1 inhibition on SREBP1 target genes expression in GB cells, U87 and U251 cells were treated with the SOAT1 inhibitors mitotane at 100 µM and ATR101 at 13 µM in medium containing 10% FCS medium, using ethanol as a solvent control. U87 cells were treated with mitotane at 6 and 24 hours, while U251 cells were only treated for 24 hours. There was a strong reduction in mRNA levels of *SCD, SREBP1, HMGCR* downstream of SOAT1 in both cell lines upon treatment with mitotane compared to the solvent control (Fig 4.54A). Similarly, the SOAT1 inhibitor ATR101 used at a concentration of 13 µM also showed reduction in mRNA levels of *SCD, SREBP1, HMGCR* in both U87 and U251 cells (Fig 4.54B). However, both experiments were exploratory and only performed in single replicates precluding statistical analysis.

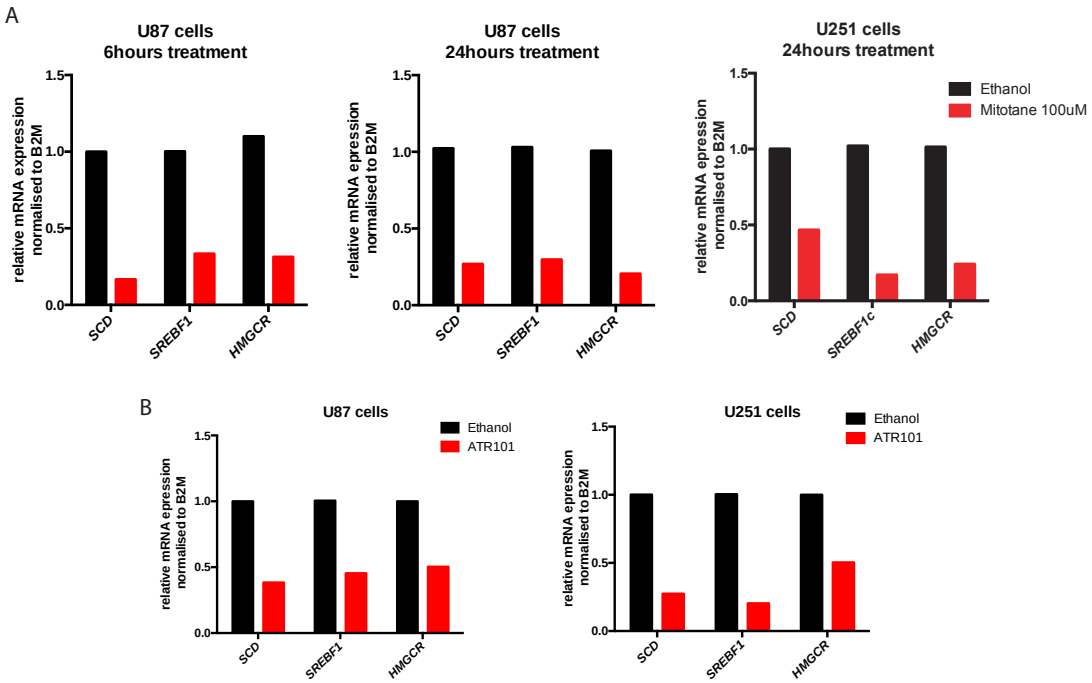

Figure 4.54: Inhibitors targeting SOAT1 reduce mRNA levels of SREBP targets

A) qRT-PCR showing mRNA levels of *SCD*, *SREBF1* and *HMGCR* in U87 cells treated with 100 µM mitotane for either 6 or 24 hours and U251 cells for 24hours in 10%FCS medium.
B) qRT-PCR showing mRNA levels of *SCD*, *SREBF1* and *HMGCR* in U87 and U251 cells treated with ATR101 13 µM for 24 hours in 10%FCS medium.

As cell viability was reduced in U87 cells upon SOAT1 knockdown in cells cultured in 1% FCS condition, mitotane was also used to investigate the effect of SOAT1 inhibition on cell viability of U87 and U251. Cells were treated with mitotane at a concentration of 100 µM in medium containing 10% or 1% FCS for 24hours with ethanol used as solvent control. The mTORC1 inhibitor rapamycin was used at a concentration of 50 nM as positive control for decrease in SREBP1 transcriptional output. Rapamycin reduced cell viability by up to 50% in U87 cells both in the 10% and 1% FCS condition, but not in U251 cells (Fig 4.55A-B). Mitotane reduced cell viability by about 50% in the 10% FCS condition in U87 cells, and to a minor extent in U251 cells (Fig 4.55A-B). However, in the 1% FCS condition, there was a drastic reduction in cell viability in both cell lines (Fig 4.55A-B).

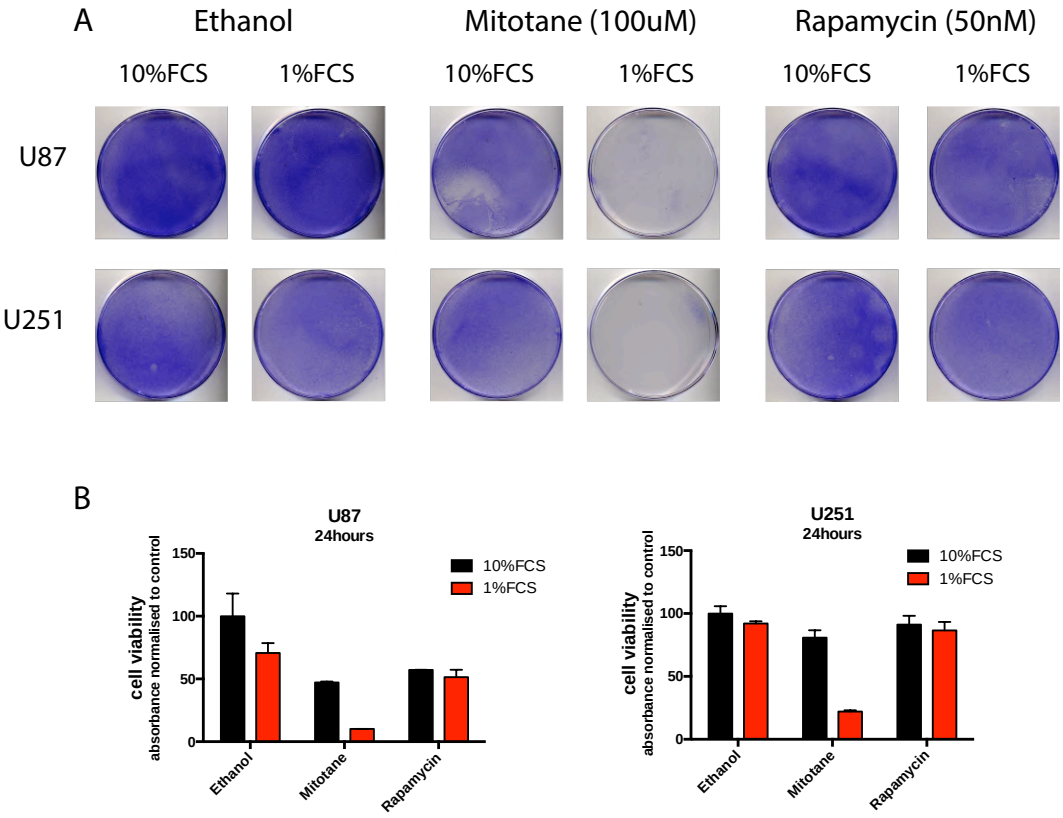

Figure 4.55: Decrease in cell viability of U87 and U251 cells treated with mitotane in low serum condition

A) Crystal violet staining of U87 and U251 cells treated with ethanol, 100 µM mitotane or 50nM rapamycin in medium containing 10% FCS or 1%FCS for 24hours.

B) Quantification of crystal violet staining shown in (A). Values are normalised to ethanol controls in 10% FCS conditions. Bars represent mean ± SEM (n=2, each biological replicate in technical duplicate).

While these results suggest that inhibition of SREBP function by blocking the esterification of cholesterol could impair the viability of GB cells exposed to serum-depleted condition, the drastic effect of mitotane could also have been due to higher availability of the drug in the 1% FCS condition, as mitotane is known to bind to lipoproteins and BSA in serum (Kroiss et al., 2016). Even though reduction in cell viability of U87 cells was observed upon SOAT1 knockdown, it was not entirely clear if the reduction in cell viability by mitotane was due to the inhibition of the SREBP1 pathway. To explore this further, cell viability assays were performed with different mitotane concentrations in medium supplemented with 10, 5 and 1% FCS in both U87 and U251 cells (Fig 4.56A-B). This experiment showed that only the1% FCS condition revealed a drastic reduction in cell viability at both 50 and 100μM of mitotane. In cells cultured in 5 and 10% FCS, only 100 μM of mitotane caused a reduction in cell viability (Fig 4.56A-B).

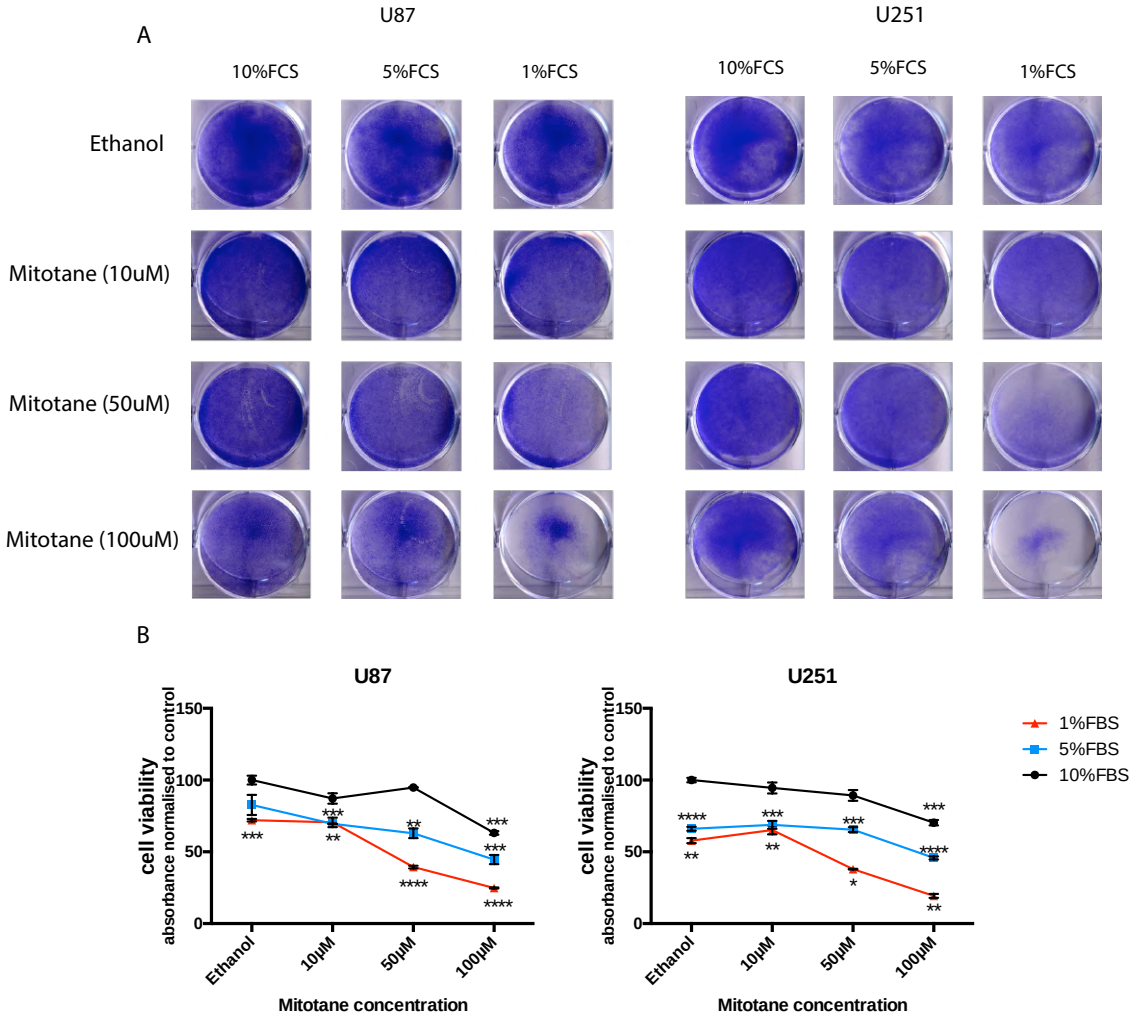

Figure 4.56: Cell viability of U87 and U251 cells treated with different mitotane concentrations in medium containing various FCS concentrations

A) Crystal violet staining of U87 and U251 cells treated with 10, 50 or 100 μM mitotane in medium containing 1, 5 or 10% FCS for 24hours. Ethanol was used as solvent control.

B) Quantification of crystal violet staining in (A) shown as dose-response curves. The values of quantification are normalised to ethanol controls in 10% FCS. Each point on the growth curve represent mean ± SEM (n=3). p-values were calculated using a two tailed student's t-test (p-values are represented as * ≤ 0.05, ** ≤ 0.01, *** ≤ 0.001 and **** ≤ 0.0001).

To confirm the reduction in cell viability observed upon SOAT1 inhibition using mitotane, U87 and U251 cells were treated with another small-molecule SOAT1 inhibitor, avasimibe, in a dose-response experiment with increasing concentration ranging from 1 to 50μM in medium containing 1% or 10% FCS for 24hours. The two cell lines showed differential sensitivity to this compound, but both cell lines responded with a complete reduction in cell viability when treated with 10 to 50 μM of avasimibe in 1% FCS medium (Fig 4.57). Out of the two cell lines, U87 cells were more sensitive

to avasimibe and displayed a 50% reduction in viability at a concentration of approx. 20 µM in 10% FCS medium and at 1.5 µM in 1% FCS medium (Fig 4.57A). U251 cells reduced viability by 50% at a concentration of 30 µM in 10% FCS medium and at 5 µM in 1% FCS medium (Fig 4.57B).

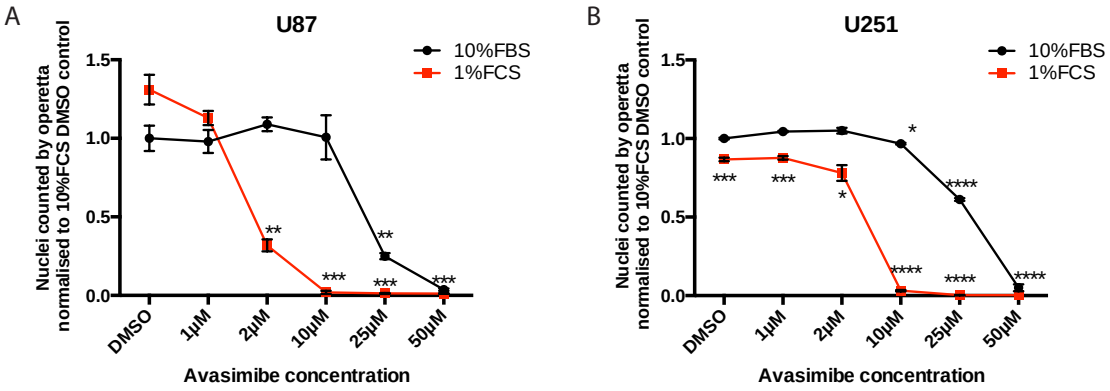

Figure 4.57: Cell viability of U87 and U251 cells treated with different avasimibe concentrations in medium containing 10% or 1% FCS

U87 (A) and U251 (B) cells were treated with increasing concentration of avasimibe (1 to 50 µM) or ethanol (solvent control) in medium containing either 1% or 10% FCS for 24hours. Cell viability was quantified based on nuclei staining by DAPI and counted on an automated microscope (Perkin Elmer, Operetta). Quantifications were used to generate dose-response curves. Values of quantification are normalized to ethanol controls in 10% FCS sample. Each point on the growth curve represent mean ± SEM (n=3).
p-values were calculated using a two tailed student's t-test (p-values are represented as * ≤ 0.05, ** ≤ 0.01, *** ≤ 0.001 and **** ≤ 0.0001).

Next, rescue experiments were performed on cells treated with mitotane by addition of oleic acid coupled to BSA. U87 and U251 cells were treated with mitotane at 50 and 100 µM in medium containing 10% or 1%FCS. In addition, either BSA or BSA-coupled oleic acid was added to the 1% FCS condition. All treatments were conducted for 24 hours. As observed before, U87 cells showed more sensitivity to mitotane in the 10% FCS condition, resulting in a substantial reduction of cell number at 50 and 100 µM of the drug, while U251 cells were not affected under these conditions (Fig 4.58A-B). In contrast, both cell lines showed a similar response to mitotane at 50 and 100 µM in medium containing 1% FCS (Fig 4.58A-B). Moreover, addition of BSA reduced the effect of mitotane in both U87 and U251 cells in media with 1% FCS, suggesting that mitotane binds to BSA reducing its toxicity. This was most apparent in U251 cells, where BSA alone completely abolished the mitotane

effect. Addition of oleic acid to mitotane treated cells cultured in medium with 1% FCS induced a complete rescue of cell viability in U87 cells (Fig 4.58A). However, as viability in U251 cells was already restored by BSA alone, it was impossible to determine the effect of oleic acid in these cells (Fig 4.58B).

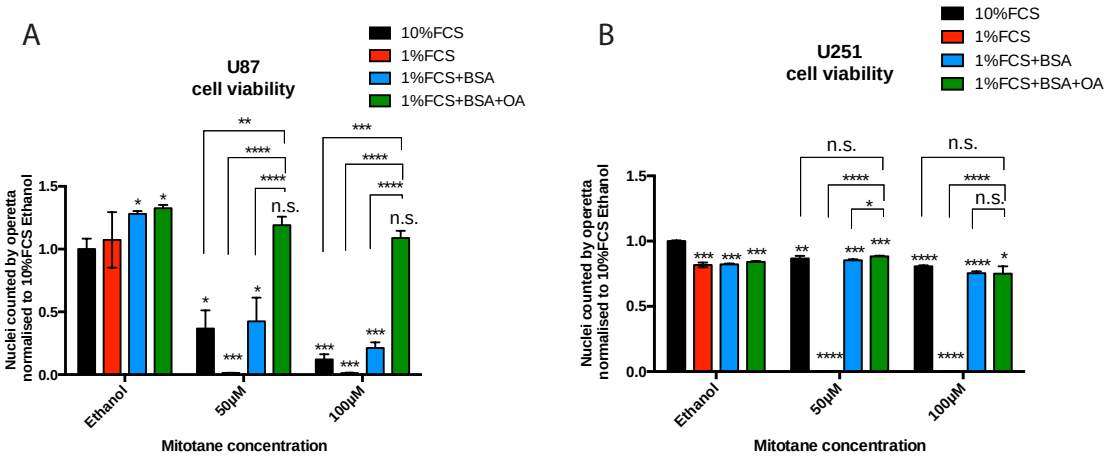

Figure 4.58: Rescue of cell viability in U87 and U251 cells treated with mitotane in low serum medium with oleic acid

U87 (A) and U251 (B) cells were treated with mitotane (50 or 100 μM) or ethanol (solvent) in medium containing 1% or 10% FCS for 24hours. Oleic acid coupled to BSA was added at 300 μM with equal concentration of BSA added as controls. Cell viability was quantified based on nuclei staining by DAPI and counted on an automated microscope (Perkin Elmer, Operetta). The values of quantification are normalised to ethanol controls in 10% FCS samples. Bars represent mean ± SEM (n=3).
p-values were calculated using a two tailed student's t-test (p-values are represented as * ≤ 0.05, ** ≤ 0.01, *** ≤ 0.001, **** ≤ 0.0001, n.s.= not significant).

4.6.2 Understanding the regulation of SOAT1 by upstream signalling pathways in GB

As SOAT1 is an important modulator of SREBP activity, understanding the regulation of SOAT1 in GB cells by upstream signalling molecules, such as PI3K, EGFR, AKT and mTORC1, could be important as mutations in pathways involving these factors are commonly seen in GB. To explore this, U87 and U251 cells were treated with different inhibitors targeting PI3K (NVPBKM120, used at 1μM), EGFR (lapatinib, used at 1μM), AKT (MK2206, used at 1μM) or mTORC1 (rapamycin, used at 100nM) in cells grown in medium containing 10% FCS for 72 hours. SOAT1 protein

levels decreased upon PI3K and mTORC1 inhibition in U87 cells, while U251 cells showed a decrease of SOAT1 protein after exposure to PI3K, AKT and mTORC1 inhibitors (Fig 4.59A). mRNA levels of *SOAT1* and *SREBPF1* showed a similar response to these inhibitors in U87 cells (Fig 4.59B-C). U251 cells showed a reduction in SOAT1 mRNA only in response to rapamycin, while SREBF1 mRNA was reduced only mildly with rapamycin in both cell lines (Fig 4.59B-C). However, it should be noted that SOAT1 regulates the activity rather than the expression of SREBP1. Thus, additional analysis of SREBP1 target genes could be required to confirm this effect. Moreover, this experiment was only exploratory and conducted in a single biological replicate thus precluding statistical analysis.

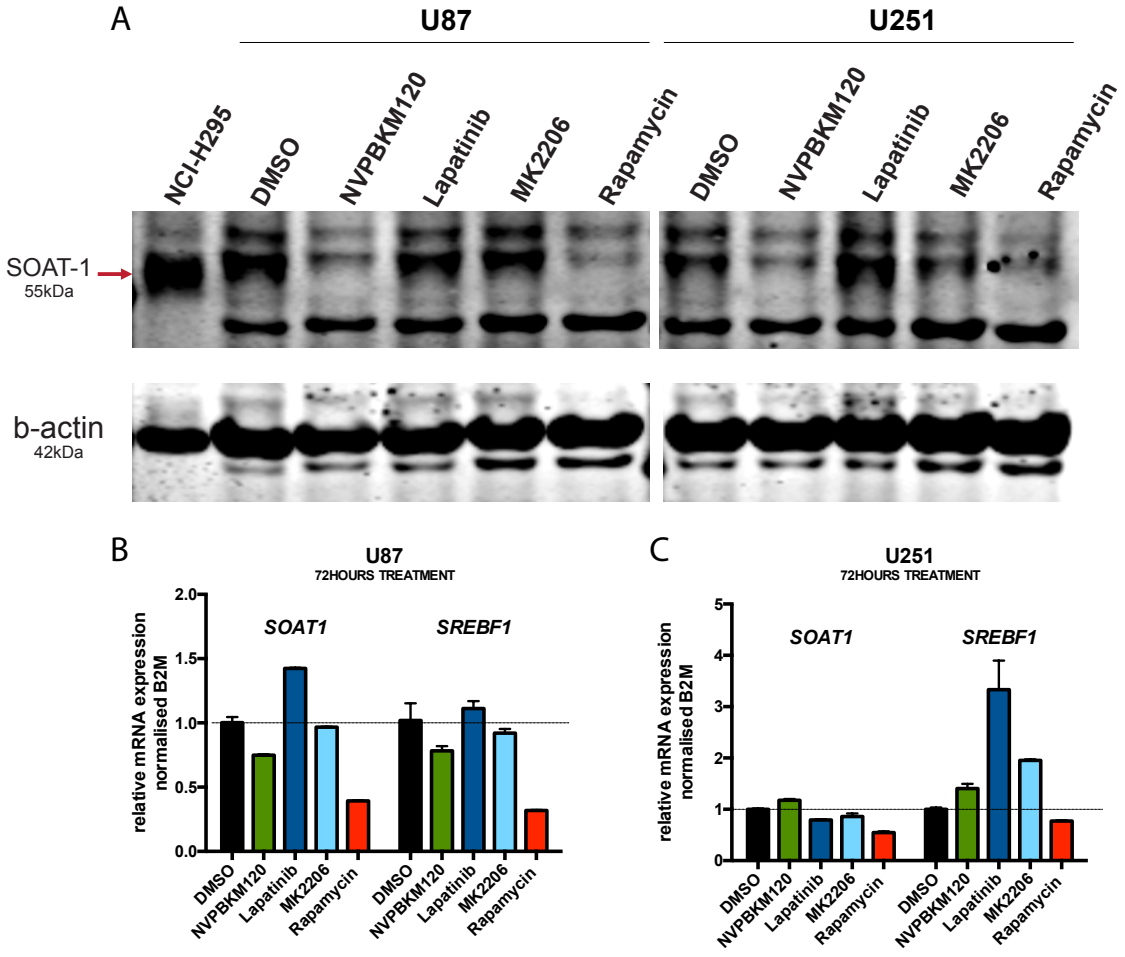

Figure 4.59: SOAT1 protein and mRNA levels are altered upon inhibition of signalling molecules in GB cells

A) WB showing SOAT1 protein levels in U87 and U251 cells treated with 1µM of the PI3K inhibitor NVPBKM120, 1µM of the EGFR inhibitor Lapatinib, 1µM of the AKT inhibitor MK2206, 100nM of mTORC1 inhibitor rapamycin or DMSO as solvent control in medium containing 10% FCS for 72 hours. β-actin serves as loading control. NCI-H295 cells serve as positive control for SOAT1 protein.

B) qRT-PCR showing mRNA levels of *SOAT1* and *SREBF1* in U87 and U251 cells under the same conditions as in (A). mRNA levels are shown relative to DMSO condition. Bars represent mean ± SEM of technical replicates (n=1).

In a parallel experiment, U87 and U251 cells were treated with the same inhibitors in medium containing 10% FCS for 24 hours to understand if there were short term changes observed in mRNA levels of *SOAT1, SREBP1* and *SCD*. To check the efficacy of the inhibitor treatment, phosphorylation status of AKT and S6 proteins was analysed. Decrease in phospho-Ser 473 in the AKT protein upon treatment with PI3K and AKT inhibitors and a decrease in phospho-Ser 240/244 in the S6 protein upon treatment with rapamycin confirmed the efficacy of these compounds in both cell lines (Fig 4.60A). In U87 cells, PI3K and mTORC1 inhibitors significantly reduced mRNA levels of *SOAT1*, while PI3K, AKT and mTORC1 inhibitors significantly reduced mRNA levels of *SREBF1* and *SCD* (Fig 4.60B). In U251 cells, AKT and mTORC1 inhibitors significantly reduced mRNA levels of *SOAT1,* while only the mTORC1 inhibitor reduced mRNA levels of *SREBF1* and *SCD* (Fig 4.60C). Overall, rapamycin showed the best decrease in SOAT1 protein and mRNA levels in both cell lines after treatment for 24 and 72hours. Further experiments are required to unravel the molecular mechanism of the regulation of SOAT1 by the PI3K, AKT and mTORC1 pathways.

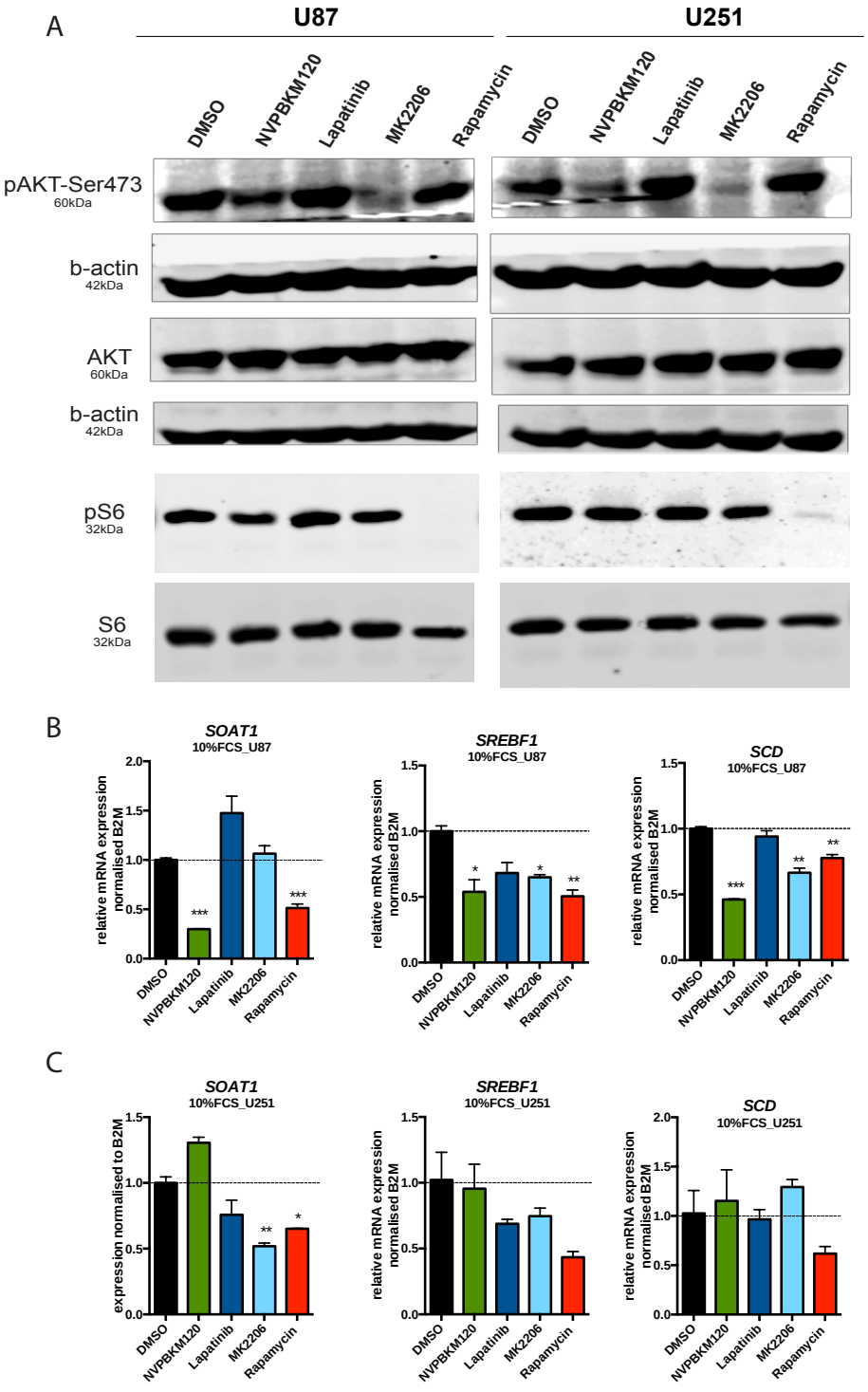

Figure 4.60: Validation of upstream signalling inhibition and effects on SOAT1, SREBP1 and SCD expression

A) WB showing protein levels of AKT, phopho-AKT (serine 473), S6 and phospho-S6 (serine 240/244) in U87 and U251 cells treated with DMSO, 1μM of the PI3K inhibitor NVPBKM120, 1μM of the EGFR inhibitor lapatinib, 1μM of the AKT inhibitor MK2206 or 100nM of the mTORC1 inhibitor rapamycin in medium containing 10% FCS for 24hours. β-actin serves as loading control.

B) qRT-PCR showing mRNA levels of *SOAT1*, *SREBF1* and *SCD* under the same conditions as in (A). mRNA levels are shown relative to the DMSO condition. Bars represent mean ± SEM (n=3).

p-values were calculated using a two tailed student's t-test (p-values are represented as * ≤ 0.05, ** ≤ 0.01).

4.6.3 Cell proliferation is reduced upon knockdown of SOAT1 in GB stem-like cells

NCH644 GB patient derived stem like cells described in chapter 4.5, showed that SREBP1 plays a crucial role in their proliferation and their ability to form neurospheres. To understand whether knockdown of SOAT1 would also impact GSC, shRNA sequences targeting SOAT1 (LT3-SOAT1_02 and 03) that had already been validated in U87 cells, were introduced into NCH644 cells. NCH644 cells expressing these sequences were grown in GSC media 1 containing 2.25 µM Dox or ethanol (solvent control) for 6 days to form neurospheres, with Dox and ethanol being replenished every 48 hours (Fig. 4.61A). mRNA levels of *SOAT1*, *SCD*, *PLA2G3* and *HMGCR* were reduced upon SOAT1 knockdown in GSCs (Fig 4.61C). Also, cell numbers were significantly reduced upon depletion of SOAT1, with both shRNA sequences showing equivalent results (Fig 4.61B). Hence, these results re-confirm the importance of SREBP1 in the maintenance of GB stem cells and place SOAT1 upstream of this regulation. Further experiments are required to establish whether pharmaceutical inhibition of SOAT1 can be used to impair GSC function *in vitro* and *in vivo*.

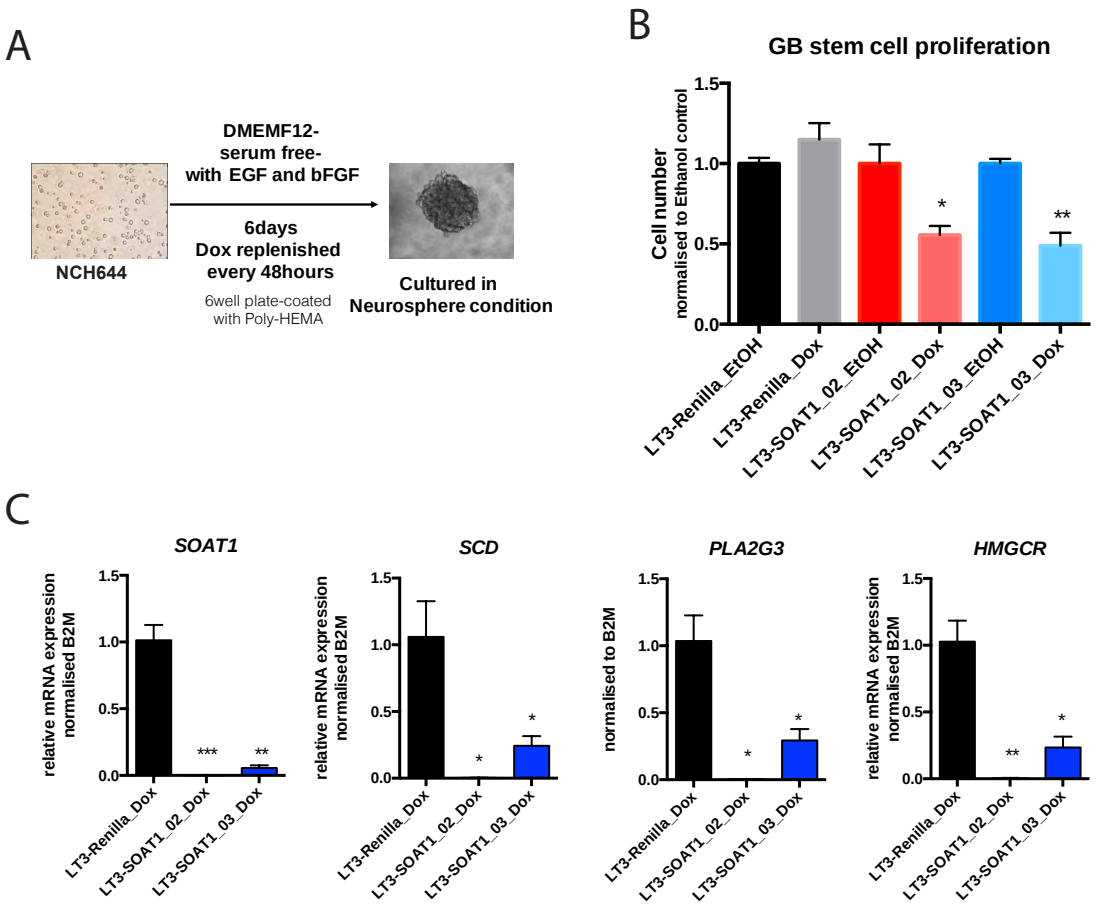

Figure 4.61: SOAT1 knockdown reduces proliferation of GB stem like cells

A) Diagram representing the experimental conditions where NCH644 patient derived GB cells were cultured as neurospheres in the presence or absence of Dox to induce shRNA expression.

B) Cell number of NCH644 cells expressing shRenilla, shSOAT1_02 and 03 sequences cultured as in A. Values are normalised to shRenilla treated with ethanol.

C) qRT-PCR showing mRNA levels of *SOAT1, SCD*, *PLA2G3* and *HMGCR* in NCH644 cells expressing shRenilla, shSOAT1_02 and 03 sequences. Cells were cultured as in A. mRNA levels are shown relative to shRenilla controls.

Bars represent mean ± SEM (n=3). p-values were calculated using a two tailed student's t-test (p values are represented as * ≤ 0.05, **≤ 0.01, ***≤ 0.001).

Chapter 5: Discussion

Cancer is one of the major causals of deaths worldwide and even though we have made major advances to improve treatment for cancer, there is still a great demand for better therapeutic treatments for cancers with advanced stages. GB is one of the utmost feared and the most aggressive type of brain tumours with a median survival rate of only 15 months (Osuka and Van Meir, 2017). These tumours are known to mostly grow asymptomatic causing late diagnosis, leading to low survival rate among patients and posing challenges for its treatment. Additionally, brain being a difficult organ for treatment, many of the normal treatment strategies fail due to the blood brain barrier (BBB) - a system that tightly regulates the transport of nutrients to brain and separates it from the rest of its body and also, surgeries can be rather challenging to even skilled neurosurgeons depending on the position of the tumour and its accessibility. Even with precision surgeries in patients that are fortunate enough to have huge portion of the tumour bulk removed, have to undergo rigorous radio and chemotherapy to improve their length of survival (Osuka and Van Meir, 2017). After all the few possible treatments these tumours are known to relapse in almost all cases, posing the death sentence to people diagnosed with GB (Osuka and Van Meir, 2017; Roy et al., 2015).

There are several known reasons for the high recurrence rate of these tumours and some of them are being studied extensively to understand them better and also to improve treatment strategies. First, their extraordinary capability of infiltration into different parts of the brain from their primary tumour bulk probably allows them to stay dormant after resection of the primary tumours and form secondary tumours at a later stage (Osuka and Van Meir, 2017). Second, high heterogeneity in these tumours poses difficulties to target all cell types with one treatment strategy. They are known to have high mutational burden and have several different populations within the tumour bulk and also have high infiltration of surrounding normal cells such as microglial cells which can almost make up to 50% of the tumour bulk (Hambardzumyan *et al.*, 2016). Additionally, these tumours are also known to have stem-like cells that are highly resistant to radio and chemotherapy, thus constituting the major cell population contributing to relapse in patients (Lathia et al., 2015; Peixoto and Lima, 2018). Third, these tumours exhibit vast neoangiogenic features that could also facilitate not only

transfer of nutrients from the system but also transfer of signalling molecules or metastatic cells from the tumour bulk to other parts of the brain. Hence, novel therapeutic strategies with possible combinatorial treatments are necessary to target different aspects of these tumours to effectively cure GB.

5.1 Glioblastoma cells under reduced serum depend on SREBP1 pathway

Growth and proliferation of cancer cells can be determined by the environment in which the tumour resides and the availability of the necessary nutrients to satisfy their enhanced biosynthetic demand. Cancer cells in a microenvironment with limited nutrients have to rewire their metabolism to perform *de novo* synthesis of macromolecules to proliferate and survive. Brain is a lipid rich organ and is composed of 60% of lipids (An and Weiss, 2016; Villa et al., 2016). But the availability of free lipids is limited (Patel et al., 2019; Villa *et al.*, 2016) and hence the tumour cells have to rely on *de novo* synthesis of lipids or rewiring their metabolism to release signalling molecules to obtain the lipids from their environment. GB tumours are already known to have large hypoxic areas which further push the tumours to be self-reliant and dependent on *de novo* synthesis (Jawhari et al., 2016; Monteiro et al., 2017). PI3K/AKT pathway is one of the most mutated pathways identified by TCGA in a comprehensive analysis on genes and core pathways in GB patients (Cancer Genome Atlas Research, 2008). PI3K/AKT/mTORC1 is an important axis and upstream regulators of the transcription factor SREBP1, that regulate *de novo* fatty acid synthesis in cells(Lewis et al., 2011; Porstmann et al., 2005; Porstmann *et al.*, 2008; Porstmann et al., 2009). The reliability of cells to rewire their metabolism makes them more reliant on alternative pathways such as SREBP1 network to support tumours under nutrient limited conditions. Hence, such distinct pathways become relevant only in cancer cells and set them apart from normal cells, providing a window of opportunity for effective cancer treatment.

5.1.1 Upregulation of SREBP1 network in serum limited environment

Fatty acids are among the necessary building blocks for growth and survival of cells. Fatty acids are known to be involved in many important cellular functions like membrane biogenesis, energy storage and are also involved in the formation of signalling molecules (Snaebjornsson *et al.*, 2020). When sterol levels are low in the surrounding environment, cells activate the translocation of the inactive precursor (full length) of SREBP1 bound to SCAP in the ER membrane via cop-2 mediated vesicles to the Golgi apparatus. The proteases present in the Golgi apparatus proteolytically cleaves the n-terminus of SREBP1 (known as mature SREBP1) which then enters the nucleus and binds as homodimers to the SRE elements and transcriptionally regulates the expression of the enzymes involved in fatty acid synthesis (Rohrig and Schulze, 2016). Accordingly, increased levels of mature SREBP1 were observed upon incubating both GB cells U87 and U251 in media containing low serum (Fig 4.1A). The mRNA levels of *SREBF1* and its target *SCD* were upregulated in low serum conditions in both cell lines (Fig 4.1B). Upregulation of SREBP1 and its increased transcriptional output in low or serum free conditions are in line with different studies (Bertolio et al., 2019; Griffiths *et al.*, 2013; Lewis *et al.*, 2015; Lo et al., 2018). The upregulation of *SREBF1*, *SREBF2* and their targets was observed in media containing serum replacement without lipids and cholesterol but with growth factors, as opposed to cells grown in full serum media (Fig 4.2), suggesting that low availability of fatty acids and lipids rewire their metabolism to upregulate *de novo* fatty acid synthesis. Even though the serum replacement increased *SREBF1* and *F2* and their targets to even greater extent than low serum condition, as this media without any free lipids could have accounted for the difference in the higher activation of the pathway.

5.1.2 SREBP1 knockdown with shRNAs are validated in two vector backbones

shRNA mediated genetic ablation of *SREBF1* was performed in 2 different vector systems, i.e., pLKO-Tet-On and pLT3-GEPIR. Both vector systems were inducible with doxycycline (Dox) treatment to induce shRNA expression and deplete *SREBF1* in the cells. The shRNA sequence shBP1_07 used in the LKO backbone was already shown to significantly reduce SREBP1 and its target genes in U87 cells and reduce tumour volume in subcutaneous tumours grown in nude mice (Griffiths *et al.*, 2013). Similar reduction in mRNA levels of *SREBF1* and its targets *SCD, FASN, ACLY*

and *ACACA* was observed upon SREBP1 silencing in this thesis (Fig 4.3B). This was also confirmed by the depletion of mSREBP1 in cells incubated in both 10% and 1% serum (Fig 4.3C). Upregulation of mSREBP1 in control cells upon incubation in 1% FCS compared to the 10% condition was observed, showing that overall the conditions replicated earlier studies performed in U87 cells (Fig 4.3C) (Griffiths *et al.*, 2013; Lewis *et al.*, 2015). Further, depletion of SREBP1 also led to a decrease in protein levels of SCD, confirming the effectiveness of inhibiting gene expression downstream of SREBP1 (Fig 4.3D). Binding of SREBP1 to the promoter regions of its targets was also captured by ChIP experiments and a strong reduction of promoter binding of SREBP1 to its targets *FASN, ACLY, ACACA, RAB5* and *SCD* was observed upon knockdown (Fig 4.3E). The different sites within the *FASN* promoter tested for SREBP1 binding were obtained from different sources. The first *FASN* primer sequence, amplifying a region spanning the proximal site and used in Fig 4.3E, was obtained from a SREBP1 ChIP sequencing data set that was validated to confirm SREBP1 binding (Reed et al., 2008). The other *FASN* primer sequence, amplifying a region spanning the distal site used in Fig 4.3E, was obtained from a ChIP sequencing experiment performed with MYC antibody (Gouw *et al.*, 2019). This region not only shows binding of MYC but also a weaker binding of SREBP1 (Gouw *et al.*, 2019). It was clear that binding to both the distal site, with low binding efficiency, and the proximal site, with strong binding efficiency to SREBP1 in low serum condition, was efficiently abrogated by SREBP1 knockdown (Fig 4.3E). Taken together, these results positively confirmed the loss of SREBP1 activity in U87 cells upon its knock down with the pLKO-Tet-On system.

For the pLT3-GEPIR system, shRNAs targeting SREBP1 were obtained from a genome wide collection of sensor based shRNA predictions provided by Fellmann et al (Fellmann *et al.*, 2013). This vector system was used as the miR-E backbone boosts the knockdown efficiency of shRNAs by several fold by enhancing the pri-miRNA processing. Also, a second system with shRNA targeting SREBP1 was used to exclude off-target effects and to better understand the biological consequences of SREBP1 knockdown. Out of the five miR-E-based shRNA sequences targeting SREBP1 tested, only three showed a substantial reduction in *SREBF1* mRNA levels while all significantly reduced the mRNA levels of *SCD* (Fig 4.4). SREBP1 transcriptionally regulates its own expression and hence the three sequences 01, 03

and 06 were chosen for further experiments, despite the observed reduction in SCD levels for all sequences.

It has been shown previously that cells exposed to lipid-deplete conditions upregulate SREBP1 and its targets (Griffiths *et al.*, 2013; Lewis *et al.*, 2015; Reed *et al.*, 2008). Hence, U87 cells expressing the three shRNA sequences 01, 03 and 06 targeting SREBP1 were further investigated in medium containing 1% FCS to enhance the activity of the SREBP1 network, and mRNA levels of *SREBF1* and *SCD* upon SREBP1 knockdown were determined. Indeed, a substantial decrease in mRNA levels of *SREBF1* and *SCD* in both 10% and 1% FCS condition was observed with all three shRNA sequences (Fig 4.5). However, the shRNA sequence expressed from the LT3-BP1_03 vector did not reduce the mRNA levels of *SREBF1* to the same extent as the other sequences and in 1% FCS condition failed to reach significance. Also, the mRNA levels of *SCD* were not depleted to the same extent in cells expressing this vector compared to the other sequences. SCD catalyses the formation of a double bond at the D9 position of the two saturated fatty acyl-CoAs: palmitoyl- (C16:0) and stearoyl-(C18:0) CoAs into monounsaturated fatty acyl-CoAs: palmitoleoyl- (C16:1) and oleoyl-(C18:1) CoAs. Indeed, monounsaturated oleic acid (C18:1) is one of the most abundant non-essential fatty acids in the cells, and ablation of SCD in low serum condition leads to accumulation of saturated FAs (SFA) and a decrease in mono-unsaturated FAs (MUFA), resulting in ER stress and apoptosis due to the build-up of reactive oxygen species, which can be rescued by addition of MUFAs (Ariyama *et al.*, 2010; Griffiths *et al.*, 2013; Williams *et al.*, 2013; Young et al., 2013). Hence, mRNA levels of *DDIT3* gene that codes for the protein CHOP were analysed, as it was previously shown to be induced upon ER stress (Griffiths *et al.*, 2013; Roongta *et al.*, 2011). mRNA levels of *DDIT3* were significantly upregulated upon knockdown of SREBP1 with shRNA sequences LT3-BP1_01 and 06 in medium containing 10% FCS and to an even larger extent in the 1% FCS condition (Fig 4.5). But there was no significant change in *DDIT3* mRNA levels with the sequence LT3-BP1_03 (Fig 4.5). This might be due to insufficient knockdown of SREBP1, in which case the residual SREBP1 is enough to retain sufficient SCD activity and maintain the balance of saturated and unsaturated FAs, thus not resulting in ER stress. These results were confirmed using the shRenilla sequence as control to exclude any effects caused by Dox used for the shRNA induction. We observed substantial reduction in mRNA levels

of *SREBF1* and *SCD* upon SREBP1 knockdown with all three sequences, still LT3-BP1_03 did not reduce *SCD* levels to the same extent or increase *DDIT3* as the other 2 sequences in 1% FCS condition (Fig 4.6). Next, the cells with LT3-BP1_01 and 06 shRNA sequences were tested in a cell viability assay. Reduction in cell viability in low serum conditions was in line with the induction of ER stress leading to apoptosis and consistent with earlier studies (Fig 4.7), thus validating the new system to match results obtained with the LKO-BP1_07 sequence or other methods of SREBP1 inhibition (Griffiths *et al.*, 2013; Roongta *et al.*, 2011).

5.1.3 SREBP1 is essential for GB cell survival under reduced serum condition

The SREBP1 network is upregulated in low serum and becomes indispensable for survival under this condition, as serum is the only source of exogenous lipids in tissue culture (Griffiths *et al.*, 2013; Lewis *et al.*, 2015; Reed *et al.*, 2008). Growth rates of U87 cells in 10%, 1% and 0% FCS with and without SREBP1 expression using LKO-BP1_07 and LT3-BP1_06 shRNA sequences and LKO-Scr and LT3-Renilla as controls were assessed. Cells grown in 10% FCS condition were able to proliferate similar to control cells upon SREBP1 knockdown for 72 hours with the shRNA sequences expressed in the LT3-GEPIR system, while at 96hours cells with LKO-BP1_07 showed significant reduction in proliferation compared to its control LKO-Scr (Fig 4.8). SREBP proficient cells in the 1% FCS condition are able to proliferate, as they can upregulate SREBP1 to accommodate for lower availability of exogenous fatty acids, even though they do not proliferate to the same extent as cells in the 10% FCS condition. The cells did not reach a good knockdown of SREBP1 until 72 hours, and at 96 hours we generally saw the maximal decrease of SREBP1 and its targets (Fig 4.13). In line with this, we start to see the reduction in cell growth at 72 hours of Dox treatment with both shRNA sequences compared to control and a significant difference in proliferation at 96 hours (Fig 4.8). Hence this confirms that SREBP1 becomes crucial for cell survival and proliferation under low serum condition. Cells without any serum were able to survive but not able to proliferate either with or without SREBP1 (Fig 4.8). This might be due to arrest in cell growth as we also deplete essential fatty acids from the media (McGregor et al., 2020).

5.2 SREBP1 transcriptionally controls genes involved in fatty acid synthesis and phospholipid modification in GB

Previous studies using overexpression of SREBP1 in GB cells revealed a gene expression signature that was also found to be overexpressed in patients with poor survival (Lewis *et al.*, 2015). To obtain a comprehensive insight into gene expression networks controlled by SREBP1 and to identify genes that are regulated by SREBP1 in GB, a genome wide RNA sequencing analysis was performed in U87 cells following shRNA-mediated gene silencing of SREBP1 in cells cultured in both full and reduced serum conditions.

5.2.1 Analysing the SREBP1 network by gene expression analysis in GB

RNAseq analysis in U87 cells after SREBP1 silencing in the two serum conditions confirmed that many SREBP1 target genes are induced by low serum culture. SREBP1 silencing in the 10% FCS condition resulted in reduced expression of 53 genes, while 218 genes showed reduced expression when SREBP1 was silenced in cells cultured in 1% FCS (Fig 4.9A). Performing gene set enrichment analysis on RNAseq data obtained from U87 cells after SREBP1 knockdown in 1% FCS condition showed significant down regulation of HORTON_SREBP1 targets (Fig 4.10). This gene set had been obtained by Horton et al by performing gene expression analysis on livers of mice transgenic for SREBP1a, SREBP2 and from SCAP knock out mice and identifies genes that are controlled by the family of SREBP transcription factors (Horton *et al.*, 2003). Downregulation of genes in the HORTON gene set further confirmed the efficient depletion of SREBP1 function in GB cells by the shRNA strategy and increased the confidence in the expression data. We also observed a downregulation of ISHIDA_E2F targets upon SREBP1 knock down (Fig 4.10). This gene list was generated by Ishida et al and identified genes related to cell proliferation that are controlled by E2F proteins (Ishida *et al.*, 2001). Downregulation of genes in this gene list confirmed our findings that loss of SREBP1 leads to ER stress and arrests cell growth and proliferation in the low serum condition (Fig 4.6, 4.7 and 4.8). We also

saw that SREBP1 knock down in the low serum condition leads to upregulation of genes related to transcriptional response to salirasib, a specific inhibitor of Ras farnesylation (Blum *et al.*, 2007). Further interrogation revealed that this gene list also contains genes involved in apoptosis, cell death and stress response pathways (Blum *et al.*, 2007), suggesting that the depletion of SREBP1 induces loss of viability and stress in GB cells. Accordingly, we also saw PHONG_TNF targets upregulated upon SREBP1 depletion. This gene set consists of genes related to the tumour necrosis factor (TNF) signalling pathway, which controls cell survival, stress response and the induction of pro-inflammatory cytokines (Phong *et al.*, 2010). Even though we have not explored the mechanism underlying the induction of both pro-survival and apoptotic pathways, we concluded that the pro-inflammatory response might be induced due to the stress that is induced by SREBP1 depletion under low serum conditions that can eventually lead to loss of cell viability due to the induction of apoptosis or other cell death pathways (Griffiths *et al.*, 2013; Lewis *et al.*, 2015).

Some of the genes downregulated by SREBP1 (shown in Fig 4.9A) found in the RNA-seq data were also validated by RT-qPCR using the same RNA samples. These results also re-confirmed the upregulation of the SREBP1 pathway when cells were grown in low serum compared to cells grown in 10% FCS (Fig 4.9B). *SREBF1* and its targets *SCD, FASN, FADS1, FADS2* and *FABP3* were significantly downregulated upon SREBP1 depletion.

5.2.2 PLA2G3 is regulated by SREBP1 in GB cells under low serum condition

Expression data obtained from the SREBP1 overexpression studies in U87 cells (Lewis *et al.*, 2015) was overlapped with genes from RNAseq data with SREBP1 knockdown and a gene list consisting of 72 genes was defined (Fig 4.11A). This 72 gene list consisted of genes that were upregulated in the overexpression data set and downregulated following SREBP1 depletion, resulting in genes that were strongly and consistently regulated by SREBP1. Next, this gene list was used in a pathway analysis to identify processes that are impacted by SREBP1. This analysis revealed SREBP1's strong involvement in several lipid related processes, and notably one of the pathways that was revealed in this analysis was phospholipid metabolism (Fig 4.11B). PLA2G3

was the most depleted gene upon SREBP1 silencing in the RNAseq data and all genes involved in phospholipid metabolic process were significantly downregulated (Fig 4.11C). Interestingly, *PLA2G3* was strongly induced by the low serum condition and significantly reduced upon SREBP1 knockdown (Fig 4.11D) and was therefore identified as a novel target regulated by SREBP1 in GB. SREBP1 is known to regulate PLA2G3 by binding to its promoter region and this regulation is preserved between humans and several other species (Gijs *et al.*, 2015). PLA2G3 is a phospholipase that hydrolyses the ester bond linking the fatty acid present at the sn-2 position in phospholipids (Park *et al.*, 2012). The products of this reaction are used as precursors for the synthesis of signalling molecules, in particular prostaglandins and LPA. Hence, this pathway could play a prominent role in supporting tumour growth and proliferation under lipid-deplete conditions in GB. The regulation of PLA2G3 upon SREBP1 depletion was confirmed also using the LT3-GEPIR system and a similar regulation of *PLA2G3* mRNA with all 3 shRNA sequences targeting SREBP1 was observed (Fig 4.12B). SREBP1 regulated PLA2G3 also on the protein level in both 1% and 10% FCS condition, as SREBP1 silencing reduced its levels in both conditions (Fig 4.12A). However, it was surprising that SREBP1 also regulated PLA2G3 protein levels in the 10% FCS condition as the expression of *PLA2G3* mRNA was extremely low in 10% FCS compared to the 1% FCS condition. Also, the PLA2G3 protein levels were not increased in 1% FCS compared to 10% FCS condition, suggesting that mRNA and protein levels are regulated differently in response to low serum. However, PLA2G3 is a secreted protein and the amount detected in cell lysates may only represent a fraction of the total protein produced. Due to the lack of detailed studies on PLA2G3, it remains to be analysed further to understand its regulation.

Cells expressing shRNA sequences targeting PLA2G3 obtained from Fellmann et al (Fellmann *et al.*, 2013) showed a reduction in protein and mRNA levels of PLA2G3 upon Dox treatment compared to the shRenilla control (Fig 4.14). PLA2G3 protein levels upon SREBP1 knockdown showed the strongest reduction in the 53 kDa form, while direct PLA2G3 knockdown reduced all three bands that were detected with the antibody. PLA2G3 is a secreted protein and glycosylated at several sites (Murakami *et al.*, 2005). Further experiments are needed to identify the different bands observed and assign them to specific forms of glycosylated-PLA2G3. Silencing of PLA2G3 for 96 hours and incubating the cells in media without serum for the last 24 hours did not

result in reduced cell viability (Fig 4.16). This suggests that PLA2G3 is not essential for cell proliferation and survival of GB cells *in vitro*, at least not under the conditions studied here, but that might be involved in non-autonomous functions of cancer cells, for example cell-cell communication mechanisms that depend on the formation of certain lipid mediators.

5.3 SREBP1 controls the composition of fatty acids and lipids

After confirmation of the efficient decrease in SREBP1 regulated enzymes (Fig 4.9), analyses of fatty acids and lipid species were performed, as changes in fatty acids and lipids would allow us to further understand the downstream effects of SREBP1 depletion in GB. Global profiling of fatty acids and lipids upon SREBP1 depletion using thin layer chromatography did not show any gross changes in the total levels of these lipids (Fig 4.17) and a deeper analysis of individual fatty acids and lipid species across several classes was performed.

5.3.1 Decrease in total MUFA and increase in total PUFA upon SREBP1 and PLA2G3 depletion

Upon measuring total fatty acids in the cells, a significant reduction of oleic acid was observed upon SREBP1 silencing with all three shRNA sequences in the two different vector systems (Fig 4.18 and 4.19). This reduction in oleic acid was shown in several earlier studies with SREBP1 depletion or SCD inhibition and was known to induce ER stress due to loss of MUFA and increase in saturated FAs (Ariyama *et al.*, 2010; Griffiths *et al.*, 2013; Williams *et al.*, 2013). Further interrogation on the changes in the total fatty acid profile upon SREBP1 silencing was done as most enzymes involved in the fatty synthesis network regulated by SREBP1 were downregulated upon its depletion (Fig 4.9). As SREBP1 transcriptionally regulates enzymes involved in fatty acid desaturation and elongation, in particular SCD and ELOVL6, the ratio of oleic acid over palmitic acid (C18:1/C16:0) was analysed. This analysis showed a clear reduction in the ability to convert palmitic acid to oleic acid in SREBP1 depleted cells. We also measured ratios of eicosadienoic acid over linoleic acid (C20:2/C18:2), which

requires ELOVL5 activity (Baenke et al., 2013; Snaebjornsson *et al.*, 2020). This analysis also showed a significant reduction in this ratio, indicating that the activity of ELOVL5 is reduced after SREBP1 depletion. The significant reduction in these ratios upon SREBP1 depletion confirmed that the output of the SREBP1 network, i.e., *de novo* fatty acid synthesis and desaturation as well as the elongation of some essential fatty acids, was decreased (Fig 4.18 and 4.19). In addition, we also observed that SREBP1 depletion caused the accumulation of several PUFA species within the total fatty acid pool. The vast majority of fatty acids represented in the total fatty acid pool are those that are released from membrane phospholipids and cholesterol esters upon saponification. These fatty acids are relatively stable and represent membrane fatty acid composition. As PLA2G3 was strongly downregulated upon SREBP1 silencing, the increase of PUFA in the total fatty acid pool could indicate a reduction in the release of PUFA-containing acyl-chains that are known to reside preferentially on the sn-2 position (Murase *et al.*, 2017). To confirm this, a further analysis of total fatty acids in cells after knockdown of PLA2G3 was performed and a similar increase in PUFA was observed (Fig 4.20). Hence, both SREBP1 and PLA2G3 silencing showed a comparable increase in PUFA (Fig 4.21), indicating that PLA2G3 contributes to the modulation of cellular lipid composition by SREBP1. Also, it was evident that oleic acid was similarly decreased by both SREBP1 and PLA2G3 depletion. However, it is not clear whether the decrease seen in PLA2G3 depleted cells was a direct effect of reduced PLA2G3 function or an indirect effect, for example due to higher activity of phospholipases which act on the sn-1 position. Further experiments are required to understand the decrease on oleic acid upon PLA2G3 knockdown.

5.3.2 SREBP1 depletion changes the composition of phospholipids and their derivatives

Lipidomic analysis of the cells with SREBP1 and PLA2G3 silencing was studied further to unravel the specific lipid composition alterations and connect them to the changes observed in total fatty acids. Upon SREBP1 silencing, there was an overall decrease in the ratio of unsaturated to saturated fatty acids, showing that SREBP1 regulates the composition of phospholipids and their derivatives (Fig 4.24). Analysing different PC and PE species, we observed that PC-C32:0, PC-C34:0, PC-C36:4 and PC-C38:4 was significantly upregulated upon SREBP1 silencing (Fig 4.22). Even

though MS2 analysis was not performed on these lipids to correctly annotate the fatty acid chains associated with the lipid species, the identity of phospholipids was only inferred based on the abundance of fatty acids in the total fatty acid profile of the cells. PC comprises the major component of lipids in the cell membranes followed by PE (Harayama and Riezman, 2018). Both lipid species showed a similar trend that led to conclusion that SREBP1 changes the composition of phospholipids by reducing the amount of MUFA-containing acyl-chains but increasing the amount of PUFA. This also corresponds with the changes in the fatty acid composition observed. Surprisingly, these changes in phospholipids were not observed in cells following PLA2G3 silencing even though similar fatty acid changes were seen (Fig 4.25).

Further analysis of different lysophospholipid species derived from PC and PE was performed to determine whether SREBP1 and PLA2G3 gave rise to similar changes. As LPC, LPE and LPA contain only one acyl-chain, it was possible to directly determine the identity of these molecules from the MS spectra. A significant increase in saturated LPC (C16:0 and C18:0), LPE (only C18:0) and LPA (C14:0, C16:0 and C18:0) was seen upon SREBP1 silencing. Also, a significant decrease in MUFA-containing LPC (C16:1 and C18:1), LPE (C16:1 and a trend in C18:1) and LPA (C16:1 and C18:1) was observed. Changes in the PUFA lysophospholipids differed a bit from those seen in the total fatty acid profile. In LPC there was an increase in C18:2, C18:3 and C20:3 while other species did not change; in LPE there was an increase in the PUFA-containing species C18:2, C18:3, C20:4 but a decrease in C22:5 and C22:6. As the total fatty acid profile shows a summary of all the lipid species in the cells, it is hard to explain differences between fatty acids and lysophospholipids. However, changes in LPA species were more pronounced than the changes in the other two classes of lysophospholipids. Moreover, PLA2G3 silencing did not completely recapitulate the changes observed in LPA species after SREBP1 depletion. There were no strong changes in PUFA-containing LPA species upon PLA2G3 depletion (Fig 4.25). The differences observed between cells with SREBP1 silencing and PLA2G3 silencing were not completely unexpected, as total fatty acids and lipid species are the result of multiple metabolic reactions and SREBP1 depletion alters the expression of multiple enzymes in the lipid biosynthesis pathway in addition to PLA2G3. Importantly, LPA is not only produced from membrane lipids through the action of different lipases but is also an intermediate of the biosynthetic pathway leading to phosphoglyceride

synthesis. Thus, the changes in LPA observed in response to SREBP1 silencing most likely represent alterations in phosphoglyceride synthesis. Further experiments with lipid standards for specific lipid classes are required to validate these results and MS2 analysis is needed to identify specific lipid species and to fully unravel the impact of SREBP1 on the cellular lipidome in GB.

5.4 Involvement of SREBP1 in the production of angiogenic mediators to promote angiogenesis in GB

Identifying the processes that are affected by the changes seen in fatty acids and the lipid species upon SREBP1 knockdown would be crucial to provide better insights for its role in GB biology. As some of the lipid mediators that are produced as an output of the SREBP1 network such as LPA and PGE2, are known to be involved in signalling events that support cell migration, invasion and angiogenesis (Auciello et al., 2019; Form and Auerbach, 1983; Hisano and Hla, 2019; Knowles et al., 2005; Namkoong et al., 2005; Ning *et al.*, 2011; Tabuchi, 2015), it was investigated whether SREBP1 could also modulate non-cell autonomous processes in GB.

5.4.1 SREBP1 silencing reduces angiogenic mediators in conditioned medium

Whether SREBP1 contributes to angiogenesis in GB was studied by incubating HUVECs with conditioned medium (CM) obtained from U87 cells with or without SREBP1 silencing and conclusions were drawn based on the ability of the CM to induce sprouting or tube formation in the endothelial cells. Lack of sprouting in blank medium and the induction of sprouting by addition of VEGF or the LSGS supplement were used as controls in the assay. A significant decrease in the ability of HUVECs to sprout upon incubating them with CM from SREBP1 silenced cells was observed (Fig 4.26). Also, HUVECs incubated with medium from U87 cells that were depleted for SREBP1 using three individual shRNA sequences showed a significant reduction in the number of loops, branching points and tubes in a tube-formation assay (Fig 4.27). Both assays clearly showed that SREBP1 depletion reduces the ability of cancer cells to secrete pro-angiogenic factors that drive angiogenesis in endothelial cells. This led to further analysis of the CM to identify the crucial factors that are reduced upon SREBP1 knockdown that could be involved in the regulation of angiogenesis by SREBP1.

First, expression levels of a panel of angiogenesis related proteins were analysed in CM from cells with and without SREBP1 silencing. Many of the proteins

that were detected by the antibody array were above the set cut off limit for detection and several of these were changed (Fig 4.28). VEGF is one of the best-known inducers of neovascularization in normal and tumour tissues, and there is a vast body of literature showing the role of VEGF specifically in tumour angiogenesis (Carmeliet, 2005; Jain *et al.*, 2007; Leung *et al.*, 1989; Sheng and Xu, 2016). Importantly, anti-angiogenic therapy is a crucial part of present clinical trials investigating combinatorial therapy in GB, although anti-angiogenic drugs such as Bevacizumab have so far not been so successful as a single agent therapy (Cuncannon et al., 2019; Kim *et al.*, 2018; Li *et al.*, 2017b). But there was only a marginal decrease in VEGF protein detected in the CM upon SREBP1 silencing and its intracellular levels were not altered (Fig 4.28 and 4.29). Hence, VEGF levels were not depleted upon SREBP1 silencing and this led to the conclusion that SREBP1 might not modulate angiogenesis by reducing VEGF levels in cancer cells.

A strong reduction in angiogenin, endothelin-I and IL-8 was observed upon SREBP1 silencing by analysing their protein levels in the CM (Fig 4.28). Angiogenin is a polypeptide member of the RNase A superfamily and is known to be associated with cancer cell survival, proliferation and neovascularization *in vitro* and *in vivo* (Miyake et al., 2015). Angiogenin is known to enter endothelial cells by endocytosis, where it accumulates in the nucleolus to regulate rRNA transcription and ribosome biogenesis and therefore plays an important role in angiogenesis. Also, it has been already shown that depletion of angiogenin ablates angiogenic capacity in endothelial cells (Kishimoto *et al.*, 2005). Angiogenin is also known to induce tumour cell proliferation and plays an important role in tumour growth and survival. Angiogenin is shown to be regulated downstream of AKT pathway in prostate cancer (Yoshioka et al., 2006). This is particularly interesting, as SREBP1 is also regulated downstream of the PI3K/AKT pathway (Porstmann *et al.*, 2005; Porstmann *et al.*, 2008; Porstmann *et al.*, 2009). Further analysis is required to unravel the molecular regulation of angiogenin by SREBP1, its relation to angiogenesis and whether its control is related to a lipid molecule regulated downstream of AKT/SREBP1.

Endothelin-I, another factor that was reduced upon SREBP1 silencing in CM, is a known G-protein coupled receptor agonist that is involved in angiogenesis. Endothelin-I is involved in the regulation of proliferation, migration, invasion and

neovascularisation in tumours (Bagnato and Spinella, 2003). Like angiogenin, endothelin-I is also known to be regulated by hypoxia and downstream of AKT and acts through endothelin receptors (Bagnato and Spinella, 2003). Endothelin-I stimulates endothelial cells to produce VEGF and thereby regulates angiogenesis (Wu et al., 2014). Furthermore, it is known that endothelin-I can indirectly induce angiogenesis by promoting the secretion of angiogenic proteases from cancer cells and fibroblasts (Knowles *et al.*, 2005). But it is still not clear how endothelin-I is regulated by SREBP1 downstream of the AKT pathway and further research is needed to understand the mechanism of its regulation.

Another important known regulator of tumour angiogenesis that was downregulated upon SREBP1 silencing was IL-8. This was rather unexpected, as the RNA-seq data showed a strong upregulation of pro-inflammatory signalling and cytokine signatures, including IL-8, upon SREBP1 depletion in low serum condition. IL-8 is a pro-inflammatory chemokine which is a known regulator of tumour growth, metastasis and angiogenesis in many cancers (Ning *et al.*, 2011). IL-8 is also known to regulate endothelial cell survival, proliferation and the production of matrix metalloproteinases (Li *et al.*, 2003). Also, it is known that exposing endothelial cells to IL-8 induces synthesis of VEGF and increased angiogenesis (Shi and Wei, 2016). The regulation of IL-8 by SREBP1 is novel and the molecular mechanisms governing this relationship needs to be explored in further studies.

Overall, these observed changes point to a connection between SREBP1 and angiogenesis. It is still unclear whether SREBP1 regulates these proteins and thereby alters VEGF production in endothelial cells indirectly affecting angiogenesis. Further analysis of VEGF levels should be conducted in HUVEC upon incubation with CM obtained from cells with or without SREBP1 silencing or media containing angiogenin, endothelin-I and IL-8, to understand whether the specific regulation of angiogenesis is dependent or independent of VEGF.

5.4.1 Lipid mediators induce sprouting in endothelial cells

It was hypothesised that the depletion of SREBP1, the transcription factor that regulates fatty acid biosynthesis and phospholipid composition, could lead to changes

in lipid mediator synthesis that could also impact non-cell autonomous functions. It was still unclear whether changes in fatty acid synthesis and the composition of phospholipids can also lead to changes in the lipid secretome of cancer cells that are involved in autocrine and paracrine signalling. The activity of group 2 phospholipases is vital in cancer cells to mediate signalling processes, as these enzymes are involved in the degradation of phospholipids to lysophospholipids by releasing the fatty acids that are present on the sn-2 position (Hisano and Hla, 2019). Acyl-groups present on sn-2 positions in phospholipids are mostly PUFAs, such as arachidonic acid (C20:4) or DHA which are precursors for synthesis of prostaglandins and leukotrienes (Park *et al.*, 2012). Once the fatty acids are cleaved off by phospholipases, the different lysophospholipids released are either further modified to synthesise signalling molecules, such as LPA, or new fatty acid chains are added during the process of lipid remodelling for membrane biogenesis (Moessinger *et al.*, 2014; Shindou and Shimizu, 2009). As lipid mediators are already known to be involved in angiogenesis (Beloribi-Djefaflia et al., 2016; Hisano and Hla, 2019), it was determined whether the lipids produced downstream of SREBP1 are responsible for the regulation of angiogenesis. U87 CM that had previously been boiled at 95°C for 10 mins retained the ability to induce endothelial cell sprouting (Fig 4.30). Moreover, lipids that had been extracted from CM of U87 cells also induced sprouting to a similar extent as the untreated control medium (Fig 4.30). This indicated that lipid mediators present in the medium can induce angiogenesis even when all proteins are denatured by boiling (Bazzani et al., 2017; Liu et al., 2012). Similarly, the lipid fraction derived from CM alone was sufficient to induce sprouting.

The reaction catalysed by phospholipases produces precursors for the synthesis of lysophospholipids and proinflammatory lipid molecules. Both end products of these reactions, LPA-18:1 and PGE2, were added to the assay to test their ability to induce angiogenesis. Indeed, addition of either LPA-18:1 or PGE2 was able to induce angiogenesis to a similar level also observed with CM from U87 cells (Fig 4.31 and 4.32).

Endothelial spheroids were also incubated with LPA-C18:1 or with lipids extracted from CM and tested in the sprouting assay using a specific inhibitor of the LPA receptor (LPARi, KI 16425) (Ohta et al., 2003). It was clear that addition of the

inhibitor blocked endothelial cell sprouting induced by LPA-C18:1 but, importantly, also by the lipids purified from CM of cancer cells (Fig 4.30 and 31). These results strongly suggest that the mediator lipid present in the CM could indeed be LPA. LPA regulates angiogenesis by binding to LPAR, belonging to the family of G protein-coupled receptors, and many studies have shown that LPA is involved in the regulation of endothelial cell proliferation, migration and wound healing, and play a vital role in tumour progression (Rivera-Lopez et al., 2008; Teo *et al.*, 2009).

Similarly, HUVECs spheroids incubated with increasing concentration of PGE2 showed an increase in sprouting in a concentration dependent manner (Fig 4.32). PGE2 is also a known inducer of angiogenesis and is involved in the regulation of proliferation and signalling in both cancer and endothelial cells (Form and Auerbach, 1983; Namkoong *et al.*, 2005). Even though it was clear that lipid mediators that are linked to the SREBP1 network were able to induce angiogenesis, it was not clear which nodes of the pathway were necessary for the process. Hence, the SREBP1 pathway was inhibited at several points by treating U87 cells with selective inhibitors during CM production (termed as pre-treatment). Alternatively, the inhibitor was added to the CM obtained from untreated U87 cells (termed as post-treatment). Next, the ability of the different media to induce endothelial sprouting was assessed (as represented in Fig 4.33A). Interestingly, SCD inhibition using the inhibitor CAY10566 (SCDi) showed a decrease in sprouting only with pre-treated CM, while post-treatment did not alter the ability of CM to induce sprouting in endothelial cells (Fig 4.33B-D). This suggests that SCD inhibition in cancer cells affects the formation of factors that are involved in the induction of angiogenesis and that SCD inhibition does not affect endothelial cells directly. Hence, it can be concluded that SCD is necessary for cancer cells to produce mediator lipids and influence angiogenesis in a paracrine fashion. Next, an inhibitor of secreted phospholipase, thioetheramide-PC (sPLA2i), was used to assess the effect of loss of PLA2G3 activity. This compound acts as a competitive inhibitor and binds to both catalytic and activator site of the enzyme and thereby reduces the activity of secreted phospholipases (Plesniak et al., 1993; Yu et al., 1990). The pre-treated CM obtained by using sPLA2i showed a significant reduction in the ability to induce sprouting, while post-treated CM failed to reduce sprouting to the same extent (Fig 4.34A-C). This was similar to the observations made with SCDi. In addition, CM from PLA2G3 knockdown U87 cells were used to further assess the contribution of this

enzyme. Indeed, PLA2G3 silencing caused a significant decrease in sprouting of endothelial cells that was comparable to the effect of the inhibitor (Fig 4.34D-E). These results implied that, similar to SCD, PLA2G3 is also necessary for the production of pro-angiogenic factors by the cancer cells. Even though the role of PLA2G3 in tumour angiogenesis downstream of SREBP1 is novel and needs to be further investigated, previous results have shown that overexpression of PLA2G3 in colorectal cancer cells implanted in nude mice results in larger tumours with increased tumour neo-vascularization, supporting its involvement in tumour growth and angiogenesis via PGE2 synthesis (Murakami *et al.*, 2005).

Further inhibitors of lipid modifying reactions downstream of PLA2G3 were also used to block either the processing of lysophospholipids to LPA or the activity of the LPA receptors. HA-130 inhibits autotaxin (ATX) (Auciello *et al.*, 2019), a secreted enzyme that has lysophospholipase activity and catalyses the conversion of different lysophospholipids to LPA. The inhibition of ATX reduced sprouting in endothelial cells with CM obtained from both pre- and post-treatment (Fig 4.35A-C). It is known that ATX is involved in angiogenesis by promoting the growth of endothelial cells and inducing vessel formation (Nam et al., 2001). Incubation with pro-angiogenic growth factors, such as bFGF, induces high expression of ATX in endothelial cells and ATX influences angiogenesis through the production of LPA. Also, a study in GB has shown that ATX inhibition renders cancer cells sensitive to radiation treatment, with a strong reduction in tumour vascularisation and delayed tumour growth, thus highlighting the important role of this enzyme in GB (Bhave et al., 2013). Since LPA is capable of inducing angiogenesis, we further tested its effect by adding the LPA receptor inhibitor KI 16425 that inhibits LPAR1, LPAR2 and LPAR3 (Ohta *et al.*, 2003). Both pre- and post-treated CM with LPA receptor inhibitor showed reduced ability for sprouting induction in endothelial cells (Fig 4.35D-F). These results together confirmed that LPA is important for inducing sprouting by U87 cells and implicate this lipid as one of the mechanisms through which cancer cells can promote angiogenesis. These results are in accordance with earlier studies that have shown LPA's involvement in angiogenesis (Lee et al., 2000; Rivera-Lopez *et al.*, 2008; Tabuchi, 2015; Teo *et al.*, 2009). Moreover, LPA induced blood vessel formation was shown to be more robust compared to VEGF in a chicken chorioallantoic membrane angiogenesis model, suggesting its involvement not only in vessel formation but also in vessel maturation (Rivera-Lopez

et al., 2008). The same study also showed that LPAR1, LPAR2 and LPAR3 are involved in the LPA-mediated effects in vessel formation and that its inhibition reduces angiogenic capability in cancer cells (Rivera-Lopez *et al.*, 2008). Taken together, the results obtained with inhibitors targeting ATX or the LPA receptors strongly suggest that production of LPA is involved in the induction of endothelial cell sprouting. However, it is possible that LPA might also function in a paracrine manner to connect pro-angiogenic signalling between tumour and endothelial cells.

5.4.2 Analysis of lipid mediators in conditioned medium

The results shown so far indicate that mediator lipids secreted from U87 cancer cells can induce sprouting of endothelial cells, though it was still unclear whether these factors can indeed be detected in CM and whether they are altered upon SREBP1 silencing. To analyse medium lipid composition globally, total levels of different lipid species in CM were analysed by TLC. However, levels of most lipids were far too low to identify any changes in CM with or without SREBP1 silencing (Fig 4.36). Hence, changes in the relative fractions of both free and total fatty acids were analysed in CM from U87 cells upon SREBP1 silencing by MS, following a direct injection protocol.

The main change observed in total fatty acids in the CM was an increase in the fraction of several PUFA species (Fig 4.37), similar to the effect of SREBP1 silencing on the cellular total fatty acid pool. This suggested that lipids secreted from the cancer cells contain higher levels of fatty acids that are typically present in the sn-2 position of phospholipids. Unexpectedly, no decrease in the amount of MUFA was detected in the total fatty acid pool present in condition medium from SREBP1 silenced cells. But indeed, a significant decrease in MUFAs in the free fatty acid pool present in condition medium from SREBP1 silenced cells was observed (Fig 4.37) and this data aligns with the free fatty acid profile of cells with SREBP1 silencing, shown in other studies (Griffiths *et al.*, 2013). Further investigation is necessary to identify the individual lipid species in the medium and to understand the discrepancy between the cellular and medium lipidomes.

Next, PGE2 levels were assessed in the CM obtained from cancer cells using MS following direct injection. This analysis only showed a minor trend towards lower

levels of PGE2 upon SREBP1 silencing, albeit with large variability (Fig 4.38A). As CM are obtained from cancer cells cultured with serum-free medium, it was challenging to measure lipid signalling molecules that are generally very close to the detection threshold of the mass spectrometer, leading to high variation. However, PGE2 levels measured by ELISA showed a significant reduction upon SREBP1 silencing (Fig 4.38 B). Next, addition of oleic acid (C18:1) was tested to determine if this could restore the production of PGE2 in SREBP1 silenced cells. Oleic acid can prevent the induction of ER stress caused by the accumulation of saturated fatty acids and depletion of mono-unsaturated fatty acids (Griffiths *et al.*, 2013). While addition of oleic acid somewhat increased PGE2 levels in CM from SREBP1 silenced cells, the effect was only partial, suggesting that a reduction in oleic acid did not completely account for the decrease in PGE2 synthesis induced by SREBP1 silencing (Fig 4.38B). In contrast, arachidonic acid (C20:4), which is the direct substrate for PGE2 synthesis, was added to SREBP1 silenced cells before CM was collected, and this strongly induced PGE2 levels to a much higher extent than in control medium (Fig 4.38B). This observation confirmed that arachidonic acid is the limiting factor for the synthesis of PGE2 upon SREBP1 silencing. PLA2G3 silencing also led to a reduction in PGE2 levels, but this was only observed with one of the shRNA sequences (Fig 4.38C) and further investigation is necessary to understand the differences between the two shRNA sequences. However, taken together the total fatty acid profiles obtained from both SREBP1 and PLA2G3 silenced cells, it seems likely that the decrease in PGE2 levels observed after SREBP1 silencing could be attributed to a reduction in the releasing of arachidonic acid from the sn-2 position of membrane phospholipids, making this fatty acid available as a substrate for PGE2 synthesis.

Next, the analysis of LPA-C18:1 in the CM from U87 cells by mass spectrometry was performed and only showed a trend towards a decrease following SREBP1 silencing, most likely due to its low abundance and the detection limit of the instrument (Fig 4.39). A commercially available ELISA showed that SREBP1 silencing led to an increase in total LPA levels, but this experiment was conducted with only one shRNA sequence. Moreover, PLA2G3 silencing did not change total LPA levels (Fig 4.39). This data was hard to interpret, as LPA-C18:1 needs to be analysed specifically to draw conclusions, so other more sensitive methods have to be established to obtain these results. Nevertheless, addition of increasing amounts of LPA-C18:1 to CM from

SREBP1 silenced cells efficiently restored endothelial cell sprouting, starting at a concentration of 100 nM and fully restoring sprouting at around 1μM with no further increase observed beyond that concentration (Fig 4.40). These results, together with the LPARi results, convincingly showed that LPA contributes to the regulation of endothelial cell sprouting downstream of SREBP1.

5.4.3 Xenografts of SREBP1 silenced cells show reduced blood vessels density

As it is important to analyse if SREBP1 reduction affects angiogenesis in tumours and validate our findings *in vivo,* tumour sections from an earlier study that showed reduction in tumour volume upon SREBP1 depletion (Griffiths *et al.*, 2013) were used to analyse changes in vessel density. The tumours with SREBP1 silencing were not only smaller but also paler in comparison to control tumours (Fig 4.41 A). Staining of blood vessels with an antibody detecting mouse endomucin showed a significant reduction in blood vessel density (Fig 4.41 B-D). This observation confirmed that SREBP1 depletion reduced blood vessel formation in tumours *in vivo* and thus was in agreement with our results *in vitro*. Taken together, our data suggests that SREBP1 depletion affects several proteins and lipids involved in angiogenesis in GB. Even though we have not been able to attribute this reduction to a specific mediator, our data supports a model in which changes in fatty acid and phospholipid composition induced as a result of the decreased expression of several targets of the SREBP1 transcriptional network affect endothelial cells. In addition, we have uncovered several novel downstream targets that are altered upon SREBP1 depletion in GB cells (as shown in Fig 4.42). At this stage, the data shows that regulation of angiogenesis by SREBP1 works through a cascade of several factors. It can be concluded that SREBP1 not only regulates cell proliferation and survival but is also involved in the control of tumour angiogenesis, thus posing itself as a potential target in GB patients to limit tumour growth and prevent relapse of this aggressive tumour.

5.5 SREBP1 is indispensable for survival of glioblastoma stem-like cells

Another important factor that contributes to relapse in almost all cases of GB patients is the presence of cancer stem-like cells (CSC), also known as tumour initiating cells (TIC). CSC often escape surgery and are mostly resistant to radio- and chemotherapy (Batlle and Clevers, 2017; Lathia *et al.*, 2015). Many studies have prioritized on understanding and targeting specifically cancer cells that have stem-like properties to improve treatment strategies and increase the overall survival of GB patients (Prasad *et al.*, 2015; Zhu et al., 2014). CSC are characterised similar to stem cells with self-renewal properties and are known to have a distinct metabolism compared to differentiated cancer cells (Li et al., 2017a; Peixoto *et al.*, 2021; Peixoto and Lima, 2018; Pinkham et al., 2019; Wang et al., 2017) and this feature adds advantage to targeting them specifically, making them attractive for the development of novel treatments.

5.5.1 The SREBP1 pathway is upregulated in glioblastoma stem-like cells and its depletion leads to decreased cell viability

A large body of literature has shown that lipid metabolism plays an important role in the survival and proliferation of cancer stem-like cells (Ben-David et al., 2013; Li *et al.*, 2017a; Rios-Esteves and Resh, 2013; Wen et al., 2018; Yasumoto et al., 2016). The study presented in this thesis characterised both U87 and NCH644 patient-derived GB stem-like cells by cultivating them either as monolayer or as neurospheres (Fig 4.43A). Growing cancer cells in suspension on Poly-HEMA coated plates in serum free media with growth factors and supplements is known to enrich the culture for stem-like cells capable of forming neurospheres, while differentiated cells undergo anoikis (Campos et al., 2010). The cells grown in neurosphere culture show high expression of stem cells markers, such as nestin and CD133, and decreased expression of differentiated markers, such as GFAP (Fig 4.43C) (Ardebili et al., 2011; Campos *et al.*, 2010). Gene expression analysis using RNAseq revealed that U87 cells grown as neurospheres show upregulation of HORTON_SREBP1 targets compared to monolayer cells, suggesting the induction of the SREBP1 pathway in neurospheres (Fig 4.43B). Also, upregulation of mRNA levels of the canonical SREBP1 target genes

SCD, PLA2G3 and *FABP3* was observed in NCH644 cells grown in neurospheres compared to monolayer cultures (Fig4.43C). *GFAP* mRNA levels were massively downregulated in neurospheres, validating the enrichment of GSCs in this culture system, in line with the literature (Ardebili *et al.*, 2011; Campos *et al.*, 2010). Several studies have already highlighted the importance of fatty acid desaturation by SCD in GSC survival and proliferation (Ben-David *et al.*, 2013; Li *et al.*, 2017a; Pinkham *et al.*, 2019; Rios-Esteves and Resh, 2013), and high SCD protein levels were observed in GSC compared to monolayer cells (Fig 4.43D). So, further analyses were performed to understand if the genetic depletion of SREBP1 using shRNAs (validated in U87 cells and discussed in earlier chapters) could have an impact on GSC growth and proliferation. Knockdown of SREBP1 also successfully depleted mRNA levels of *SREBF1* and its targets *SCD* and *PLA2G3* in neurospheres derived from NCH644 cells (Fig 4.44B). A significant decrease in GSC cell number was seen upon SREBP1 depletion, showing the importance of this pathway for survival in these cells (Fig 4.44C). Upon analysing total fatty acid profiles in these cells upon SREBP1 depletion, a decrease in desaturation ratios for C16:1/C16:0 and C18:1/C18:0, and a slight increase in arachidonic acid levels were seen (Fig 4.44D). These results are similar to a study utilizing Raman spectroscopy in ovarian CSC, revealing the increased presence of unsaturated fatty acids over saturated fatty acids and highlighting the importance of SCD in CSC (Li *et al.*, 2017a). Together, these results emphasise the importance of the SREBP1 pathway in supporting the survival of GSC. As it was still unclear whether depletion of SREBP1 affected stem-like properties of GCSs, serial neurosphere formation assays were performed to further unravel the role of SREBP1 in GSC maintenance. The depletion of SREBP1 did not alter size of the neurospheres formed over 10 days (Fig 4.45A and D). However, SREBP1 silencing caused a significant decrease in the number of neurospheres formed and decreased the total number of cells present in the cultures at the end of the assay (Fig 4.45B-C).

A study previously showed that loss of SCD leads to ER stress in CSC and renders them sensitive to treatment with temozolomide, an alkylating agent used as first and second line treatment of GB, and thereby resulted in reduced tumour growth (Pinkham *et al.*, 2019). FASN, another enzyme in the SREBP1 network, is also known to be associated with an increase in stem cell markers (Yasumoto *et al.*, 2016), and the inhibition of FASN leads to a decrease in CSC survival in breast cancer (Pandey

et al., 2011). Also, ELOVL2, which is involved in the synthesis of some poly-unsaturated fatty acid species, was shown to be important to maintain cell membrane integrity, and its inhibition was detrimental for CSC survival(Gimple et al., 2019). Hence, SREBP1 and its target genes may play an important role in maintaining specific cellular functions that are indispensable for CSC survival.

5.5.2 Oleic acid rescues loss of cell viability and neurosphere formation upon SREBP1 knockdown

The most important readout of the neurosphere assay is the number of neurospheres formed by seeding a limited cell number in every condition, as each cell is thus tested for its ability to initiate the formation of a neurosphere. Even though this assay is originally derived from the neurosphere assay used for neuronal stem cells (Reynolds and Weiss, 1992) and has been since used in mammosphere assays to determine stemness of breast cancer cells (Bailey et al., 2018; Lombardo et al., 2015), it has also been adapted to monitor CSC growth in glioma. To be able to determine the stemness of individual cells and to avoid potential clumping, a modified neurosphere assay with the addition of methylcellulose was developed. This increases the viscosity of the medium and allows single cells to be embedded with limited movement and this protocol was used to determine the stemness of the cells (Kaufman et al., 2001). A methylcellulose assay using NCH644 cells with or without SREBP1 knockdown was assessed with serial generation of neurospheres (Fig 4.46). Cells were also interrogated by the addition of BSA-coupled oleic acid or BSA alone as control. This experiment showed that the number of neurosphere and the total cell number at the end of the primary neurosphere assay were decreased upon SREBP1 silencing, while no change was observed in neurosphere area, similar to the results seen using the first assay protocol (Fig 4.46). Interestingly, addition of oleic acid was able to restore both number of neurospheres and cell number that was decreased due to loss of SREBP1 (Fig 4.46 A-B). A decrease in number of neurospheres and cell number upon SREBP1 silencing and rescue with oleic acid was also observed in secondary neurospheres, generated from cells seeded from primary neurospheres (Fig 4.47 A-B). It had previously been shown that inhibition of SCD in ovarian CSC could be rescued with addition of oleic acid (Li *et al.*, 2017a). In this system, SCD was important in CSCs to induce sphere formation in *in vitro* assays and also crucial in the induction

of tumours *in vivo.* Moreover, fatty acid desaturation levels in the cells was shown to play an important role in the maintenance of stem cell markers and to govern the cancer-relevant NFkB pathway (Li *et al.*, 2017a). Also, in human pluripotent stem cells, fatty acids desaturation inhibitors were identified as being detrimental to survival and causing ER stress and apoptosis, emphasizing the significance of oleic acid in stem cells (Ben-David *et al.*, 2013).

Performing methylcellulose assays on U87 cells with LKO-BP1_07 also showed a decrease in the number of neurospheres and overall cell number in primary neurospheres (Fig 4.48A-B). Additionally, a strong decrease in neurosphere area was observed upon SREBP1 knockdown, but also to some extent in the dox in control conditions (Fig 4.48C-D). Similar results were obtained by seeding cells into secondary neurospheres, where the effect of SREBP1 knockdown was much stronger, and almost completely abolished neurosphere numbers. It has to be noted that U87 cells were not adapted to neurosphere culture before the experiment, and that these cells are known to have strong heterogeneity of both differentiated and stem-like cells. However, U87 cells even without prior adaptation were still able to survive for 20 days as neurospheres in the control conditions. This indicates that U87 cells do not undergo anoikis, a specific form of cell death of cells in suspension culture (Ayla and Karahuseyinogluc, 2019; Gilmore, 2005), and also confirms the importance of SREBP1 in the adaptation to suspension culture and the formation of neurospheres. However, although further investigation is required to understand the difference seen between the two cell lines and to determine whether oleic acid would also restore neurosphere formation in SREBP1 silenced U87 cells, it is clear that SREBP1 is necessary for neurosphere formation in GB cells.

Understanding the role of SREBP1 pathway in stemness could help to uncover the Achilles heel of GSC that could be targeted to eliminate both stem and differentiated cancer cells. It is known that MUFAs are involved in the regulation of Wnt/b-catenin signalling and promote the maintenance of stem like features in CSC. Activation of Wnt protein requires post-translational acylation that is regulated by the porcupine O-acyltransfaerase (PORCN), that adds acyl chains to conserved cysteine and serine residues on the Wnt protein (Nusse, 2008; Nusse et al., 2008). This translational modification is necessary for the translocation of Wnt proteins from the

ER to the plasma membrane and is essential for their secretion, which is important for their function in stem cells (Herr et al., 2012; Nusse, 2008; Nusse *et al.*, 2008). It was specifically shown that PORCN prefers MUFAs for acylating Wnt, as these molecules can bend and fit perfectly into the hydrophobic groove of these proteins, thus facilitating their activation compared to a saturated fatty acid, that is stiff or PUFAs, that have long carbon chains (Asciolla et al., 2017; Rios-Esteves and Resh, 2013). Utilizing radioactively labelled palmitic acid, it was shown that Wnt proteins are biased towards utilising palmitic acid over other fatty acids for acylation at Ser209 by PORCN (Takada et al., 2006). To facilitate availability of MUFAs, SCD activity becomes obligatory for WNT acylation and activation by PORCN (Rios-Esteves and Resh, 2013). Also downstream of Wnt signalling, ß-catenin regulation is connected to fatty acid availability. Unsaturated fatty acids are also required to stabilize ß-catenin and prevent its binding to FAS associated proteins (FAF1), which normally degrade ß-catenin, thus facilitating its nuclear localization (Kim et al., 2015). It remains to be further investigated if oleic acid can substitute for palmitic acid in our rescue experiment, but together with the evidence obtained from the literature it is clear that SCD activity is necessary and indispensable for Wnt activation and maintenance of stem cell features.

5.6 SREBP1 is regulated by the upstream regulator SOAT1

The PI3K/AKT pathway is one of the most prominent and most frequently mutated pathways in GB patients (Cancer Genome Atlas Research, 2008), and it is know that SREBP is regulated downstream of this pathway (Lewis *et al.*, 2011; Porstmann *et al.*, 2005; Porstmann *et al.*, 2008). Hence, other nodes within the pathway that are involved in this regulation were studied. A study in prostate cancer with loss of PTEN showed upregulation of the PI3K/AKT pathway, resulting in increased uptake of lipoproteins from the environment (Yue *et al.*, 2014). These cells also showed high levels of cholesterol esterification, as free cholesterol can inhibit lipid synthesis by limiting SREBP processing. It was shown that these prostate cancer cells modulate cholesterol levels by esterifying via SOAT1, thereby keeping both lipid uptake and lipid synthesis active, thus promoting cell growth and metastatic behaviour (Peck and Schulze, 2014; Yue *et al.*, 2014). Inhibition of cholesterol esterification led to a significant reduction in cancer cell proliferation, invasion and tumour growth, and overall decreased the aggressiveness of these tumours in mouse xenografts (Yue *et al.*, 2014). This study opened up to a new possible node of SREBP regulation in cancer cells. Also, GB tumours obtained from orthotopic mouse xenografts using several GB cell lines, patient-derived cancer cells and also patient biopsies showed high levels of lipid droplet accumulation and cholesterol esterification (Geng *et al.*, 2016). Hence, understanding the regulation of SREBP and its targets by SOAT1 could provide an alternative mechanism to inhibit the pathway.

5.6.1 SOAT1 depletion reduces SREBP targets

2 shRNAs targeting SOAT1 obtained from Fellmann et al (Fellmann *et al.*, 2013) showed significant downregulation of *SOAT1* mRNA levels in 10% and 1% FCS compared to the control (Fig 4.50). Adrenocortical carcinoma cell line NCI-H295 was used as a positive control for SOAT1 protein detection, as these cells are well characterised and known to have overexpression of SOAT1 (Sbiera *et al.*, 2015). Surprisingly, SOAT1 protein levels were significantly less in 1% FCS compared to 10%FCS (Fig 4.51A). It was clear that shRNA against SOAT1 reduced their protein levels in 10%FCS but since low FCS condition had low SOAT1 levels it was hard to interpret the loss of SOAT1 (Fig 4.51A). Interestingly, upon SOAT1 knockdown *SCD* mRNA levels decreased significantly with both shRNAs in 10%FCS and no change

was seen in 1%FCS condition (Fig 4.51B-C). Also, *HMGCR* mRNA levels were significantly decreased upon SOAT1 silencing in 10% FCS condition and also slightly reduced in 1%FCS condition (Fig 4.51B-C). Further, treatment of U87 and U251 cells with SOAT1 inhibitors Mitotane and ATR101 (also known as PD-132301) also showed reduction in *SREBF1c*, *SCD* and *HMGCR* mRNA levels (Fig 4.54) (Kroiss and Fassnacht, 2016). Taken together these results show that depletion of SOAT1 reduces SREBP1 targets in 10%FCS condition. Knockdown of SOAT1 and its inhibition by Avasimibe, a SOAT1 inhibitor was shown to reduce SREBP1 targets mRNA and protein levels and also mature SREBP1 and 2 in glioma cells (Geng *et al.*, 2016).

In this thesis, analysis of GB cell viability upon knockdown of SOAT1 showed no effect in medium containing 10% FCS. However, cells cultured in 1% FCS showed a significant reduction in cell viability (Fig 4.52). Treating U87 and U251 cells with mitotane showed small reduction in cell viability in 10% FCS, and in 1% FCS mitotane caused massive cell death eliminating almost the entire population (Fig 4.55). Mitotane is known to induce apoptosis in cells via ER stress, but it is also known to have strong affinity towards BSA (Kroiss *et al.*, 2016). Binding of Mitotane to BSA present in serum could explain the large difference in its effect observed between 1% and 10% FCS conditions. Hence, we tested the effect of increasing mitotane concentrations in medium with different FCS levels and observed that mitotane caused a reduction in cell number already at lower concentrations in 1% FCS medium compared to the other conditions in both U87 and U251 cells (Fig 4.56). However, the effect of BSA in this context was not studied. In order to understand the effect of inhibition of SOAT1 despite the problems caused by potential BSA binding, we used another compound, Avasimibe, that is already known to specifically inhibit SOAT1 (Cheng *et al.*, 2018; Li et al., 2016). It was clear that cells in 1% FCS medium compared to 10% FCS were more susceptible to the inhibition of SOAT1 with Avasimibe in both cell lines (Fig 4.57). These results confirmed that depletion of SOAT1 activity, either by genetic ablation or by inhibitor treatment, reduces cell viability in 1% FCS to a larger extent than in 10% FCS. As there was no induction of *DDIT3* (CHOP) upon SOAT1 silencing in 1% FCS in U87 cells (Fig 4.53) and no reduction in the expression of SCD, this indicates that these cells are not undergoing ER stress that is usually caused by SREBP1 silencing. Most likely, SOAT1 silencing did not reduce SREBP1 activity to the extent needed to fully inactivate the pathway. Nevertheless, it is still possible that treatment with

inhibitors, such as mitotane, ATR101 or Avasimibe, could cause cell death by ER stress that also leads to apoptosis (Kroiss and Fassnacht, 2016; Sbiera *et al.*, 2015). Indeed, also in GB cells, it had been shown that oleic acid addition was able to rescue cell viability upon inhibition of SOAT1 (Cheng *et al.*, 2018). Similarly, we found that oleic acid restored cell viability in the presence of mitotane, at least in U87 cells, while, U251 cells, which already showed a lower sensitivity towards the drug, addition of BSA alone could already partially restore cell viability (Fig 4.58).

Interestingly, we found that the expression of SOAT1 is controlled by components of the PI3K/AKT/mTORC1 pathway. Inhibition of PI3K or mTORC1 reduced SOAT1 levels in both U87 and U251 cells, while inhibition of AKT only affected SOAT1 levels in U251 cells (Fig 4.59). Interestingly, U87 cells also showed a reduction in the mRNA levels of *SOAT1* upon PI3K and mTORC1 inhibition, suggesting that a transcriptional process is involved in its regulation, while U251 cells showed a small reduction in *SOAT1* mRNA only after mTORC1 inhibition, suggesting a different mechanism of regulation (Fig 4.59). Moreover, expression of *SREBF1* mRNA resembled that of *SOAT1* mRNA in U87 cells, and U251 cells showed an inconsistent response. These results were obtained after 72 hours of inhibitor treatment and we anticipated signalling events could already take effect at shorter time points. Indeed, 24 hours of inhibitor treatment already showed an effective reduction in the phosphorylation of key components within the PI3K/AKT/mTORC1 pathway (Fig 4.60) and hence, analysis of gene expression was conducted also at an earlier time point. Here, U87 cells showed a significant reduction of *SOAT1* mRNA upon PI3K and mTORC1 inhibitor already after 24 hours of inhibitor treatment, while expression of *SREBF1* and *SCD* were significantly downregulated by inhibition of PI3K, AKT or mTORC1 (Fig 4.60). In contrast, U251 cells did show significant reduction in mRNA levels of *SOAT1* with AKT and mTORC1 inhibition, while *SREBF1* and *SCD* did not show significant effects. It is unclear how inhibition of the same upstream pathway leads to different outcomes in these 2 cell lines, but it was clear that PI3K and mTORC1 regulated SOAT1 in both cell lines. Even though many studies have related SOAT1 to the regulation of lipid biosynthesis, the transcriptional regulation of SOAT1 by the PI3K/AKT/mTORC1 signalling axis is novel and interesting and further studies are necessary to shed light on mechanistic regulation of SOAT1 by these upstream pathways.

5.6.2 SOAT1 silencing decreases GSC proliferation

To also investigate the role of SOAT1 in the regulation of stem cell function, shRNA sequences targeting SOAT1 that were already validated in U87 cells were also used in NCH644 patient derived GB stem-like cells. These sequences efficiently reduced SOAT1 mRNA levels and also caused a significant depletion in the SREBP1 targets *SCD, PLA2G3* and *HMGCR* (Fig 4.61). Loss of SOAT1 also reduced cell proliferation in NCH644 cells cultured as neurospheres (Fig 4.61), similar to the results observed with SREBP1. As SOAT1 regulates SREBP1 activity by reducing the amount of free cholesterol in the cells, these results re-confirmed that SREBP1 is important in GB stem-like cells. It had been previously shown in GB30 patient-derived glioma cells that inhibition of either SREBP1 or SOAT1 leads to a decrease in tumour formation, highlighting the importance of this pathway in this disease entity (Cheng *et al.*, 2018). Another study reported that SOAT1 inhibition reduced Wnt acylation and activation, thereby reducing metastatic capacity in prostate cancer (Lee *et al.*, 2018). Further *in vivo* experiments with orthotopic models using limiting dilution assays that account for stemness regulation are necessary to delineate the mechanism of this pathway in controlling the function of cancer stem cells in GB.

Chapter 6: Appendix

Abbreviations

AA: arachidonic acid, a fatty acid with 20 carbon units and 4 double bonds (C20:4)
ACACA: acetyl-coA carboxylase alpha
ACYL: ATP citrate lyase
AKT: Protein Kinase B, a set of three serine/threonine-specific protein kinases
ATXi: autotaxin inhibitor
BIT ad: BIT admixture
BSA: bovine serum albumin
BUME: butanol: methanol extraction for total lipids
cDNA: complementary DNA
CSCs: Cancer stem like cells
DDIT3: DNA Damage Inducible Transcript 3, also called CHOP
Dox: doxycycline
DNA: deoxyribonucleic acid
EGF: epidermal growth factor
EGFr: EGF receptor
ELOVL: elongation of very long chain fatty acids
ER: endoplasmic reticulum membranes
FADS: fatty acid desaturase
FASN: fatty acid synthase
FCS: fetal bovine serum
FGF: fibroblast growth factor
GB: glioblastoma
GO: gene ontology
GSCs: glioblastoma stem like cells
GSEA: gene set enrichment analysis
HMGCR: HMG-coA reductase
IL8: Interleukin 8
INSIG: insulin-induced genes
LDL: low-density lipoproteins
LPA: lysophosphatidic acid

LPAR1/2: lysophosphatidic acid receptor 1 or 2

LPARi: lysophosphatidic acid receptor inhibitor

LPC: lysophosphatidyl choline

LPE: lysophosphatidyl ethanolamine

MeOH: methanol

MS2: fragmented mass spectra or MS/MS

MUFA: monounsaturated fatty acids

MBTPS1/2: membrane-bound transcription factor site 1 protease and 2

MMP2: matrix metalloproteinase 2

mTORC: Mammalian target of rapamycin

Neg: negative

NF-κB: Nuclear factor kappa B

OA: oleic acid (C18:1)

PA: phosphatidic acid

PC: phosphatidyl choline

PE: phosphatidyl ethanolamine

PFA: paraformaldehyde

PGE2: prostaglandin E2

PI3K: Phosphoinositide 3-kinase

PLA2G3: Phospholipase A2 Group III

polyHEMA: poly-2-hydroxyethyl methacrylate

PORCN: porcupine O-acyltransferase

Pos: positive

PUFA: poly unsatured fatty acids

RB: retinoblastoma tumor suppressor

Rheb: Ras homolog enriched protein in brain

RNA-seq: Ribonucleic acid sequencing

RTK: Receptor tyrosine kinases

RT-qPCR: quantitative reverse transcription polymerase chain reaction

SCAP: SREBP cleavage activating protein

SCD: stearoyl-coA desaturase

SCDi: SCD inhibitor

Scr: scramble control sequence

SOAT1: sterol O-acyltransferase 1

sPLA2i: secreted phospholipase A2 inhibitor

SRE: sterol regulatory elements

SREBF1: gene encoding Sterol regulatory binding protein 1

SREBF2: gene encoding Sterol regulatory binding protein 2

SREBP1/BP1: Sterol regulatory binding protein 1

SREBP2/BP2: Sterol regulatory binding protein 2

TCGA: The cancer genome atlas

TICs: Tumour initiating cells

TLC: thin layer chromatography

VEGF: Vascular endothelial growth factor

VEGFR: Vascular endothelial growth factor receptor

WB: western blot

WHO: World health organization

Acknowledgements

I would like to express my gratitude to my supervisor Prof. Almut Schulze, who gave me an opportunity to work as a PhD student in her group. I was so fortunate to be under her guidance and mentorship for all these years. Thank you for being so kind, patient, supportive and a great advisor to me. You believed and nurtured in my abilities and let me grow and learn to be a good scientist. The long meetings and discussions were one of the best parts of my PhD journey and without them I would not have had opportunity to learn so much. Without you I would not have been able to love research and enjoy working as much as I do today. Thank you so much for the encouraging hand you have lend me to cross this PhD life and being a major part of building my scientific career.

I would also like to thank the members of my thesis committee Prof. Dr. Svenja Meierjohan and Prof. Dr Matthias Kroiss. Thank you for the feedback and encouragement you gave me during my thesis committee meetings and the advice you provided me to move forward with my project. You both were so supportive and made the thesis committee efficient and rewarding at the same time. Without your assistance finishing my PhD would not be possible and thank you so much for the guidance and kindness you have shown to me during my PhD.

I would like to thank the Graduate School of Life Science (GSLS) for all the support and guidance during my PhD. All of you have been helpful to me in so many ways from the beginning to the end. Thank you for being so supportive and helping me graduate.

It would not be possible to finish this PhD journey without the help and great support from all the past and present members of the Chair of Biochemistry and Molecular Biology. Thank you so much.

I would like to specially thank Werner Schmitz, whose guidance and support has been a major part of my PhD journey and carving my career path. Thank you, Werner, for always believing in me, even when I doubted myself.

I would like to extend special thanks to all present and past members of Prof. Schulze's lab. I will always cherish the time I spent with everyone. Bea, thank you for always being kind and helpful to me since the day I started in the lab. Thank you, Matti, Charis, Flo and Felix, for all the interesting discussions we had and especially the laughs you added. Jessica, you have been a big part of my PhD life since the day I started in the lab, we have grown to be such close friends. Thank you for always being there for me and motivating me throughout my PhD. Irem, even though we did not get a good start, you have been a great friend I found along the way, thank you always being there for me and adding spice and drama to my PhD life. Carina, you have been a great friend to me, and I thank you for all the great discussions we had both scientifically and personally. You have been a great support even after I left and always offered to help me, thank you so much. Markus, even though you came along a bit later, you have always been helpful and nice to me. Without your help I would not be able to submit my thesis, thank you for translating my abstract, helping me print my thesis and I will always remain grateful for your help. I think having great PhD buddies is the biggest part in getting through the hurdles, and specially without you Joana, my PhD life would not be the same. You have always been there for me, even now you have been a great friend and supporting and helping me all along. Thank you so much.

Roberta, thank you for introducing me to Almut and giving my scientific career a great start. You have always been a great mentor and a friend who made me keep my goals in check and focus on being a better scientist. Karin, you have been a great friend to me and always been so kind and supportive to me. Eweline, you have been such a great flatmate and my family through my PhD life. I would not be able to get through all the ups and downs without our friendship. Also, thank you for making my life outside the lab such fun. Sarah, even though we knew each other for a short time, you have always been so motivating with your fresh mind and ideas and I will always be grateful for your support during my thesis writing.

It would have been hard to finish my thesis without the support of my present boss Justin, colleagues and friends at MSK. All of you have been so kind and supportive, it was hard to push through the last bit and thank you for being there for me and motivating me.

Harry, you have been such a great and supportive partner throughout my PhD journey. You have always listened to me and gave me advice when I needed to move further. Thank you for being a great pillar of support and standing strong with me while it got hard for me to finish. I also thank your family, who have been kind and supportive to me.

My family has always been my greatest support throughout my life. Dad, thank you for your unconditional love, your belief in me and letting me chase my dreams. Without your support I could not have been able to accomplish this. Usha and Sushma, you both believed in me and motivated me even when I did not. Thank you for being there no matter what and loving the crazy me.

Mom, thank you for being the biggest strength in my life and always being with me.

Publications

Beta-hydroxybutyrate (3-OHB) can influence the energetic phenotype of breast cancer cells but does not impact their proliferation and the response to chemotherapy or radiation.

Cancer & Metab (Jun 2018)

Catharina Bartmann, **Sudha R. Janaki Raman**, Jessica Flöter, Almut Schulze, Katrin Bahlke, Jana Willingstorfer, Maria Strunz, Achim Wöckel, Rainer J. Klement, Michaela Kapp, Cholpon S. Djuzenova, Christoph Otto, Ulrike Kämmerer

Protein kinase D1 deletion in adipocytes enhances energy dissipation and protects against adiposity.

EMBO J (Nov 2018)

Mona C. Löffler, Alexander E. Mayer, Jonathan Trujillo Viera, Angel Loza Valdes, Rabih El-Merahbi, Carsten P. Ade, Till Karwen, Werner Schmitz, Anja Slotta, Manuela Erk, **Sudha Janaki-Raman**, Nuria Matesanz, Jorge L. Torres, Miguel Marcos, Guadalupe Sabio, Martin Eilers, Almut Schulze, and Grzegorz Sumara

Connecting lysosomes and mitochondria – a novel role for lipid metabolism in cancer cell death.

Cell Communication and Signaling (Jul 2019)

Karin Bartel; Helmut Pein; Bastian Popper; Sabine Schmitt; **Sudha Janaki-Raman**; Almut Schulze; Florian Lengauer; Andreas Koeberle; Oliver Werz; Hans Zischka; Rolf Müller; Angelika M. Vollmar; Karin von Schwarzenberg

MYC with SREBP1 Regulates Lipogenesis Essential for Neoplastic Growth

Cell Metabolism (Sep 2019)

Arvin M. Gouw, Katherine Margulis, Natalie S. Liu, **Sudha J. Raman**, Anthony Mancuso, Georgia G. Toal, Ling Tong, Adriane Mosley, Annie L. Hsieh, Delaney K. Sullivan, Zachary E. Stine, Brian J. Altman, Almut Schulze, Chi V. Dang, Richard N. Zare, Dean W. Felsher

Greasing the wheels of the cancer machine – the role of lipid metabolism in cancer (Review)

Cell Metabolism (Jan 2020)

Marteinn Snaebjornsson, **Sudha Janaki-Raman**, Almut Schulze

HGF-induced glycolytic reprogramming in HNSCC depends on Met receptor level

International journal of Molecular Sciences (Jan 2020)

Verena Boschert, Nicola Klenk, Alexander Abt, **Sudha Janaki Raman**, Roman C. Brands, Axel Seher, Christian Linz, Thorsten Bischler and Stefan Hartmann

mTOR signaling and SREBP activity increase FADS2 expression and can activate sapienate biosynthesis.

Cell Reports (Jun 2020)

Mouna Triki, Gianmarco Rinaldi, Melanie Planque, Dorien Broekaert, Alina Winkelkotte, Carina Maier, **Sudha Janaki Raman**, Anke Vandekerre, Joke Van Elsen, Martin F. Orth, Thomas G. P. Grünewald, Almut Schulze and Sarah-Maria Fendt

Neutral sphingomyelinase-2 (NSM 2) controls T cell metabolic homeostasis and reprogramming during activation

Front. Mol.Biosci. (Sep 2020)

Maria Nathalia De Lira, **Sudha Janaki-Raman**, Almut Schulze, Sibylle Schneider-Schaulies, Elita Avota.

Metabolic adaptation of acute lymphoblastic leukemia to the central nervous system microenvironment is dependent on Stearoyl CoA desaturase

Nat Cancer (October 2020)

Angela Maria Savino, Sara Isabel Fernandes, Orianne Olivares, Anna Zemlyansky, Antony Cousins, Elke K Markert, Shani Barel, Ifat Geron, Liron Frishman, Yehudit Birger, Cornelia Eckert, Sergey Tumanov, Gillian MacKay, Jurre J Kamphorst, Pawel Herzyk, Jonatan Fernández-García, Ifat Abramovich, Inbal Mor, Michela Bardini, Ersilia Barin, **Sudha Janaki-Raman**, Justin R Cross, Michael G Kharas, Eyal Gottlieb, Shai Izraeli, Christina Halsey

Chlamydia trachomatis stabilizes the proto-oncogene c-Myc to de-route glutamine metabolism for its survival.

Nature Microbiology (Nov 2020)

Karthika Rajeeve, Nadine Vollmuth, **Sudha Janaki-Raman**, Thomas Wulff, Maximilian Schmalhofer, Werner Schmitz, Apoorva Baluapuri, Claudia Huber, Francesca Dejure, Elmar Wolf, Wolfgang Eisenreich, Almut Schulze, Thomas Rudel

Integrated Metabolomics and Transcriptomics Analysis of Monolayer and Neurospheres from Established Glioblastoma Cell Lines

Cancer (Basel) (March 2021)

Joana Peixoto*, **Sudha Janaki-Raman***, Lisa Schlicker, Werner Schmitz, Susanne Walz, Alina M Winkelkotte, Christel Herold-Mende, Paula Soares, Almut Schulze, Jorge Lima

* Authors contributed equally

c-Myc is the key player in IFN-γ induced Chlamydia trachomatis dormancy

Manuscript submitted

Nadine Vollmuth, **Sudha Janaki-Raman**, Werner Schmitz, Almut Schulze, Thomas Rudel, Karthika Rajeeve.

Concerted metabolic and genetic regulation of α-ketoglutarate pools dictates the viability of stem-like or non-stem-like subpopulations in glioblastoma.

Manuscript under preparation

Joana Peixoto, **Sudha Janaki-Raman**, Werner Schmitz, Susanne Walz, Paula Soares, Valdemar Máximo, Almut Schulze, Jorge Lima.

References

1 Aldape, K., Brindle, K.M., Chesler, L., Chopra, R., Gajjar, A., Gilbert, M.R., Gottardo, N., Gutmann, D.H., Hargrave, D., Holland, E.C., et al. (2019). Challenges to curing primary brain tumours. Nat Rev Clin Oncol *16*, 509-520. 10.1038/s41571-019-0177-5.

2 An, Z., and Weiss, W.A. (2016). Cholesterol: An Achilles' Heel for Glioblastoma? Cancer Cell *30*, 653-654. 10.1016/j.ccell.2016.10.011.

3 Ardebili, S.Y., Zajc, I., Gole, B., Campos, B., Herold-Mende, C., Drmota, S., and Lah, T.T. (2011). CD133/prominin1 is prognostic for GBM patient's survival, but inversely correlated with cysteine cathepsins' expression in glioblastoma derived spheroids. Radiol Oncol *45*, 102-115. 10.2478/v10019-011-0015-6.

4 Ariyama, H., Kono, N., Matsuda, S., Inoue, T., and Arai, H. (2010). Decrease in membrane phospholipid unsaturation induces unfolded protein response. J Biol Chem *285*, 22027-22035. 10.1074/jbc.M110.126870.

5 Asciolla, J.J., Miele, M.M., Hendrickson, R.C., and Resh, M.D. (2017). An in vitro fatty acylation assay reveals a mechanism for Wnt recognition by the acyltransferase Porcupine. J Biol Chem *292*, 13507-13513. 10.1074/jbc.C117.800136.

6 Auciello, F.R., Bulusu, V., Oon, C., Tait-Mulder, J., Berry, M., Bhattacharyya, S., Tumanov, S., Allen-Petersen, B.L., Link, J., Kendsersky, N.D., et al. (2019). A Stromal Lysolipid-Autotaxin Signaling Axis Promotes Pancreatic Tumor Progression. Cancer Discov *9*, 617-627. 10.1158/2159-8290.CD-18-1212.

7 Ayla, S., and Karahuseyinogluc, S. (2019). Cancer Stem Cells, Their Microenvironment and Anoikis. Crit Rev Oncog *24*, 27-34. 10.1615/CritRevOncog.2018029433.

8 Baenke, F., Peck, B., Miess, H., and Schulze, A. (2013). Hooked on fat: the role of lipid synthesis in cancer metabolism and tumour development. Dis Model Mech *6*, 1353-1363. 10.1242/dmm.011338.

9 Bagnato, A., and Spinella, F. (2003). Emerging role of endothelin-1 in tumor angiogenesis. Trends Endocrinol Metab *14*, 44-50. 10.1016/s1043-2760(02)00010-3.

10 Bailey, P.C., Lee, R.M., Vitolo, M.I., Pratt, S.J.P., Ory, E., Chakrabarti, K., Lee, C.J., Thompson, K.N., and Martin, S.S. (2018). Single-Cell Tracking of Breast Cancer Cells Enables Prediction of Sphere Formation from Early Cell Divisions. iScience *8*, 29-39. 10.1016/j.isci.2018.08.015.

11 Batlle, E., and Clevers, H. (2017). Cancer stem cells revisited. Nat Med *23*, 1124-1134. 10.1038/nm.4409.

12 Bazzani, L., Donnini, S., Finetti, F., Christofori, G., and Ziche, M. (2017). PGE2/EP3/SRC signaling induces EGFR nuclear translocation and growth through EGFR ligands release in lung adenocarcinoma cells. Oncotarget *8*, 31270-31287. 10.18632/oncotarget.16116.

13 Becker, A.P., Sells, B.E., Haque, S.J., and Chakravarti, A. (2021). Tumor Heterogeneity in Glioblastomas: From Light Microscopy to Molecular Pathology. Cancers (Basel) *13*. 10.3390/cancers13040761.

14 Bellacosa, A., Kumar, C.C., Di Cristofano, A., and Testa, J.R. (2005). Activation of AKT kinases in cancer: implications for therapeutic targeting. Adv Cancer Res *94*, 29-86. 10.1016/S0065-230X(05)94002-5.

15 Beloribi-Djefaflia, S., Vasseur, S., and Guillaumond, F. (2016). Lipid metabolic reprogramming in cancer cells. Oncogenesis *5*, e189. 10.1038/oncsis.2015.49.

16 Ben-David, U., Gan, Q.F., Golan-Lev, T., Arora, P., Yanuka, O., Oren, Y.S., Leikin-Frenkel, A., Graf, M., Garippa, R., Boehringer, M., et al. (2013). Selective elimination of human pluripotent stem cells by an oleate synthesis inhibitor discovered in a high-throughput screen. Cell Stem Cell *12*, 167-179. 10.1016/j.stem.2012.11.015.

17 Bengoechea-Alonso, M.T., and Ericsson, J. (2009). A phosphorylation cascade controls the degradation of active SREBP1. J Biol Chem *284*, 5885-5895. 10.1074/jbc.M807906200.

18 Bertolio, R., Napoletano, F., Mano, M., Maurer-Stroh, S., Fantuz, M., Zannini, A., Bicciato, S., Sorrentino, G., and Del Sal, G. (2019). Sterol regulatory element binding protein 1 couples mechanical cues and lipid metabolism. Nat Commun *10*, 1326. 10.1038/s41467-019-09152-7.

19 Bhave, S.R., Dadey, D.Y., Karvas, R.M., Ferraro, D.J., Kotipatruni, R.P., Jaboin, J.J., Hallahan, A.N., Dewees, T.A., Linkous, A.G., Hallahan, D.E., and Thotala, D. (2013).

Autotaxin Inhibition with PF-8380 Enhances the Radiosensitivity of Human and Murine Glioblastoma Cell Lines. Front Oncol *3*, 236. 10.3389/fonc.2013.00236.

20 Blum, R., Elkon, R., Yaari, S., Zundelevich, A., Jacob-Hirsch, J., Rechavi, G., Shamir, R., and Kloog, Y. (2007). Gene expression signature of human cancer cell lines treated with the ras inhibitor salirasib (S-farnesylthiosalicylic acid). Cancer Res *67*, 3320-3328. 10.1158/0008-5472.CAN-06-4287.

21 Campos, B., Wan, F., Farhadi, M., Ernst, A., Zeppernick, F., Tagscherer, K.E., Ahmadi, R., Lohr, J., Dictus, C., Gdynia, G., et al. (2010). Differentiation therapy exerts antitumor effects on stem-like glioma cells. Clin Cancer Res *16*, 2715-2728. 10.1158/1078-0432.CCR-09-1800.

22 Cancer Genome Atlas Research, N. (2008). Comprehensive genomic characterization defines human glioblastoma genes and core pathways. Nature *455*, 1061-1068. 10.1038/nature07385.

23 Cantley, L., Whitman, M., Kaplan, D.R., Chahwala, S.B., Fleischman, L., Endemann, G., Schaffhausen, B.S., and Roberts, T.M. (1986). Phosphatidylinositol kinases and cell transformation. Symp Fundam Cancer Res *39*, 165-172.

24 Carmeliet, P. (2005). VEGF as a key mediator of angiogenesis in cancer. Oncology *69 Suppl 3*, 4-10. 10.1159/000088478.

25 Carmeliet, P., and Jain, R.K. (2000). Angiogenesis in cancer and other diseases. Nature *407*, 249-257. 10.1038/35025220.

26 Chakravarty, B., Gu, Z., Chirala, S.S., Wakil, S.J., and Quiocho, F.A. (2004). Human fatty acid synthase: structure and substrate selectivity of the thioesterase domain. Proc Natl Acad Sci U S A *101*, 15567-15572. 10.1073/pnas.0406901101.

27 Cheng, C., Geng, F., Cheng, X., and Guo, D. (2018). Lipid metabolism reprogramming and its potential targets in cancer. Cancer Commun (Lond) *38*, 27. 10.1186/s40880-018-0301-4.

28 Collins, V.P. (1993). Amplified genes in human gliomas. Semin Cancer Biol *4*, 27-32.

29 Cuncannon, M., Wong, M., Jayamanne, D., Guo, L., Cove, N., Wheeler, H., and Back, M. (2019). Role of delayed salvage bevacizumab at symptomatic progression of chemorefractory glioblastoma. BMC Cancer *19*, 445. 10.1186/s12885-019-5678-1.

30 David, J.M., Dominguez, C., Hamilton, D.H., and Palena, C. (2016). The IL-8/IL-8R Axis: A Double Agent in Tumor Immune Resistance. Vaccines (Basel) *4*. 10.3390/vaccines4030022.

31 DeBerardinis, R.J., Lum, J.J., Hatzivassiliou, G., and Thompson, C.B. (2008). The biology of cancer: metabolic reprogramming fuels cell growth and proliferation. Cell Metab *7*, 11-20. 10.1016/j.cmet.2007.10.002.

32 Fellmann, C., Hoffmann, T., Sridhar, V., Hopfgartner, B., Muhar, M., Roth, M., Lai, D.Y., Barbosa, I.A., Kwon, J.S., Guan, Y., et al. (2013). An optimized microRNA backbone for effective single-copy RNAi. Cell Rep *5*, 1704-1713. 10.1016/j.celrep.2013.11.020.

33 Finck, B.N., Gropler, M.C., Chen, Z., Leone, T.C., Croce, M.A., Harris, T.E., Lawrence, J.C., Jr., and Kelly, D.P. (2006). Lipin 1 is an inducible amplifier of the hepatic PGC-1alpha/PPARalpha regulatory pathway. Cell Metab *4*, 199-210. 10.1016/j.cmet.2006.08.005.

34 Fleischmann, M., and Iynedjian, P.B. (2000). Regulation of sterol regulatory-element binding protein 1 gene expression in liver: role of insulin and protein kinase B/cAkt. Biochem J *349*, 13-17. 10.1042/0264-6021:3490013.

35 Form, D.M., and Auerbach, R. (1983). PGE2 and angiogenesis. Proc Soc Exp Biol Med *172*, 214-218. 10.3181/00379727-172-41548.

36 Geng, F., Cheng, X., Wu, X., Yoo, J.Y., Cheng, C., Guo, J.Y., Mo, X., Ru, P., Hurwitz, B., Kim, S.H., et al. (2016). Inhibition of SOAT1 Suppresses Glioblastoma Growth via Blocking SREBP-1-Mediated Lipogenesis. Clin Cancer Res *22*, 5337-5348. 10.1158/1078-0432.CCR-15-2973.

37 Gijs, H.L., Willemarck, N., Vanderhoydonc, F., Khan, N.A., Dehairs, J., Derua, R., Waelkens, E., Taketomi, Y., Murakami, M., Agostinis, P., et al. (2015). Primary cilium suppression by SREBP1c involves distortion of vesicular trafficking by PLA2G3. Mol Biol Cell *26*, 2321-2332. 10.1091/mbc.E14-10-1472.

38 Gilmore, A.P. (2005). Anoikis. Cell Death Differ *12 Suppl 2*, 1473-1477. 10.1038/sj.cdd.4401723.

39 Gimple, R.C., Kidwell, R.L., Kim, L.J.Y., Sun, T., Gromovsky, A.D., Wu, Q., Wolf, M., Lv, D., Bhargava, S., Jiang, L., et al. (2019). Glioma Stem Cell-Specific Superenhancer Promotes

Polyunsaturated Fatty-Acid Synthesis to Support EGFR Signaling. Cancer Discov *9*, 1248-1267. 10.1158/2159-8290.CD-19-0061.

40 Golebiewska, A., Bougnaud, S., Stieber, D., Brons, N.H., Vallar, L., Hertel, F., Klink, B., Schrock, E., Bjerkvig, R., and Niclou, S.P. (2013). Side population in human glioblastoma is non-tumorigenic and characterizes brain endothelial cells. Brain *136*, 1462-1475. 10.1093/brain/awt025.

41 Gouw, A.M., Margulis, K., Liu, N.S., Raman, S.J., Mancuso, A., Toal, G.G., Tong, L., Mosley, A., Hsieh, A.L., Sullivan, D.K., et al. (2019). The MYC Oncogene Cooperates with Sterol-Regulated Element-Binding Protein to Regulate Lipogenesis Essential for Neoplastic Growth. Cell Metab *30*, 556-572 e555. 10.1016/j.cmet.2019.07.012.

42 Griffiths, B., Lewis, C.A., Bensaad, K., Ros, S., Zhang, Q., Ferber, E.C., Konisti, S., Peck, B., Miess, H., East, P., et al. (2013). Sterol regulatory element binding protein-dependent regulation of lipid synthesis supports cell survival and tumor growth. Cancer Metab *1*, 3. 10.1186/2049-3002-1-3.

43 Hambardzumyan, D., Gutmann, D.H., and Kettenmann, H. (2016). The role of microglia and macrophages in glioma maintenance and progression. Nat Neurosci *19*, 20-27. 10.1038/nn.4185.

44 Han, J., Li, E., Chen, L., Zhang, Y., Wei, F., Liu, J., Deng, H., and Wang, Y. (2015). The CREB coactivator CRTC2 controls hepatic lipid metabolism by regulating SREBP1. Nature *524*, 243-246. 10.1038/nature14557.

45 Hanahan, D., and Folkman, J. (1996). Patterns and emerging mechanisms of the angiogenic switch during tumorigenesis. Cell *86*, 353-364. 10.1016/s0092-8674(00)80108-7.

46 Hanahan, D., and Weinberg, R.A. (2000). The hallmarks of cancer. Cell *100*, 57-70. 10.1016/s0092-8674(00)81683-9.

47 Harayama, T., and Riezman, H. (2018). Understanding the diversity of membrane lipid composition. Nat Rev Mol Cell Biol *19*, 281-296. 10.1038/nrm.2017.138.

48 Herr, P., Hausmann, G., and Basler, K. (2012). WNT secretion and signalling in human disease. Trends Mol Med *18*, 483-493. 10.1016/j.molmed.2012.06.008.

49 Hisano, Y., and Hla, T. (2019). Bioactive lysolipids in cancer and angiogenesis. Pharmacol Ther *193*, 91-98. 10.1016/j.pharmthera.2018.07.006.

50 Holz, M.K., Ballif, B.A., Gygi, S.P., and Blenis, J. (2005). mTOR and S6K1 mediate assembly of the translation preinitiation complex through dynamic protein interchange and ordered phosphorylation events. Cell *123*, 569-580. 10.1016/j.cell.2005.10.024.

51 Horton, J.D. (2002). Sterol regulatory element-binding proteins: transcriptional activators of lipid synthesis. Biochem Soc Trans *30*, 1091-1095. 10.1042/bst0301091.

52 Horton, J.D., Shah, N.A., Warrington, J.A., Anderson, N.N., Park, S.W., Brown, M.S., and Goldstein, J.L. (2003). Combined analysis of oligonucleotide microarray data from transgenic and knockout mice identifies direct SREBP target genes. Proc Natl Acad Sci U S A *100*, 12027-12032. 10.1073/pnas.1534923100.

53 Hsieh, A.C., Liu, Y., Edlind, M.P., Ingolia, N.T., Janes, M.R., Sher, A., Shi, E.Y., Stumpf, C.R., Christensen, C., Bonham, M.J., et al. (2012). The translational landscape of mTOR signalling steers cancer initiation and metastasis. Nature *485*, 55-61. 10.1038/nature10912.

54 Hua, X., Yokoyama, C., Wu, J., Briggs, M.R., Brown, M.S., Goldstein, J.L., and Wang, X. (1993). SREBP-2, a second basic-helix-loop-helix-leucine zipper protein that stimulates transcription by binding to a sterol regulatory element. Proc Natl Acad Sci U S A *90*, 11603-11607. 10.1073/pnas.90.24.11603.

55 Ishida, S., Huang, E., Zuzan, H., Spang, R., Leone, G., West, M., and Nevins, J.R. (2001). Role for E2F in control of both DNA replication and mitotic functions as revealed from DNA microarray analysis. Mol Cell Biol *21*, 4684-4699. 10.1128/MCB.21.14.4684-4699.2001.

56 Jain, R.K., di Tomaso, E., Duda, D.G., Loeffler, J.S., Sorensen, A.G., and Batchelor, T.T. (2007). Angiogenesis in brain tumours. Nat Rev Neurosci *8*, 610-622. 10.1038/nrn2175.

57 Jakobsson, A., Westerberg, R., and Jacobsson, A. (2006). Fatty acid elongases in mammals: their regulation and roles in metabolism. Prog Lipid Res *45*, 237-249. 10.1016/j.plipres.2006.01.004.

58 Jawhari, S., Ratinaud, M.H., and Verdier, M. (2016). Glioblastoma, hypoxia and autophagy: a survival-prone 'menage-a-trois'. Cell Death Dis *7*, e2434. 10.1038/cddis.2016.318.

59 Jump, D.B. (2009). Mammalian fatty acid elongases. Methods Mol Biol *579*, 375-389. 10.1007/978-1-60761-322-0_19.

60 Kaufman, D.S., Hanson, E.T., Lewis, R.L., Auerbach, R., and Thomson, J.A. (2001). Hematopoietic colony-forming cells derived from human embryonic stem cells. Proc Natl Acad Sci U S A *98*, 10716-10721. 10.1073/pnas.191362598.

61 Kim, D.H., Sarbassov, D.D., Ali, S.M., King, J.E., Latek, R.R., Erdjument-Bromage, H., Tempst, P., and Sabatini, D.M. (2002). mTOR interacts with raptor to form a nutrient-sensitive complex that signals to the cell growth machinery. Cell *110*, 163-175. 10.1016/s0092-8674(02)00808-5.

62 Kim, H., Rodriguez-Navas, C., Kollipara, R.K., Kapur, P., Pedrosa, I., Brugarolas, J., Kittler, R., and Ye, J. (2015). Unsaturated Fatty Acids Stimulate Tumor Growth through Stabilization of beta-Catenin. Cell Rep *13*, 495-503. 10.1016/j.celrep.2015.09.010.

63 Kim, M.M., Umemura, Y., and Leung, D. (2018). Bevacizumab and Glioblastoma: Past, Present, and Future Directions. Cancer J *24*, 180-186. 10.1097/PPO.0000000000000326.

64 Kishimoto, K., Liu, S., Tsuji, T., Olson, K.A., and Hu, G.F. (2005). Endogenous angiogenin in endothelial cells is a general requirement for cell proliferation and angiogenesis. Oncogene *24*, 445-456. 10.1038/sj.onc.1208223.

65 Knowles, J., Loizidou, M., and Taylor, I. (2005). Endothelin-1 and angiogenesis in cancer. Curr Vasc Pharmacol *3*, 309-314. 10.2174/157016105774329462.

66 Kroiss, M., and Fassnacht, M. (2016). Inhibition of Cholesterol Esterification in the Adrenal Gland by ATR101/PD132301-2, A Promising Case of Drug Repurposing. Endocrinology *157*, 1719-1721. 10.1210/en.2016-1210.

67 Kroiss, M., Plonne, D., Kendl, S., Schirmer, D., Ronchi, C.L., Schirbel, A., Zink, M., Lapa, C., Klinker, H., Fassnacht, M., et al. (2016). Association of mitotane with chylomicrons and serum lipoproteins: practical implications for treatment of adrenocortical carcinoma. Eur J Endocrinol *174*, 343-353. 10.1530/EJE-15-0946.

68 Lai, A., Kharbanda, S., Pope, W.B., Tran, A., Solis, O.E., Peale, F., Forrest, W.F., Pujara, K., Carrillo, J.A., Pandita, A., et al. (2011). Evidence for sequenced molecular evolution of IDH1 mutant glioblastoma from a distinct cell of origin. J Clin Oncol *29*, 4482-4490. 10.1200/JCO.2010.33.8715.

69 Lally, J.S.V., Ghoshal, S., DePeralta, D.K., Moaven, O., Wei, L., Masia, R., Erstad, D.J., Fujiwara, N., Leong, V., Houde, V.P., et al. (2019). Inhibition of Acetyl-CoA Carboxylase by Phosphorylation or the Inhibitor ND-654 Suppresses Lipogenesis and Hepatocellular Carcinoma. Cell Metab *29*, 174-182 e175. 10.1016/j.cmet.2018.08.020.

70 Lathia, J.D., Mack, S.C., Mulkearns-Hubert, E.E., Valentim, C.L., and Rich, J.N. (2015). Cancer stem cells in glioblastoma. Genes Dev *29*, 1203-1217. 10.1101/gad.261982.115.

71 Lee, H., Goetzl, E.J., and An, S. (2000). Lysophosphatidic acid and sphingosine 1-phosphate stimulate endothelial cell wound healing. Am J Physiol Cell Physiol *278*, C612-618. 10.1152/ajpcell.2000.278.3.C612.

72 Lee, H.J., Li, J., Vickman, R.E., Li, J., Liu, R., Durkes, A.C., Elzey, B.D., Yue, S., Liu, X., Ratliff, T.L., and Cheng, J.X. (2018). Cholesterol Esterification Inhibition Suppresses Prostate Cancer Metastasis by Impairing the Wnt/beta-catenin Pathway. Mol Cancer Res *16*, 974-985. 10.1158/1541-7786.MCR-17-0665.

73 Lee, S.S., Li, J., Tai, J.N., Ratliff, T.L., Park, K., and Cheng, J.X. (2015). Avasimibe encapsulated in human serum albumin blocks cholesterol esterification for selective cancer treatment. ACS Nano *9*, 2420-2432. 10.1021/nn504025a.

74 Leung, D.W., Cachianes, G., Kuang, W.J., Goeddel, D.V., and Ferrara, N. (1989). Vascular endothelial growth factor is a secreted angiogenic mitogen. Science *246*, 1306-1309. 10.1126/science.2479986.

75 Lewis, C.A., Brault, C., Peck, B., Bensaad, K., Griffiths, B., Mitter, R., Chakravarty, P., East, P., Dankworth, B., Alibhai, D., et al. (2015). SREBP maintains lipid biosynthesis and viability of cancer cells under lipid- and oxygen-deprived conditions and defines a gene signature associated with poor survival in glioblastoma multiforme. Oncogene *34*, 5128-5140. 10.1038/onc.2014.439.

76 Lewis, C.A., Griffiths, B., Santos, C.R., Pende, M., and Schulze, A. (2011). Regulation of the SREBP transcription factors by mTORC1. Biochem Soc Trans *39*, 495-499. 10.1042/BST0390495.

77 Li, A., Dubey, S., Varney, M.L., Dave, B.J., and Singh, R.K. (2003). IL-8 directly enhanced endothelial cell survival, proliferation, and matrix metalloproteinases production and regulated angiogenesis. J Immunol *170*, 3369-3376. 10.4049/jimmunol.170.6.3369.

78 Li, J., Condello, S., Thomes-Pepin, J., Ma, X., Xia, Y., Hurley, T.D., Matei, D., and Cheng, J.X. (2017a). Lipid Desaturation Is a Metabolic Marker and Therapeutic Target of Ovarian Cancer Stem Cells. Cell Stem Cell *20*, 303-314 e305. 10.1016/j.stem.2016.11.004.

79 Li, J., Gu, D., Lee, S.S., Song, B., Bandyopadhyay, S., Chen, S., Konieczny, S.F., Ratliff, T.L., Liu, X., Xie, J., and Cheng, J.X. (2016). Abrogating cholesterol esterification suppresses growth and metastasis of pancreatic cancer. Oncogene *35*, 6378-6388. 10.1038/onc.2016.168.

80 Li, Y., Ali, S., Clarke, J., and Cha, S. (2017b). Bevacizumab in Recurrent Glioma: Patterns of Treatment Failure and Implications. Brain Tumor Res Treat *5*, 1-9. 10.14791/btrt.2017.5.1.1.

81 Liu, L., Ge, D., Ma, L., Mei, J., Liu, S., Zhang, Q., Ren, F., Liao, H., Pu, Q., Wang, T., and You, Z. (2012). Interleukin-17 and prostaglandin E2 are involved in formation of an M2 macrophage-dominant microenvironment in lung cancer. J Thorac Oncol *7*, 1091-1100. 10.1097/JTO.0b013e3182542752.

82 Lo, A.K., Lung, R.W., Dawson, C.W., Young, L.S., Ko, C.W., Yeung, W.W., Kang, W., To, K.F., and Lo, K.W. (2018). Activation of sterol regulatory element-binding protein 1 (SREBP1)-mediated lipogenesis by the Epstein-Barr virus-encoded latent membrane protein 1 (LMP1) promotes cell proliferation and progression of nasopharyngeal carcinoma. J Pathol *246*, 180-190. 10.1002/path.5130.

83 Lombardo, Y., de Giorgio, A., Coombes, C.R., Stebbing, J., and Castellano, L. (2015). Mammosphere formation assay from human breast cancer tissues and cell lines. J Vis Exp. 10.3791/52671.

84 Louis, D.N. (2006). Molecular pathology of malignant gliomas. Annu Rev Pathol *1*, 97-117. 10.1146/annurev.pathol.1.110304.100043.

85 Lu, M., Wan, M., Leavens, K.F., Chu, Q., Monks, B.R., Fernandez, S., Ahima, R.S., Ueki, K., Kahn, C.R., and Birnbaum, M.J. (2012). Insulin regulates liver metabolism in vivo in the absence of hepatic Akt and Foxo1. Nat Med *18*, 388-395. 10.1038/nm.2686.

86 Lupo, G., Caporarello, N., Olivieri, M., Cristaldi, M., Motta, C., Bramanti, V., Avola, R., Salmeri, M., Nicoletti, F., and Anfuso, C.D. (2016). Anti-angiogenic Therapy in Cancer: Downsides and New Pivots for Precision Medicine. Front Pharmacol *7*, 519. 10.3389/fphar.2016.00519.

87 Mason, P., Liang, B., Li, L., Fremgen, T., Murphy, E., Quinn, A., Madden, S.L., Biemann, H.P., Wang, B., Cohen, A., et al. (2012). SCD1 inhibition causes cancer cell death by depleting mono-unsaturated fatty acids. PLoS One *7*, e33823. 10.1371/journal.pone.0033823.

88 McGregor, G.H., Campbell, A.D., Fey, S.K., Tumanov, S., Sumpton, D., Blanco, G.R., Mackay, G., Nixon, C., Vazquez, A., Sansom, O.J., and Kamphorst, J.J. (2020). Targeting the Metabolic Response to Statin-Mediated Oxidative Stress Produces a Synergistic Antitumor Response. Cancer Res *80*, 175-188. 10.1158/0008-5472.CAN-19-0644.

89 Miyake, M., Goodison, S., Lawton, A., Gomes-Giacoia, E., and Rosser, C.J. (2015). Angiogenin promotes tumoral growth and angiogenesis by regulating matrix metallopeptidase-2 expression via the ERK1/2 pathway. Oncogene *34*, 890-901. 10.1038/onc.2014.2.

90 Moessinger, C., Klizaite, K., Steinhagen, A., Philippou-Massier, J., Shevchenko, A., Hoch, M., Ejsing, C.S., and Thiele, C. (2014). Two different pathways of phosphatidylcholine synthesis, the Kennedy Pathway and the Lands Cycle, differentially regulate cellular triacylglycerol storage. BMC Cell Biol *15*, 43. 10.1186/s12860-014-0043-3.

91 Monteiro, A.R., Hill, R., Pilkington, G.J., and Madureira, P.A. (2017). The Role of Hypoxia in Glioblastoma Invasion. Cells *6*. 10.3390/cells6040045.

92 Montemagno, C., and Pages, G. (2020). Resistance to Anti-angiogenic Therapies: A Mechanism Depending on the Time of Exposure to the Drugs. Front Cell Dev Biol *8*, 584. 10.3389/fcell.2020.00584.

93 Moon, S.H., Huang, C.H., Houlihan, S.L., Regunath, K., Freed-Pastor, W.A., Morris, J.P.t., Tschaharganeh, D.F., Kastenhuber, E.R., Barsotti, A.M., Culp-Hill, R., et al. (2019). p53 Represses the Mevalonate Pathway to Mediate Tumor Suppression. Cell *176*, 564-580 e519. 10.1016/j.cell.2018.11.011.

94 Murakami, M., Kambe, T., Shimbara, S., Higashino, K., Hanasaki, K., Arita, H., Horiguchi, M., Arita, M., Arai, H., Inoue, K., and Kudo, I. (1999). Different functional aspects of the group II subfamily (Types IIA and V) and type X secretory phospholipase A(2)s in regulating

arachidonic acid release and prostaglandin generation. Implications of cyclooxygenase-2 induction and phospholipid scramblase-mediated cellular membrane perturbation. J Biol Chem *274*, 31435-31444. 10.1074/jbc.274.44.31435.

95 Murakami, M., Masuda, S., Shimbara, S., Bezzine, S., Lazdunski, M., Lambeau, G., Gelb, M.H., Matsukura, S., Kokubu, F., Adachi, M., and Kudo, I. (2003). Cellular arachidonate-releasing function of novel classes of secretory phospholipase A2s (groups III and XII). J Biol Chem *278*, 10657-10667. 10.1074/jbc.M211325200.

96 Murakami, M., Masuda, S., Shimbara, S., Ishikawa, Y., Ishii, T., and Kudo, I. (2005). Cellular distribution, post-translational modification, and tumorigenic potential of human group III secreted phospholipase A(2). J Biol Chem *280*, 24987-24998. 10.1074/jbc.M502088200.

97 Murase, R., Taketomi, Y., Miki, Y., Nishito, Y., Saito, M., Fukami, K., Yamamoto, K., and Murakami, M. (2017). Group III phospholipase A2 promotes colitis and colorectal cancer. Sci Rep *7*, 12261. 10.1038/s41598-017-12434-z.

98 Nam, S.W., Clair, T., Kim, Y.S., McMarlin, A., Schiffmann, E., Liotta, L.A., and Stracke, M.L. (2001). Autotaxin (NPP-2), a metastasis-enhancing motogen, is an angiogenic factor. Cancer Res *61*, 6938-6944.

99 Namkoong, S., Lee, S.J., Kim, C.K., Kim, Y.M., Chung, H.T., Lee, H., Han, J.A., Ha, K.S., Kwon, Y.G., and Kim, Y.M. (2005). Prostaglandin E2 stimulates angiogenesis by activating the nitric oxide/cGMP pathway in human umbilical vein endothelial cells. Exp Mol Med *37*, 588-600. 10.1038/emm.2005.72.

100 Ning, Y., Manegold, P.C., Hong, Y.K., Zhang, W., Pohl, A., Lurje, G., Winder, T., Yang, D., LaBonte, M.J., Wilson, P.M., et al. (2011). Interleukin-8 is associated with proliferation, migration, angiogenesis and chemosensitivity in vitro and in vivo in colon cancer cell line models. Int J Cancer *128*, 2038-2049. 10.1002/ijc.25562.

101 Nobusawa, S., Watanabe, T., Kleihues, P., and Ohgaki, H. (2009). IDH1 mutations as molecular signature and predictive factor of secondary glioblastomas. Clin Cancer Res *15*, 6002-6007. 10.1158/1078-0432.CCR-09-0715.

102 Nohturfft, A., and Zhang, S.C. (2009). Coordination of lipid metabolism in membrane biogenesis. Annu Rev Cell Dev Biol *25*, 539-566. 10.1146/annurev.cellbio.24.110707.175344.

103 Nusse, R. (2008). Wnt signaling and stem cell control. Cell Res *18*, 523-527. 10.1038/cr.2008.47.

104 Nusse, R., Fuerer, C., Ching, W., Harnish, K., Logan, C., Zeng, A., ten Berge, D., and Kalani, Y. (2008). Wnt signaling and stem cell control. Cold Spring Harb Symp Quant Biol *73*, 59-66. 10.1101/sqb.2008.73.035.

105 Ohgaki, H., and Kleihues, P. (2013). The definition of primary and secondary glioblastoma. Clin Cancer Res *19*, 764-772. 10.1158/1078-0432.CCR-12-3002.

106 Ohta, H., Sato, K., Murata, N., Damirin, A., Malchinkhuu, E., Kon, J., Kimura, T., Tobo, M., Yamazaki, Y., Watanabe, T., et al. (2003). Ki16425, a subtype-selective antagonist for EDG-family lysophosphatidic acid receptors. Mol Pharmacol *64*, 994-1005. 10.1124/mol.64.4.994.

107 Ostrom, Q.T., Cioffi, G., Gittleman, H., Patil, N., Waite, K., Kruchko, C., and Barnholtz-Sloan, J.S. (2019). CBTRUS Statistical Report: Primary Brain and Other Central Nervous System Tumors Diagnosed in the United States in 2012-2016. Neuro Oncol *21*, v1-v100. 10.1093/neuonc/noz150.

108 Osuka, S., and Van Meir, E.G. (2017). Overcoming therapeutic resistance in glioblastoma: the way forward. J Clin Invest *127*, 415-426. 10.1172/JCI89587.

109 Palm, W., and Thompson, C.B. (2017). Nutrient acquisition strategies of mammalian cells. Nature *546*, 234-242. 10.1038/nature22379.

110 Pandey, P.R., Okuda, H., Watabe, M., Pai, S.K., Liu, W., Kobayashi, A., Xing, F., Fukuda, K., Hirota, S., Sugai, T., et al. (2011). Resveratrol suppresses growth of cancer stem-like cells by inhibiting fatty acid synthase. Breast Cancer Res Treat *130*, 387-398. 10.1007/s10549-010-1300-6.

111 Park, D.M., Sathornsumetee, S., and Rich, J.N. (2010). Medical oncology: treatment and management of malignant gliomas. Nat Rev Clin Oncol *7*, 75-77. 10.1038/nrclinonc.2009.221.

112 Park, J.B., Lee, C.S., Jang, J.H., Ghim, J., Kim, Y.J., You, S., Hwang, D., Suh, P.G., and Ryu, S.H. (2012). Phospholipase signalling networks in cancer. Nat Rev Cancer *12*, 782-792. 10.1038/nrc3379.

113 Parsons, D.W., Jones, S., Zhang, X., Lin, J.C., Leary, R.J., Angenendt, P., Mankoo, P., Carter, H., Siu, I.M., Gallia, G.L., et al. (2008). An integrated genomic analysis of human glioblastoma multiforme. Science *321*, 1807-1812. 10.1126/science.1164382.
114 Patel, D., Ahmad, F., Kambach, D.M., Sun, Q., Halim, A.S., Kramp, T., Camphausen, K.A., and Stommel, J.M. (2019). LXRbeta controls glioblastoma cell growth, lipid balance, and immune modulation independently of ABCA1. Sci Rep *9*, 15458. 10.1038/s41598-019-51865-8.
115 Peck, B., Schug, Z.T., Zhang, Q., Dankworth, B., Jones, D.T., Smethurst, E., Patel, R., Mason, S., Jiang, M., Saunders, R., et al. (2016). Inhibition of fatty acid desaturation is detrimental to cancer cell survival in metabolically compromised environments. Cancer Metab *4*, 6. 10.1186/s40170-016-0146-8.
116 Peck, B., and Schulze, A. (2014). Cholesteryl esters: fueling the fury of prostate cancer. Cell Metab *19*, 350-352. 10.1016/j.cmet.2014.02.012.
117 Peiffer, J., and Kleihues, P. (1999). Hans-Joachim Scherer (1906-1945), pioneer in glioma research. Brain Pathol *9*, 241-245. 10.1111/j.1750-3639.1999.tb00222.x.
118 Peixoto, J., Janaki-Raman, S., Schlicker, L., Schmitz, W., Walz, S., Winkelkotte, A.M., Herold-Mende, C., Soares, P., Schulze, A., and Lima, J. (2021). Integrated Metabolomics and Transcriptomics Analysis of Monolayer and Neurospheres from Established Glioblastoma Cell Lines. Cancers (Basel) *13*. 10.3390/cancers13061327.
119 Peixoto, J., and Lima, J. (2018). Metabolic traits of cancer stem cells. Dis Model Mech *11*. 10.1242/dmm.033464.
120 Perry, A., and Wesseling, P. (2016). Histologic classification of gliomas. Handb Clin Neurol *134*, 71-95. 10.1016/B978-0-12-802997-8.00005-0.
121 Peterson, T.R., Sengupta, S.S., Harris, T.E., Carmack, A.E., Kang, S.A., Balderas, E., Guertin, D.A., Madden, K.L., Carpenter, A.E., Finck, B.N., and Sabatini, D.M. (2011). mTOR complex 1 regulates lipin 1 localization to control the SREBP pathway. Cell *146*, 408-420. 10.1016/j.cell.2011.06.034.
122 Phong, M.S., Van Horn, R.D., Li, S., Tucker-Kellogg, G., Surana, U., and Ye, X.S. (2010). p38 mitogen-activated protein kinase promotes cell survival in response to DNA damage but is not required for the G(2) DNA damage checkpoint in human cancer cells. Mol Cell Biol *30*, 3816-3826. 10.1128/MCB.00949-09.
123 Pinkham, K., Park, D.J., Hashemiaghdam, A., Kirov, A.B., Adam, I., Rosiak, K., da Hora, C.C., Teng, J., Cheah, P.S., Carvalho, L., et al. (2019). Stearoyl CoA Desaturase Is Essential for Regulation of Endoplasmic Reticulum Homeostasis and Tumor Growth in Glioblastoma Cancer Stem Cells. Stem Cell Reports *12*, 712-727. 10.1016/j.stemcr.2019.02.012.
124 Plesniak, L.A., Boegeman, S.C., Segelke, B.W., and Dennis, E.A. (1993). Interaction of phospholipase A2 with thioether amide containing phospholipid analogues. Biochemistry *32*, 5009-5016. 10.1021/bi00070a006.
125 Porstmann, T., Griffiths, B., Chung, Y.L., Delpuech, O., Griffiths, J.R., Downward, J., and Schulze, A. (2005). PKB/Akt induces transcription of enzymes involved in cholesterol and fatty acid biosynthesis via activation of SREBP. Oncogene *24*, 6465-6481. 10.1038/sj.onc.1208802.
126 Porstmann, T., Santos, C.R., Griffiths, B., Cully, M., Wu, M., Leevers, S., Griffiths, J.R., Chung, Y.L., and Schulze, A. (2008). SREBP activity is regulated by mTORC1 and contributes to Akt-dependent cell growth. Cell Metab *8*, 224-236. 10.1016/j.cmet.2008.07.007.
127 Porstmann, T., Santos, C.R., Lewis, C., Griffiths, B., and Schulze, A. (2009). A new player in the orchestra of cell growth: SREBP activity is regulated by mTORC1 and contributes to the regulation of cell and organ size. Biochem Soc Trans *37*, 278-283. 10.1042/BST0370278.
128 Prasad, S., Gaedicke, S., Machein, M., Mittler, G., Braun, F., Hettich, M., Firat, E., Klingner, K., Schuler, J., Wider, D., et al. (2015). Effective Eradication of Glioblastoma Stem Cells by Local Application of an AC133/CD133-Specific T-cell-Engaging Antibody and CD8 T Cells. Cancer Res *75*, 2166-2176. 10.1158/0008-5472.CAN-14-2415.
129 Raught, B., and Gingras, A.C. (1999). eIF4E activity is regulated at multiple levels. Int J Biochem Cell Biol *31*, 43-57. 10.1016/s1357-2725(98)00131-9.
130 Reed, B.D., Charos, A.E., Szekely, A.M., Weissman, S.M., and Snyder, M. (2008). Genome-wide occupancy of SREBP1 and its partners NFY and SP1 reveals novel functional roles

and combinatorial regulation of distinct classes of genes. PLoS Genet *4*, e1000133. 10.1371/journal.pgen.1000133.

131 Regad, T. (2015). Targeting RTK Signaling Pathways in Cancer. Cancers (Basel) *7*, 1758-1784. 10.3390/cancers7030860.

132 Reynolds, B.A., and Weiss, S. (1992). Generation of neurons and astrocytes from isolated cells of the adult mammalian central nervous system. Science *255*, 1707-1710. 10.1126/science.1553558.

133 Rios-Esteves, J., and Resh, M.D. (2013). Stearoyl CoA desaturase is required to produce active, lipid-modified Wnt proteins. Cell Rep *4*, 1072-1081. 10.1016/j.celrep.2013.08.027.

134 Rivera-Lopez, C.M., Tucker, A.L., and Lynch, K.R. (2008). Lysophosphatidic acid (LPA) and angiogenesis. Angiogenesis *11*, 301-310. 10.1007/s10456-008-9113-5.

135 Rohrig, F., and Schulze, A. (2016). The multifaceted roles of fatty acid synthesis in cancer. Nat Rev Cancer *16*, 732-749. 10.1038/nrc.2016.89.

136 Roongta, U.V., Pabalan, J.G., Wang, X., Ryseck, R.P., Fargnoli, J., Henley, B.J., Yang, W.P., Zhu, J., Madireddi, M.T., Lawrence, R.M., et al. (2011). Cancer cell dependence on unsaturated fatty acids implicates stearoyl-CoA desaturase as a target for cancer therapy. Mol Cancer Res *9*, 1551-1561. 10.1158/1541-7786.MCR-11-0126.

137 Roy, S., Lahiri, D., Maji, T., and Biswas, J. (2015). Recurrent Glioblastoma: Where we stand. South Asian J Cancer *4*, 163-173. 10.4103/2278-330X.175953.

138 Salway, J.G. (2017). Metabolism at a Glance, Fourth Edition (John Wiley and sons).

139 Sarbassov, D.D., Guertin, D.A., Ali, S.M., and Sabatini, D.M. (2005). Phosphorylation and regulation of Akt/PKB by the rictor-mTOR complex. Science *307*, 1098-1101. 10.1126/science.1106148.

140 Saxton, R.A., and Sabatini, D.M. (2017). mTOR Signaling in Growth, Metabolism, and Disease. Cell *169*, 361-371. 10.1016/j.cell.2017.03.035.

141 Sbiera, S., Leich, E., Liebisch, G., Sbiera, I., Schirbel, A., Wiemer, L., Matysik, S., Eckhardt, C., Gardill, F., Gehl, A., et al. (2015). Mitotane Inhibits Sterol-O-Acyl Transferase 1 Triggering Lipid-Mediated Endoplasmic Reticulum Stress and Apoptosis in Adrenocortical Carcinoma Cells. Endocrinology *156*, 3895-3908. 10.1210/en.2015-1367.

142 Scheid, M.P., Parsons, M., and Woodgett, J.R. (2005). Phosphoinositide-dependent phosphorylation of PDK1 regulates nuclear translocation. Mol Cell Biol *25*, 2347-2363. 10.1128/MCB.25.6.2347-2363.2005.

143 Scheithauer, B.W. (2009). Development of the WHO classification of tumors of the central nervous system: a historical perspective. Brain Pathol *19*, 551-564. 10.1111/j.1750-3639.2008.00192.x.

144 Sheng, J., and Xu, Z. (2016). Three decades of research on angiogenin: a review and perspective. Acta Biochim Biophys Sin (Shanghai) *48*, 399-410. 10.1093/abbs/gmv131.

145 Shi, J., and Wei, P.K. (2016). Interleukin-8: A potent promoter of angiogenesis in gastric cancer. Oncol Lett *11*, 1043-1050. 10.3892/ol.2015.4035.

146 Shindou, H., and Shimizu, T. (2009). Acyl-CoA:lysophospholipid acyltransferases. J Biol Chem *284*, 1-5. 10.1074/jbc.R800046200.

147 Snaebjornsson, M.T., Janaki-Raman, S., and Schulze, A. (2020). Greasing the Wheels of the Cancer Machine: The Role of Lipid Metabolism in Cancer. Cell Metab *31*, 62-76. 10.1016/j.cmet.2019.11.010.

148 Sounni, N.E., Cimino, J., Blacher, S., Primac, I., Truong, A., Mazzucchelli, G., Paye, A., Calligaris, D., Debois, D., De Tullio, P., et al. (2014). Blocking lipid synthesis overcomes tumor regrowth and metastasis after antiangiogenic therapy withdrawal. Cell Metab *20*, 280-294. 10.1016/j.cmet.2014.05.022.

149 Stupp, R., Mason, W.P., van den Bent, M.J., Weller, M., Fisher, B., Taphoorn, M.J., Belanger, K., Brandes, A.A., Marosi, C., Bogdahn, U., et al. (2005). Radiotherapy plus concomitant and adjuvant temozolomide for glioblastoma. N Engl J Med *352*, 987-996. 10.1056/NEJMoa043330.

150 Sundqvist, A., Bengoechea-Alonso, M.T., Ye, X., Lukiyanchuk, V., Jin, J., Harper, J.W., and Ericsson, J. (2005). Control of lipid metabolism by phosphorylation-dependent degradation of the SREBP family of transcription factors by SCF(Fbw7). Cell Metab *1*, 379-391. 10.1016/j.cmet.2005.04.010.

151 Tabuchi, S. (2015). The autotaxin-lysophosphatidic acid-lysophosphatidic acid receptor cascade: proposal of a novel potential therapeutic target for treating glioblastoma multiforme. Lipids Health Dis *14*, 56. 10.1186/s12944-015-0059-5.

152 Takada, R., Satomi, Y., Kurata, T., Ueno, N., Norioka, S., Kondoh, H., Takao, T., and Takada, S. (2006). Monounsaturated fatty acid modification of Wnt protein: its role in Wnt secretion. Dev Cell *11*, 791-801. 10.1016/j.devcel.2006.10.003.
153 Tamura, K., Sakurai, T., and Kogo, H. (2006). Relationship between prostaglandin E2 and vascular endothelial growth factor (VEGF) in angiogenesis in human vascular endothelial cells. Vascul Pharmacol *44*, 411-416. 10.1016/j.vph.2006.02.009.
154 Teo, S.T., Yung, Y.C., Herr, D.R., and Chun, J. (2009). Lysophosphatidic acid in vascular development and disease. IUBMB Life *61*, 791-799. 10.1002/iub.220.
155 Thoreen, C.C., Chantranupong, L., Keys, H.R., Wang, T., Gray, N.S., and Sabatini, D.M. (2012). A unifying model for mTORC1-mediated regulation of mRNA translation. Nature *485*, 109-113. 10.1038/nature11083.
156 van Meer, G., Voelker, D.R., and Feigenson, G.W. (2008). Membrane lipids: where they are and how they behave. Nat Rev Mol Cell Biol *9*, 112-124. 10.1038/nrm2330.
157 Vander Heiden, M.G., Plas, D.R., Rathmell, J.C., Fox, C.J., Harris, M.H., and Thompson, C.B. (2001). Growth factors can influence cell growth and survival through effects on glucose metabolism. Mol Cell Biol *21*, 5899-5912. 10.1128/mcb.21.17.5899-5912.2001.
158 Villa, G.R., Hulce, J.J., Zanca, C., Bi, J., Ikegami, S., Cahill, G.L., Gu, Y., Lum, K.M., Masui, K., Yang, H., et al. (2016). An LXR-Cholesterol Axis Creates a Metabolic Co-Dependency for Brain Cancers. Cancer Cell *30*, 683-693. 10.1016/j.ccell.2016.09.008.
159 Vivanco, I., and Sawyers, C.L. (2002). The phosphatidylinositol 3-Kinase AKT pathway in human cancer. Nat Rev Cancer *2*, 489-501. 10.1038/nrc839.
160 Walker, A.K., Jacobs, R.L., Watts, J.L., Rottiers, V., Jiang, K., Finnegan, D.M., Shioda, T., Hansen, M., Yang, F., Niebergall, L.J., et al. (2011). A conserved SREBP-1/phosphatidylcholine feedback circuit regulates lipogenesis in metazoans. Cell *147*, 840-852. 10.1016/j.cell.2011.09.045.
161 Wang, X., Huang, Z., Wu, Q., Prager, B.C., Mack, S.C., Yang, K., Kim, L.J.Y., Gimple, R.C., Shi, Y., Lai, S., et al. (2017). MYC-Regulated Mevalonate Metabolism Maintains Brain Tumor-Initiating Cells. Cancer Res *77*, 4947-4960. 10.1158/0008-5472.CAN-17-0114.
162 Watanabe, K., Tachibana, O., Sata, K., Yonekawa, Y., Kleihues, P., and Ohgaki, H. (1996). Overexpression of the EGF receptor and p53 mutations are mutually exclusive in the evolution of primary and secondary glioblastomas. Brain Pathol *6*, 217-223; discussion 223-214. 10.1111/j.1750-3639.1996.tb00848.x.
163 Wen, Y.A., Xiong, X., Zaytseva, Y.Y., Napier, D.L., Vallee, E., Li, A.T., Wang, C., Weiss, H.L., Evers, B.M., and Gao, T. (2018). Downregulation of SREBP inhibits tumor growth and initiation by altering cellular metabolism in colon cancer. Cell Death Dis *9*, 265. 10.1038/s41419-018-0330-6.
164 Whitman, M., Kaplan, D.R., Schaffhausen, B., Cantley, L., and Roberts, T.M. (1985). Association of phosphatidylinositol kinase activity with polyoma middle-T competent for transformation. Nature *315*, 239-242. 10.1038/315239a0.
165 Williams, K.J., Argus, J.P., Zhu, Y., Wilks, M.Q., Marbois, B.N., York, A.G., Kidani, Y., Pourzia, A.L., Akhavan, D., Lisiero, D.N., et al. (2013). An essential requirement for the SCAP/SREBP signaling axis to protect cancer cells from lipotoxicity. Cancer Res *73*, 2850-2862. 10.1158/0008-5472.CAN-13-0382-T.
166 Wu, M.H., Huang, C.Y., Lin, J.A., Wang, S.W., Peng, C.Y., Cheng, H.C., and Tang, C.H. (2014). Endothelin-1 promotes vascular endothelial growth factor-dependent angiogenesis in human chondrosarcoma cells. Oncogene *33*, 1725-1735. 10.1038/onc.2013.109.
167 Yan, H., Parsons, D.W., Jin, G., McLendon, R., Rasheed, B.A., Yuan, W., Kos, I., Batinic-Haberle, I., Jones, S., Riggins, G.J., et al. (2009). IDH1 and IDH2 mutations in gliomas. N Engl J Med *360*, 765-773. 10.1056/NEJMoa0808710.
168 Yang, H., Rudge, D.G., Koos, J.D., Vaidialingam, B., Yang, H.J., and Pavletich, N.P. (2013). mTOR kinase structure, mechanism and regulation. Nature *497*, 217-223. 10.1038/nature12122.
169 Yasumoto, Y., Miyazaki, H., Vaidyan, L.K., Kagawa, Y., Ebrahimi, M., Yamamoto, Y., Ogata, M., Katsuyama, Y., Sadahiro, H., Suzuki, M., and Owada, Y. (2016). Inhibition of Fatty Acid Synthase Decreases Expression of Stemness Markers in Glioma Stem Cells. PLoS One *11*, e0147717. 10.1371/journal.pone.0147717.
170 Yokoyama, C., Wang, X., Briggs, M.R., Admon, A., Wu, J., Hua, X., Goldstein, J.L., and Brown, M.S. (1993). SREBP-1, a basic-helix-loop-helix-leucine zipper protein that controls transcription of the low density lipoprotein receptor gene. Cell *75*, 187-197.

171 Yoshioka, N., Wang, L., Kishimoto, K., Tsuji, T., and Hu, G.F. (2006). A therapeutic target for prostate cancer based on angiogenin-stimulated angiogenesis and cancer cell proliferation. Proc Natl Acad Sci U S A *103*, 14519-14524. 0606708103 [pii]
172 10.1073/pnas.0606708103.
173 Young, R.M., Ackerman, D., Quinn, Z.L., Mancuso, A., Gruber, M., Liu, L., Giannoukos, D.N., Bobrovnikova-Marjon, E., Diehl, J.A., Keith, B., and Simon, M.C. (2013). Dysregulated mTORC1 renders cells critically dependent on desaturated lipids for survival under tumor-like stress. Genes Dev *27*, 1115-1131. 10.1101/gad.198630.112.
174 Yu, L., Deems, R.A., Hajdu, J., and Dennis, E.A. (1990). The interaction of phospholipase A2 with phospholipid analogues and inhibitors. J Biol Chem *265*, 2657-2664.
175 Yue, S., Li, J., Lee, S.Y., Lee, H.J., Shao, T., Song, B., Cheng, L., Masterson, T.A., Liu, X., Ratliff, T.L., and Cheng, J.X. (2014). Cholesteryl ester accumulation induced by PTEN loss and PI3K/AKT activation underlies human prostate cancer aggressiveness. Cell Metab *19*, 393-406. 10.1016/j.cmet.2014.01.019.
176 Zhu, J., and Thompson, C.B. (2019). Metabolic regulation of cell growth and proliferation. Nat Rev Mol Cell Biol *20*, 436-450. 10.1038/s41580-019-0123-5.
177 Zhu, Z., Khan, M.A., Weiler, M., Blaes, J., Jestaedt, L., Geibert, M., Zou, P., Gronych, J., Bernhardt, O., Korshunov, A., et al. (2014). Targeting self-renewal in high-grade brain tumors leads to loss of brain tumor stem cells and prolonged survival. Cell Stem Cell *15*, 185-198. 10.1016/j.stem.2014.04.007.